FACULTY OF ENGINEERING AND APPLIED SCIENCE

INSTITUTE OF SOUND AND VIBRATION RESEARCH

ORIGINS OF NOISE AND VIBRATION IN VEE FORM DIESEL ENGINES WITH EMPHASIS ON PISTON SLAP

by

S.D. HADDAD

A Thesis submitted for the Degree

of

Doctor of Philosophy

University of Southampton

April 1974

ABSTRACT

FACULTY OF ENGINEERING AND APPLIED SCIENCE

INSTITUTE OF SOUND AND VIBRATION RESEARCH

Doctor of Philosophy

Origins of Noise and Vibration in Vee Form Diesel Engines with Emphasis on Piston Slap

by Sulaiman David Haddad

The investigations described in this thesis deal with Vee engine vibration and noise characteristics induced by combustion and piston impact forces in both conventional and low noise engine structures.

It has been shown that the bank to bank mode of Vee engine vibration is basically due to piston slap excitation while the conical mode, mainly resulting from combustion, is accentuated by piston to bore oil film pressure. These modes were also seen to persist on specifically designed low noise engine structures. Cylinder block vibration, and the resultant noise radiated, is mainly due to piston slap.

Simulations of piston slap on an experimental rig and an analogue computer have illustrated that the rate of rise of the piston sideways force is the most important parameter controlling the resultant cylinder block vibration. Block vibration acceleration is proportional to the logarithm of the rate of rise of the side force.

Oscillographic and change of parameter studies have shown that piston slap can be as important a source of noise as combustion. Up to 3 dBA reduction of the overall engine noise, in the frequency range from 1000 Hz upwards, is practicable in existing engines by minimising piston slap.

Study of piston behaviour in a running engine has shown that piston movement in the bore initiates dynamic pressures which are due to both squeeze film and hydrodynamic effects. The impulsive squeeze film pressure

predominates over combustion excitation for most engine conditions and therefore can control the vibration characteristics of engine structure.

Comparison of measured and calculated piston movements has stressed the importance of the oil film in the evaluation of piston behaviour.

ACKNOWLEDGEMENTS

I owe a considerable debt to my supervisor, Professor T. Priede, for his encouragement and constructive criticism throughout this work. He has taught me much and I count it a priviledge to have worked under him. Particular thanks are extended to Dr. R.G. White and Mr. P.W. Fortescue for the considerable assistance towards the simulation work.

Thanks are due to Cummins Engine Company for their active support of the project and for the provision of engines and experimental equipment, and to AED-Cawston and Wellworthy Ltd. for making available component parts and computations.

I wish to express my appreciation to all members of the Automotive Group of ISVR, especially Mr. E.C. Grover and Dr. N. Lalor, for their help and valued discussions. Also to Mr. R. Hooper for his enthusiastic assistance in the numerous engine test installations and rigs.

Other members of ISVR deserve my compliments, especially Mr. R. Pacifico for his assistance in the analogue hardware, Mrs. S. Probert for assisting with computation and Mrs. M. Strickland for her efficient typing of the manuscript.

Finally, but by no means least, my wife, Basima, deserves my admiration for being so patient while conducting this research.

CONTENTS

LIST OF FIGURES

LIST OF TABLES

CHAPTER 1

INTRODUCTION

In the commercial field, in order to meet the legislated power to weight ratio, vehicles with more powerful engines are required. To increase the power output, the engine can be made larger or can run faster or its specific load can be increased. Generally until recently, the parameter chosen for increasing the power output of an engine has been the speed, which also unfortunately, increases the noise (ref. 1.1). The result is that automotive diesel engine noise has increased by about 6 to 8 dBA over the past 20 years. The introduction of the high speed diesel engine, however, has offered very great economic advantages since the same power output has been possible from a physically smaller and lighter unit.

The combustion process in the diesel engine has always been identified by subjective impressions of the resultant noise. This characteristic noise of diesel combustion is generally known as 'diesel knock' which distinguishes it from the smoother combustion of the spark ignition petrol engine. At the same time, noises of mechanical origin can also be recognised such as 'piston slap', gear noise, tappet noise and bearing impact noise. These mechanical noises can be of such a high level that, no difference is observed between the noise of the engine when motoring and running.

The forces producing these distinctive noises are of widely different character. The gas force resulting from combustion may be assumed to be the direct exciting force of the engine, while the mechanical impacts are the indirect forces which are dependent on the direct exciting forces in some non-linear manner.

In recent years there has been great pollution awareness in most parts of the industrialised world. Road transport is considered to be a main contributor and public concern is forcing engine manufacturers to produce

engines with lower exhaust emissions. A comprehensive account by Pischinger and Cartellieri (ref. 1.2) shows that reductions of emissions are feasible to meet the projected world-wide standards. Gaseous emissions, smoke and noise are, to a great extent, independent: an understanding of their basic relationships is therefore of value.

When the basic relationships between carbon monoxide, hydrocarbon, oxides of nitrogen, smoke, specific fuel consumption and noise with injection timing for a given fuel injection system are considered, only the noise and oxides of nitrogen reduce with retarded timing while all the other parameters tend to increase. In practice therefore a compromise between the two groups of parameters has to be carefully considered. It can be observed, however, that methods used to control the formation of oxides of nitrogen in a diesel engine also tend to reduce the combustion induced noise.

It is mainly the control of oxides of nitrogen that has dictated new approaches to combustion system design. For this reason Indirect Injection (I.D.I.) combustion systems, where the smoke reduces with retarded timing, are again being considered for larger capacity engines. In D.I. engines it has been found that retarded timing can be acceptable provided at the same time the engine is turbocharged. Turbocharging effectively cleans the smoke and also reduces the carbon monoxide and hydrocarbon emissions. Turbocharging is also one of the most effective methods for reducing the combustion noise of the engine which is achieved even with a substantially greater engine output (refs. 1.3, 1.4).

The pressure diagrams of the pressure charged engine closely resemble that of a petrol engine. The reduction of combustion induced noise (cylinder pressure level) in comparison with the normally aspirated engines is of the order of 6 to 8 dB.

From investigations on a number of turbocharged engines of different make it has been found that the reduction of noise is considerably smaller than the reduction of the cylinder pressure level. The reductions of the overall noise of the engines are between 2 to 4 dBA or the noise can even be greater. This suggests that noises of mechanical origin are becoming more predominant in smoother combustion turbocharged engines.

In any reciprocating engine certain clearances must be maintained between the running parts. This applies to the piston in the bore, journal in bearings and mating gears. In all these moving parts the gas forces which act on the piston are modified by alternating forces generated in the crank mechanism, the result being that the force between the two moving parts, or between moving and stationary parts, changes its direction (or "sign"). During the operation of the engine the moving parts are accelerated across the clearances, thus causing either mechanical impacts or impulsive hydraulic forces in the lubricating oil film.

There are three major sources of mechanical noise in the reciprocating engine.

(i) Piston slap - either mechanical impact or impulsive oil film force.

(ii) Bearing impacts - impulsive oil film force.

(iii) Timing gear impacts - mechanical impact force.

Any of these sources can be the cause of the predominant noise of the engine.

The piston slap is generally a prominent source in a diesel engine unless expansion controlled or crosshead pistons are used. Elimination of piston slap usually gives up to 3 dBA reduction of engine noise.

So far the bearing noise, because of the predominance of the direct combustion induced noise, has been less significant in diesel engines. In

petrol engines, however, there is evidence to suggest that the predominant high frequency noise (1000-3000 Hz) is primarily induced by the impulsive lubricating oil film pressures (ref. 1.5). The same phenomena are now being observed in some small high speed diesel engines.

If the timing gear system is located at the front of the engine the gears are subjected to fluctuating tangential forces causing impacts between the gear teeth. Front gear systems are invariably responsible for predominating frontal noise which is largely influenced by gear clearance. Experiments involving replacing the gears with a chain or locating the gears at the rear of the engine generally show some 4-6 dBA reduction of noise from the front and up to 3 dBA reduction of noise from the sides.

The intensity of the noise generated by the impacting parts of the engine depends on the characteristics of the force which accelerates the moving part across the clearance and thus depends on the characteristics of the applied force and its final kinetic energy at impact.

In the turbocharged engines, despite the very smooth cylinder pressure development the rate of side force and its peak value is markedly increased compared to the normally aspirated engine. This is a result of high cylinder pressures persisting during the initial part of the expansion stroke.

The considerations therefore indicate that with the introduction of pressure charged engines the problem of diesel engine noise will lie in better understanding of mechanical sources of noise.

The investigation presented in this thesis describes a study of a high speed vee-form automotive engine noise, its origins, characteristics of structure and structure design and the relationship between the combustion and piston slap induced noise.

The Vee engine has been chosen for this study because a far greater proportion of vibration of its radiation area (cylinder banks) is caused by piston slap.

Particular attention is being paid to the fundamental origins and the parameters which control piston slap.

Most of the work was carried out on the Cummins 'Vale' V8 470 diesel engine (Engine SA) and its low noise versions (LNA and LNB) except where stated otherwise.

References

1.1 T. PRIEDE. "Noise in engineering and transportation and its effect on the community". Automotive Engine Congress, Detroit, Michigan, 1971, Paper 710061.

1.2 R. PISCHINGER and W. CARTELLIERI. "Combustion system parameters and their effect upon diesel engine exhaust emissions". S.A.E. September 1972, Paper 720756.

1.3 C.J. WALDER. "Reduction of emissions from diesel engines". International Automotive Engineering Congress, 1973. S.A.E. Paper 730214.

1.4 W.P. MANSFIELD and W.S. MAY. "Diesel engine combustion at high m.e.p. with low compression ratio". S.A.E. paper 660343.

1.5 J.A. RAFF. "Some studies into the origins of noise of small automotive petrol engines". ISVR, Southampton University, Ph.D. Thesis, 1972.

CHAPTER 2

REVIEW OF LITERATURE

Serious attempts to understand the origins of diesel engine noise are relatively recent. One of the first comprehensive accounts was published by Bradbury (ref. 2.1). He listed that the main sources of noise from a diesel engine are piston slap, firing impulse (combustion impulse), valve gear, fuel injection equipment and crankshaft torsional vibration. Mercy (ref. 2.2) classified various sources of noise and determined their relative magnitudes as percentage contributors to the total engine noise.

Austin and Priede (ref. 2.3) presented results on engine noise and its origins. They showed that noise output from a diesel engine is constant with load, that the sound intensity increases with $(\text{speed})^3$ and that noise output increases with engine $(\text{size})^{1.33}$. Theoretical relationships were used to estimate the structural attenuation and the sound radiated from the engine surfaces. The overall attenuation (structural-acoustical attenuation) that exists between the cylinder pressure and the sound pressure measured at 3 feet from the engine was established.

Priede (ref. 2.4) evaluated some of the most important origins of noise and vibration of reciprocating engines and showed that, particularly in a diesel engine, the combustion constitutes the major source of excitation producing the noise.

The other sources of noise in the diesel engine have been investigated by various researchers with particular attention to piston slap. Studies of the phenomenon of piston slap have been either experimentally or theoretically biased. In the former, the parameters investigated were somewhat limited. In the latter, due to complexity of the theory, researchers had to assume minor simplifications for solving the problem.

Meier (ref. 2.5) was the first to measure piston sideways movement in a running engine. He outlined the cycle events in which piston slap occurs and described experiments designed to minimise piston slap by off-setting the gudgeon pin. From his theoretical analyses and experimental results he gave further recommendations regarding piston design to minimise piston slap. He concluded by discussing the effect of the piston to bore oil film.

Zinchenko (ref. 2.6) developed expressions for the impulse resulting from piston impact by calculating the net lateral force acting on the piston and solving the resulting equations of motion. He distinguished between impacts occurring at top dead centre (T.D.C.), where the gas forces are high, and impacts occurring elsewhere, where inertia forces dominate the net lateral force. However, in his analysis he did not consider separately connecting rod inertia effects but accounted for these by assigning an equivalent inertia increase to the piston.

Crane (ref. 2.7) gave more comprehensive theoretical treatment to the problem. He used a computer to evaluate piston slap impact velocities as a function of piston-cylinder clearance and engine geometry for several engines.

Hempel (ref. 2.8) presented even more extensive analytical treatment. He subdivided the motion of the piston across the cylinder clearance into various stages. The parameters used were non-dimensional and some simplifications made which, although quite valid if used to give a clearer insight into the phenomenon, were not really justified if used as a basis for a detailed experimental analysis of a particular engine.

Priede (ref. 2.9), though having established the importance of combustion excitation in diesel engines, records in a more recent work an investigation of the piston slap contribution to the overall noise level.

The method he used depended on comparison of the spectra of the gas force and the forces associated with piston slap. From this he concluded that piston slap is likely to predominate only when combustion is relatively smooth, and even then over a limited frequency range above 800 Hz.

Fielding and Skorecki (ref. 2.10) also presented a comprehensive study with excellent theoretical analysis by deriving equations for the transverse motion of the piston in a similar way to Hempel. They verified these results experimentally by varying some of the engine parameters such as piston-cylinder clearance, gudgeon pin offset, and piston lubrication, but this work was limited to a study on a single cylinder engine.

Most of the investigations considered above have been carried out on single cylinder units and therefore are not fully representative of multi cylinder automotive engines.

Others used similar techniques. These include Ungar and Ross, Heldt, Smith, Bolt, Beranek, Griffiths, Skobtsove, Haasler, Burrel, Butler and Lightowlers.

Westbrook and Munro (ref. 2.11) stress that a full understanding of piston slap can only be achieved by the study of piston behaviour in a running engine. They present a reliable method of telemetering information continuously over the whole working cycle on piston movement, temperature and strain from a running engine. In addition to specifying the transducer detail, they also compare piston movement with engine block vibration acceleration.

Laws, Parker and Turner (ref. 2.12) have used this technique successfully to measure the cyclic incidence and intensity of piston to cylinder impact as a function of engine temperature, load and speed. These results are also compared with measurements of cylinder block vibration.

Parker, Laws and Turner (ref. 2.13) also present a well developed

theoretical computation to calculate piston movement, impact velocities and side forces showing reasonable correlation with the measured values.

At ISVR, Automotive Engineering Group (ref. 2.14), research is pursued on multi-cylinder diesel engines which included realistic simulation of piston slap in a non-running engine using sideways force generators.

References

2.1 C.H. BRADBURY. "The measurement and interpretation of machinery noise with special reference to oil engines". Proc. Inst. Mech. Eng. 1952-53. Vol. 1B, pp. 1-18.

2.2 K.R. MERCY. "Analysis of the basic noise sources in the diesel engine". ASME Paper No. 55-OGP-4, March 1955.

2.3 A.E.W. AUSTIN and T. PRIEDE. "Origins of diesel engine noise". Symp. on Noise and Noise Suppression, London 1958. I. Mech. E.

2.4 T. PRIEDE. "Relation between form of cylinder pressure diagram and noise in diesel engines". Proc. I. Mech. E. (A.D.), pp. 63-77, 1960-61. No. 1.

2.5 A. MEIER. "The kinematics of piston noises". Article in A.T.Z. 54(6), 123-8. 1952.

2.6 V.I. ZINCHENKO. "Noise of marine diesel engines". Sudpromgiz (see BBN TIR No. 61, July 1962). 1957.

2.7 P.H.G. CRANE. "The initiation of diesel engine cylinder liner vibrations by piston transverse motion". Adm. Res. Lab. Report No. R2/B10. 1959.

2.8 W. HEMPEL. "Ein Beitrag zur Kenntnis der Seitenbewegung des Tauchkolbens". A.T.Z. Vol. 2, pp. 5-10. (MIRA Translation No. 39/66). 1966.

2.9 T. PRIEDE. "Some studies into origins of automotive diesel engine noise and its control". FISITA Paper C12. 1966.

2.10 B.J. FIELDING and J. SKOROCKI. "Identification of mechanical sources of noise in a diesel engine - sound originating from piston slap". I. Mech. E. Vol. 184, Pt.1 No. 46.

2.11 M.H. WESTBROOK and R. MUNRO. "The telemetering of information from a working internal combustion engine". Journal of Engineering for Power, ASME. April 1967.

2.12 A.M. LAWS, D.A. PARKER and B. TURNER. "Piston movement as a source of engine noise". FISITA Paper 1/6, p. 29-37. 1972.

2.13 D.A. PARKER, A.M. LAWS and B. TURNER. "Piston movement in the diesel engine". CIMAC Congress, Washington. 1973.

2.14 S.D. HADDAD and H.L. PULLEN. "Some investigations into the effect of piston slap on the noise and vibration of diesel engines". BAS Conference on "Prime Movers". July 1973.

CHAPTER 3

CHARACTERISTICS OF VEE FORM ENGINE VIBRATION AND NOISE AND ITS CONTROL BY STRUCTURE DESIGN

A number of vee form automotive diesel engines have been studied. A typical installation of an engine on a test bed is shown in figure 3.1 with the engine on resilient mountings. The crankshaft axis is about three feet above the floor to enable the radiation of noise to be measured from the lower part of the engine. The engine is coupled to a dynamometer via a gearbox. All tests were carried out in test cells lined with foam wedges or perforated sound absorbing tiles. To ensure that only the engine contribution to noise is evaluated, the inlet and exhaust ducts are piped away to the outside of the test cubicle. Bruel and Kjaer equipment was used for the noise and vibration measurements. It was found that the repeatability of noise tests was reasonable, but certain variations were noted as illustrated for a V8 engine in figure 3.2. It was therefore considered that before attempting a fundamental investigation into particular sources of noise, such as piston slap, a much better control and understanding of the causes of variations were essential.

3.1 Effect of Operating Parameters and Measurement Techniques on Noise and Vibration

Variations are expected due to various reasons.

(a) Acoustic conditions.

(b) Engine operating conditions, such as inlet air temperature and water and lubricating oil temperatures.

3.1.1 Acoustic conditions

Figure 3.3a illustrates the variation of overall sound pressure level when moving the microphone along the length of the engine and at constant

distance away from the engine. As can be seen, there are variations of noise. The total fluctuations are within 2 dBA. This is considered small, but it does suggest that it is important to place the microphone precisely at the same position for each test. There is also some fluctuation of noise with distance from the engine. Figure 3.3b shows this effect along a line to the side of the engine. In general, noise decays following the inverse square law up to 3 feet. Beyond 3 feet, other factors distort the characteristics of decay. It can be concluded that precision must be adhered to in the positioning of the microphone from the engine.

3.1.2 Operating conditions

In the initial stages of the investigation considerable discrepancy existed between the noise data from engines of the same type when tested at ISVR, the United States and Germany. The differences were significant, being of the order of 3 dBA. It was thought that these variations could be due to either the operating conditions in the test cells or the quality of the fuel.

One of the operating conditions which was found to have a pronounced effect was the temperature of the lubricating oil, since generally it was observed that when starting from cold the engine appeared to be considerably noisier. Controlled tests showed that some engines are more sensitive than others to varying operating conditions. Oil temperature effects were found more pronounced in engines with shallow combustion chambers.

3.1.2.1 Effect of lubricating oil temperature on the noise, vibration and combustion

To enable the control of the oil temperatures, an external oil cooler was installed. A thermostat was also set on the cooling water outlet to control the water temperatures at fixed values throughout the investigation (inlet at 65 $\pm$ 2°C, outlet at 75 $\pm$ 2°C).

The introduction of the external oil cooler served two purposes:-

1. To control the oil temperature at a constant level when measuring the cylinder pressure spectra and noise for various speeds and loads.

2. To enable the oil temperature to be varied at constant speed and load (i.e., to enable the cylinder pressure spectra to be varied).

This external oil cooler was not of sufficient capacity to control the oil temperature in the lower range (i.e., below 85°C) for long enough time to obtain a complete spectrum.

In order to overcome this difficulty, the automatic recording facility of the B & K equipment was utilised to obtain the continuous variation in cylinder pressure level in a particular 1/3 octave band over the oil temperature range. This procedure was repeated for all 1/3 octave bands enabling 1/3 octave spectra at particular oil temperatures to be built up.

Typical results of the variation of overall noise levels (dB(A)) with oil temperature is shown in Fig. 3.4. Figure 3.5 shows the variation of overall noise levels with speed at oil temperatures of 70° and 110°C giving slopes of 23 dBA/decade and 30 dBA/decade respectively, indicating some change in the mechanism of excitation with temperature

Fig. 3.6 shows photographic recordings of cylinder pressure diagrams at oil temperatures of 68, 80, 94 and 115°C which were taken to study the mechanism of the effect of oil temperature on the cylinder pressure spectrum. These diagrams were analysed and the tabulated results are shown in Fig. 3.7. It is observed that a reduction of oil temperature increases the delay period (assuming the dynamic timing is unchanged at constant speed) and gives a greater initial rate of pressure rise which can produce higher cylinder pressure and noise levels. A similar effect has been shown by

other researchers in the context of cooling water temperatures (refs. 3.1, 3.2). The higher peak pressures at higher oil temperatures are the result of reduced heat loss as the piston crown temperature is increased.

Figure 3.8 shows the variation of cylinder pressure and noise spectra for oil temperatures of 68, 94 and 115°C at 3000 revs/min full load. It is clear that the oil temperature is affecting the cylinder pressure and consequently the noise. However, the amounts by which the cylinder pressure level and sound pressure level vary do not exactly correspond. This indicates that even at full load other sources of excitation are also affecting the noise level. Approximate calculations indicate that the excitation from both combustion and mechanical sources is of similar magnitude. It is clear, therefore, that the way in which the cylinder pressure spectrum varies with oil temperature is a useful tool for determining the level of mechanically excited noise. Cylinder pressure and sound pressure levels at various frequencies plotted against log (oil temperature °C) in Fig. 3.9a-d) follow average straight lines with different slopes. Since the slope of the SPL is lower than that of the cylinder pressure level in certain frequency bands (frequencies 1000, 1250, 3000, 3150 Hz), it suggests that with increasing oil temperature the combustion induced noise is reduced where the piston slap noise is increased. Fig. 3.10 shows the overall noise levels plotted against log (oil temperature) for 3300, 3000, 2000 rev/min full load. It can be seen that an approximate straight line relationship exists enabling the following approximate correction formula to be derived for a given speed:

$$(\text{dBA})_{\substack{\text{corrected to} \\ 90^\circ\text{C}}} = (\text{dBA})_{\substack{\text{measured at} \\ \text{temp. } t^\circ\text{C}}} + \Delta \text{ dB}$$

where Δ dB $\simeq$ $12.5 \log_{10} t - 24.4$

taking 90°C as average operating oil temperature.

This relationship will enable noise levels taken at different temperatures to be correlated.

It was also found that the oil temperature affected the structure vibration and in particular the axial crankshaft vibration (indicating crankshaft bending). The latter was measured at various temperatures using a special probe shown in figure 3.11a, which has the calibration correction shown in figure 3.11b. Figure 3.11c shows relative axial crankshaft vibration acceleration spectra at 1500 revs/min full load at various oil temperatures. All the spectra show strong components at the fundamental firing frequency (100 Hz) and up to the fourth harmonic. The effect of oil temperature here may be explained in different ways:

a - Change in crankshaft damping

Starkman (ref. 3.3) has shown that crankshaft main bearing damping decreases with reduction in oil viscosity, i.e., with increased temperature. Figure 3.11d shows that in the high frequency range (4000 Hz) the reduction of damping is the dominant mechanism controlling noise and vibration with increasing oil temperature.

b - Change in combustion

As mentioned earlier, raising the oil temperature decreases the severity of combustion significantly affecting the cylinder pressure spectrum between 300 Hz and 4000 Hz.

c - Change in piston slap

At higher temperatures the viscosity of the oil between the piston and the cylinder liner will be lower augmenting piston slap effects. These could also affect the damping of the block structure.

These studies indicate the necessity for careful control of operating

conditions and suggest that piston slap and bearing impacts can be seriously affected. In addition, the fuel quality (cetane number) has been found to affect the resultant emitted noise of the engine investigated within a 3 dB(A) range.

3.2 Early Noise and Combustion Studies Showing the Importance of Mechanically Induced Noise

It is generally found that if the combustion excitation is predominant over other sources then any increase in combustion will give a corresponding increase in engine noise. If combustion changes have no effect, then other sources predominate.

3.2.1 Full load with speed

Fig. 3.12 shows the cylinder pressure spectra and noise for the engine at 3300, 3000 and 2000 rev/min full load at normal operating temperatures. The figure shows that although, in general, the noise increases with cyliner pressure level over most of the frequency range, the increments do not exactly correspond. Figure 3.13 is derived from Fig. 3.12 to clarify this effect. From this figure it can be seen that at full load conditions, the engine noise increases nearly at the same rate as cylinder pressure level over most of the frequency range and is therefore combustion controlled.

3.2.2 Full load versus no load

Fig. 3.14 shows the comparison of cylinder pressure and noise spectra for full load and no load conditions at 3000 rev/min. It is observed that there is a marked difference of cylinder pressure level between the two conditions especially in the higher frequency range where initial rate of pressure rise is the controlling factor. Fig. 3.15 shows the structural-acoustical attenuation (cylinder pressure level minus sound pressure level

.. Ref. 2.4) of the engine at operating temperatures for full and no load conditions. From this graph it will be seen that the structural-acoustical attenuation at no load is lower than at full load. If combustion were the predominant excitation in both cases, the curves could be identical as the level of attenuation is independent of the level of excitation. The fact that the attenuation is low at no load conditions indicates that some factor other than cylinder pressure is having a significant effect. It can be concluded therefore that mechanical excitation is much more significant at no load than at full load conditions. These mechanical sources of excitation include piston slap, bearing noise and gear noise.

It is clear from the above discussion that although mechanical excitation is probably predominant at no load conditions, its effect at full load is less marked.

3.3 Vee Form Engine Vibration and Emitted Noise

All conventionally designed reciprocating engines are basically similar in construction. In-line engines consist of a box divided into compartments. The top of this box is closed by the cylinder head, which is comparatively stiff, and the bottom is closed by a relatively flexible oil sump. Also at the top and about halfway down are horizontal decks that support the cylinders. Although these decks are quite thick, their stiffness is lessened by the cylinder bores. Such a structure is flexible in torsion about an axis parallel to the crankshaft, mainly because the oil sump is not stiff enough to "close the box" effectively. Considered as a beam, the engine is much stiffer in bending in the vertical plane than in the horizontal plane.

If such structures are excited by a sinusoidally varying force of constant magnitude over a range of frequencies, the vibration amplitude

measured at a point will show many resonant peaks. At the frequency corresponding to each peak, the structure will take up a different vibration pattern or mode shape.

In general the first mode of vibration occurs at a few hundred Hertz and consists of a torsional motion about an axis parallel to the crankshaft. At higher frequencies, say up to 1000 Hz, the engine starts to bend along its length like a homogeneous beam. Above this frequency the structure ceases to behave as a solid body and the panels forming the sides of the bays begin to vibrate independently.

At the higher frequencies these modes tend to fall into groups. Each individual mode in a group has the same basic characteristics, but differs in detail from the others. This phenomenon is demonstrated in Figure 3.16, which shows results of a finite element analysis of a 6-cylinder, in-line engine crankcase. In this group there are 12 versions of a particular type of panel mode. The natural frequencies are very close, with only 233 Hz total separation (ref. 3.4).

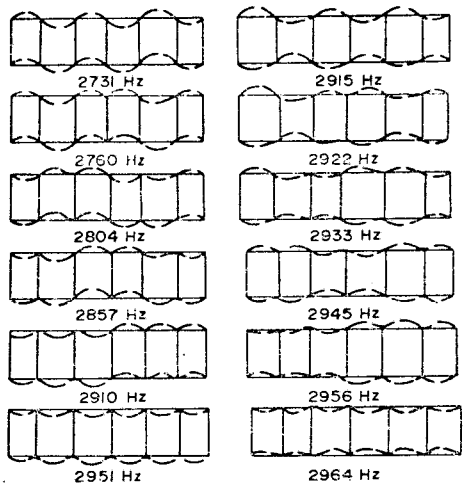

Fig. 3.16. Panel modes of a six-bay crankcase.

The Vee engine, which is a compact unit, has been developed to give much greater horse power than an in-line engine of the same length. Vee form engines consist basically of two "Siamesed" in-line engines although in this case there is little difference between the horizontal and vertical

stiffnesses.

For this reason most of the vibration modes associated with in-line engines are also present with the vee engine. However, the fact that there are now two cylinder banks introduces another mode which consists of bodily motion of one bank relative to the other.

On several vee engines it has been found that the two most acoustically important modes of structure vibration are the bank-to-bank and conical as shown in figures 3.17 and 3.18, respectively.

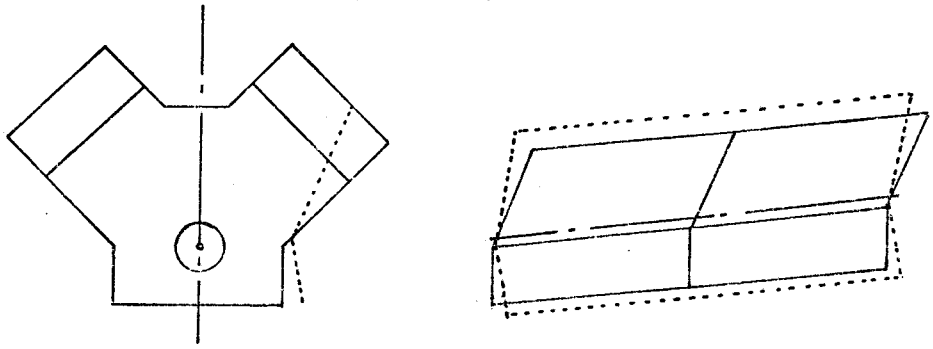

Fig. 3.17. Idealised displacement of the bank-to-bank mode on one side of a V8 engine (≈ 1250 Hz for SA).

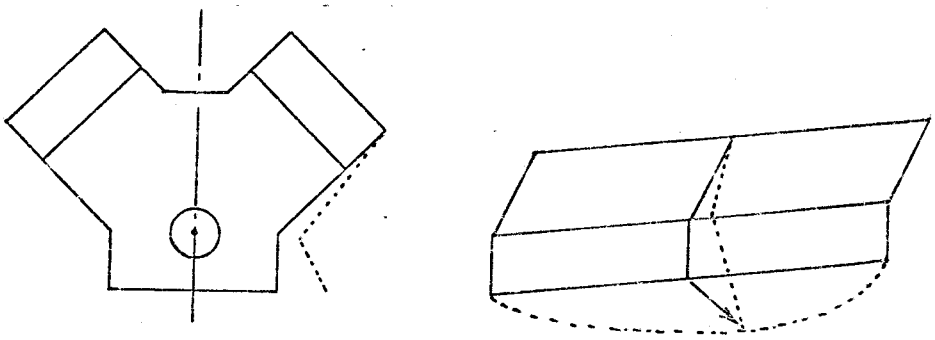

Fig. 3.18. Idealised displacement of the conical mode on one side of a V8 engine (≈ 2500 Hz for SA).

The bank-to-bank frequency of a V engine block structure can be calculated from the empirical formula:

$$f_{b.t.b.} = \left(\frac{2.79}{d}\right)^3 \text{ Hz} \qquad \text{(Reference 3.5)}$$

where d = perpendicular distance between crankshaft axis and the top face of the cylinder block in metres.

The frequency of the conical mode of the block structure can be calculated from the empirical formula:

$$f_c = \left(\frac{3.22}{\ell}\right)^5 \text{ Hz} \qquad \text{(Reference 3.5)}$$

where ℓ is the crankcase/block length in metres.

3.3.1 Design details of low noise Vee form research engine

There are three basic ways of reducing the noise radiated by the main engine structure: (1) stiffening, (2) damping, and (3) reducing the radiating area.

Control by stiffening. Radiated noise from the engine structure results from bending of the whole block in the low-frequency range and bending of the individual panels in the high frequency range. For a constant force input with frequency, the vibration amplitude at resonance is inversely proportional to the natural frequency, and therefore stiffening is effective only to the extent that the natural frequency is increased. Increasing the natural frequency can also be an advantage if it then falls within a range where the exciting forces are less. The forces from combustion tend to decrease with frequency at the rate of 30 dB/decade, as shown by the typical combustion force spectrum in Figure 3.19. Ideally, if a natural frequency is increased by a factor of two, the level of excitation would be reduced by 9 dB.

Although some improvement can be expected by the addition of webs and heavy ribbing, with only a small weight gain, it is difficult to increase significantly the whole range of natural frequencies. This can be achieved only by a general increase of thickness.

A fundamental requirement for the control of noise through increased bending stiffness is a material that makes the increase of natural frequencies possible without increasing weight.

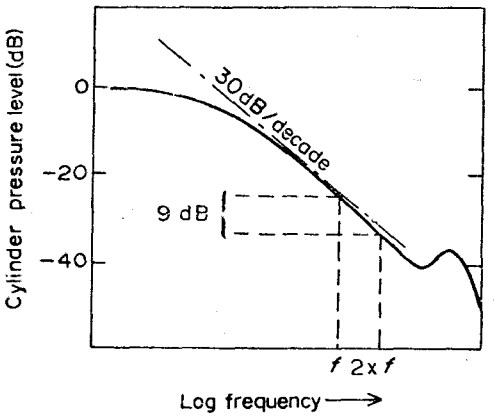

Fig. 3.19. Reduction of excitation by increase in frequency.

The frequency of plates in bending is, to a first approximation, proportional to thickness for all structural materials.

By using a low-density metal structure of the same weight as a cast iron structure, the greater thickness of the walls would make them much stiffer, and therefore the vibration amplitude for a given force would be much lower. Moreover, the natural frequency would be increased inversely to its density. This principle has been adopted in the experimental magnesium engine (ref. 3.6) in which wall thicknesses have been increased by a factor of 4 to 5.

Low-frequency modes of engine vibration depend on the overall bending stiffness of the engine structure. This stiffness is mainly controlled by the cylinder block and head. The crankcase is relatively weak because its general form is that of an open box. It has been found experimentally that an integral bearing assembly (Ref. 3.7) can increase the crankcase bending stiffness with only a small weight increase. This arrangement also has the advantage of restraining the end faces of the engine.

Control by damping. Control of engine noise by use of structural material with higher inherent damping properties is often considered. Although such materials are available, it is doubtful whether any real advantage could be gained by their use. Even with a highly resonant structure,

such as steel or cast iron, enormous damping is introduced by friction between mating and sliding surfaces. Measurements on a bare engine casting showed the dynamic magnification factor Q of over 200, but the same crankcase in a fully assembled engine showed a Q as low as 16. For further reduction to be worthwhile, additional damping of the same magnitude must be introduced into the structure. This cannot be achieved practically by attention to the basic load-carrying framework, but significant improvement can be made to individual outer panels.

One such possibility is the replacement of these outer panels with highly damped members. The feasibility of this method was illustrated by the skeleton frame engine (ref. 3.7), where a considerable reduction of high-frequency noise was obtained, by using plates of damped construction screwed to a welded steel framework.

Control by reducing the radiating area. Since it is much easier to control the noise from the covers than from the basic structure, there is a considerable advantage in redesigning the engine so that covers constitute a great percentage of the total area. It has been shown that crankcase walls are often the main noise-radiating surfaces of the basic structure, and therefore their removal holds a potential advantage. The main functions of the crankcase walls are to help support the crankshaft bearings, retain oil, and provide a location for the oil sump. If the crankcase walls are removed, a bearing beam arrangement can be made to support the bearings, and a deeper oil sump can be assembled to the bottom deck of the cylinder block to retain oil. This larger oil sump will then be attached to a stiff structural member with lower vibration levels than the normal position.

3.3.1.1 Practical low noise engine design

The basic principles of low-noise design have been indicated. By using these in conjunction with the choice of an optimum speed and bore, an entirely new engine could be constructed to take advantage of all these principles. Such an engine must satisfy other constraints such as maximum piston speed, size, weight and, of course, the required engine power.

An alternative to the complete redesign of an engine is to limit the redesign to the basic structure of an existing engine. This takes advantage of standard production parts such as cylinder head, crankshaft, rods, pistons, liners, camshaft, valve train and fuel-injection equipment.

A number of experimental in-line and Vee-form low noise engines were built at ISVR to demonstrate the worthwhile reductions of noise possible with the use of practical manufacturing techniques and conventional materials. To do this all major noise radiating surfaces had to be dealt with and the basic modes of the structural vibration controlled, necessitating entirely new main engine structures.

3.3.1.2 Low noise Vee form engine design

On the standard engine on which this design was based, the frequency of the bank-to-bank mode falls in a range which is both sensitive to the ear and where levels of excitation from combustion and mechanical origins are high.

As a major reduction of engine noise was envisaged it was decided to aim at a design giving reduced amplitude of bank-to-bank vibration by stiffening the roots of the banks. Such a design would be expected to result in a nominal increase in mass accompanied by a small increase in natural frequency.

A major weakness in the standard design is at the camshaft bearings.

The section between the banks, which can be considered as a flat plate of $\frac{1}{4}$ inch in thickness, is subjected to both compressive and tensile loads and buckling moments when the banks vibrate. Apart from the bearing annuli and the end bulkheads, this thin plate is the only tie between the banks at the top of the engine. Moreover, its effectiveness is considerably offset by general weakening in this area provided by the tappet guide bores which are closely spaced.

On the experimental engine (Figure 3.20a) this plate is of substantial thickness and extends to the full depth of the fuel pump fixing bosses. Although this section is solid for the sake of expediency it could be cored to reduce weight. The banks are further stiffned by a tie below the camshaft. However, this does not extend the full length of the engine as provision is made to insert the bearing bushes.

A tie is also provided between the banks at the front end of the engine. This consists of a rigid cast section joining the banks together at top deck level. This cast tie is cored and utilised as a water transfer duct between the banks. Ideally a similar tie is desirable at the rear of the engine but this would necessitate considerable redesign of the pump drive details.

To avoid a bending moment the bosses for the cylinder head fixing studs are extended from the top to the bottom deck of the cylinder block thus ensuring a direct tensile load.

On the standard engine frontal noise was mainly due to flexural vibration of the front bulkhead partly as a result of bank-to-bank motion. This was controlled by increasing the thickness of the section.

The crankcase walls on the normal engine are cantilevered from the bottom deck of the cylinder block and in general vibration increases from this point to the sump fixing flange. The centre three bulkheads forming the crankshaft bearings restrain the amplitude of vibration of these walls

but their effectiveness is offset by the relative displacement of the bores in the two banks which causes a bending moment at the bearing.

It was not possible to significantly increase the section of these bulkheads to restrain crankcase wall movement because of the compactness of the engine design. To increase the thickness of the crankcase walls is also not practicable without a 15% weight increase. It was therefore considered that for a low noise engine design the crankcase walls should be removed.

The lower decks of the cylinder blocks on the low noise design were extended so that they were cut by the horizontal crankshaft plane thus forming rigid attachment points for the sump (also cylinder block side wall covers) where vibration levels would be low. An integral bearing beam was fitted to replace the support previously given to the main bearing caps by the crankcase walls (Figure 3.20a).

Suitable covers were developed to replace those on the standard design. The combined effect of all modifications reduced noise over the entire high frequency range as shown in Figure 3.20b. An overall reduction of 9 dBA was obtained (ref. 3.4).

3.3.1.3 Design of engine covers

Two basic principles were applied to the cover designs: these were application of damping and isolation of vibration.

(a) Oil sump: details are shown in figure 3.21a. It was made of two sheets of 26 SWG steel bonded with thick rubber based adhesive. This sump gave a noise reduction of 2 dBA.

(b) Valve cover (figure 3.21b). This was of similar construction using aluminium sheets, giving a noise reduction of 2½ dBA.

(c) Exhaust manifold (figure 3.22). The standard iron manifold was shielded with a casing of 26 SWG steel sheet lined with ceramic fibre, giving a noise reduction of 1½ to 2 dBA.

(d) Push rod covers (see sketch): These covers were made of double skin panels spot welded together.

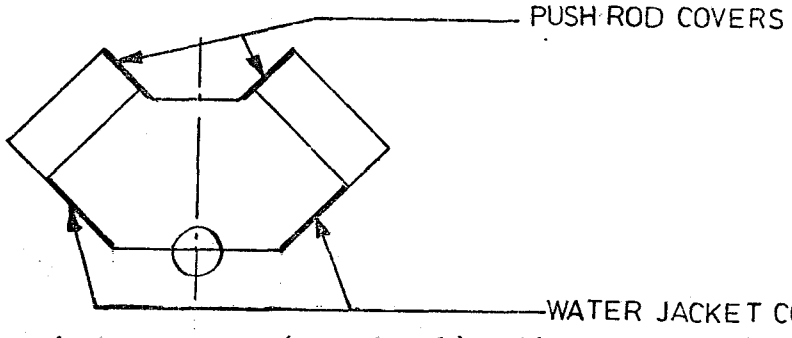

(e) Water jacket covers (see sketch). These were made of double skin damped panels bonded together at the fixing flange, thus also providing vibration isolation.

(f) Inlet manifold: Vibration isolation was employed by slitting the manifold at the base and bonding together with silicon rubber.

These covers on the low noise engine consitute about 70% of total radiating area.

3.3.2 Test results on the low noise Vee form research engine

The engine was initially designed with an integral bearing beam to increase bending stiffness and to provide axial restraint to the bearing caps normally given by bolting through the crankcase skirt. Various crankshaft supports, illustrated in figures 3.23 and 3.24, were tested as follows:

α Integral bearing beam

β Divided bearing beam

γ Ladder frame

δ Separate bearing caps

The noise spectra of the low noise engine with these crankshaft supports were taken and are compared with the integral beam (fig. 3.23a).

The results of these comparisons are shown in figures 3.25-3.28 for engine speeds of 3300, 3000, 2000 and 1500 revs/min full load. Generally the ladder frame is marginally better than the others at all speeds.

The study of the vibration characteristics of low noise engines shows that the effect of combustion is substantially reduced in relation to piston slap induced noise. This is due to the basic principle of the low noise engine design mainly because the crankcase has been eliminated (the crankcase is in general the radiating area which emits combustion induced noise), while the cylinder blocks of this engine form the major radiating area. This can be seen from vibration modes of the low noise engine as shown in figure 3.29 for 1250 and 2500 Hz. Appreciable amplitude levels of vibration only exist on cylinder blocks.

The rate of increase of noise and vibration with engine speed usually identifies the characteristics of the source of excitation. For example, combustion excitation gives an average of 30 dB/decade slope, while 20 dB/decade characterises the piston/liner impacts. Figure 3.30 shows that the overall noise of the low noise engine varies with speed at an average rate of 20 dB/decade and the standard engine at 30 dB/decade, suggesting that a different mechanism of excitation controls the resultant noise of low noise engines which is piston slap. Therefore greater emphasis has been given to the study of this phenomenon.

3.4 Conclusions

(1) Acoustic conditions and engine operating parameters are shown to affect the resultant engine noise, vibration and combustion and therefore should be carefully controlled.

(2) Lubricating oil temperature and fuel quality can affect the overall engine noise by 2-3 dBA.

(3) Reduction of noise by about 9 dBA can be produced by a new form of Vee engine load carrying structure design eliminating the crankcase and incorporating damped and isolated covers.

This engine design has a greater effect on controlling combustion noise, which is predominantly radiated from the lower part of the structure, than piston slap noise which is mainly radiated from the upper part, therefore enhancing the relative level of mechanical noise.

References

3.1 W.J. Griffiths and J. Skorecki. "Some Aspects of Vibration of a Single Cylinder Diesel Engine. A: Effect of Cooling Water on Cylinder Pressure and Surface Vibration". Journal of Sound and Vibration (1964), 1(4), p.345-364.

3.2 A.M. Rothrock. "Photographic Study of Combustion in Compression Ignition Engine". S.A.E. (1934), Trans. 29, 203.

3.3 E.S. Starkman and A. Bonora. "Some Observations of the Effect of Lubricating Oil Properties on Combustion Generated Engine Vibrations". S.A.E. Paper No. 690451.

3.4 E.C. Grover and N. Lalor. "A Review of Low Noise Diesel Engine Design at ISVR". Journal of Sound and Vibration (1973), Vol. 28(3), 403-431.

3.5 N. Lalor. "Origins of Reciprocating Engine Noise - Its Characteristics, Prediction and Control". SEE Paper - November 17th, 1971.

3.6 T. Priede, A.E.W. Austin and E.C. Grover. "Effect of Engine Structure on Noise of Diesel Engines". I. Mech. E. 179 (Pt. 2A), No. 4, 1964-5.

3.7 T. Priede, E.C. Grover and N. Lalor. "Relation between Noise and Basic Structural Vibration of Diesel Engines". SAE Paper No. 690450, 1969.

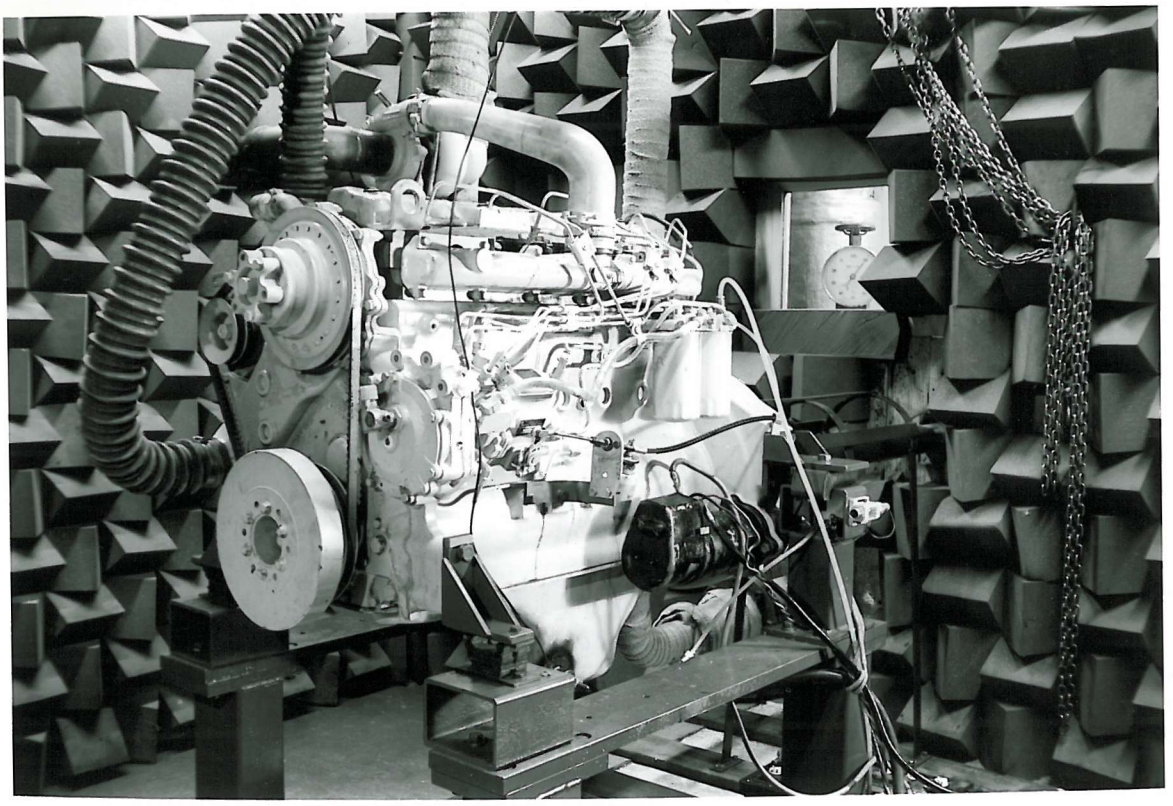

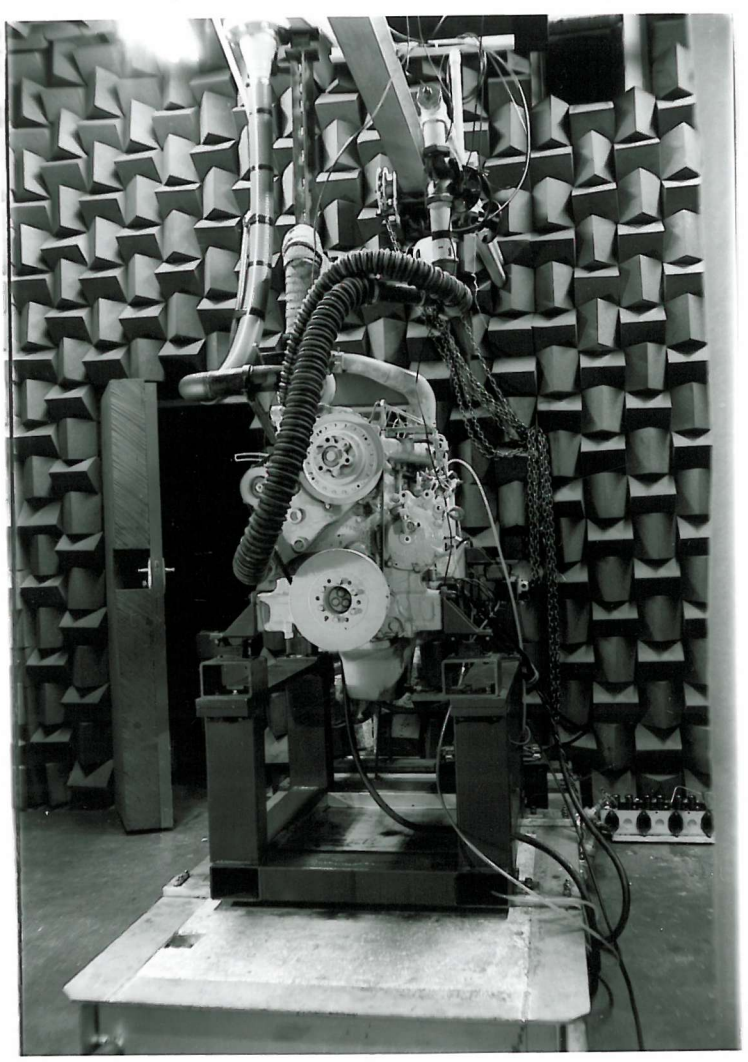

FIG. 3.1 TYPICAL INSTALLATION OF DIESEL ENGINE IN TEST CELL.

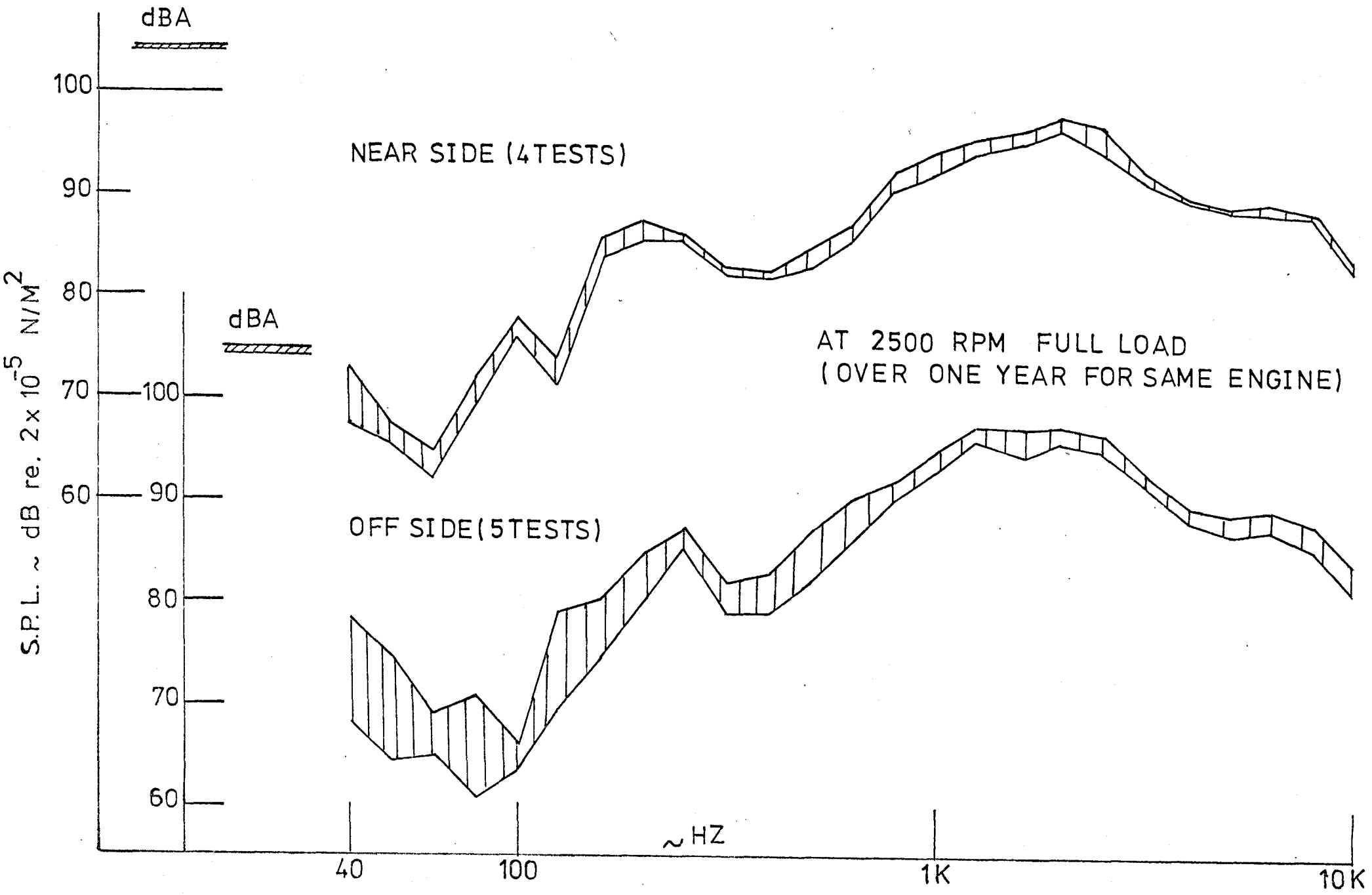

FIG. 3.2 SCATTER OF NOISE MEASUREMENTS

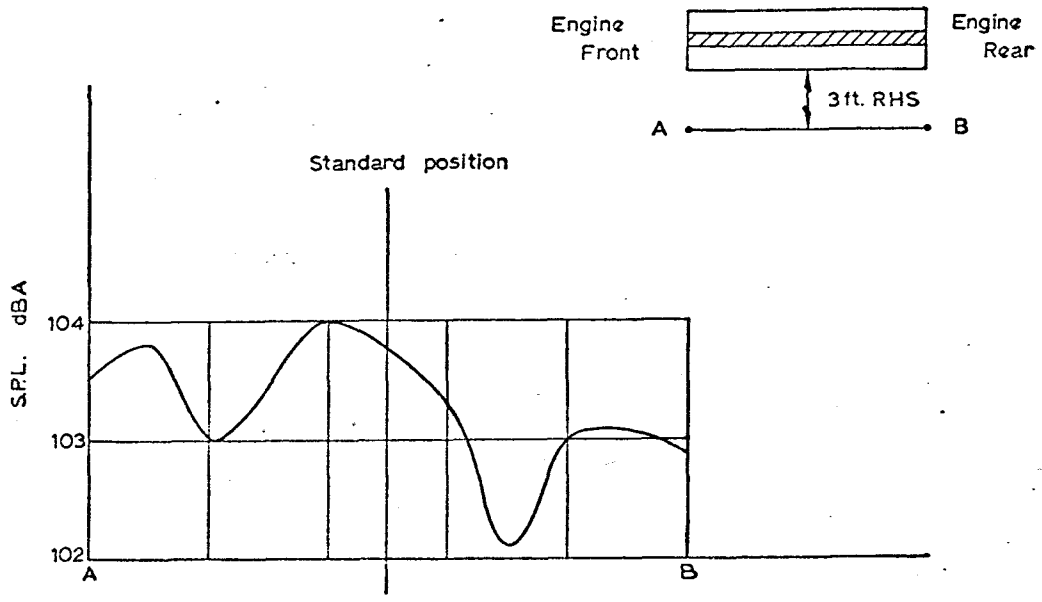

FIG.3.3a Overall S.P.L. variation when moving microphone across line AB for standard vale at 3300 full load.

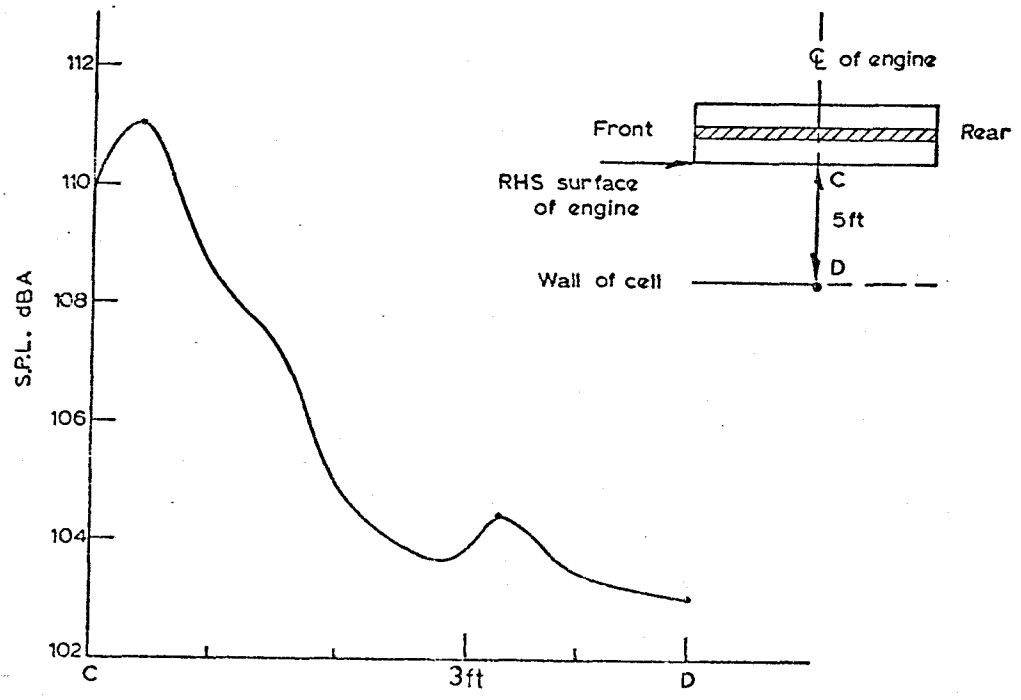

FIG.3.3 b Overall S.P.L. variation when moving microphone across line CD for standard at 3300 full load.

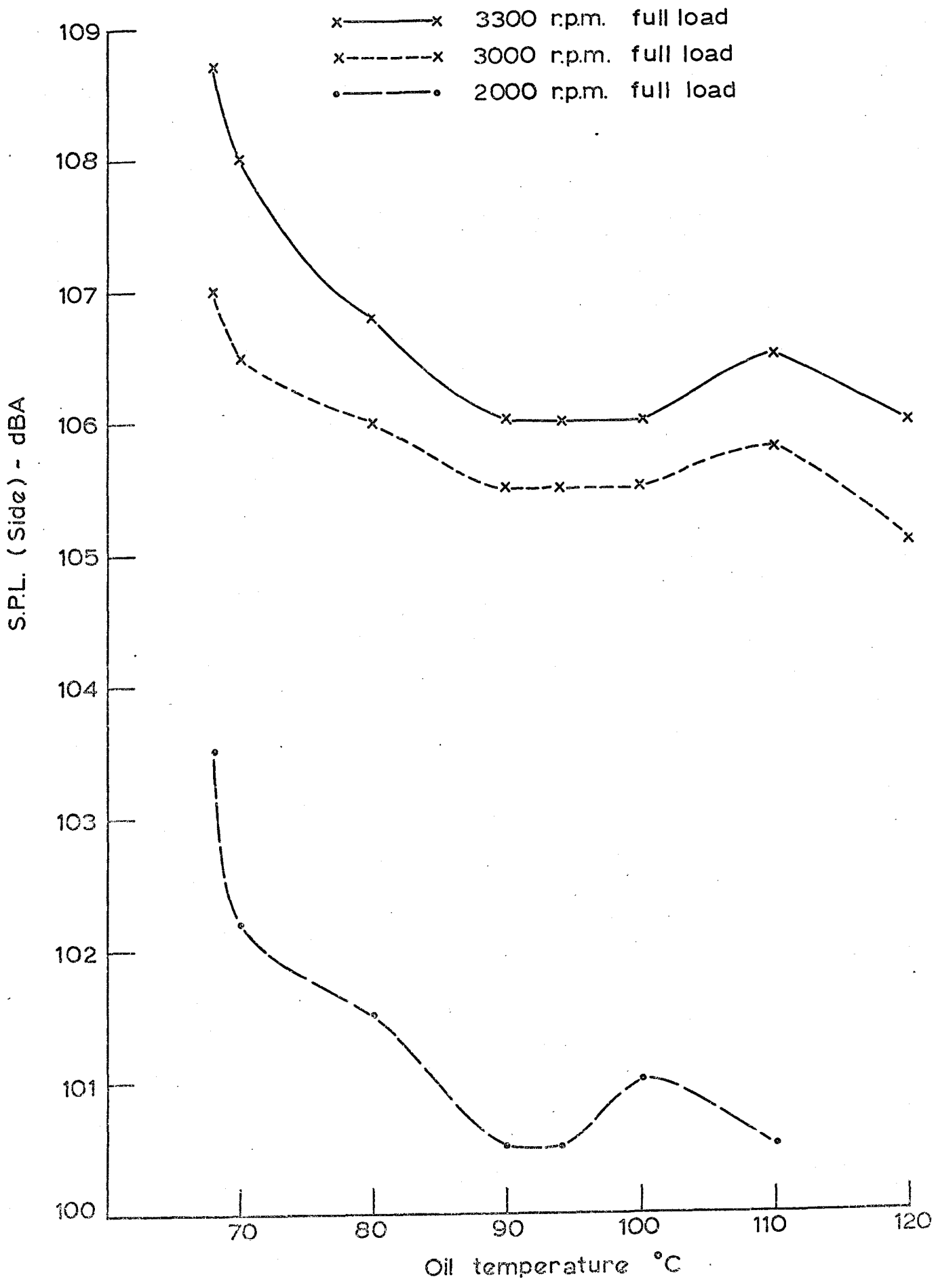

Fig. 3.4 Variation of overall noise levels with oil temperature for the SA engine.

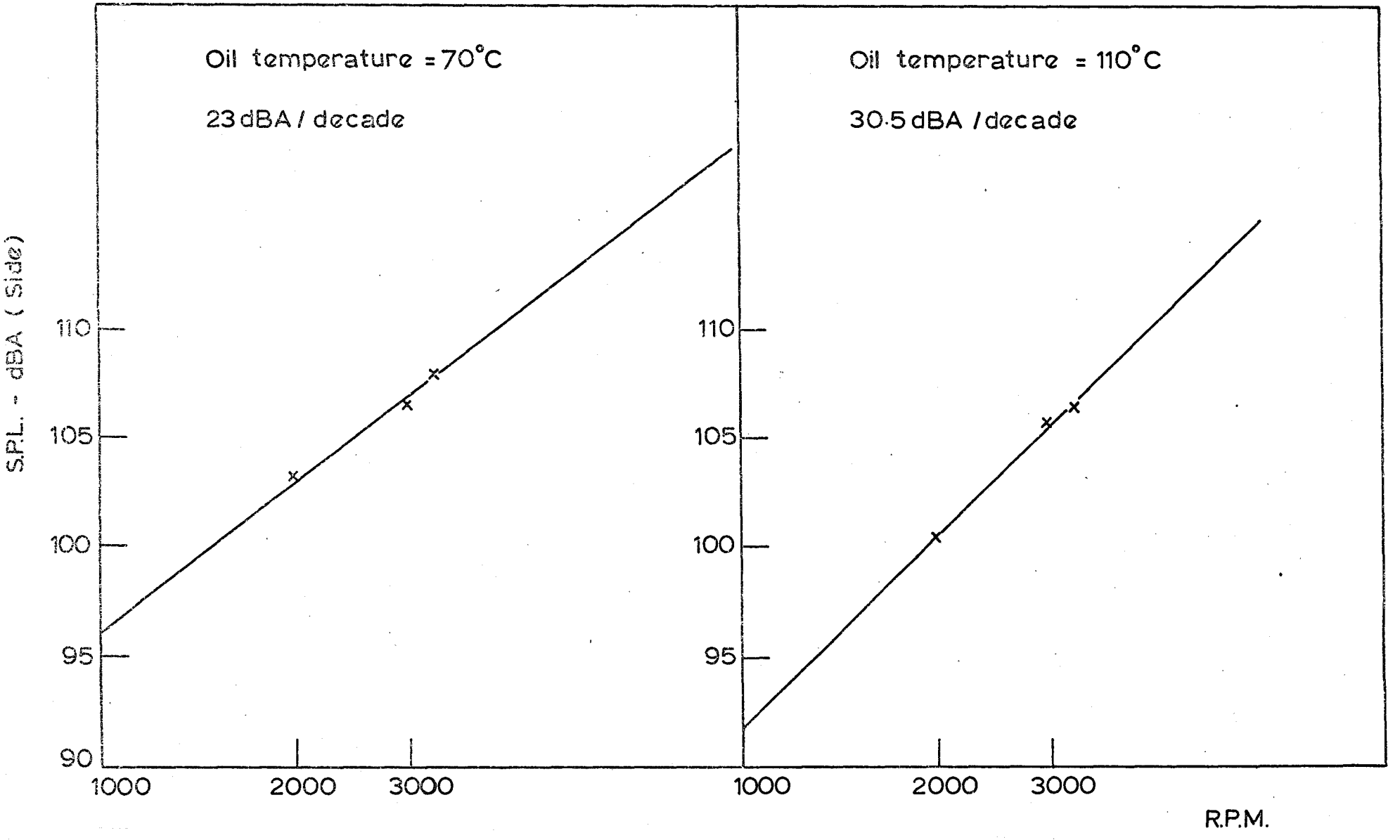

Fig. 3.5 Variation of overall noise levels with speed of the SA engine at full load for 70 and 110°C oil temperature

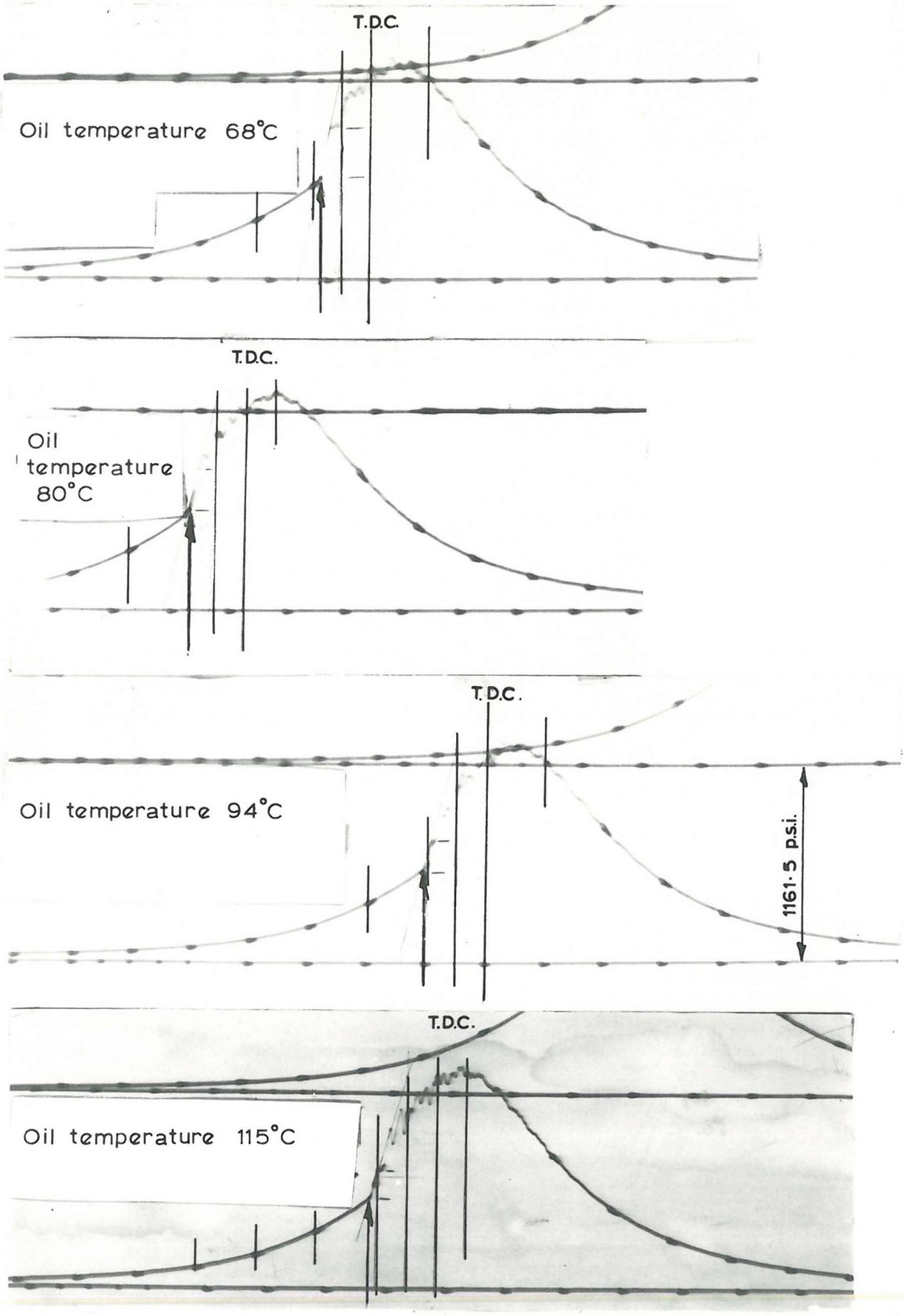

Fig. 3.6 Variation of cylinder pressure diagrams with oil temperature for the SA engine at 3000 r.p.m. full load.

Table I

Analysis of the pressure diagrams of the SA engine at 3000 r.p.m. full load of Fig. 3.6

Oil temperature °C	Initial rate of pressure rise p.s.i. / °	Amplitude of initial pressure rise P. S.I.	Initial pressure rise starts at P.S.I. - ° before T.D.C.	Peak pressure in cylinder P.S.I.
68	164	285	600 at 8° before T.D.C.	1265
80	152	235	580 at 9° before T.D.C.	1265
94 *	126	190	535 at 10.5° before T.D.C.	1280
115	122	165	525 at 11.5° before T.D.C.	1300

* Operating temperatures

Lub. oil temperature ≏ 94°C
Cooling water inlet = 65 ± 2°C
Cooling water outlet = 75 ± 2°C

FIG. 3.7

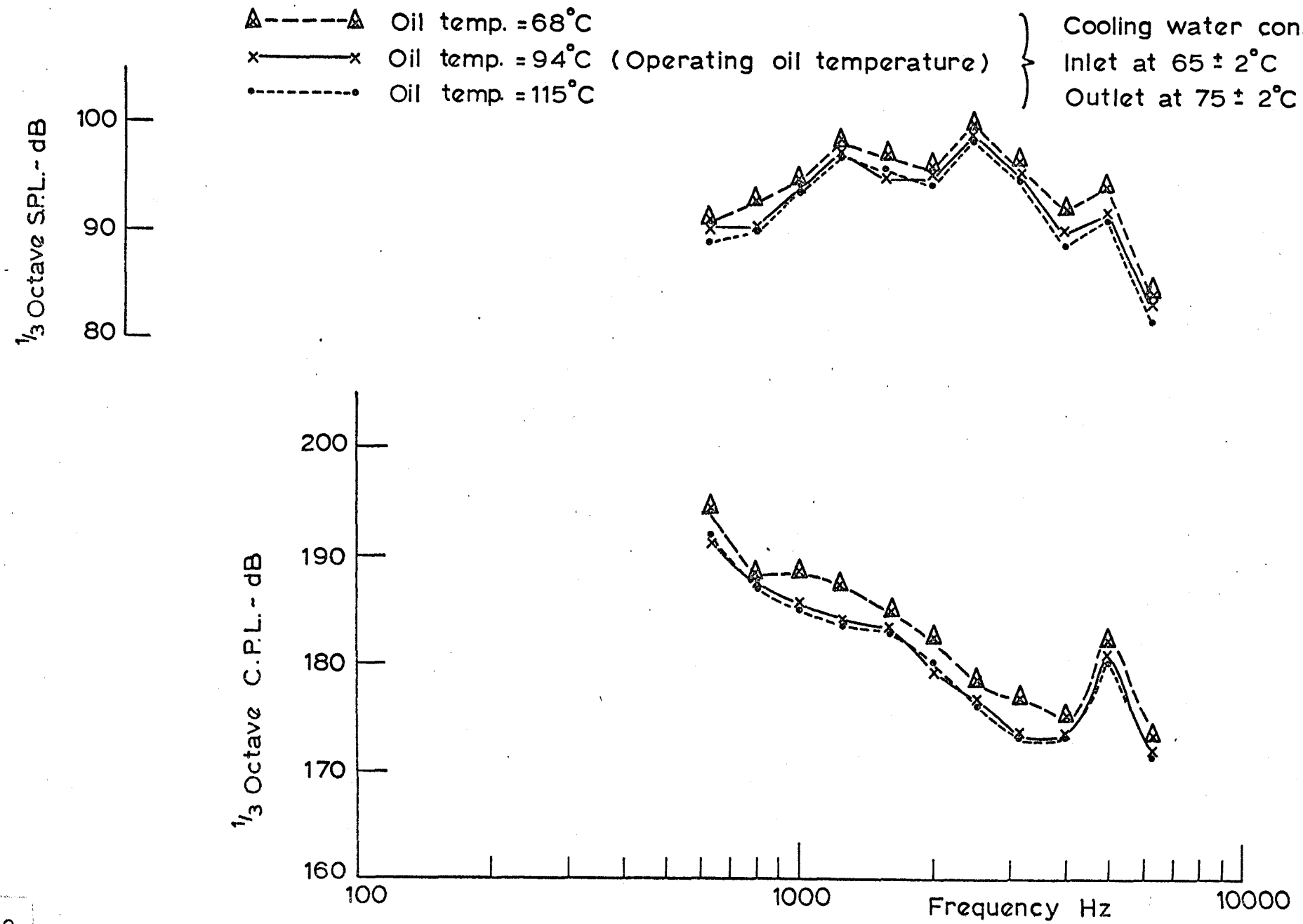

Fig. 3.8 Variation of cylinder pressure and noise spectra with change of oil temperature for the SA engine at 3000 r.p.m. full load.

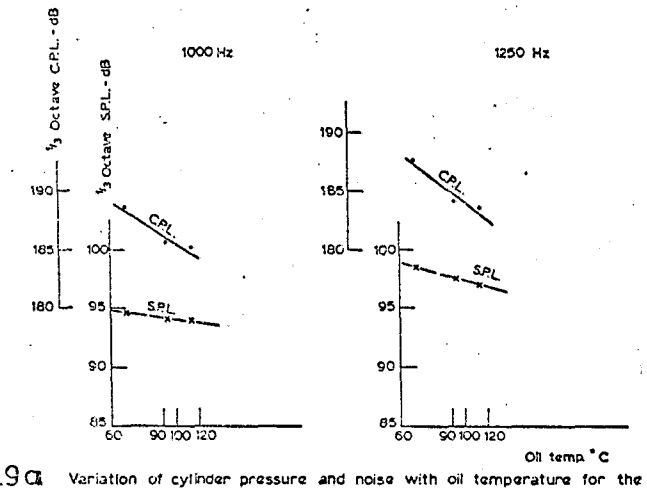

FIG. 3.9a Variation of cylinder pressure and noise with oil temperature for the standard engine at 3000 r.p.m. full load - 1000 and 1250 Hz.

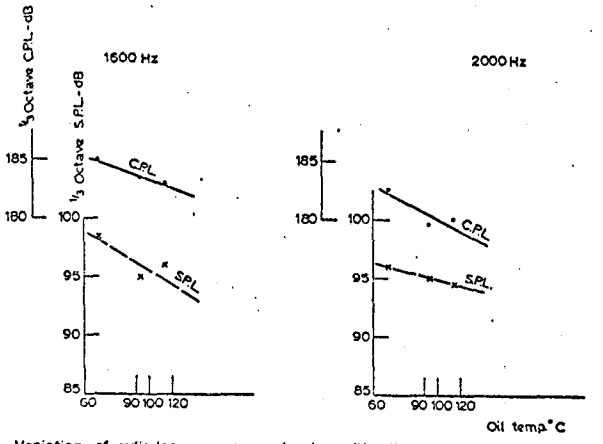

FIG. 3.9b Variation of cylinder pressure and noise with oil temperature for the standard engine at 3000 r.p.m. full load - 1600 and 2000 Hz.

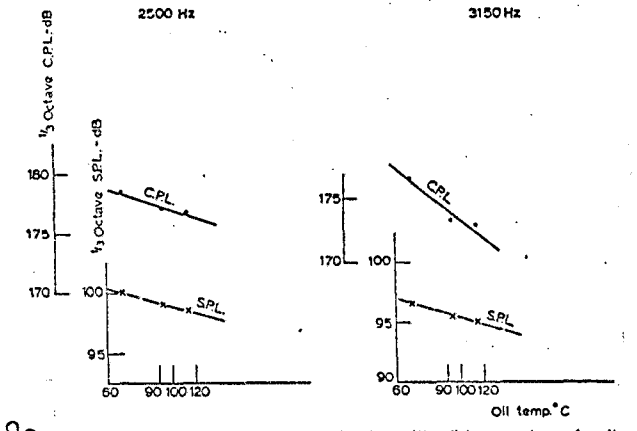

FIG. 3.9c Variation of cylinder pressure and noise with oil temperature for the standard engine at 3000 r.p.m. full load - 2500 and 3150 Hz.

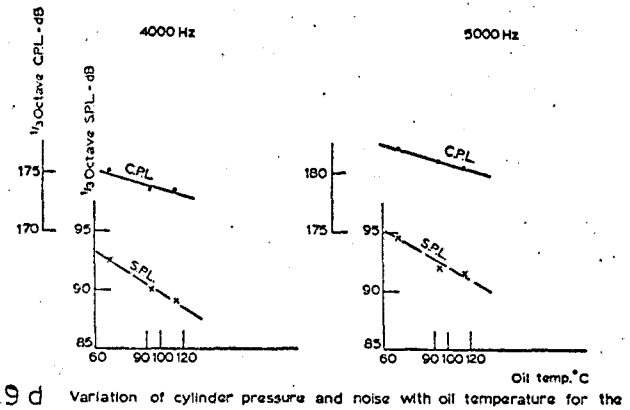

FIG. 3.9d Variation of cylinder pressure and noise with oil temperature for the standard engine at 3000 r.p.m. full load - 4000 and 5000 Hz.

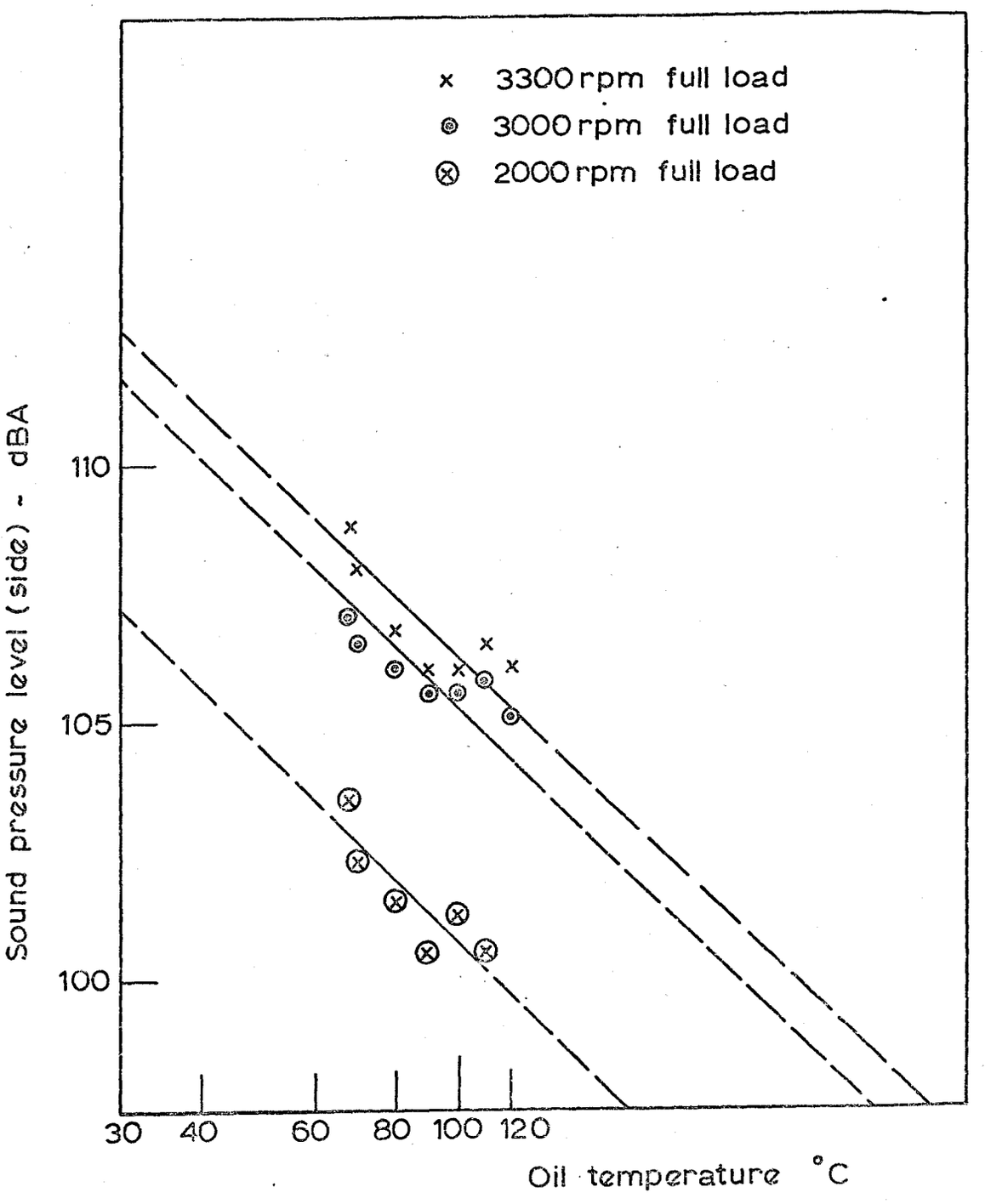

Fig. 3.10 Variation of overall noise level with oil temperature (log scale) for the SA engine - at full load.

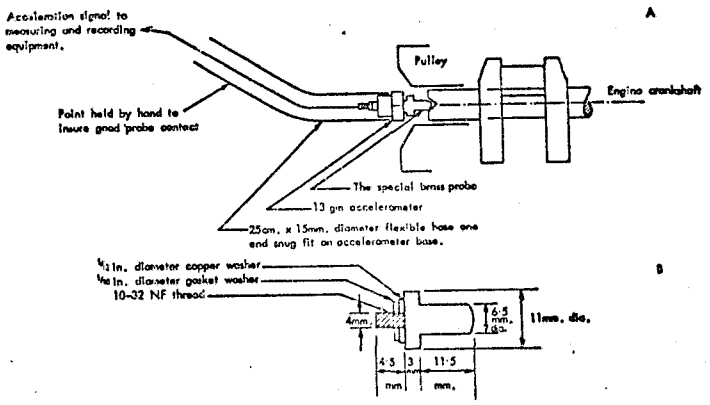

FIG. 3.11a SKETCH SHOWING THE SPECIAL BRASS PROBE AND ASSEMBLY FOR CRANKSHAFT VIBRATION MEASUREMENT.

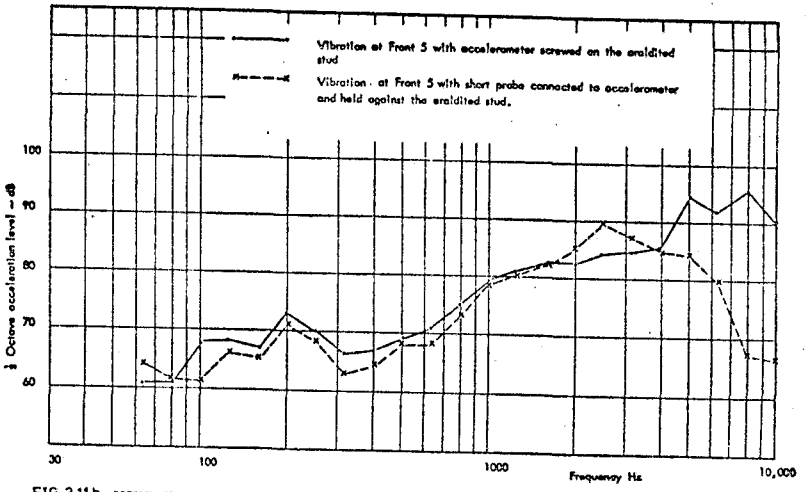

FIG. 3.11b REFERENCE CORRECTION LEVELS FOR SHORT PROBE.

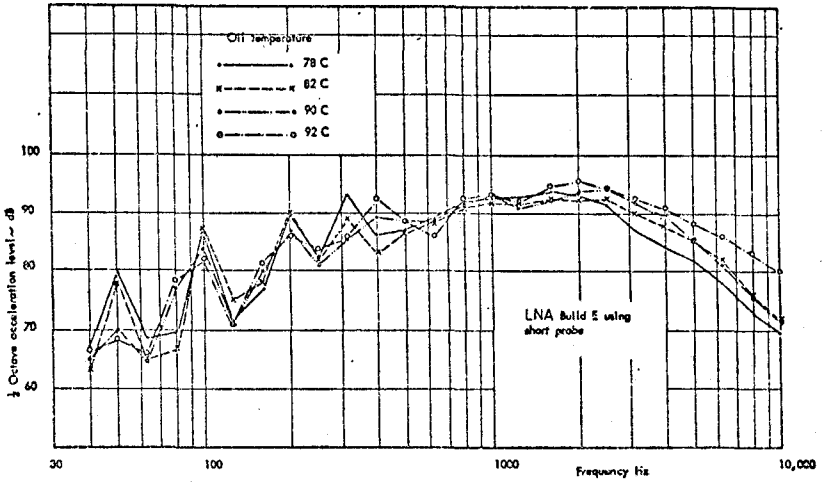

FIG. 3.11c VARIATION OF AXIAL CRANKSHAFT VIBRATION WITH OIL TEMPERATURE AT 1500 r.p.m. FULL LOAD.

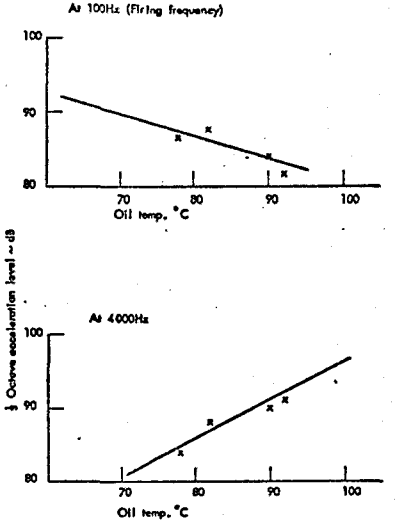

FIG. 3.11d TYPICAL LOW AND HIGH FREQUENCY CRANKSHAFT VIBRATION RESPONSE WITH OIL TEMP. FOR LNA AT 1500 r.p.m. FULL LOAD.

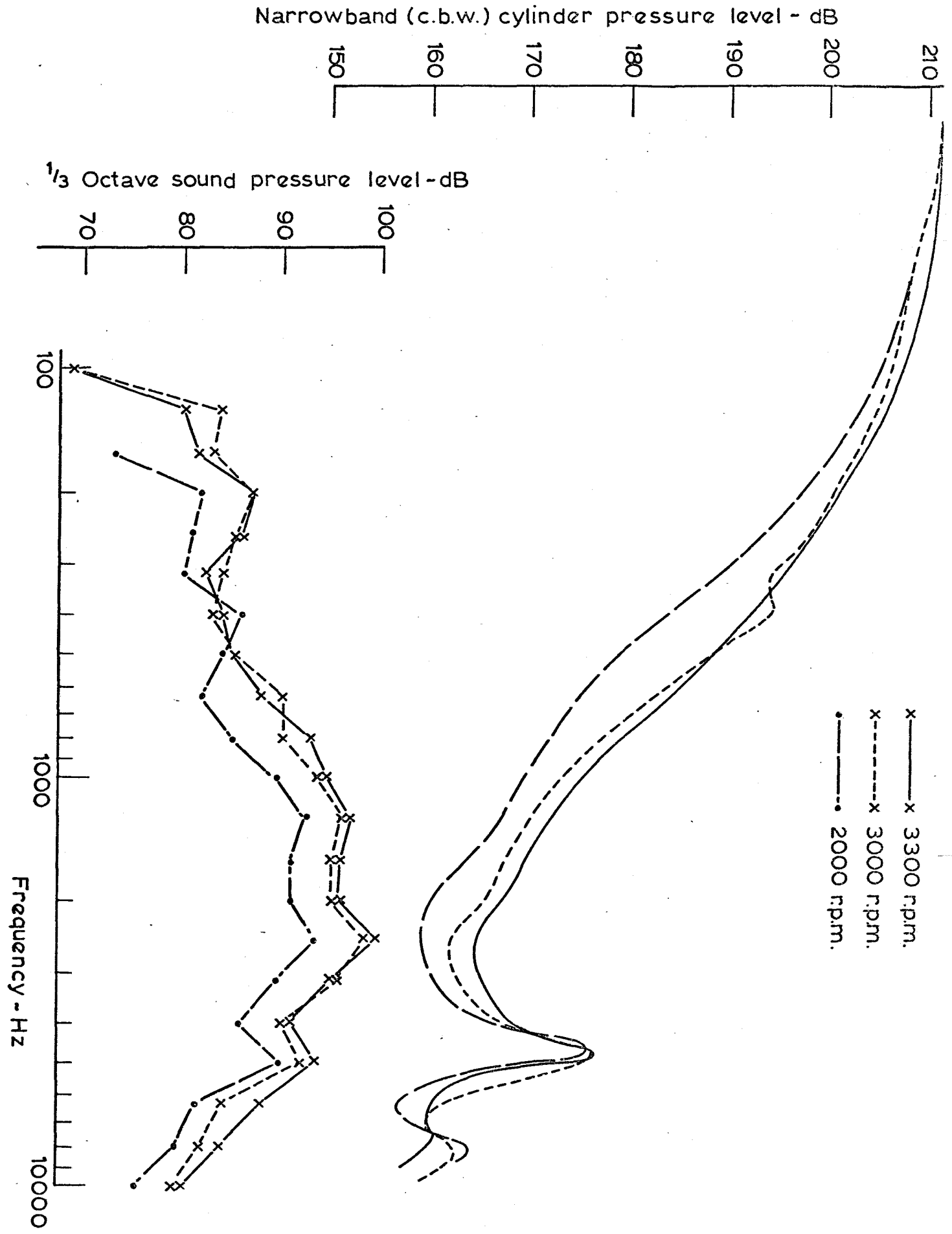

Fig. 3.12 Cylinder pressure and noise spectra at full load for the SA engine at operating temperatures.

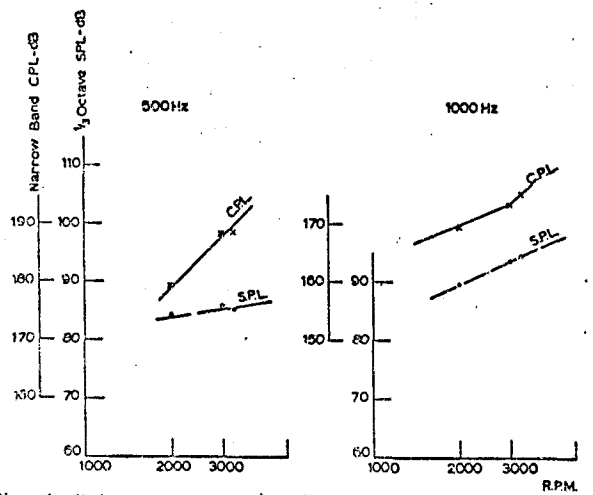

FIG. 3.13 a Variation of cylinder pressure and noise with speed for the standard engine at full load and operating temperatures - 500 and 1000 Hz.

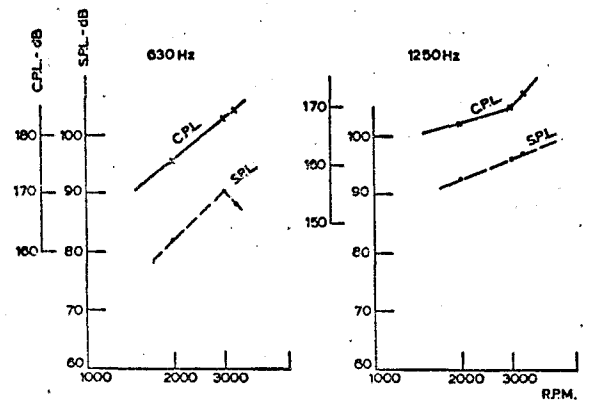

FIG. 3.13 b Variation of cylinder pressure and noise with speed for the standard engine at full load and operating temperatures - 630 and 1250 Hz.

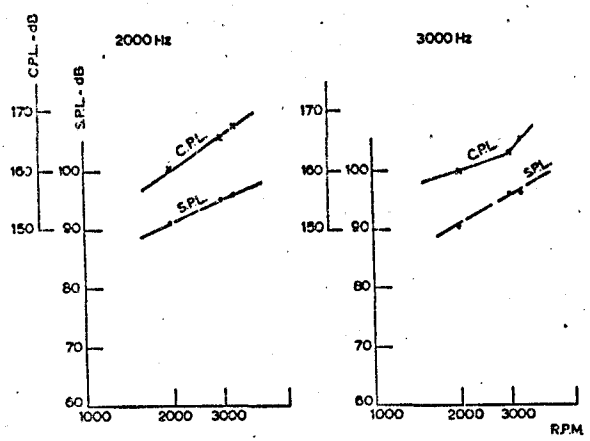

FIG. 3.13 c Variation of cylinder pressure and noise with speed for the standard engine at full load and operating temperatures - 2000 Hz and 3000 Hz.

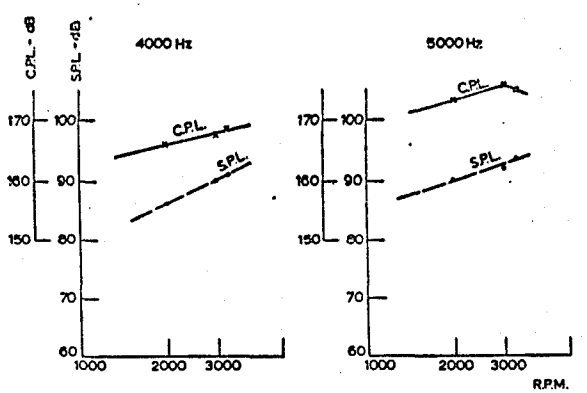

FIG. 3.13 d Variation of cylinder pressure and noise with speed for the standard engine at full load and operating temperatures - 4000 and 5000 Hz.

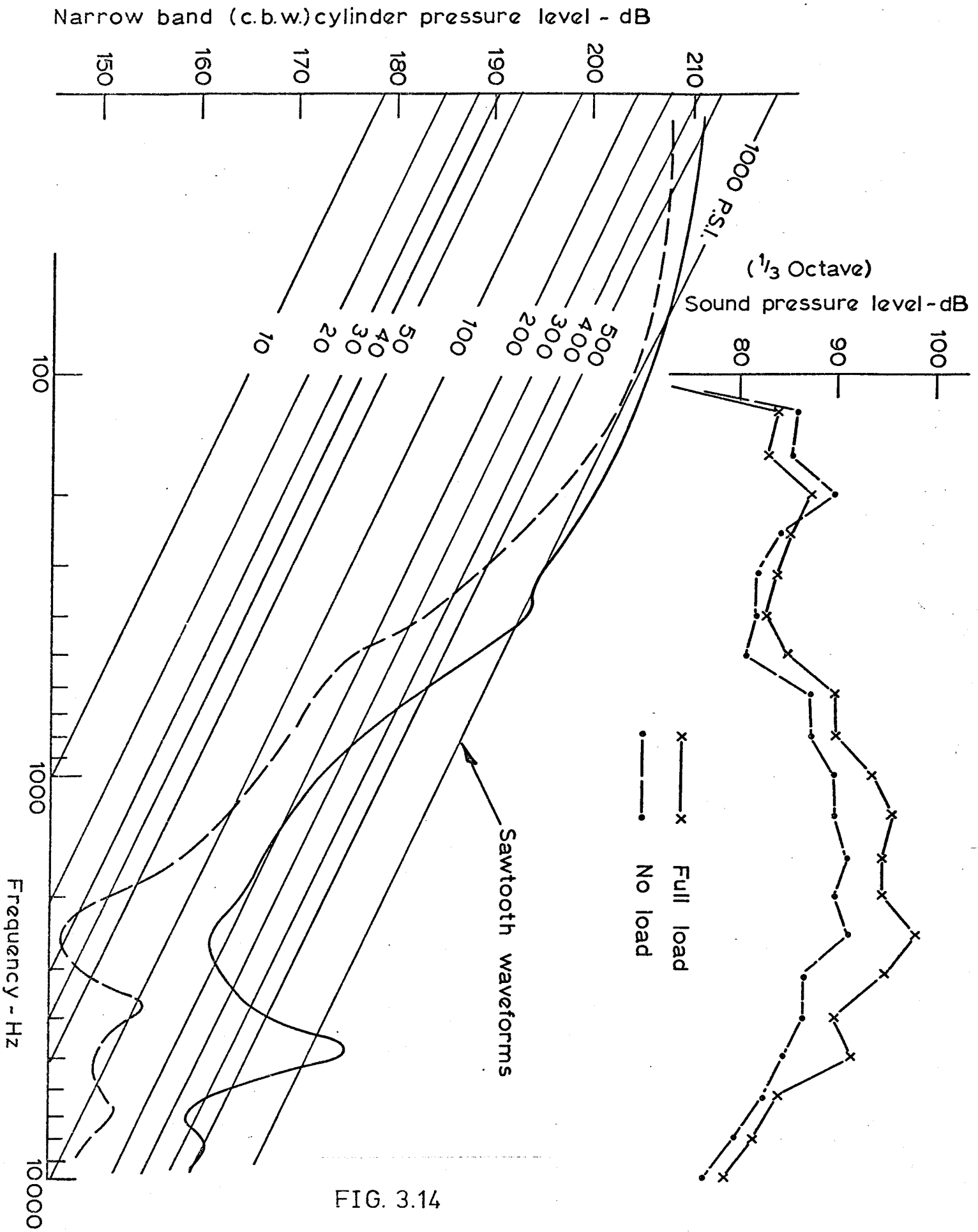

FIG. 3.14

Cylinder pressure and noise spectra at 3000r.p.m. for the SA engine at operating temperatures.

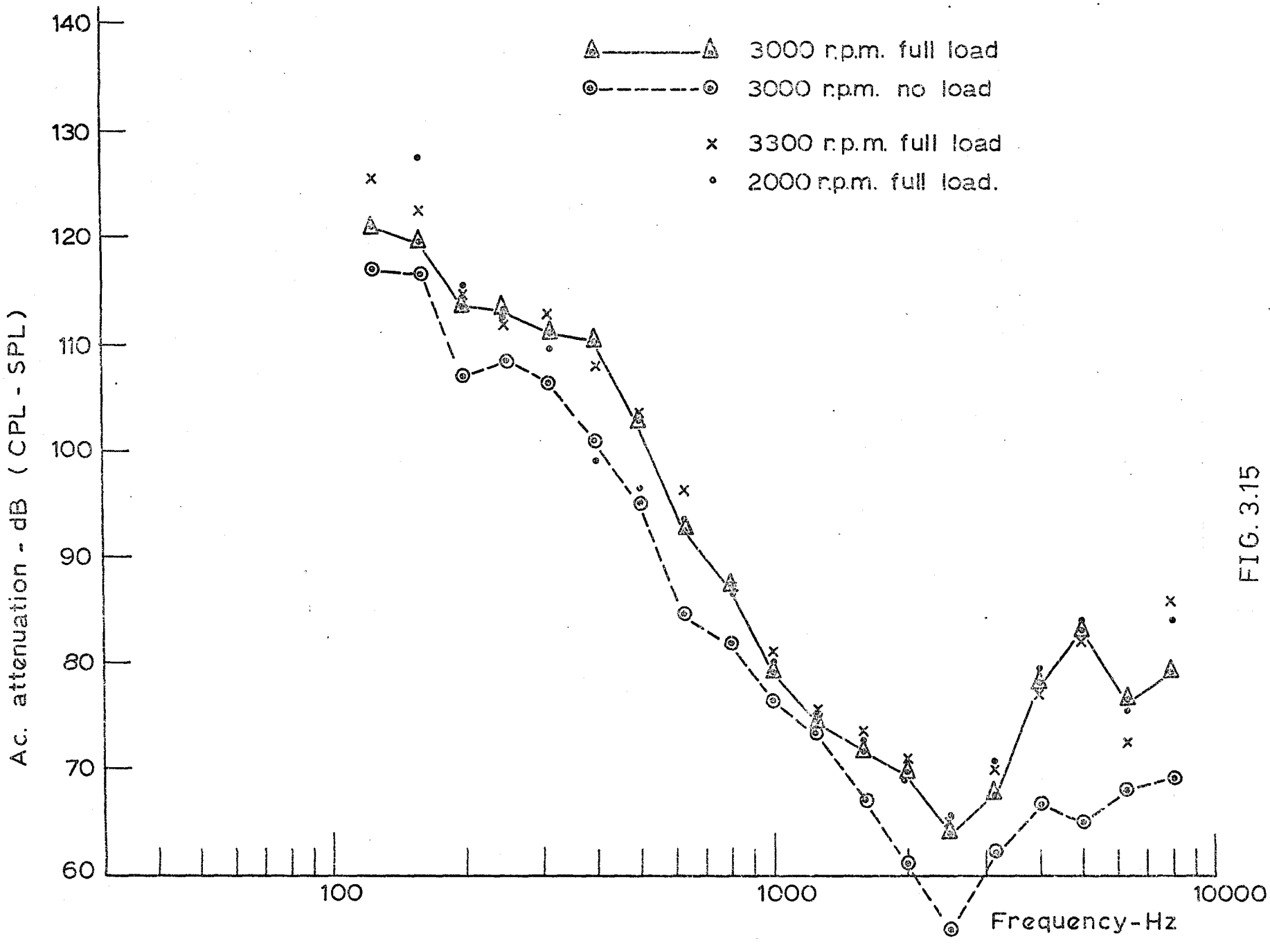

FIG. 3.15

Structural acoustical attenuation of the SA engine at operating temperatures.

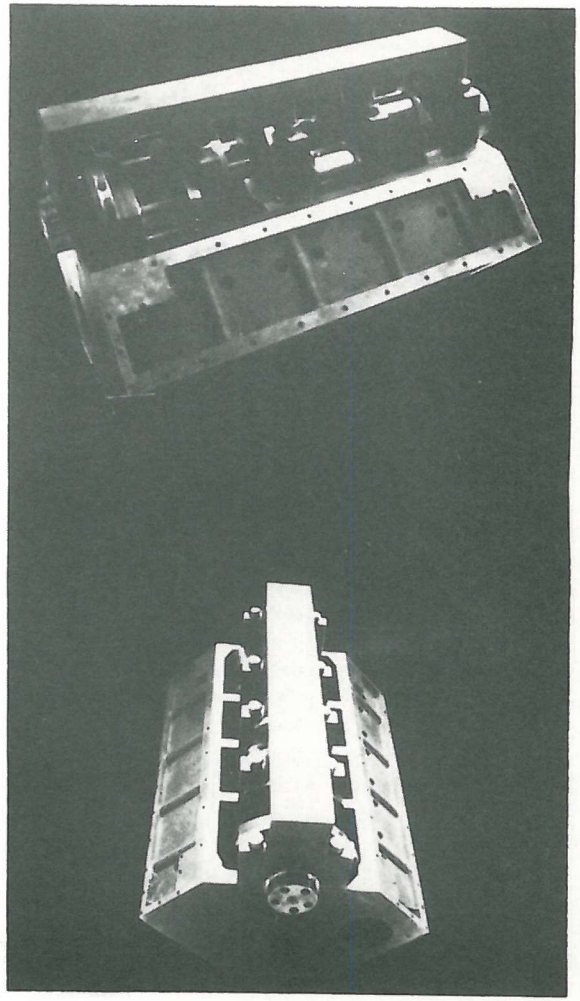

FIG. 3.20a LOW NOISE ENGINE (LNA)

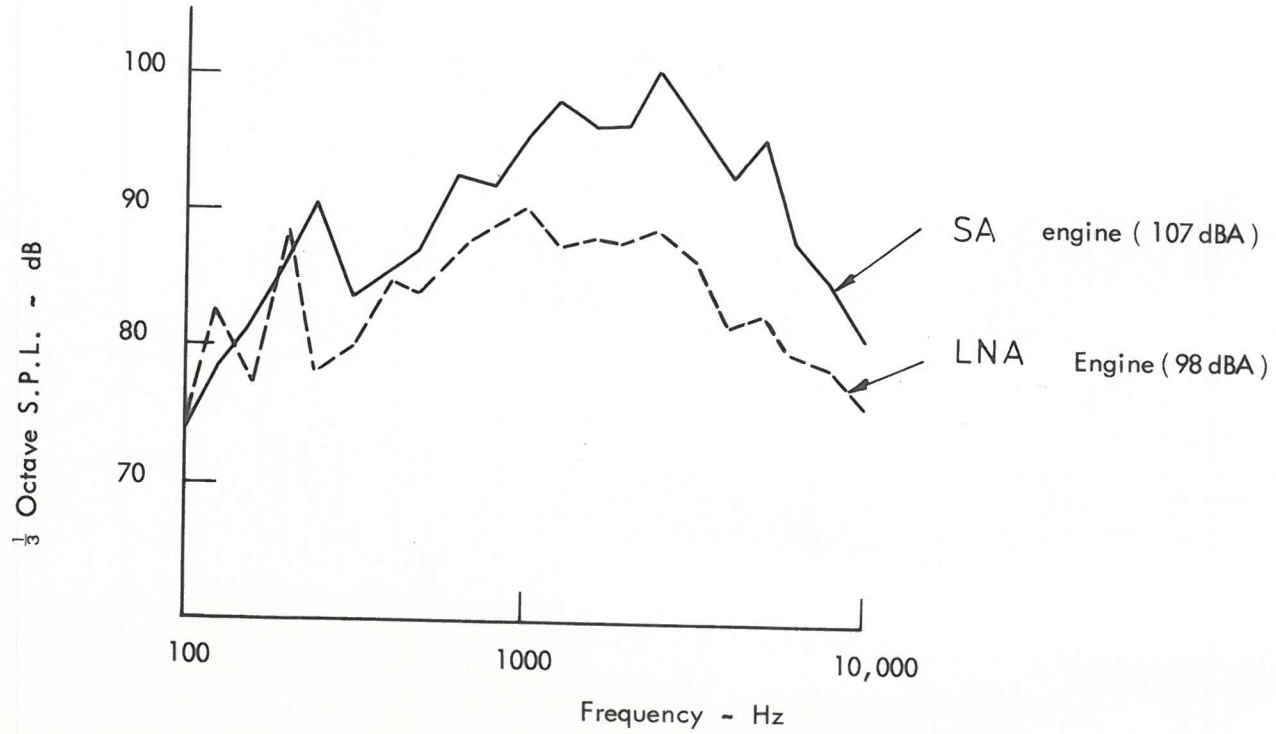

FIG. 3.20 b

NOISE REDUCTION THROUGH REDESIGN AT RATED SPEED AND FULL LOAD.

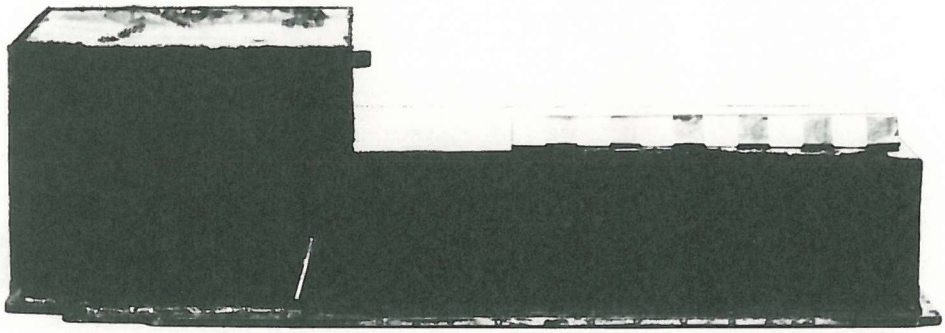

FIG. 3.21 a A new modified Sump

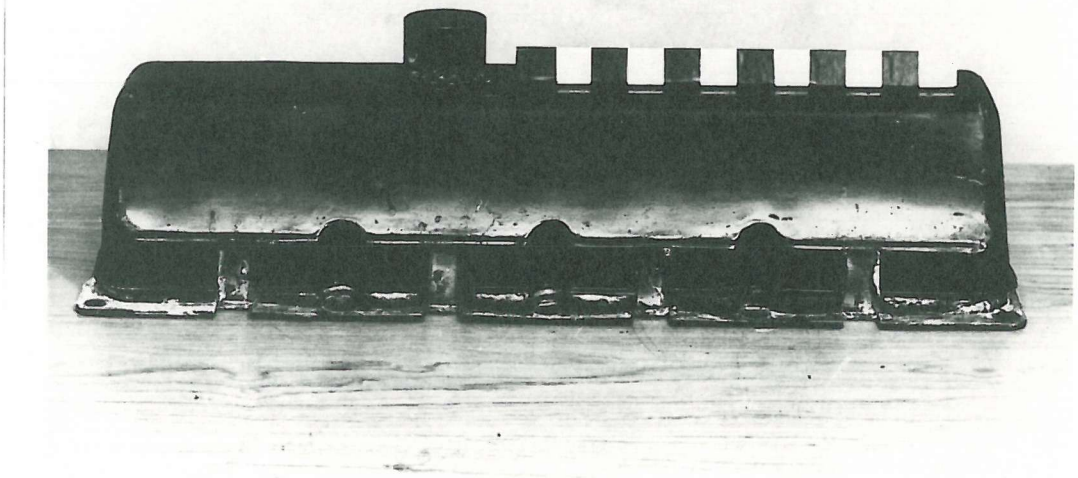

FIG. 3.21 b A double skinned valve cover

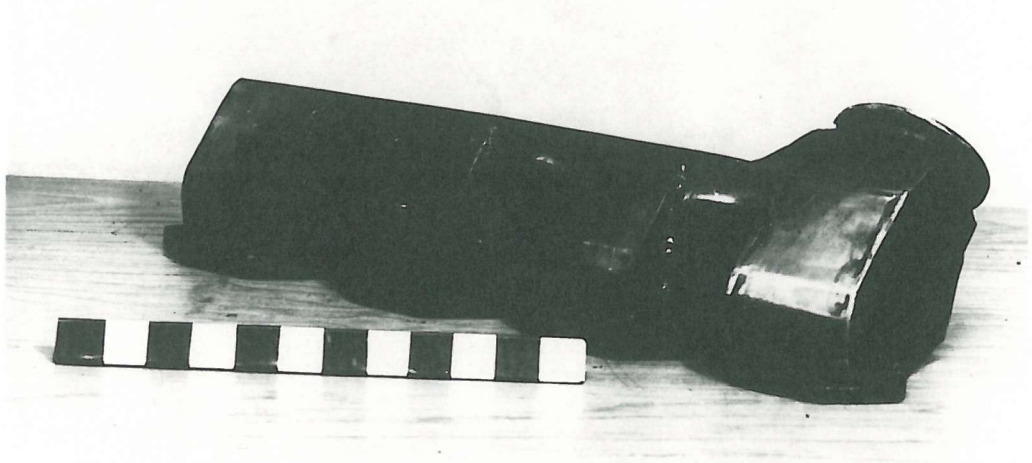

FIG. 3.22 a Exhaust manifold steel cover

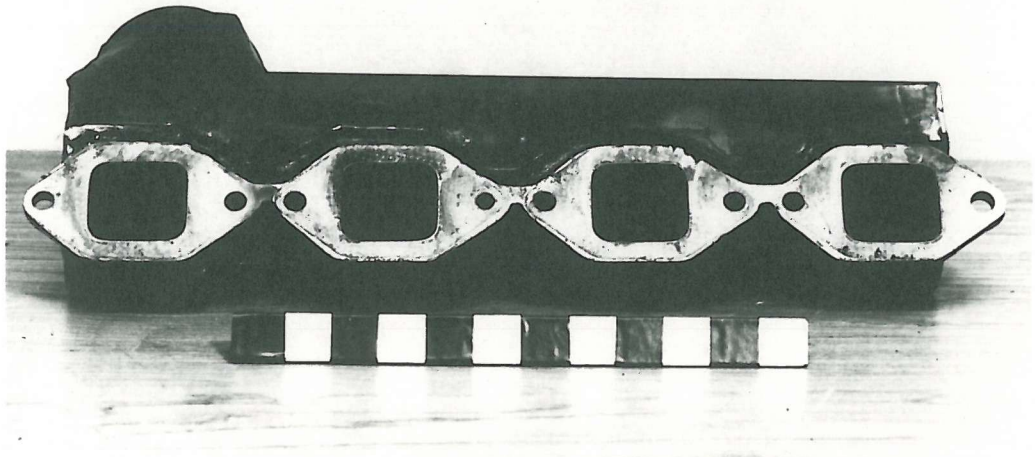

FIG. 3.22 b showing the exhaust manifold steel cover and Kao wool underneath

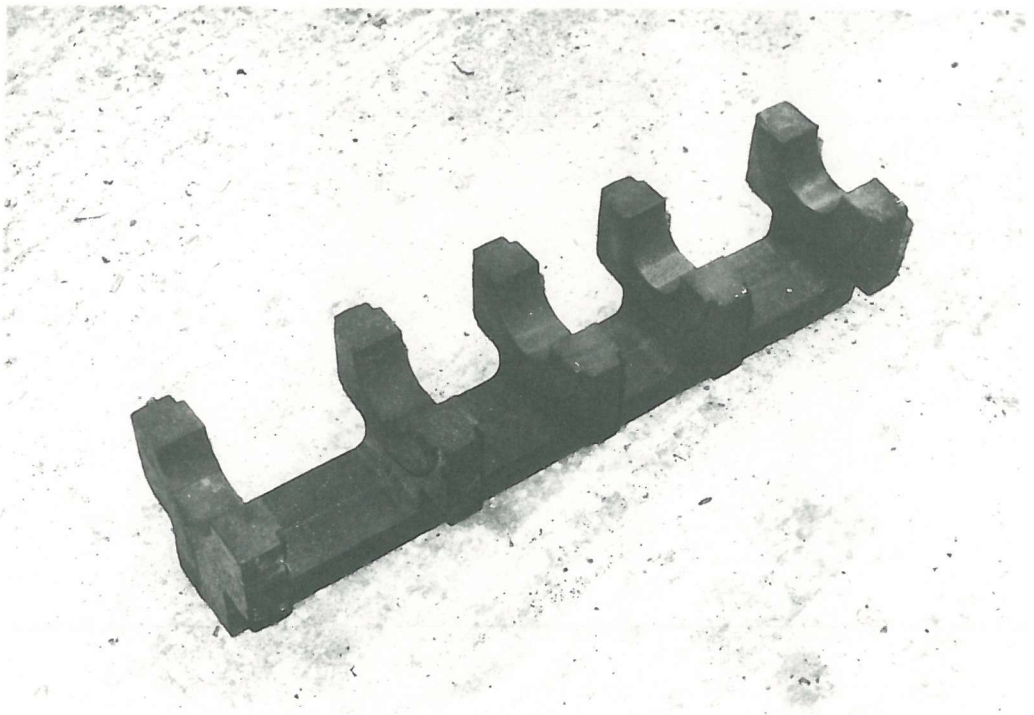

FIG. 3.23a THE INTEGRAL BEARING BEAM (α)

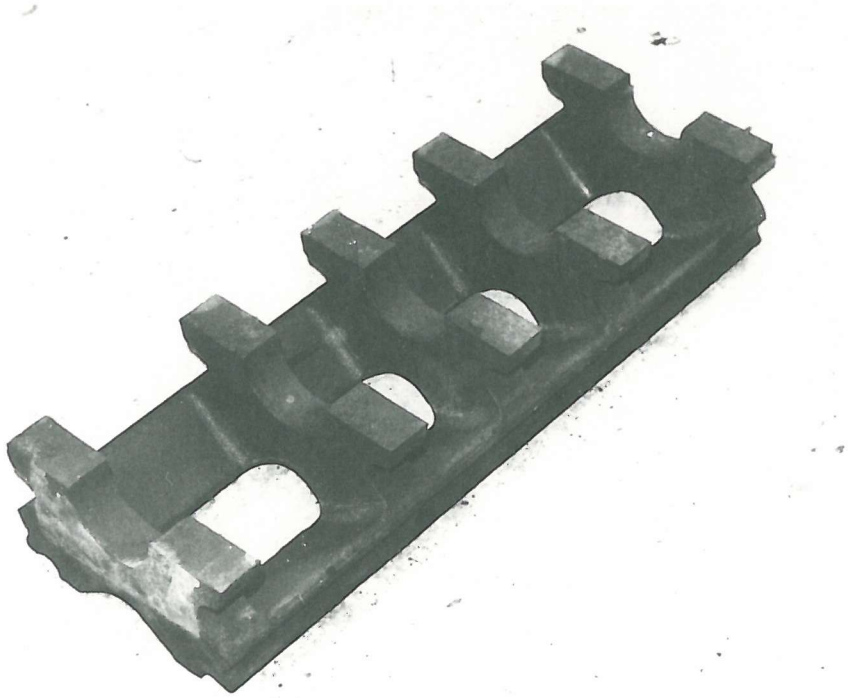

FIG. 3.23b THE TWIN BEARING BEAM (β)

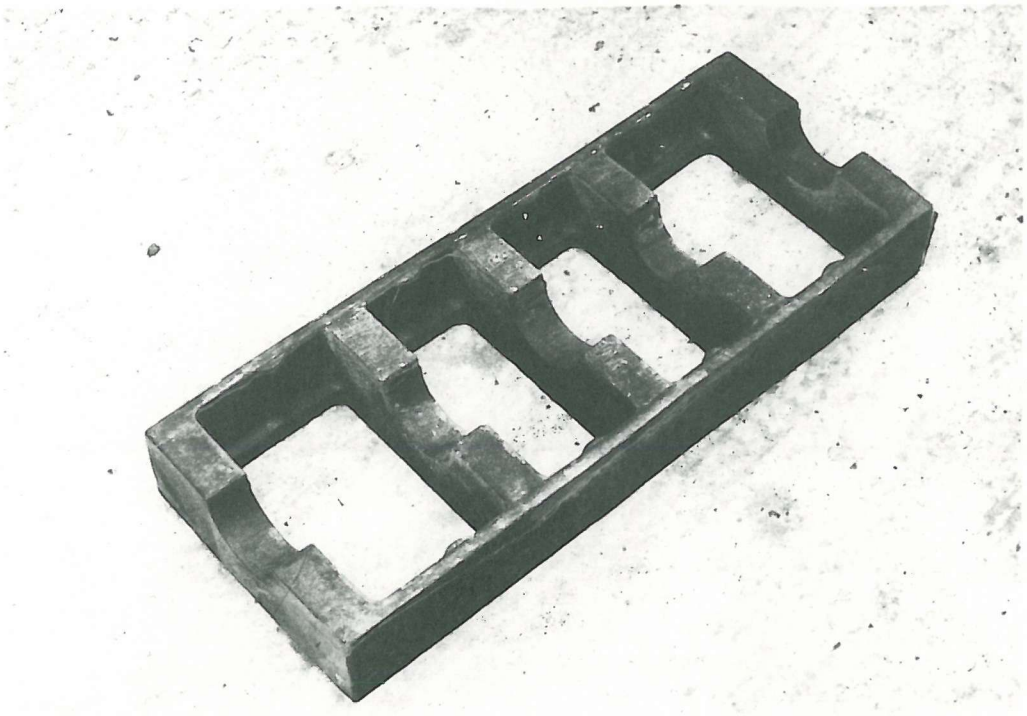

FIG. 3.24a THE LADDER FRAME (γ)

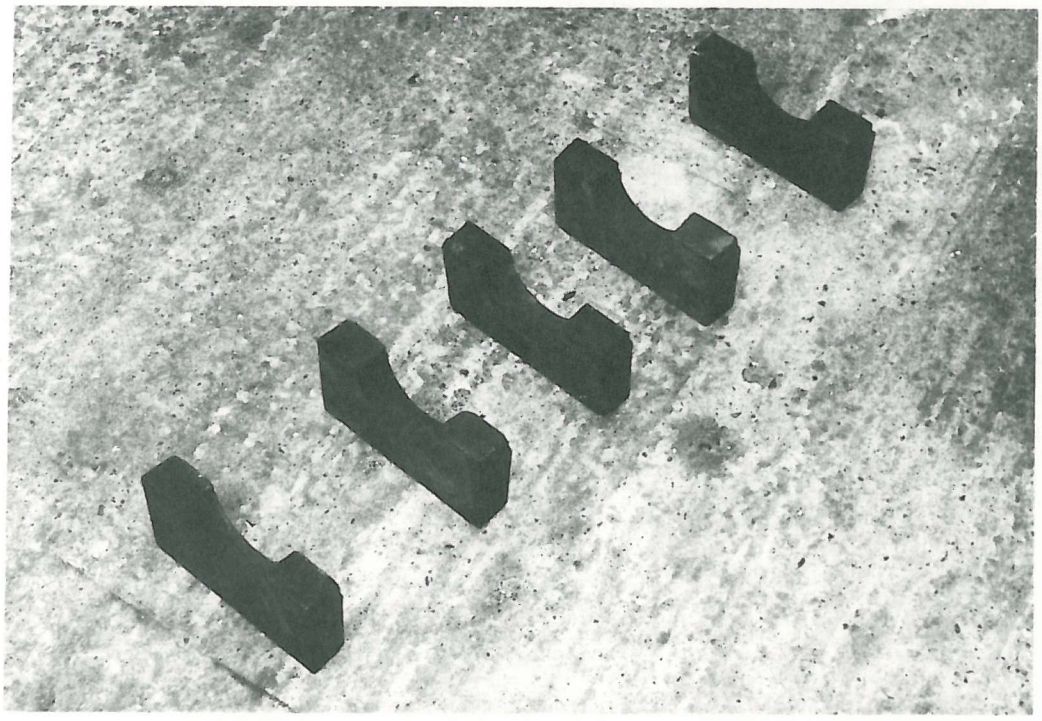

FIG. 3.24b THE SEPARATE BEARING CAPS (δ)

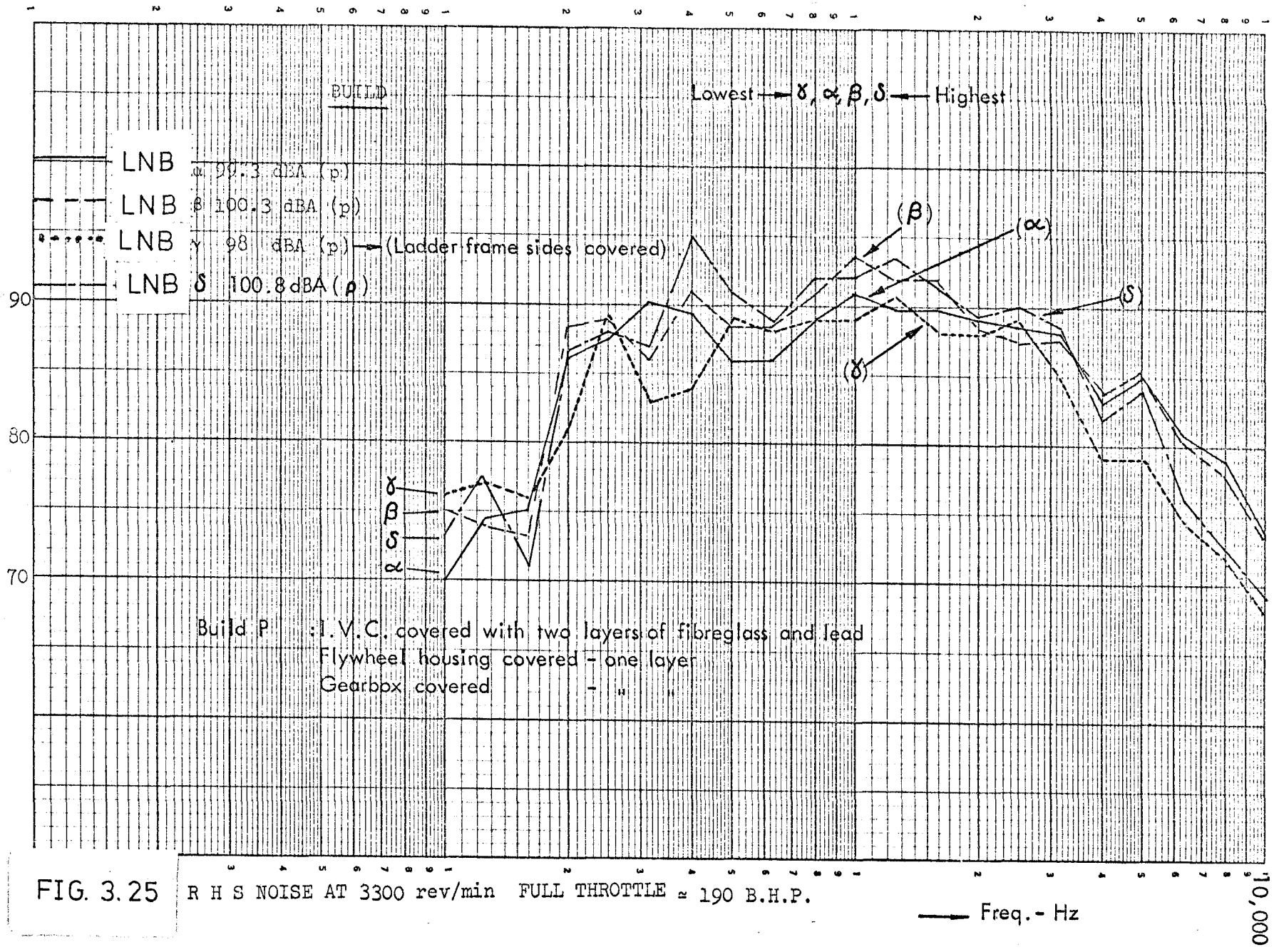
BUILD P
Lowest → γ, α, β, δ ← Highest
LNB α 99.3 dBA (p)
LNB β 100.3 dBA (p)
LNB γ 98 dBA (p) — (Ladder frame sides covered)
LNB δ 100.8 dBA (p)
(β)
(α)
(δ)
(γ)
γ
β
δ
α
90
80
70
S P L ~ dB
Build P : I.V.C. covered with two layers of fibreglass and lead
Flywheel housing covered - one layer
Gearbox covered - " "
R H S NOISE AT 3300 rev/min FULL THROTTLE ≈ 190 B.H.P.
Freq. - Hz
10,000

FIG. 3.25

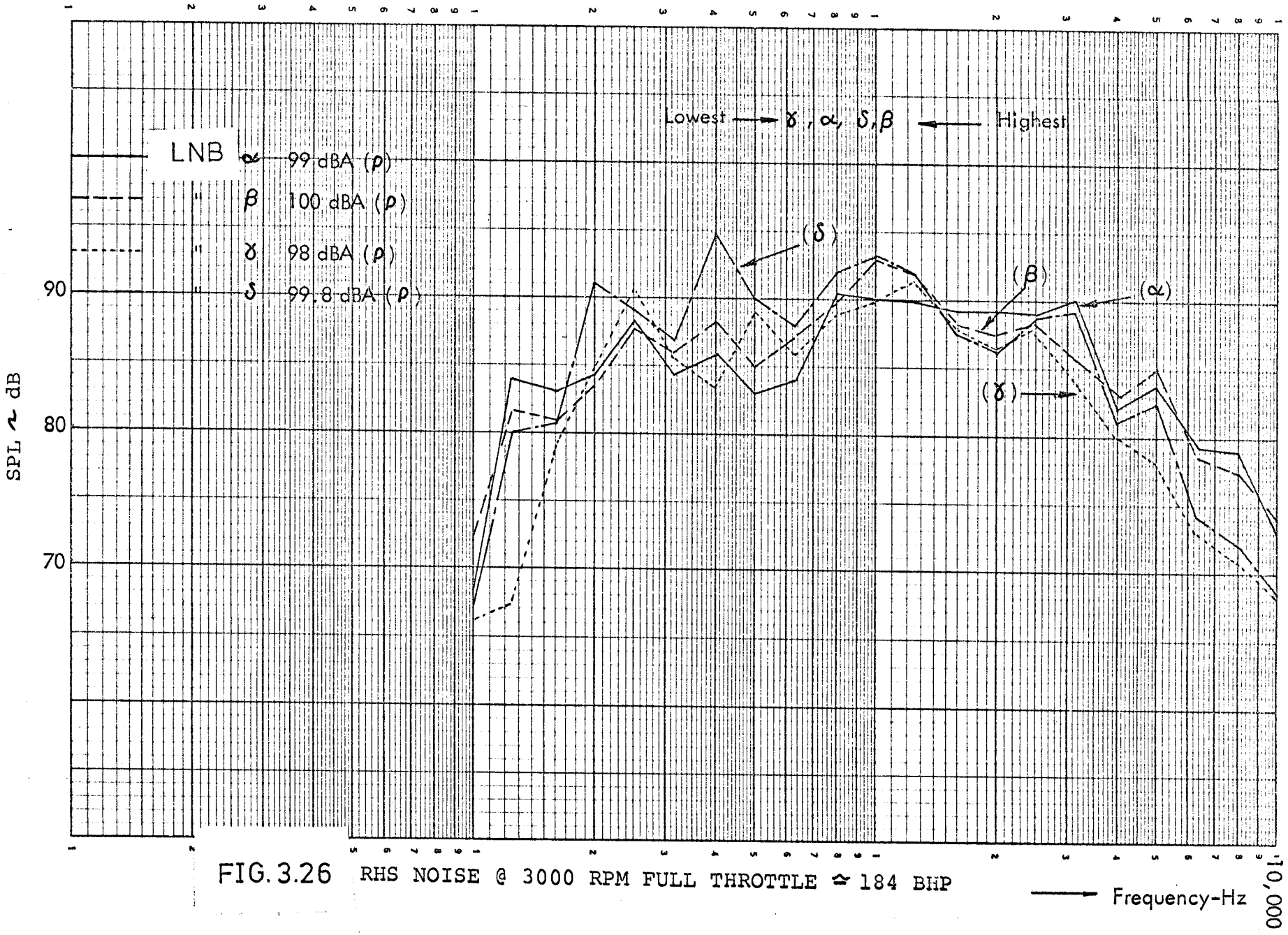

FIG. 3.26 RHS NOISE @ 3000 RPM FULL THROTTLE ≙ 184 BHP

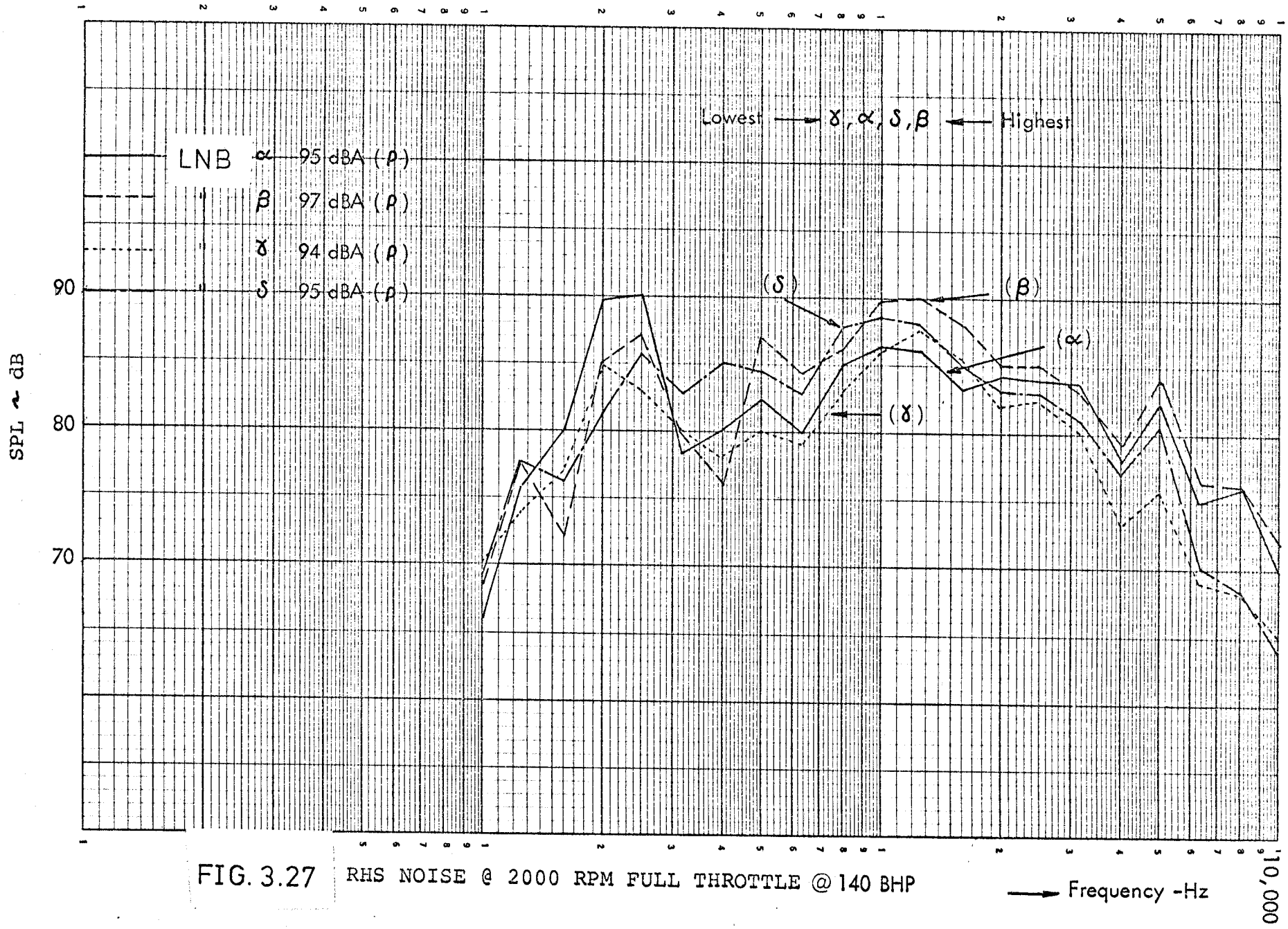

FIG. 3.27 RHS NOISE @ 2000 RPM FULL THROTTLE @ 140 BHP

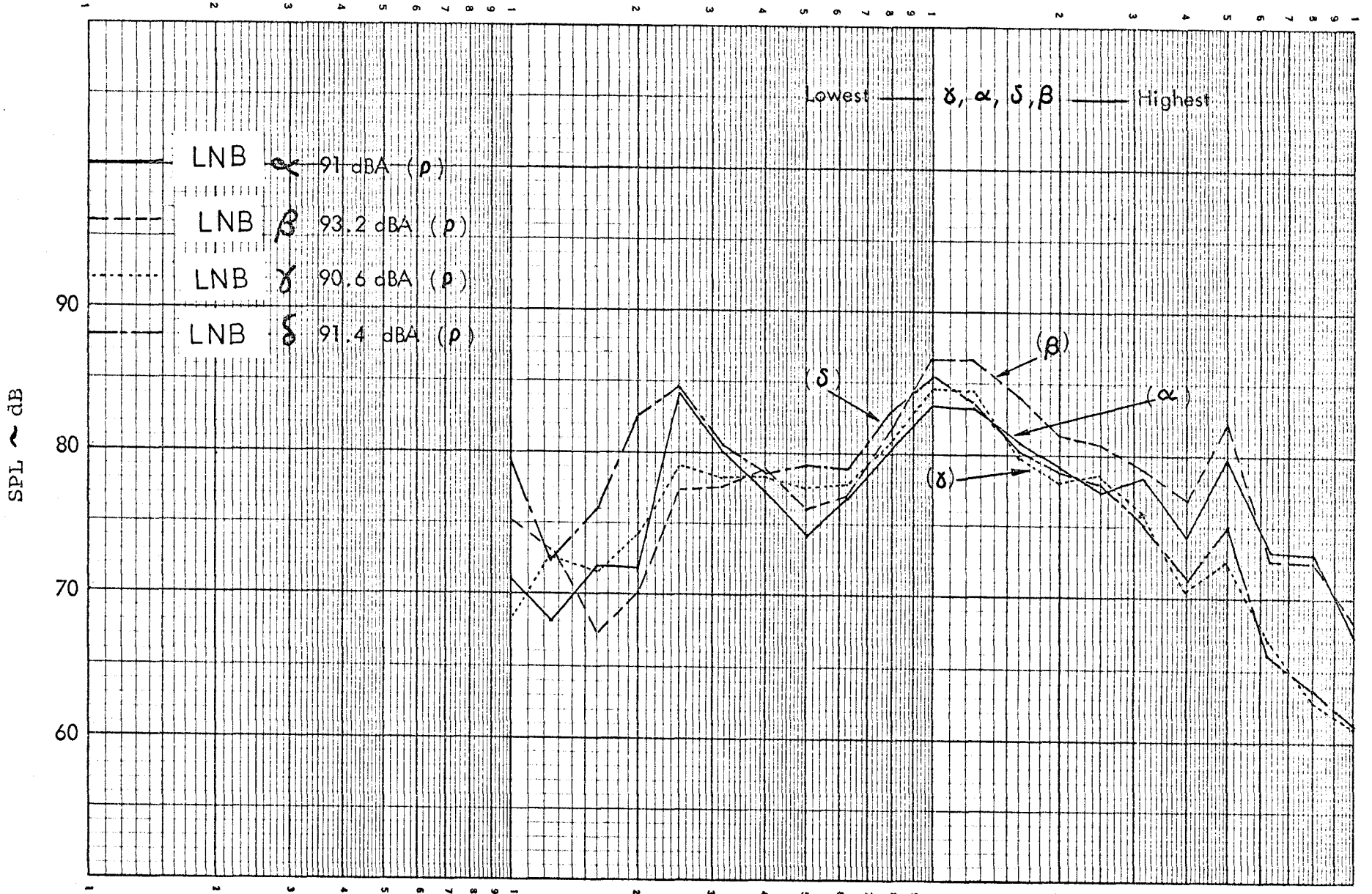

FIG. 3.28 RHS NOISE @ 1500 RPM FULL THROTTLE ≈ 106 BHP

SCALE: Large Division = 1.0 g

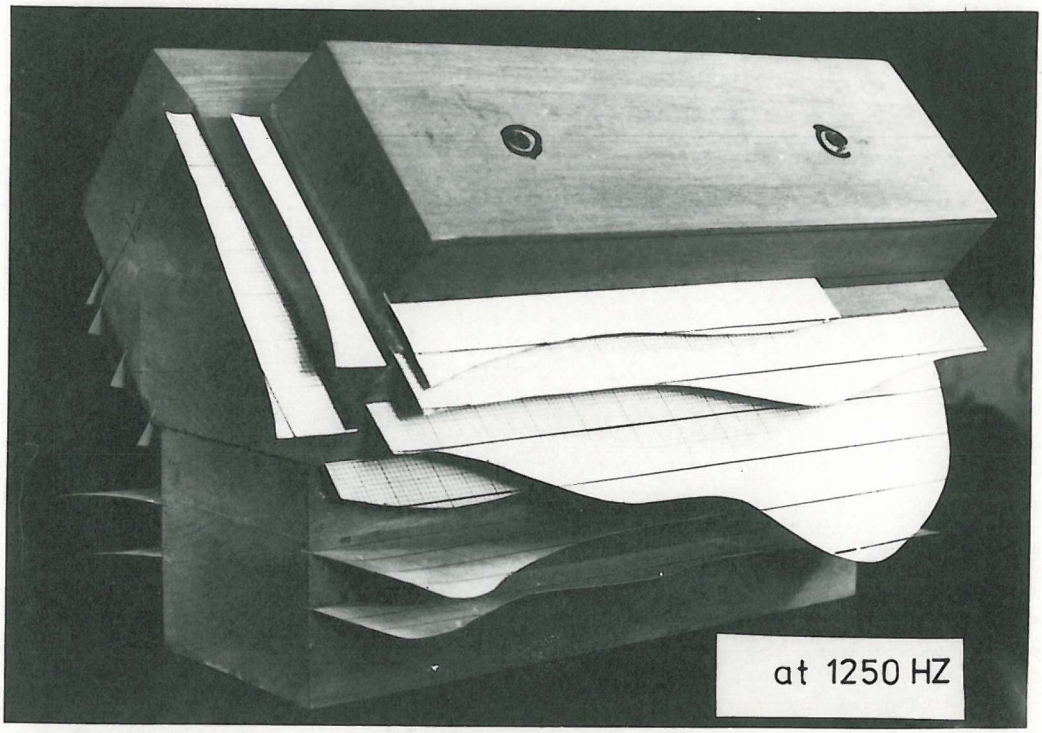

"RHS and front"

"RHS and front"

FIG. 3.29 ENGINE VIBRATION MODES (EXCLUDING IVC) OF LNB∝ AT 1500 r.p.m. FULL THROTTLE (106 B.H.P.)

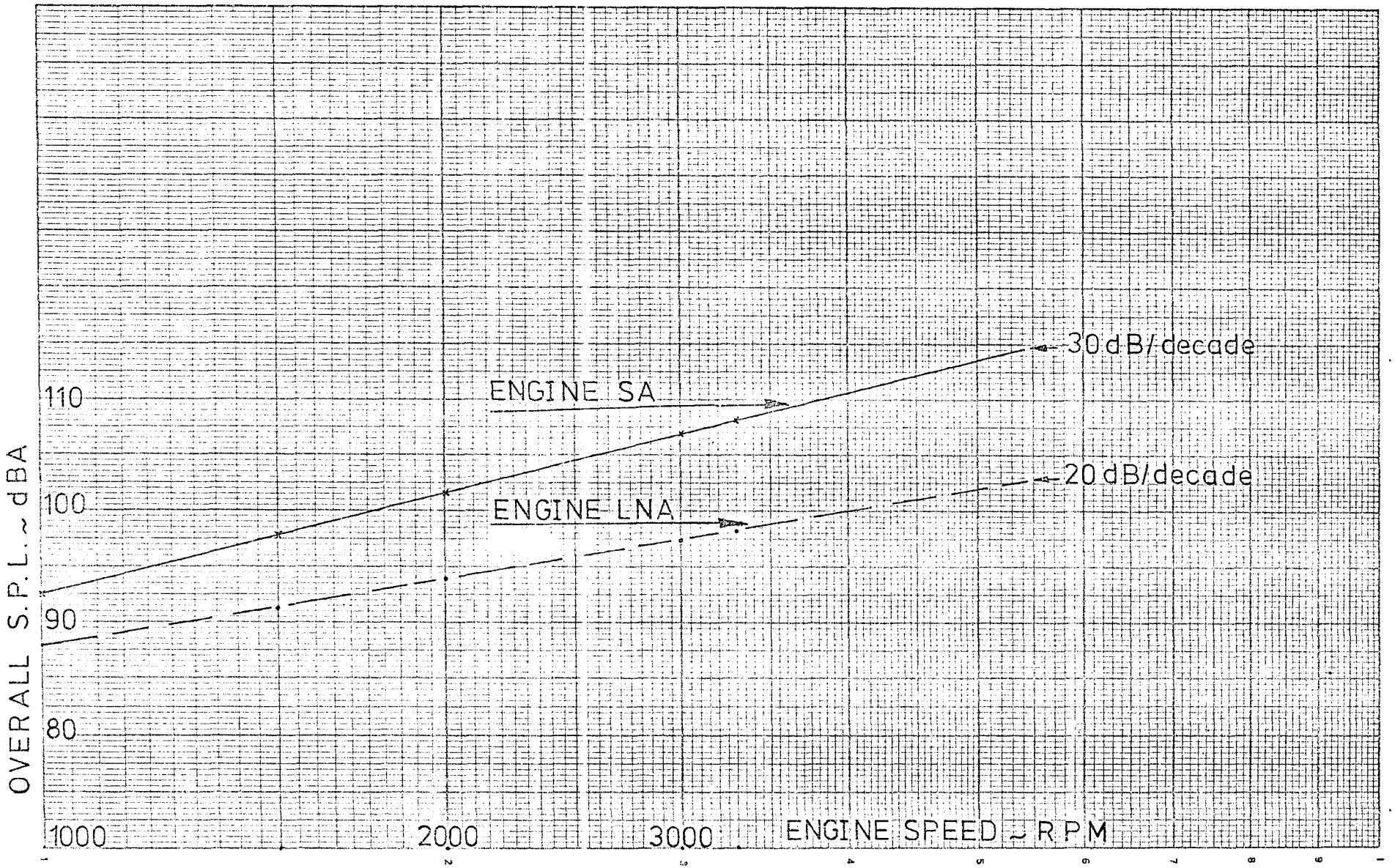

FIG. 3.30 COMPARISON OF STANDARD AND LOW NOISE ENGINE AT FULL LOAD

CHAPTER 4

IDENTIFICATION OF PISTON SLAP IN A RUNNING VEE FORM DIESEL ENGINE

4.1 Introduction

Piston slap is initiated whenever the side-thrust force changes direction. This occurs under two conditions: when the force in the connecting rod changes sign, i.e., changes from tension to compression or vice versa, or when the component of the connecting rod force normal to the cylinder axis changes direction as a result of changes in the sign of the angle between the connecting rod and cylinder axis. The latter condition always occurs at top and bottom dead centres; the former condition is realised when the total inertia-force contribution to side thrust just balances that resulting from the gas force.

In conventional diesel or reciprocating engines it is always found that piston slap occurs at or near the top and bottom dead centre, while mid-stroke slaps may be suppressed at some low-speed operating conditions where the aforementioned force balance cannot be attained.

Apart from the effect on engine noise piston slap has received considerable attention because of its effect on cavitation erosion.

In the running engine it is difficult to identify the noise produced by piston slap. The reasons are that both combustion and piston slap noise characteristics are similar and the resultant induced transient vibrations of the structure occur at close instants in time. Unless the pressure rise resulting from combustion is before T.D.C., the identification of the piston slap is almost impossible. The contribution to the noise and vibration, however, can be assessed by the introduction of relevant modifications to the piston system in order to significantly change the piston

impact characteristics (ref. 2.14).

The well known techniques employed for reduction of piston slap are summarised below:

(1) Lateral displacement of the gudgeon pin by around 3% of the piston diameter towards the thrust side and redistributing the piston weight. Similar results can also be obtained by offsetting the crankshaft from the cylinder centre line.

(2) Lengthening the piston skirt to minimise the inclination of the piston in the bore.

(3) Use of pistons with minimal piston-to-bore clearances, such as bimetallic, expansion restricted pistons and use of bearing pads.

(4) Use of overall small clearances for the piston pin.

(5) Obtain the maximum rigidity of liner to limit deformation.

(6) Isolation of the cylinder liner from the engine block and possibly increasing the damping of the liner.

(7) By suitable control of coolant so that liner expansion is more even down the length of the bore.

(8) Oil cushions between the piston and the cylinder wall (ref. 4.1).

(9) Reduction of ratio of crank radius to connecting rod length.

To limit piston slap noise on an existing engine only a limited number of these techniques can be applied. The possibility of oil cushioning on the engine was investigated but proved to be unpracticable because of the short skirt pistons in the oversquare engine investigated. Therefore it was decided to employ thermally controlled pistons with very small clearance together with careful assembly of the liners to ensure the true roundness of the bore.

4.2 General Instrumentation

The engine investigated was installed as outlined in Chapter 3 with acoustic conditions and operating parameters being carefully controlled. Engine performance was also monitored throughout the tests. All noise measurements were taken at the standard microphone position (3 ft or 0.9m from engine level with exhaust manifolds). For engine surface vibration, the accelerometer was rigidly attached by small studs cemented in position at points forming a complete grid over the engine surface as shown in figure 4.1. Cylinder pressure levels were taken using a quartz transducer installed in cylinder no. 1. This was positioned such that the diaphragm was flush with the surface of the combustion chamber. The signal being fed through a charge amplifier into a Muirhead Pametrada frequency analyser (Type D489-EM) set to "in-tune high" selectivity. The pressure transducer was statically calibrated before and after engine running.

In order to separate the individual events in the engine cycle, an oscillographic technique is employed. In this, three signals are usually displayed:

(1) degree marks to locate the sequence of firing cylinders. For this a degree marker disc with magnetic pick up was fitted to the front of the crankshaft to indicate crankshaft positions at 10^{o} intervals and T.D.C. position of No. 1 cylinder. The degree marker signal was fed into one channel of a Tektronix oscilloscope.

(2) A pressure diagram to locate the reference firing cylinder. For this the signal from the quartz transducer out of the amplifier is fed into a second channel of the oscilloscope.

(3) Vibration signal (or noise). The accelerometer (or microphone) signal is fed through a spectrometer set on the dBA weighting network into a third channel of the oscilloscope. The dBA scale was found most representative for the present comparative study.

Photographic recordings were made using a Southern Instrument Drum Camera and fitted with a continuous film feed mechanism.

4.3 Test Results

The engine was tested under two conditions:

(a) with standard pistons having radial cold clearance of .012 in;

(b) with special expansion restricted 'Autothermatik' pistons having radial cold clearance of .002 in.

The 'Autothermatik' pistons were designed and developed especially for the V8 engine investigated by Mahle K.G. Ltd., of Germany. They have four steel inserts to control the expansion of the skirt. Extra care had to be taken when assembling these pistons in the engine due to the inherent ovality of the wet liners. The liners therefore were honed insitu to obtain true roundness.

The two radial clearances give representative limits for the study of the effect of clearance on piston slap.

In the following discussion of results these two pistons will be referred to as "standard" and "Mahle" ("slapless").

4.3.1 Noise due to piston slap

Figures 4.2-4.5 compare noise spectra for the engine fitted with standard and Mahle pistons at the right hand side running at full load speeds of 3300, 3000, 2000 and 1500 revs/min. Table 4.I summarises the overall noise levels (dBA) for RHS, LHS, front and top.

In general, the Mahle pistons reduce the overall noise by an average of 2 dBA. There is however, a tendency for the difference in noise levels to increase with increasing engine speed, though it is not systematic and is observed to reverse in some cases, for example, at the top of the engine (at 3 ft from centre line of inlet manifold).

These two trends can be explained as follows:

1. With increasing speed, the piston approach velocity should increase and so piston slap impulse must increase. This would account for the increase in noise at higher speeds.

2. However, with increasing speed, the effect of the oil film between the piston and liner would increase in proportion to the sliding speed of the adjacent surface following the hydrodynamic theory of lubrication. This could result in decreased piston slap noise with speed.

The actual behaviour, however, is more complicated through the interaction of other varying factors which nullify the effect of each other resulting in a non-systematic relationship.

Table 4.II summarises the general trends in various frequency bands.

As can be seen, piston slap affects the broad frequency range from 800-8000 Hz but is most apparent in the third octave bands of 1000, 1250, 2000, 2500 and 5000 Hz where levels are affected by as much as 5 dB or more.

4.3.2 Vibration due to piston slap

Noise is generated by the normal component of the motion of a vibrating surface. When the surface is large in relation to the wavelength of sound and all points of the surface are moving in phase, the sound pressure generated is directly proportional to the normal component of the velocity of the vibrating surface. If the vibrating surfaces are small in comparison with the wavelength of the sound, and air can move easily between back and front of the emitting surface, then a parameter more directly proportional to the sound pressure is acceleration (ref. 4.2). For that reason the vibration acceleration has been used in the assessment of piston induced vibration.

Figures 4.6-4.8 compare vibration acceleration spectra for standard and Mahle pistons at selected points of the engine surface. Table 4.III

summarises the general trends of vibration for both pistons in various frequency bands for all vibration measuring positions.

As can be seen, piston slap influences the vibration of the whole engine surface in the frequency bands 1000, 1250, 2000, 2500, 3150 and 5000Hz. It tends to be more marked, however, on the engine block. Comparison of Table 4.II(noise data) and Table 4.III(vibration data) indicates that noise is closely related to the engine vibration.

4.3.3 Oscillographic identification of piston slap

In order to separate the individual events in the engine cycle an oscillographic study was carried out with both standard and Mahle pistons fitted in the engine. For this test three signals were displayed and recorded photographically using a drum camera. The degree marker signal locates the sequence of firing cylinders, the pressure diagram locates the reference firing cylinder and the third signal is that of either noise or vibration of engine structure (dBA weighted).

Figures 4.9 and 4.10 show typical oscillographs for the same point on the engine for No. 1 cylinder firing for engine fitted in turn with both standard and Mahle pistons. Vibration (and subsequently noise) is induced by the rapid pressure rise resulting from combustion, and this vibration impulse is followed closely by another impulse which is attributed to piston slap. The precise time at which piston impact takes place can be calculated theoretically, and correlated with the actual incidence in the oscillographs. The two signals are so close to each other that in most cases it is extremely difficult to separate them.

Figure 4.11 shows vibration oscillographic records along the line extending from the top of the engine cylinder head to the bottom of the oil sump parallel to the centre line of cylinder No. 5. From these records it was found that vibration at point β_2 gives the best position on the engine to detect the contributions of combustion and piston slap originated

vibration. This position would seem to be logical as piston slap should be seen more clearly at a point on the block opposite the slapping piston.

Figure 4.12 shows oscillographic records at a point between the centre lines of two adjacent cylinders. As expected, such a point tends to exhibit the contributions from both cylinders and renders this position useless for identification of pulses due to individual firing.

Therefore it was established that the top of the engine block and more specifically the points opposite the centre lines of the cylinders (β_2, β_4, β_6, β_8, β_2', β_4', β_6', β_8'), are the best places to monitor the separate contributions of combustion and piston slap. By measuring the vibration at each point opposite the centre line of the relevant cylinder, the contribution due to each cylinder firing can be shown accurately. An attempt was also made to identify the piston slap by noise oscillograms but this was found to be less clear.

The following information can be obtained from the vibration oscillographs:

1. Maximum instantaneous vibration amplitudes for
   (a) combustion contribution (full load)
   (b) compression contribution (no load)
   (c) piston slap contribution (full load and no load).
2. Instantaneous overall vibration amplitudes at any crank angle and for each case of cylinder firing and therefore instantaneous engine mode shapes.
3. Incidence of combustion and piston slap with relation to crank angle.
4. Relationship between combustion and slap induced noise with engine speed and load.
5. Amount and nature of cycle to cycle variations in combustion pressures and engine response obtained by continuous records with the drum camera.
6. Phase relationships.

The maximum instantaneous vibration amplitudes (in g) have been extracted, and are shown plotted in Figures 4.13-4.20 for both pistons at engine speeds of 1500 and 3000 revs/min full and no load conditions, and for each cylinder firing. The plotted amplitudes of the vibration along the cylinder banks illustrate the instantaneous mode shapes of the block. It can be seen that both the combustion induced and the piston slap induced mode shapes are more or less identical. It can also be observed that the firing of the front cylinder produces a torsional type mode, while the middle cylinders produce a bending type mode.

It has been shown (ref. 4.3) that at frequencies below 2000 Hz, the lateral modes of engine cylinder block vibration around cylinder head level for the engine investigated are very similar to those of a uniform free-free beam. Assume that the deflected shape of the cylinder head is composed entirely of the two translational modes and the first two free-free beam modes as shown below.

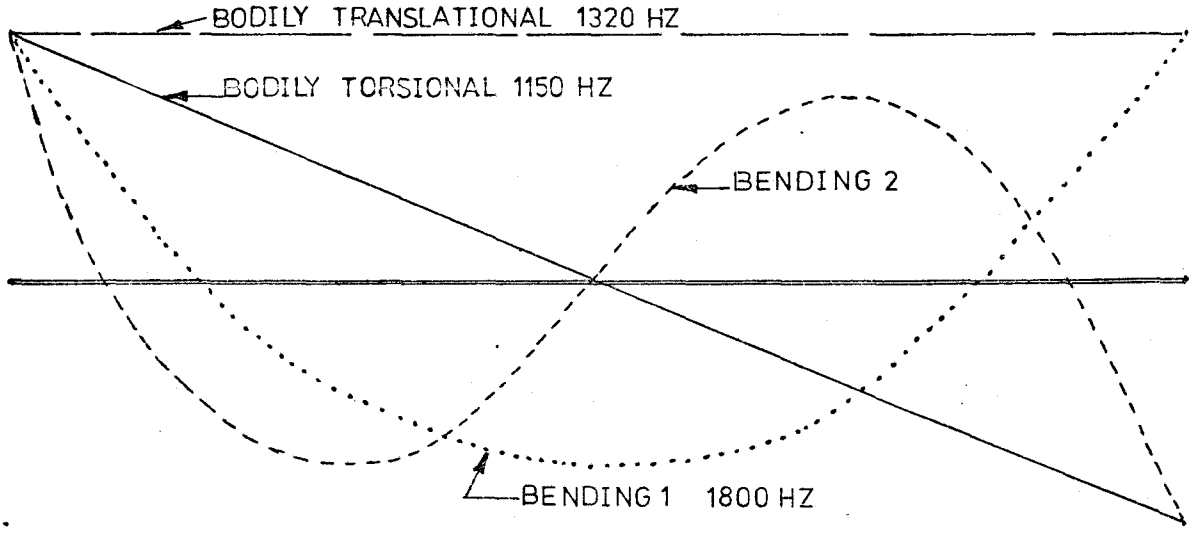

Therefore it is possible to calculate the instantaneous acceleration levels of each of the four assumed modes at every cylinder position using the general solution to the beam bending equation:

$$Y(x) = \underline{A}.\cosh(2\pi\mu.x) + \underline{B}.\cos(2\pi\mu x) + \underline{C}.\sinh(2\pi\mu.x) + \underline{D}.\sin(2\pi\mu x)$$

where x = distance from one end of block

ℓ = length of block

$$\text{Bending moment} = -EI\frac{d^2y}{dx^2}$$

$$\text{Shear force} = -EI\frac{d^3y}{dx^3}$$

$\underline{A}$, $\underline{B}$, $\underline{C}$ and $\underline{D}$ are constants

and $$\mu^4 = \frac{\rho f^2 A}{4\pi^2 EI}$$

ρ = mass density (mass/unit vol.)

f = frequency, c/s

A = cross sectional area

E = modulus of elasticity

I = moment of inertia

By using the "mode separation" technique* (ref. 4.3) it can be shown that the resultant modes obtained for the above assumed modes correspond well with those obtained from figures 4.13-4.20.

From these figures, vibration response contributions due to combustion, compression and piston slap can be seen and compared for the standard and Mahle pistons. It can be determined (using $20 \log \frac{a}{a_o}$) that with standard pistons fitted combustion induced vibration exceeds that due to piston slap by an average of 2 dBA at full load conditions over the speed range. With Mahle pistons fitted this figure is increased to 7 dBA.

---

*"Mode separation" technique uses the fact that for any linear structure, at any given instant of time the deflected shape of the structure can be represented by the sum of certain proportions of the fundamental and normal modes of the structure.

With the Mahle pistons it was found that greater damping in the engine is induced giving effect to a slight reduction also in combustion induced vibration.

It is of interest to observe from the oscillographic study that although excitation from combustion is clearly visible there is no evidence of any apparent excitation from injection equipment which suggests that it must be well below that due to combustion or piston slap.

4.4 Effect of Piston Clearance on Combustion Characteristics

There are indications that combustion characteristics of the engine may be altered when piston slap is minimised. Figures 4.21 to 4.23 show comparisons of cylinder pressure and spectra for the engine fitted with standard and Mahle pistons for 3000, 2000 and 1500 rev/min full load. Generally, there are little differences except in the higher frequency range where the cylinder pressure oscillations influence the spectra. These oscillations tend to be lower in magnitude (an average of 5-7 dB) for the Mahle pistons at around 5000 Hz but may be of equal value or even higher at around 8000 Hz. It must be stressed that the engine underwent no change whatsoever except for changing the pistons, therefore the combustion mechanism should be identical when testing with the standard and Mahle pistons. This is supported by comparison of cylinder pressure spectra from two identical standard V8 engines at 3000 and 2000 revs/min full load in figures 4.24 and 4.25. As can be seen the spectra are nearly identical for each condition. This suggests that the differences in the spectra between the Mahle and standard pistons are only due to piston design changes. The following explanations are proposed.

1. The cylinder pressure diagrams of the Mahle tend to show less fluctuations or ripples beyond the ignition point which partly explains the difference in the cylinder pressure spectra around 5000 Hz.

2. Comparing the cylinder pressure diagrams it can be seen that the start of combustion with the Mahle pistons occurs slightly earlier than on the standard pistons.

The reason is perhaps due to the fact that with smaller piston clearances, the rate of heat loss (which primarily depends on the temperature difference between the cylinder gases and the wall on one hand and the effective area exposed to the heat on the other, ref. 4.4) is smaller because of greater proximity than those with large clearances. Thus from the above explanation, the instantaneous cylinder gas temperature in the Mahle pistons is higher than that with standard pistons. The higher cylinder temperature with the Mahle is responsible for the shorter delay period. Also of importance, owing to the shorter delay period, the total fuel prepared prior to ignition is smaller and hence this could lead to a lower vibration level as confirmed by experimental results discussed earlier.

Similar 1/3 octave cylinder pressure spectra obtained in a banger rig for two different piston arrangements were presented in ref. 4.5 for:

(a) standard piston

(b) smaller diameter piston with O-rings.

Though in this experiment other factors were of importance, the general trend of the cylinder pressure spectra in these two cases resemble very closely those obtained during this investigation.

4.5 Conclusions

(1) For the V8 engine investigated, piston slap contributes up to 2½ dBA to the overall noise level of the engine.

(2) Piston slap appears to affect the noise and vibration of the engine over the acoustically important frequency range of 1000-5000 Hz.

(3) Changing piston to bore clearance in the engine influences the combustion characteristics over the frequency range from 4000-8000 Hz.

(4) The oscillographic technique was found to be a good method of identifying the various sources of engine noise and vibration, especially that due to piston slap and combustion. In addition the oscillographic records give complete information of instantaneous engine modes and thus enable a more detailed study of engine structure response to be carried out.

References

4.1 NRDC (National Research Development Corporation) British Patent No. 846995. "Oil Cushioned Piston". February 1970.

4.2 A.J. King. "Vibration and Noise of Mechanisms and Machines". Engineering, Vol. 183, p.716. 1957.

4.3 N. Lalor. "An Investigation into the Origins of Vee Engine Noise". Ph.D. Thesis. 1971. University of Southampton - Institute of Sound and Vibration Research.

4.4 A.M. Ogegbo. "Automotive Diesel Engine Combustion and Noise". Ph.D. Thesis 1973. Southampton University - Institute of Sound and Vibration Research.

4.5 E.G. Thien. "The Use of Specially Designed Covers and Shields to Reduce Diesel Engine Noise". SAE Paper No. 730244, pp. 11-12, 1973.

Revs/Min	1500				2000				3000				3300			
Microphone Position	RHS	LHS	Front	Top	RHS	LHS	Front	Top	RHS	LHS	Front	Top	RHS	LHS	Front	Top
SA Engine with standard pistons	98	98.5	98.8	97.5	101.5	101.5	101.4	100.2	106.5	106.2	106.8	103.8	107.5	107.5	107.2	103.2
SA engine with Mahle pistons	96	97	97.2	96.8	99.5	100.3	99.8	99	104	104	104.5	102	105	105.5	104.8	104
Noise diff. St.-Mahle (dBA)	2.0	1.5	1.6	0.7	2.0	1.2	1.6	1.2	2.5	2.2	2.3	1.8	2.5	2.0	2.4	-0.3

TABLE 4.I

OVERALL NOISE LEVELS (dBA) FOR THE ENGINE AT FULL THROTTLE

ENGINE SPEED (rev/min)	FREQUENCY RANGE (Hz)	PISTON SLAP EFFECT (dB) *	FREQUENCY RANGE (Hz)	PISTON SLAP EFFECT (dB) *	FREQUENCY RANGE (Hz)	PISTON SLAP EFFECT (dB) *	FREQUENCY BANDS (Hz) WHERE PISTON SLAP IS MOST EFFECTIVE
	RHS NOISE at 3 ft						
3300	(250-300)	2-3 dB	(630-3000)	2-5dB	(3000-8000)	4-12dB	800-2500, 5000, 6300
3000	L.F.	NIL	(500-2500)	2-5dB	(4000-8000)	4-12dB	630-1250, 2500, 5000, 6300
2000	L.F.	NIL	(500-2500)	2-10dB	(3000-8000)	2-12 dB	800-1250, 2500, 5000, 6300
1500	(160-400)	2-4 dB	(800-1250)	2 dB	(2500-8000)	3-10 dB	1000, 25000, 5000, 6300
	FRONT NOISE at 3 ft						
3300	L.F.	NIL	(800-2500)	2-3dB	(4000-8000)	2-4 dB	1000, 1250, 2500
3000	(100-500)	2-10 dB	(800-2500)	2-4dB	(4000-8000)	2-4 dB	800-1600, 2500, 5000, 6300
2000	L.F.	NIL	(1000-2000)	2-4dB	(4000,6300)	2-3 dB	1000-1600, 4000-6300
1500	(100-315)	1-10 dB	(1000-2000)	1-3dB	(4000-8000)	2-5 dB	1000-2500, 5000, 6300
	LHS NOISE at 3 ft						
3300	L.F.	NIL	(1000-2500)	1-4dB	(4000-6300)	2-4 dB	1000, 2000, 2500, 5000
3000	"	"	(1000-2500)	3-5dB	(4000-6300)	3-5 dB	1000-2500, 5000
2000	"	"	(1600-2500)	2 dB	(4000-6300)	1-3 dB	1000, 2000, 2500, 5000
1500	"	"	(1000-2000)	0-2dB	(4000-8000)	1-5 dB	1000, 2000, 5000
	TOP NOISE at 3 ft						
3300	L.F.	NIL	(1000-1600)	0-4dB	(4000-6300)	1-4 dB	1600, 2500
3000	(160-500)	2-7 dB	(1000-2000)	1-4dB	(4000-8000)	0-4 dB	1000, 1250, 1600, 5000
2000	(100-500)	3-12 dB	(1000-2500)	1-3dB	(4000-6300)	1-2 dB	1000, 1600, 2500
1500	(200-500)	1-4 dB	(1000-2000)	1-2dB	(4000-6300)	1-3 dB	1250, 5000

* Piston slap contribution to noise ∿ dB (or reduction in noise due to fitting the Mahle pistons)

TABLE 4. II

ENGINE NOISE DATA

	LOCATION OF VIBRATION ON ENGINE (Rows)	FREQUENCY RANGE (Hz)	* PISTON SLAP EFFECT (dB)	FREQUENCY RANGE (Hz)	* PISTON SLAP EFFECT (dB)	FREQUENCY BANDS (Hz) WHERE PISTON SLAP IS MOST EFFECTIVE
ISOLATED VALVE COVERS	(R)	L.F.	NIL	(1250-8000)	1-7 dB	2000-5000
	(b)	L.F.	NIL	(1250-6300)	1-5 dB	2000, 3150, 5000
	(c)	L.F.	NIL	(1000-6300)	1-5 dB	1000, 1250, 2500, 5000
CYLINDER HEADS	(d)	L.F.	NIL	(1000-5000)	1-6 dB	1000, 1250, 2500, 3150
	(f)	L.F.	NIL	(1000-5000)	1-5 dB	1000, 1250, 2500, 4000, 5000
ENGINE BLOCK Inclined part	(β)	(200-800)	1-4 dB	(1000-4000)	1-5 dB	1000 - 2500, 3150, 5000
	(h)	L.F.	NIL	(1000-2500)	1-10 dB	800-2500, 5000 →
	(ϕ)	(200-500)	1-7 dB	(1250-5000)	1-10 dB	1250 - 5000
Vertical part	(j)	(160-500)	2-15 dB	(1000-6300)	2-7 dB	1250, 2000, 2500, 3150, 5000
	(l)	L.F.	NIL	(1000-4000)	2-10 dB	1000, 1250, 2500, 4000
OIL PAN	(w)	L.F.	NIL	(1000-5000)	1-7 dB	1000, 1250, 1600, 2500, 3150, 5000
	(m)	(200-800)	2-5 dB	(1000-6300)	2-7 dB	1000 - 3150, 5000
	(n)	L.F.	NIL	(1000-5000)	2-4 dB	2500, 5000
	(p)	L.F.	NIL	(800-6300)	2-10 dB	1600, 2500, 3150, 5000
FLYWHEEL HOUSING	(B)	L.F.	NIL	(1000-5000)	2-5 dB	1000, 1250, 2500, 3150, 5000
ENGINE FRONT	(F)	(200-500)	1-5 dB	(1000-6300)	1-8 dB	250, 1250, 2500, 5000

* Piston slap contribution to vibration ∿ dB (or reduction in vibration due to fitting the Mahle pistons) at 1500 rev/min full throttle

TABLE III - ENGINE VIBRATION DATA

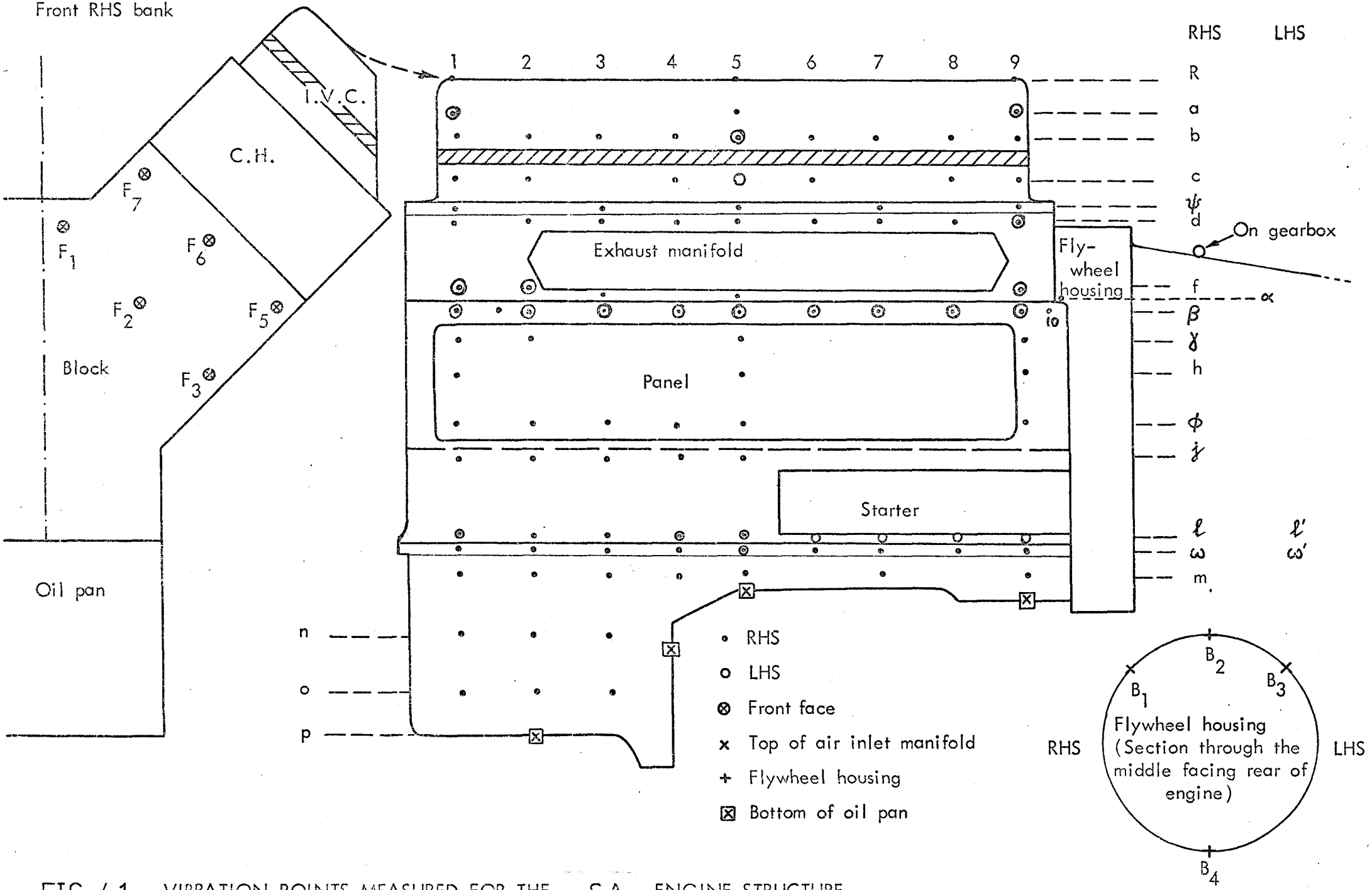

FIG. 4.1 VIBRATION POINTS MEASURED FOR THE SA ENGINE STRUCTURE.

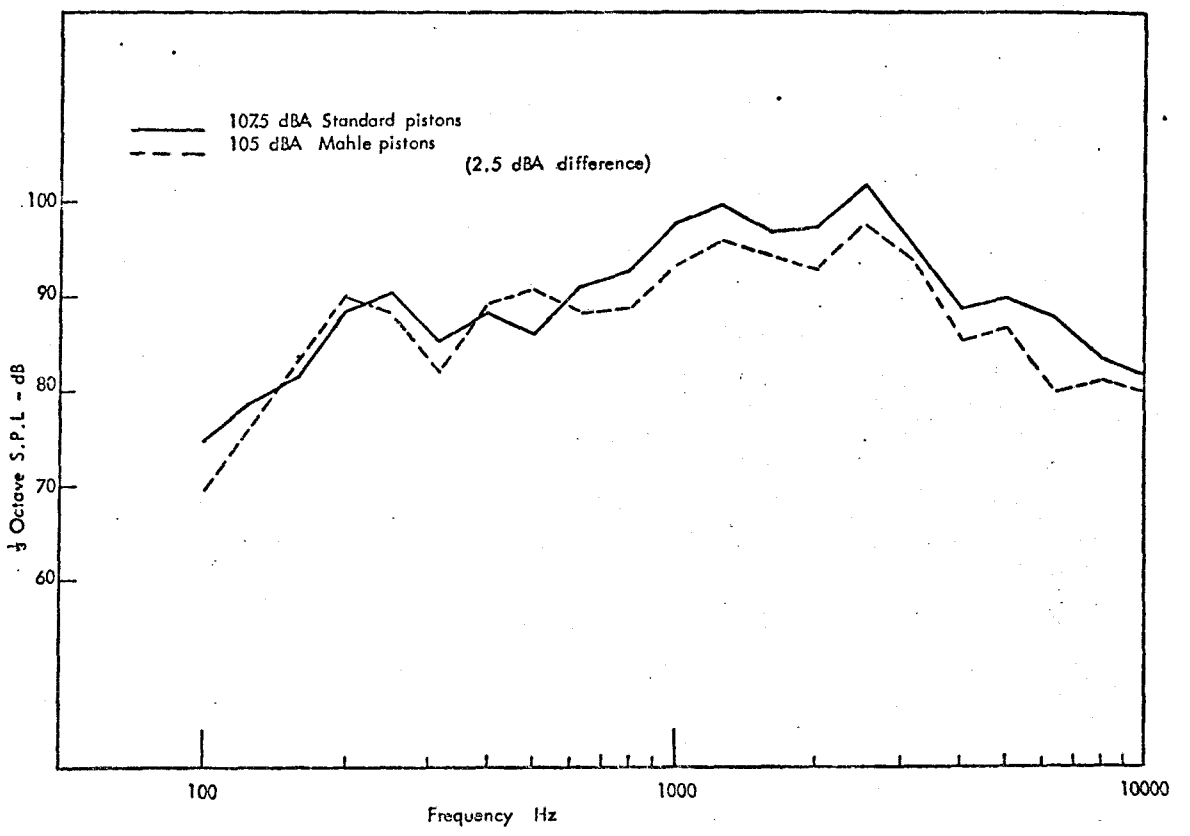

FIG. 4.2 RHS NOISE COMPARISON BETWEEN THE STANDARD AND MAHLE PISTONS FITTED ON THE ENGINE @ 3300r.p.m. FULL LOAD. SA

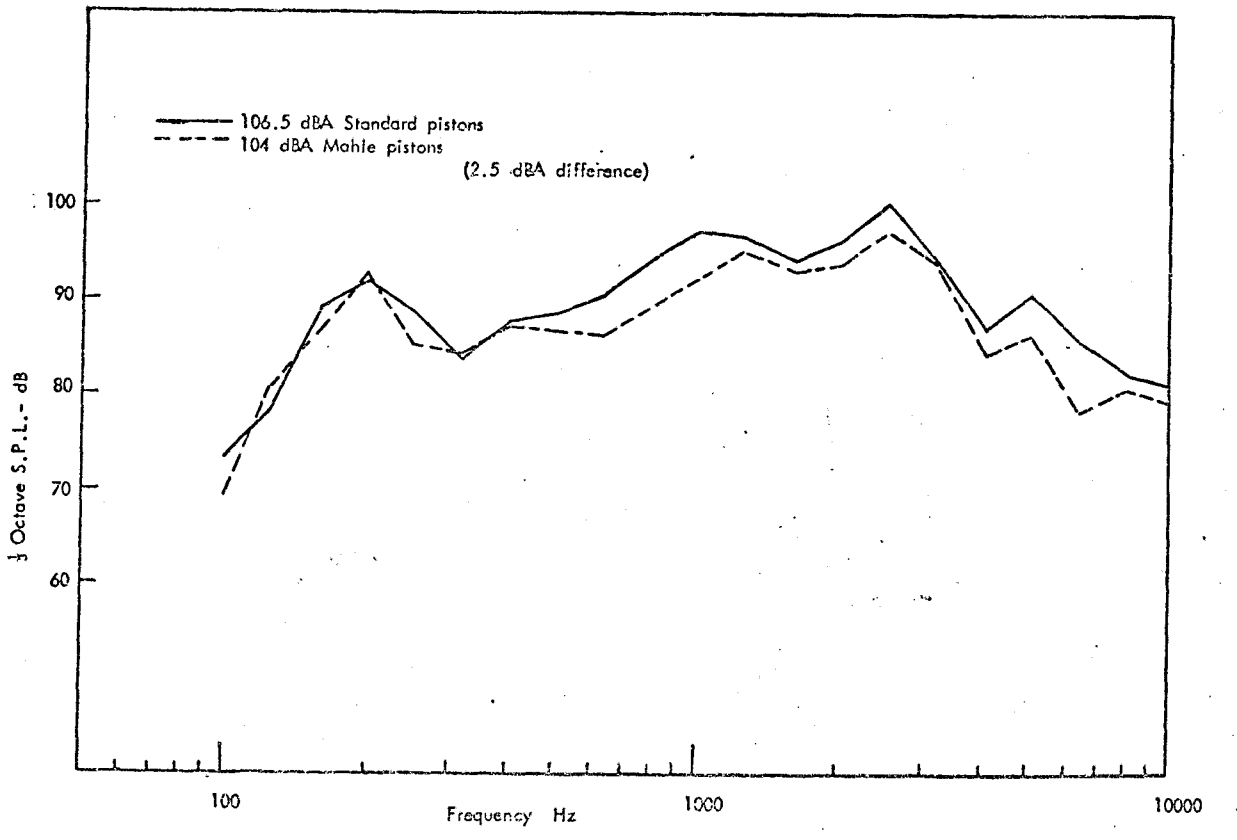

FIG. 4.3 RHS NOISE COMPARISON BETWEEN THE STANDARD AND MAHLE PISTONS FITTED ON THE ENGINE @ 3000 r.p.m. FULL LOAD. SA

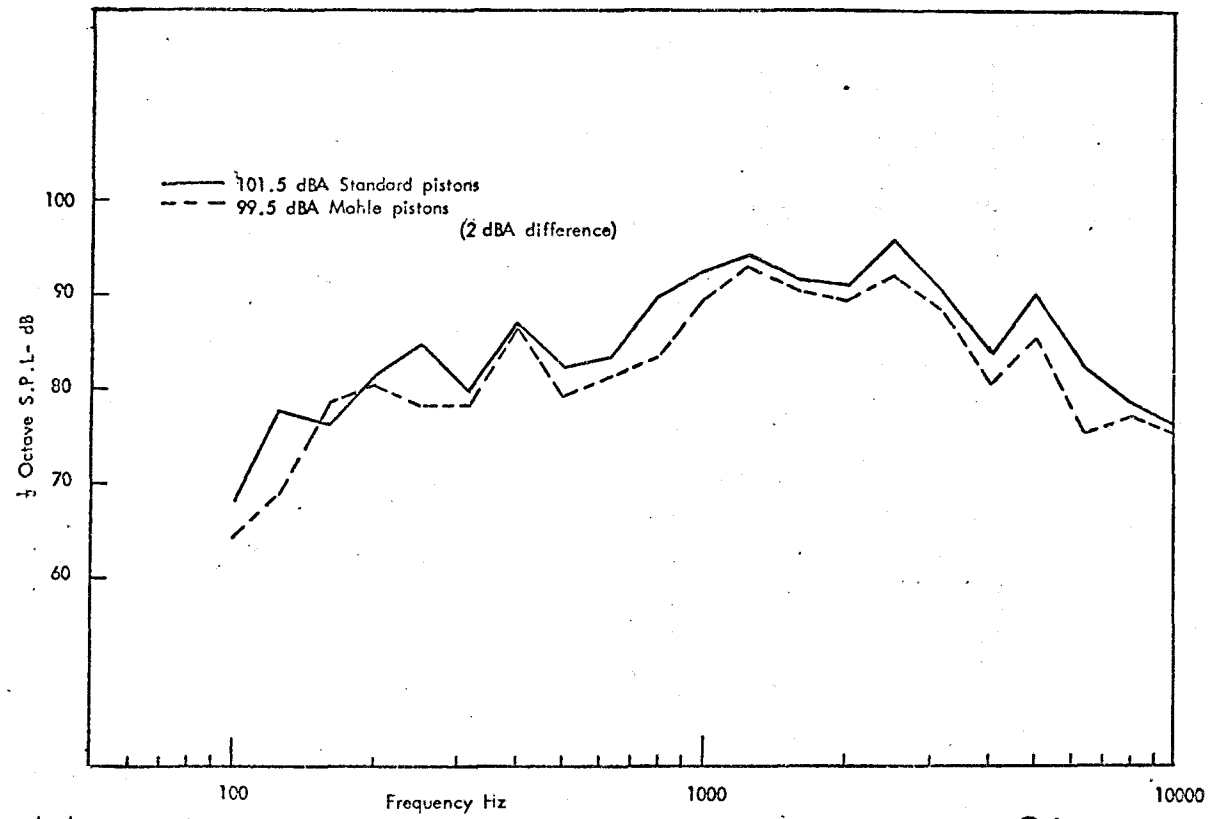

FIG. 4.4 RHS NOISE COMPARISON BETWEEN THE STANDARD AND MAHLE PISTONS FITTED ON THE ENGINE @ 2000 r.p.m. FULL LOAD. SA

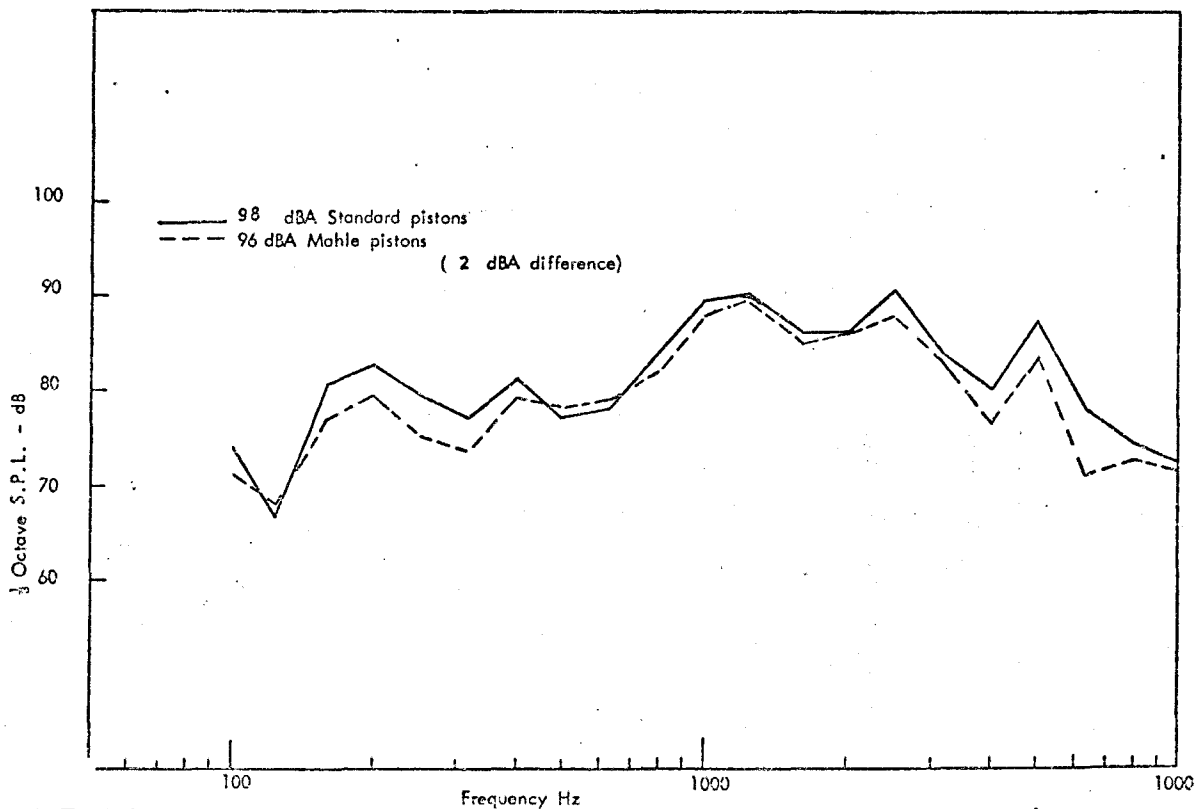

FIG. 4.5 RHS NOISE COMPARISON BETWEEN THE STANDARD AND MAHLE PISTONS FITTED ON THE ENGINE @1500 r.p.m. FULL LOAD. SA

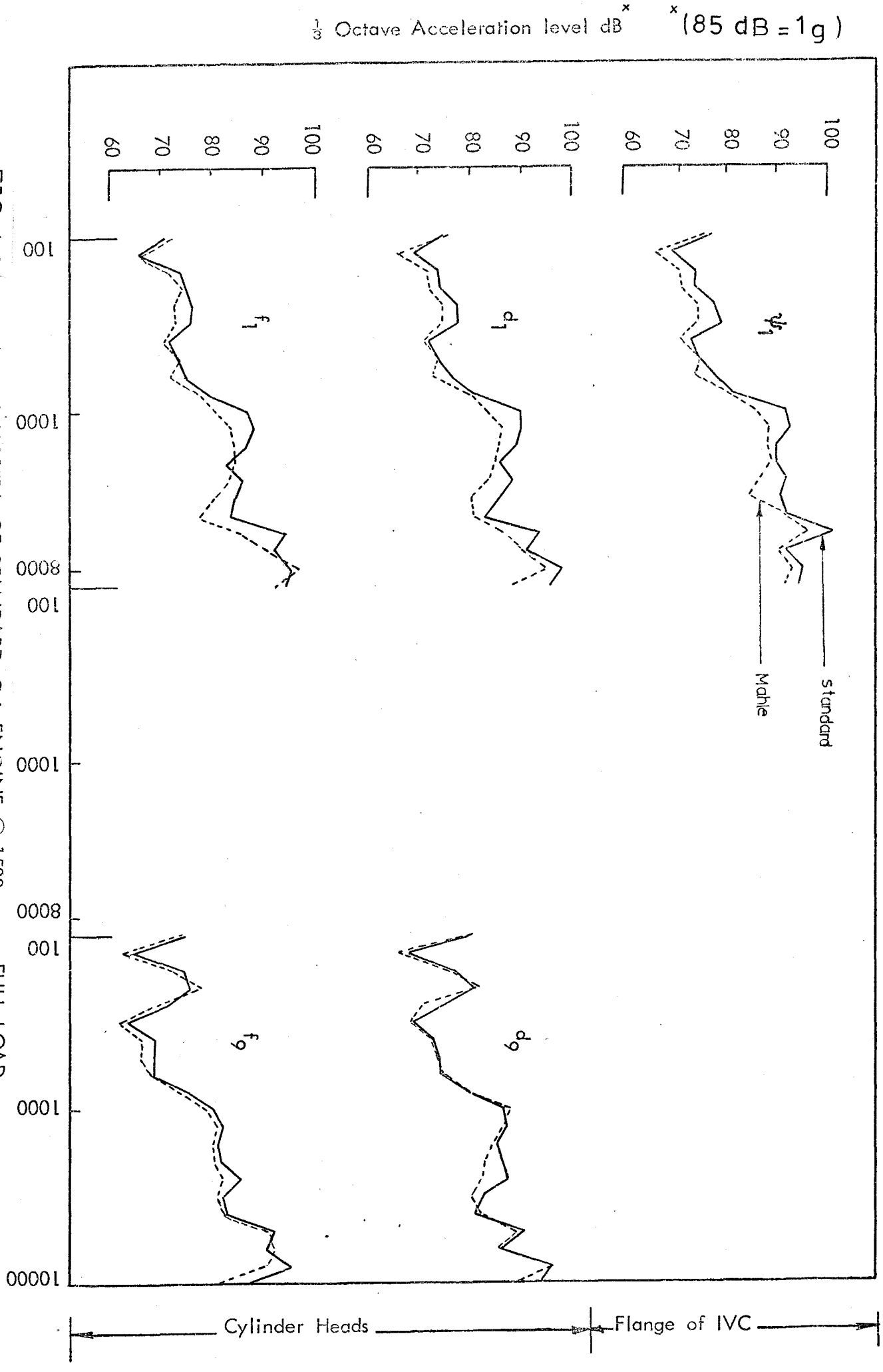

FIG. 4.6 VIBRATION SPECTRA OF STANDARD SA ENGINE @ 1500 r.p.m FULL LOAD

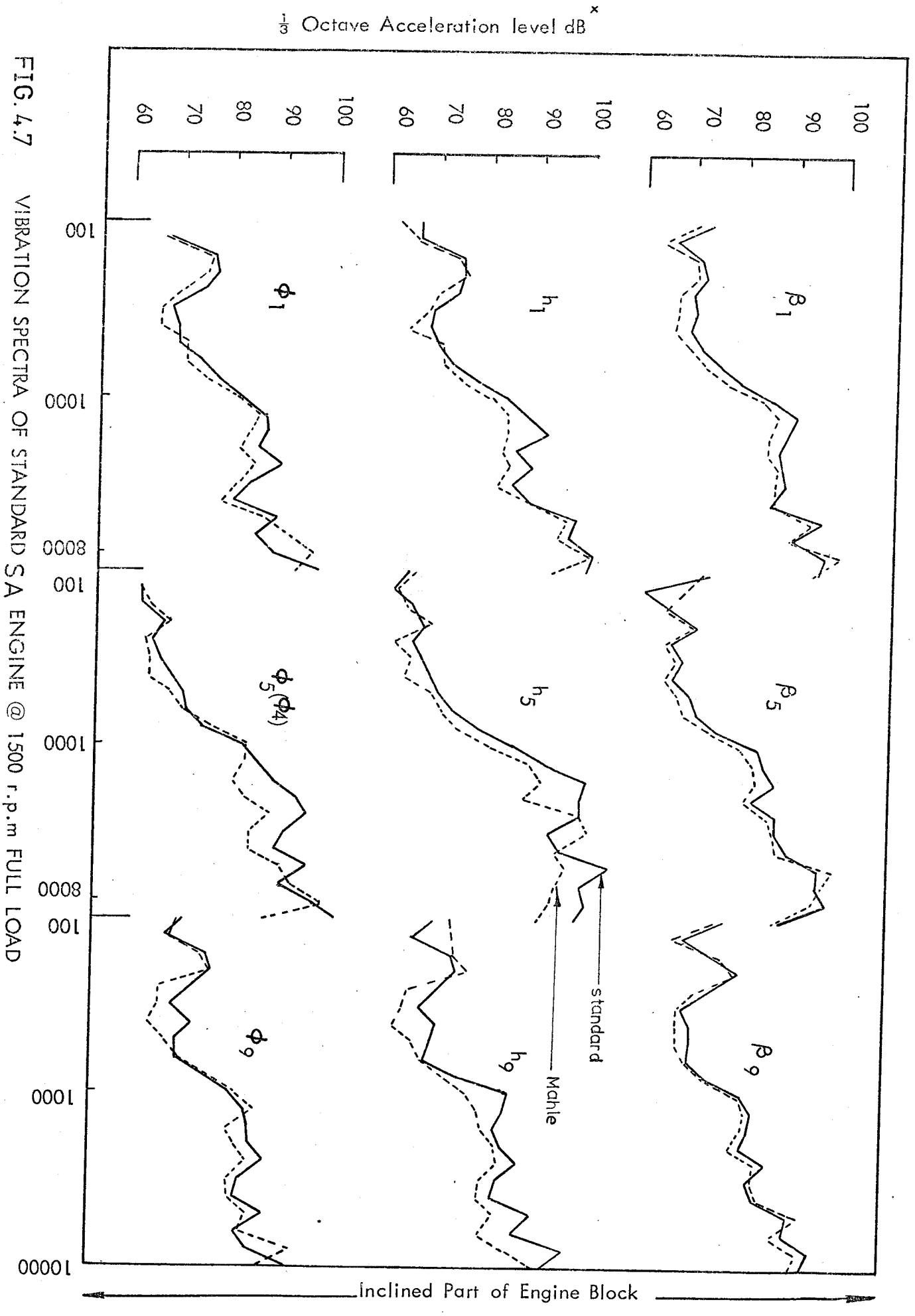

FIG. 4.7 VIBRATION SPECTRA OF STANDARD SA ENGINE @ 1500 r.p.m FULL LOAD

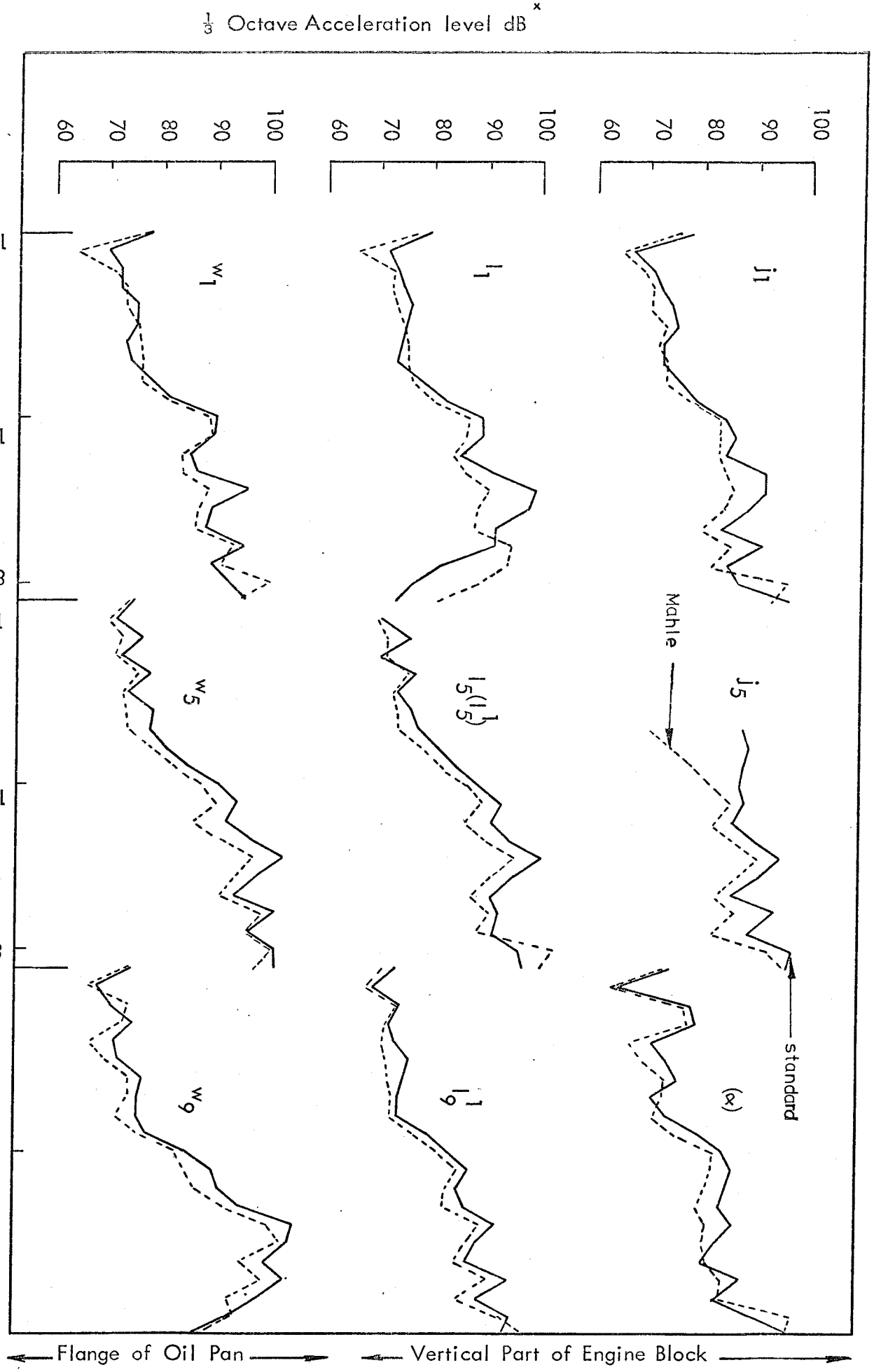

FIG. 4.8 VIBRATION SPECTRA OF STANDARD SA ENGINE @ 1500 r.p.m FULL LOAD

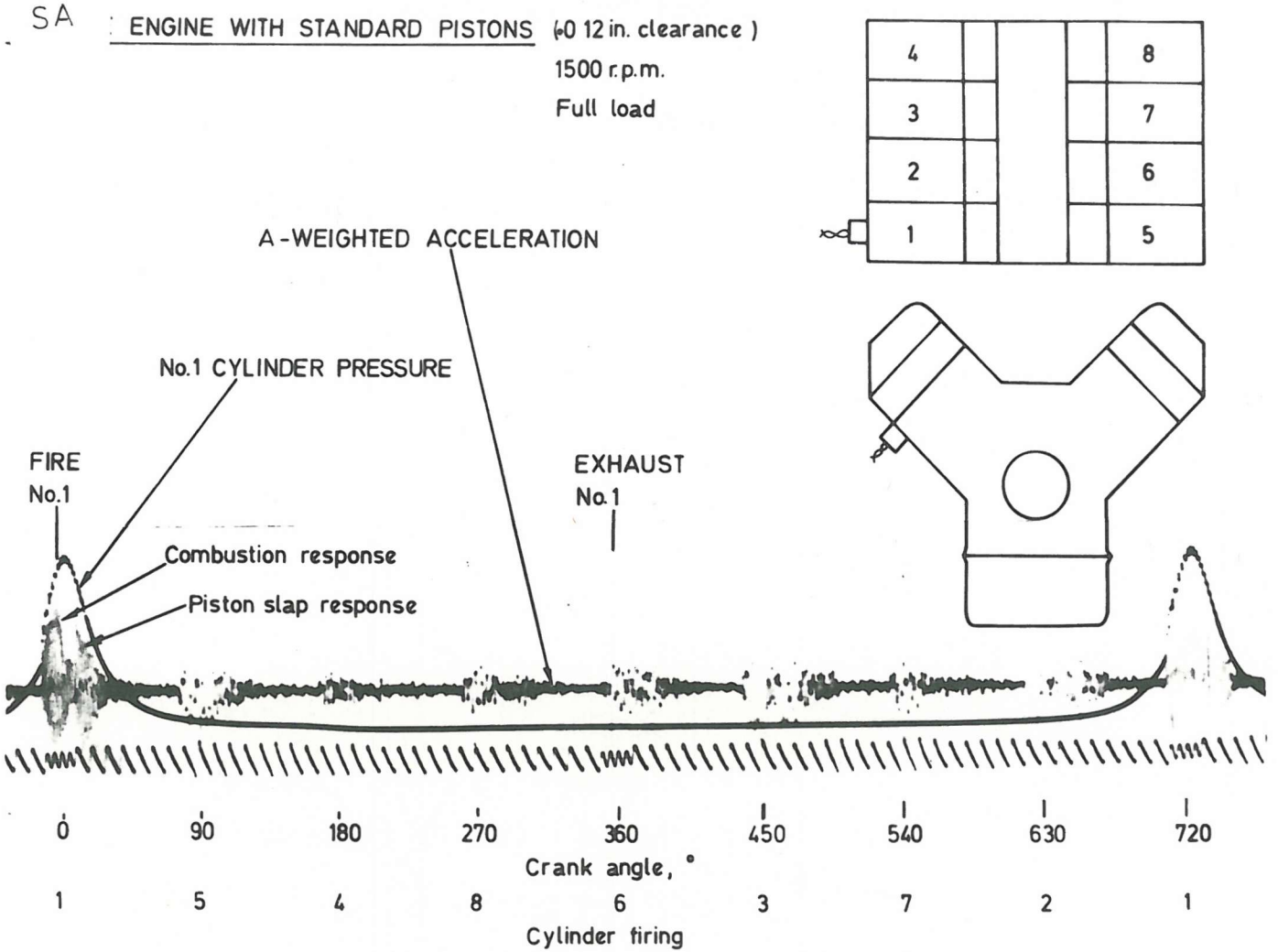

FIG. 4.9 Piston Slap Contribution to Cylinder Block Vibration IN a Running Engine

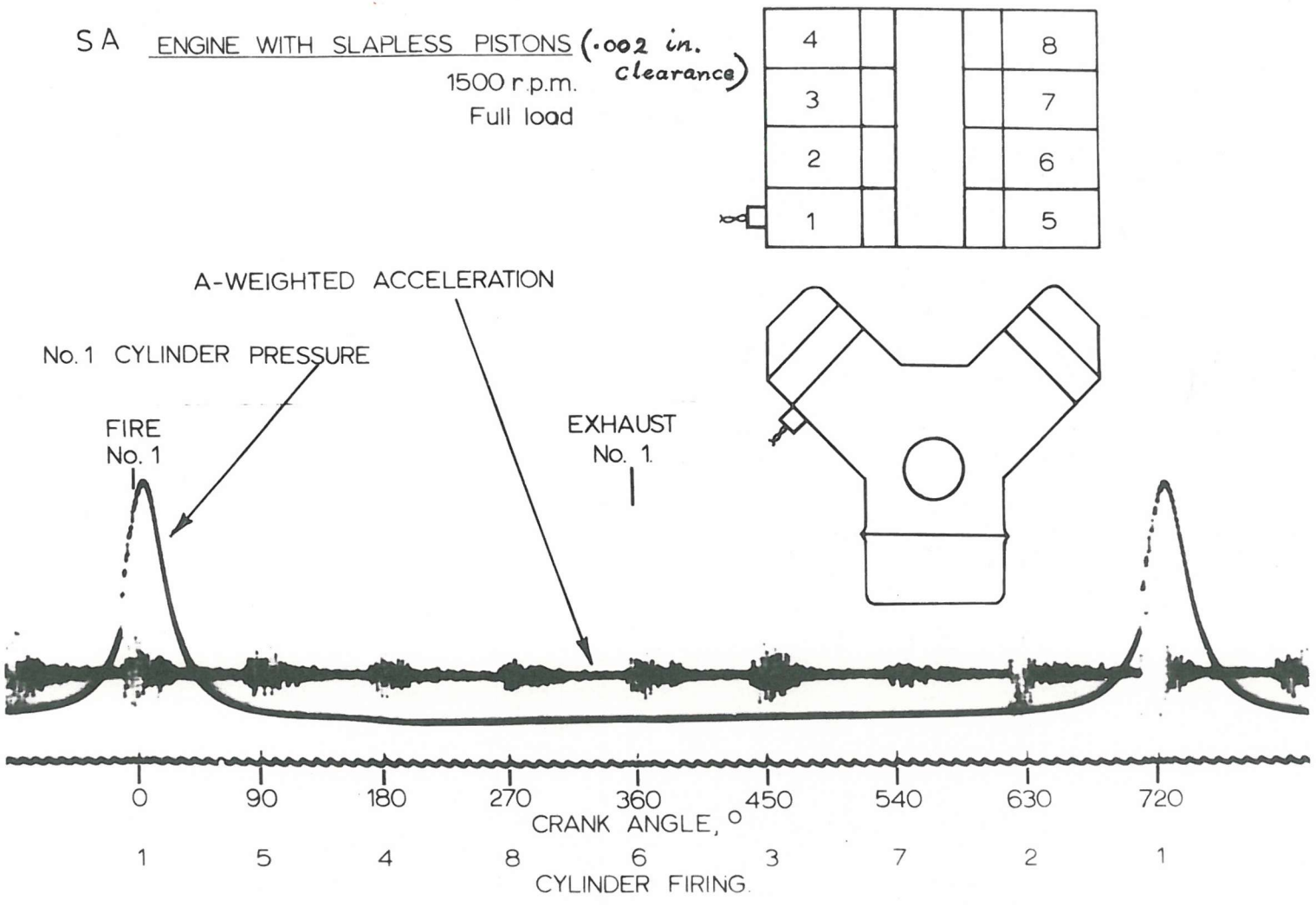

FIG. 4.10 Piston Slap Contribution to Cylinder Block Vibration in a Running Engine

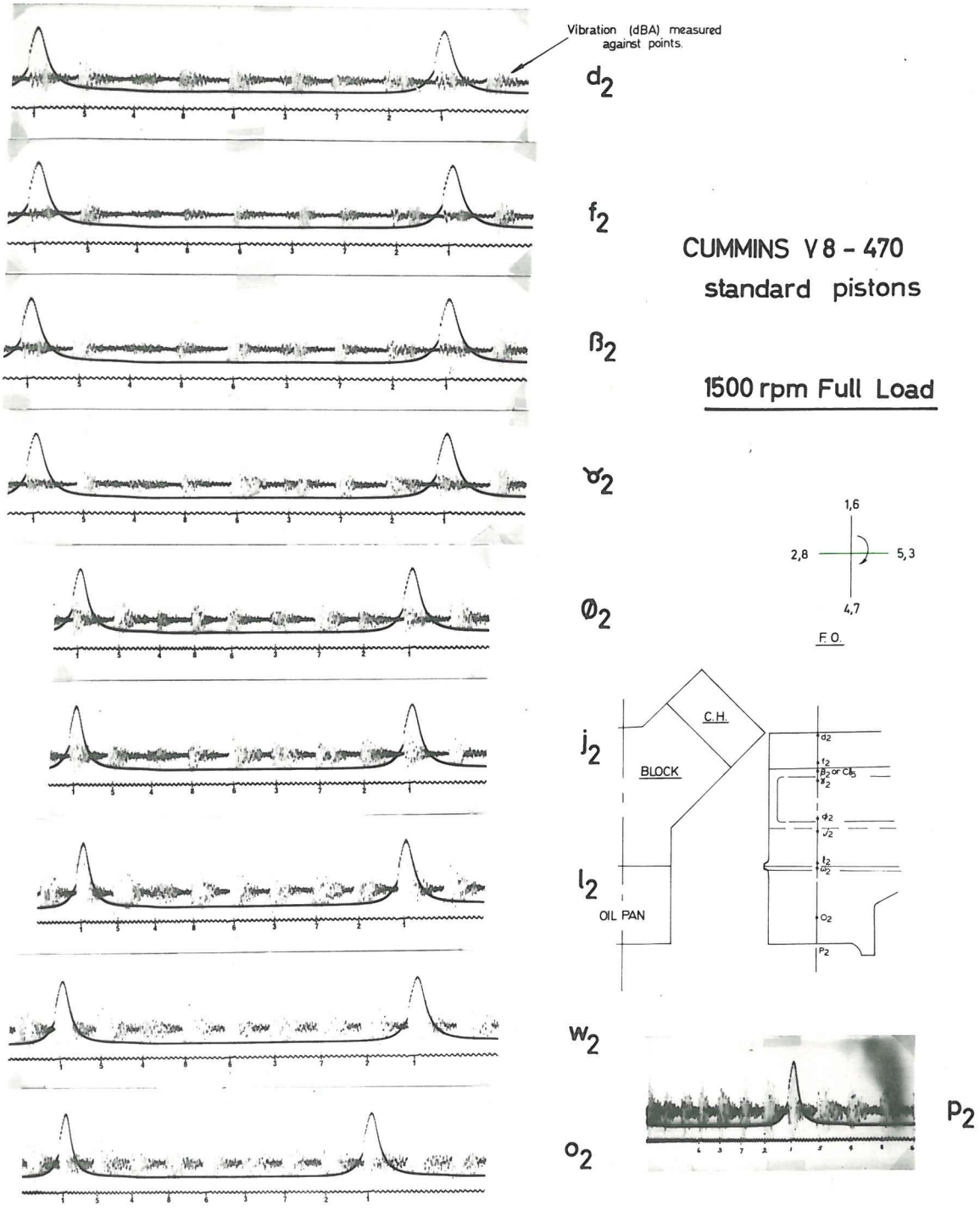

FIG. 4.11 VIBRATION CHARACTERISTICS DOWN ENGINE STRUCTURE (SA)

CUMMINS V 8 - 470 standard pistons

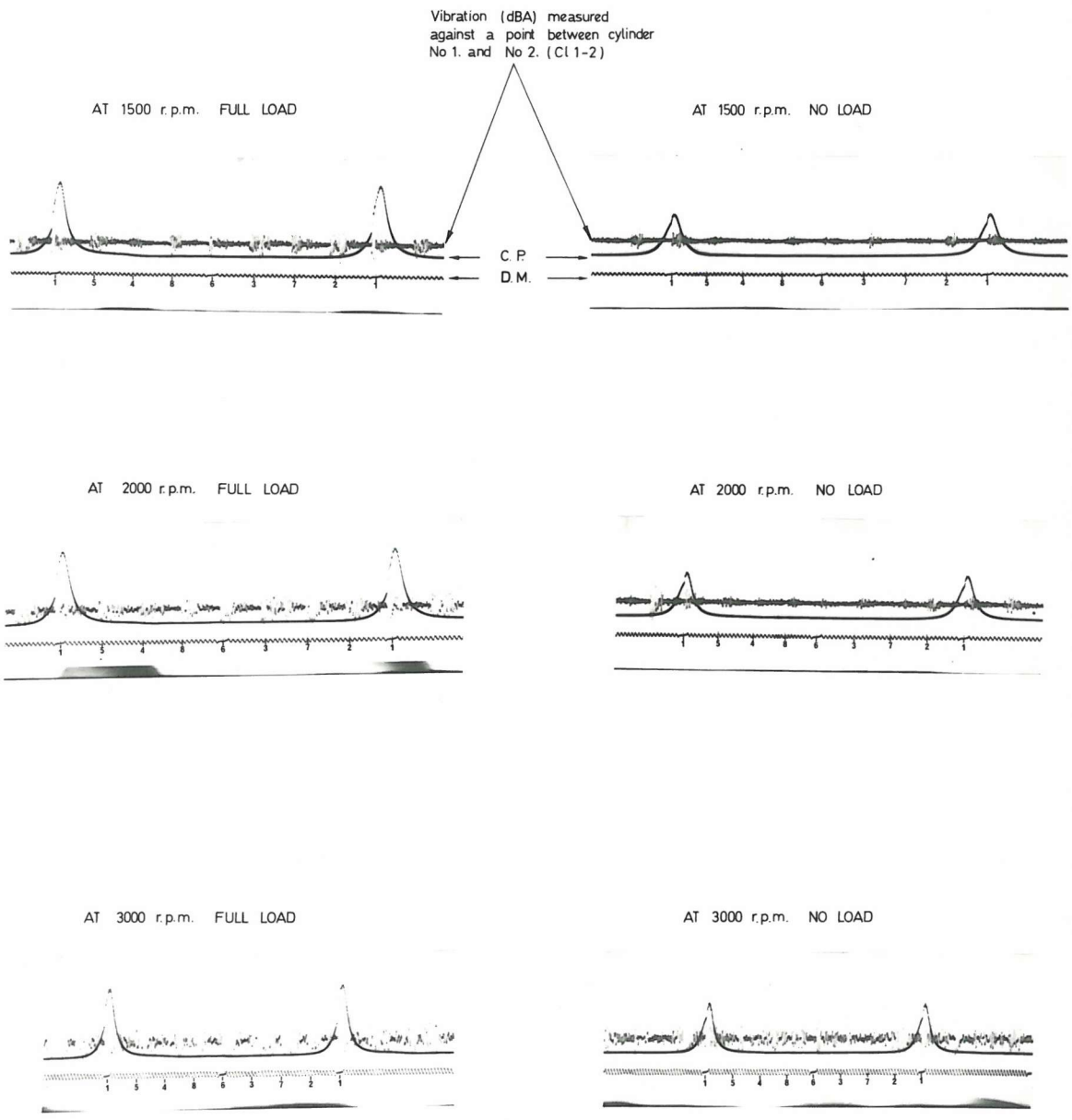

FIG. 4.12 CYLINDER BLOCK VIBRATION BETWEEN ADJACENT CYLINDERS (SA)

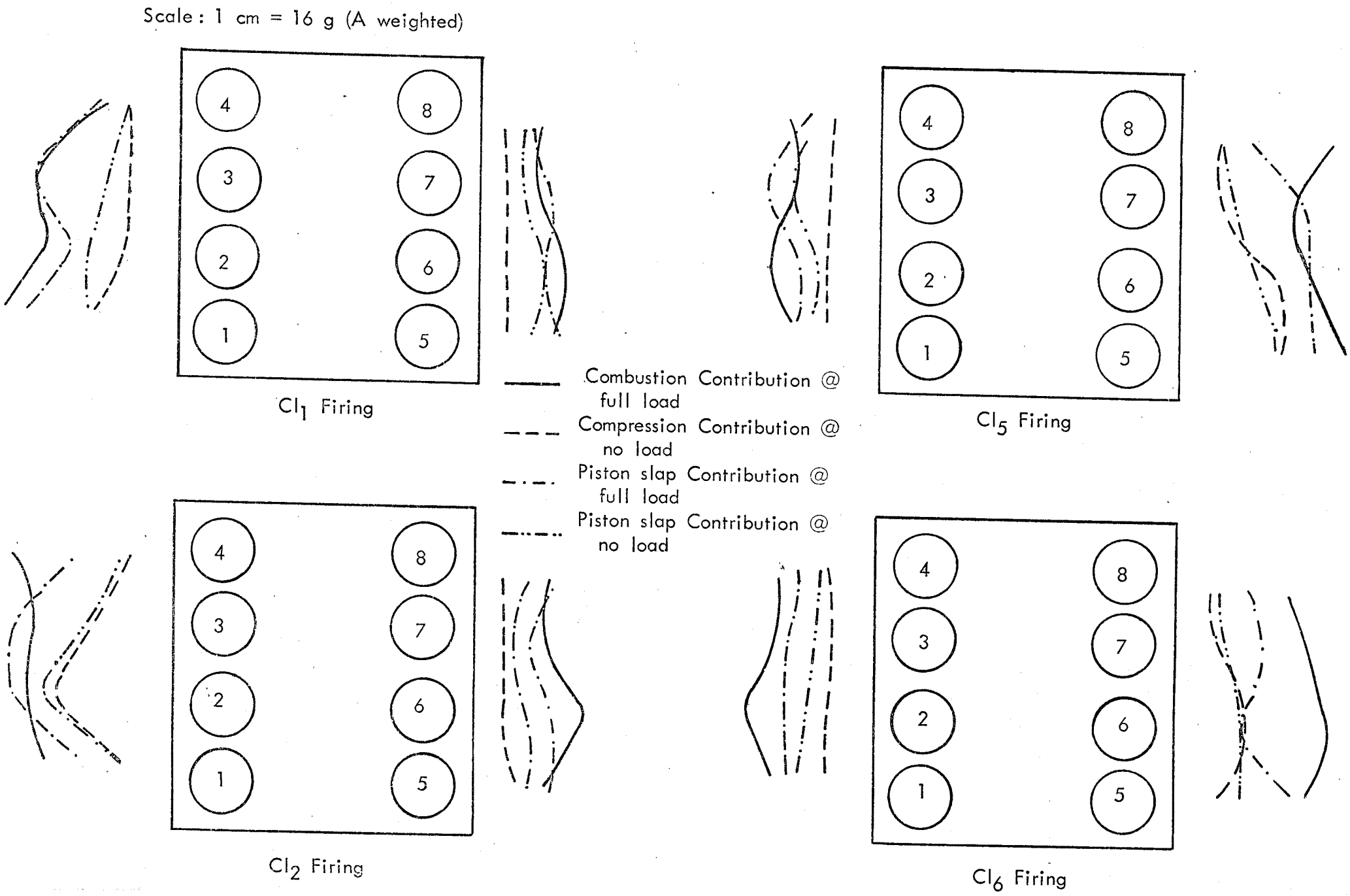

FIG. 4.13 MAXIMUM VIBRATION AMPLITUDES FOR SA ENGINE STANDARD @ 1500 r.p.m.

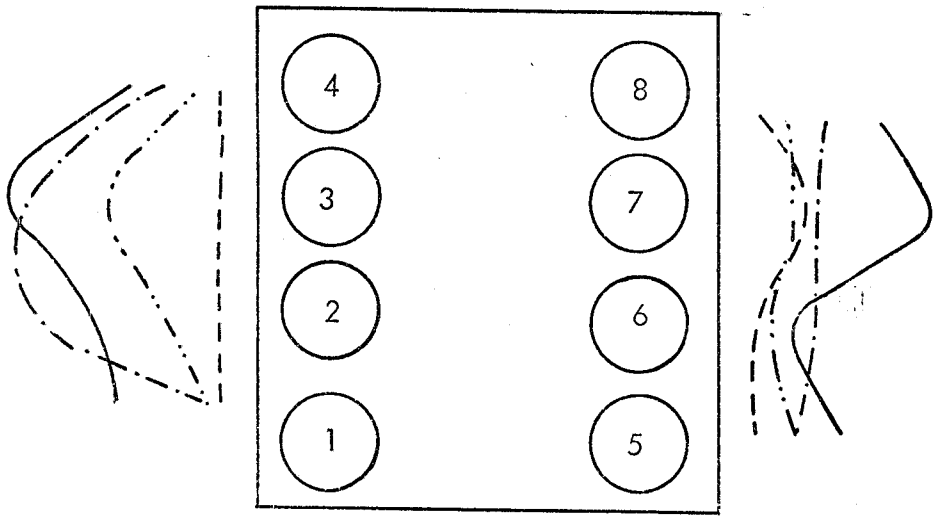

Cl_3 Firing

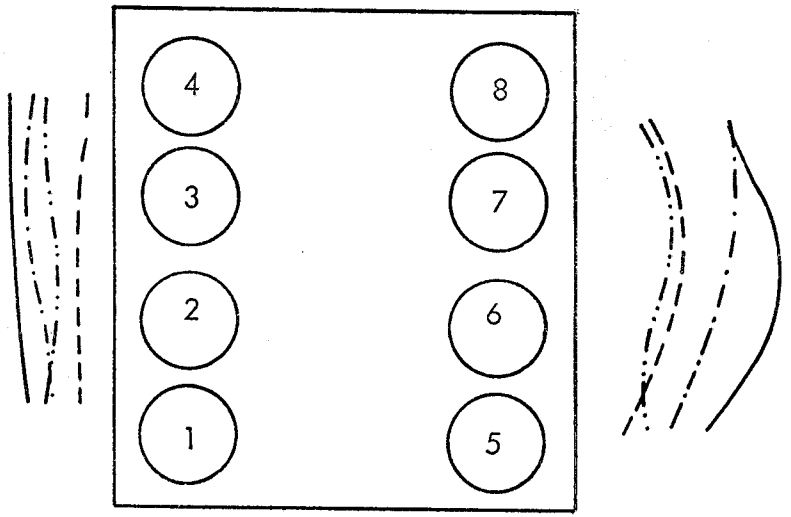

Cl_7 Firing

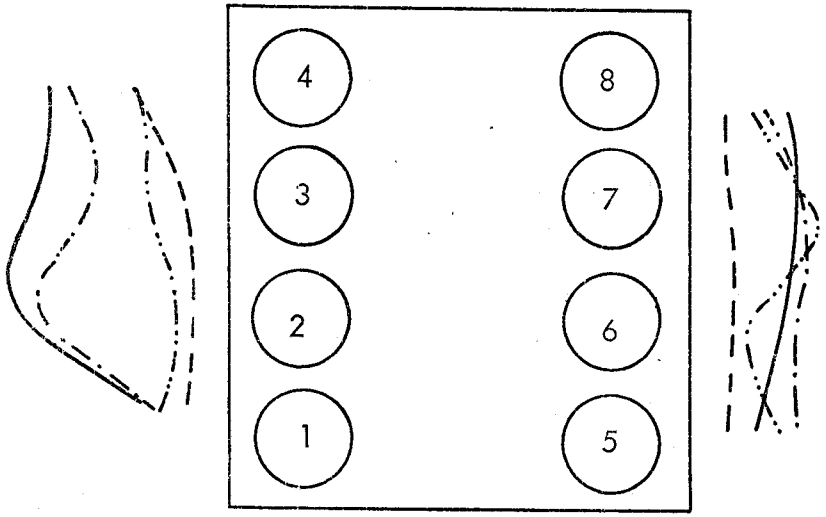

Cl_4 Firing

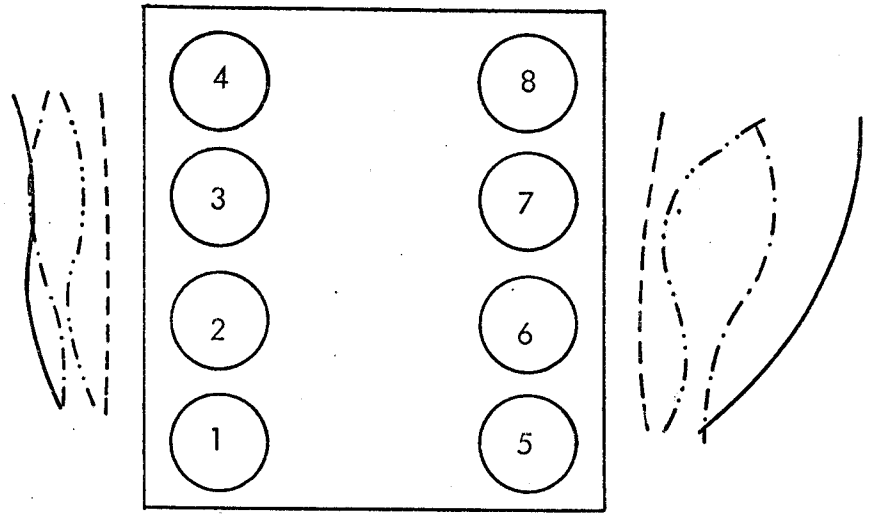

Cl_8 Firing

FIG. 4.14 MAXIMUM VIBRATION AMPLITUDES FOR SA ENGINE STANDARD @ 1500 r.p.m.

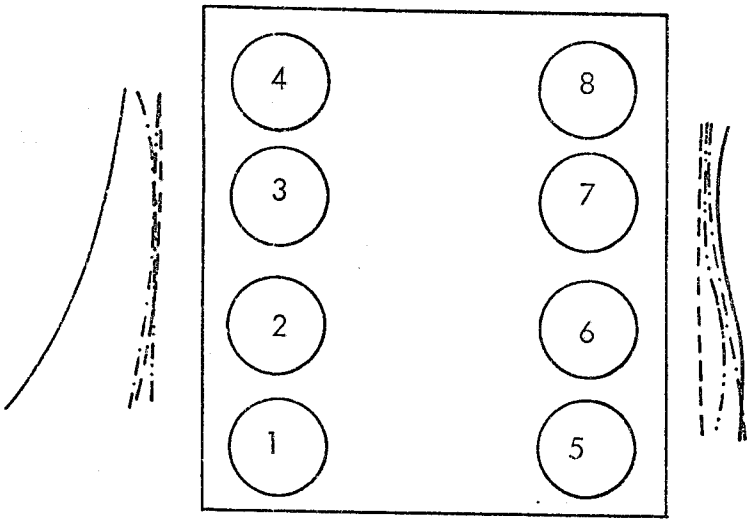

Cl_1 Firing

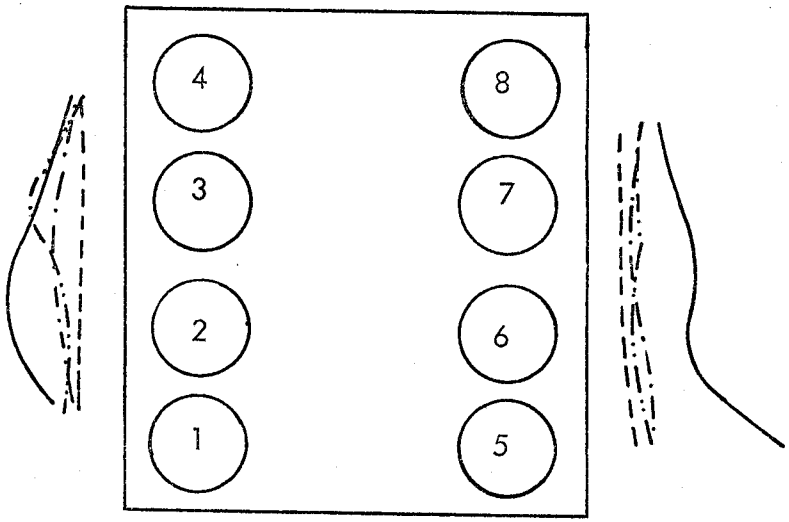

Cl_5 Firing

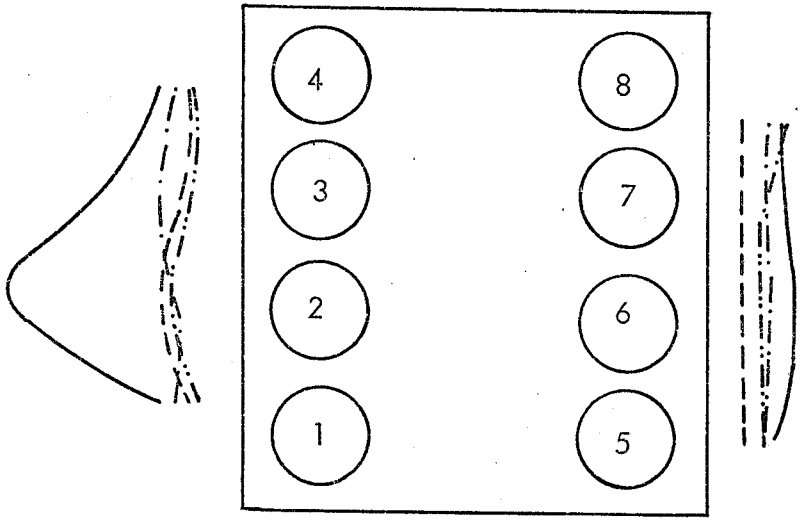

Cl_2 Firing

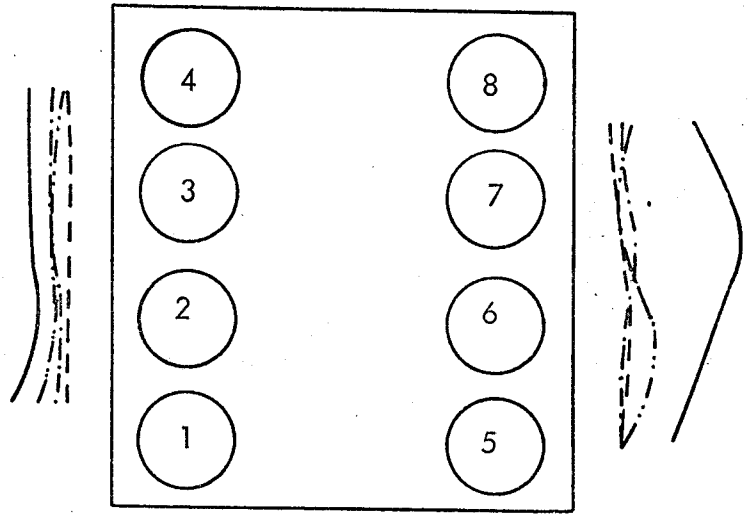

Cl_6 Firing

FIG. 4.15 MAXIMUM VIBRATION AMPLITUDES FOR SA ENGINE MAHLE @ 1500 r.p.m.

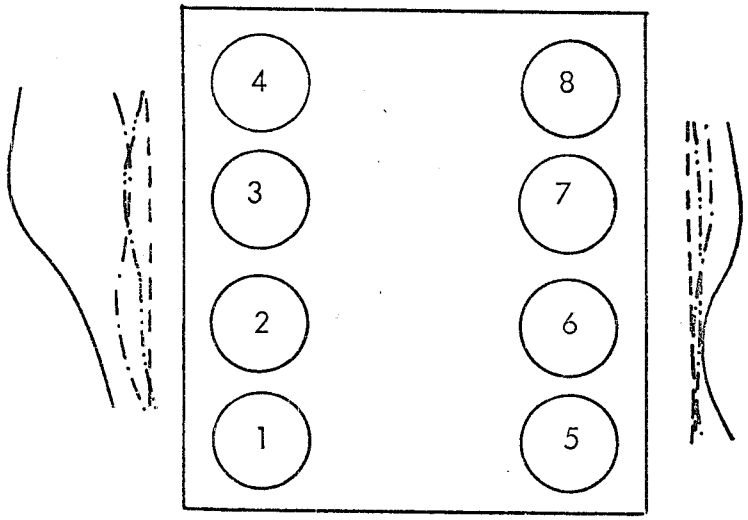

Cl_3 Firing

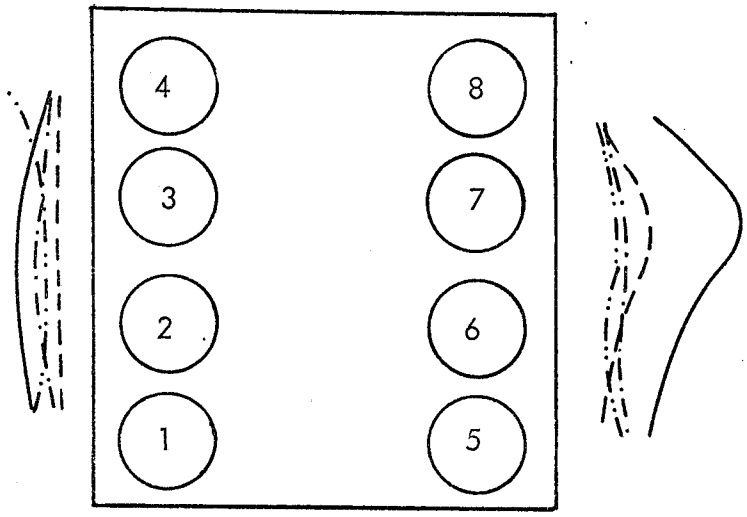

Cl_7 Firing

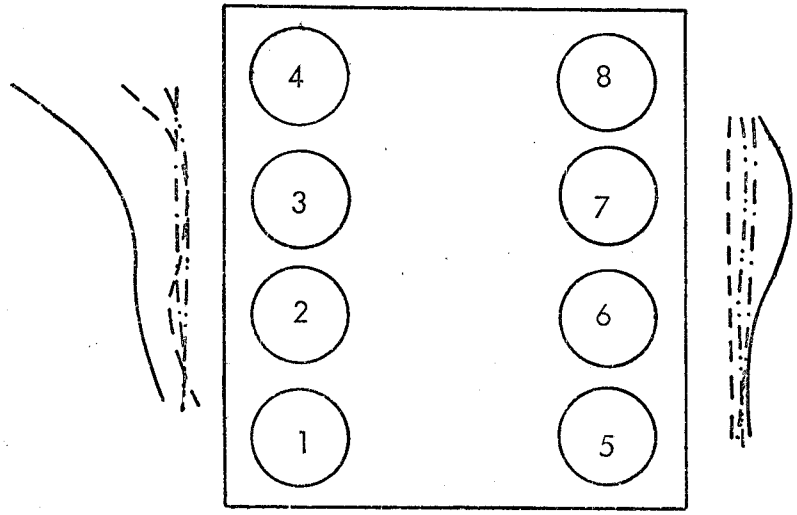

Cl_4 Firing

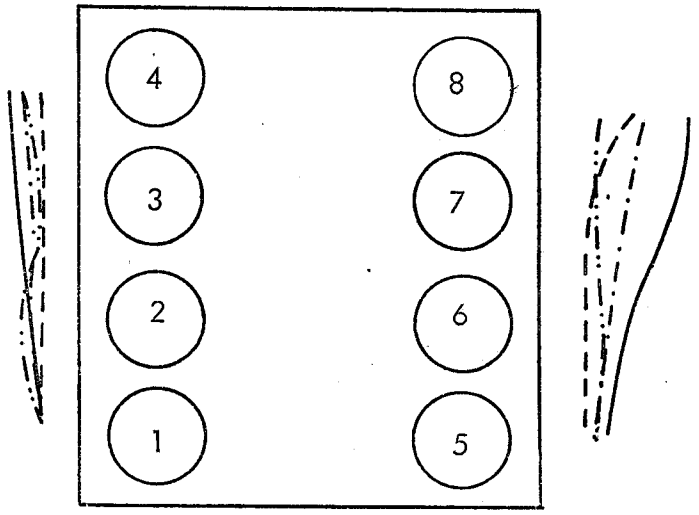

Cl_8 Firing

FIG. 4.16 MAXIMUM VIBRATION AMPLITUDE FOR SA ENGINE MAHLE @ 1500 r.p.m.

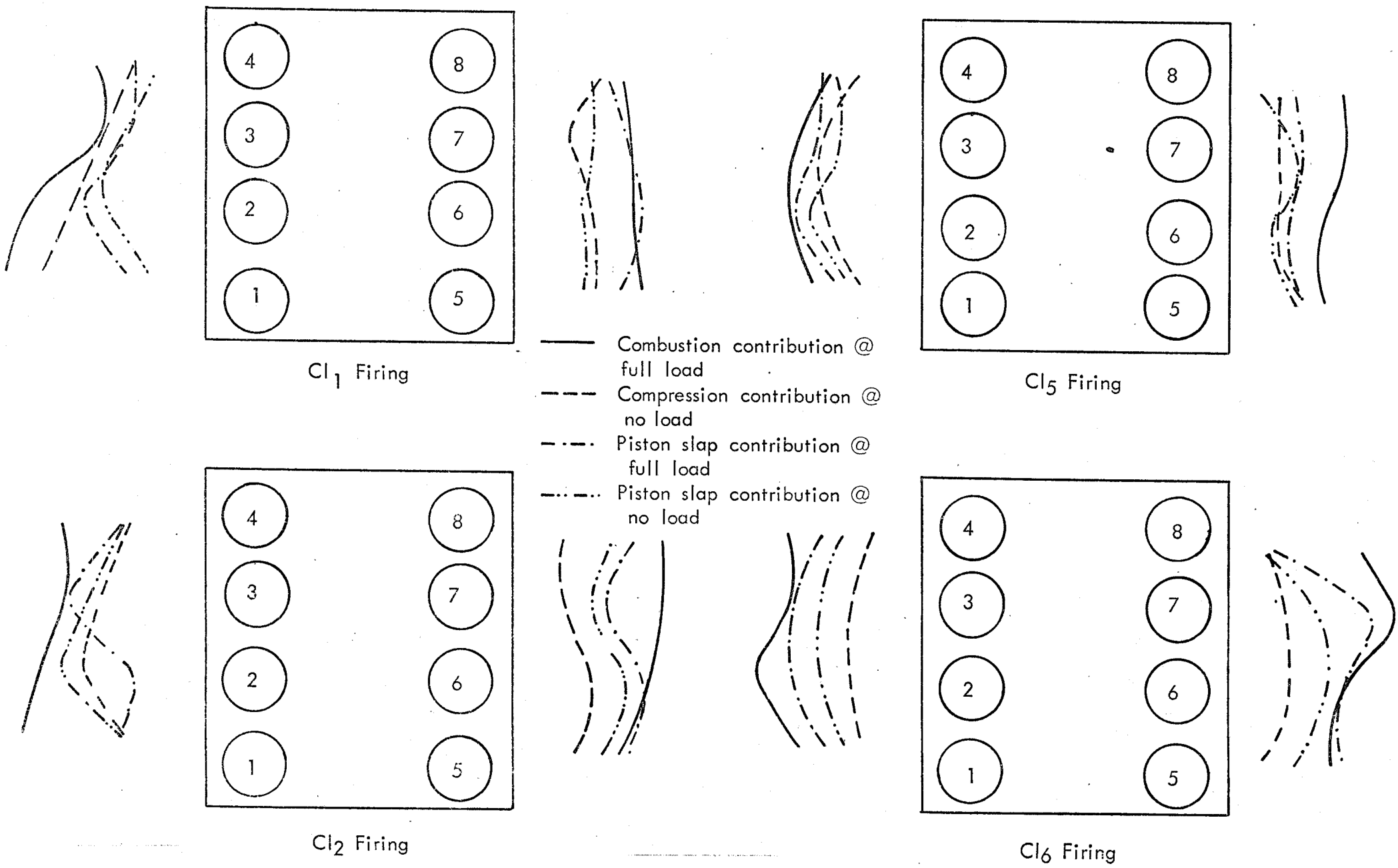

FIG. 4.17 MAXIMUM VIBRATIONS AMPLITUDES FOR SA ENGINE STANDARD @ 3000 r.p.m.

Scale: 1cm. = 16 g
"A"weighted

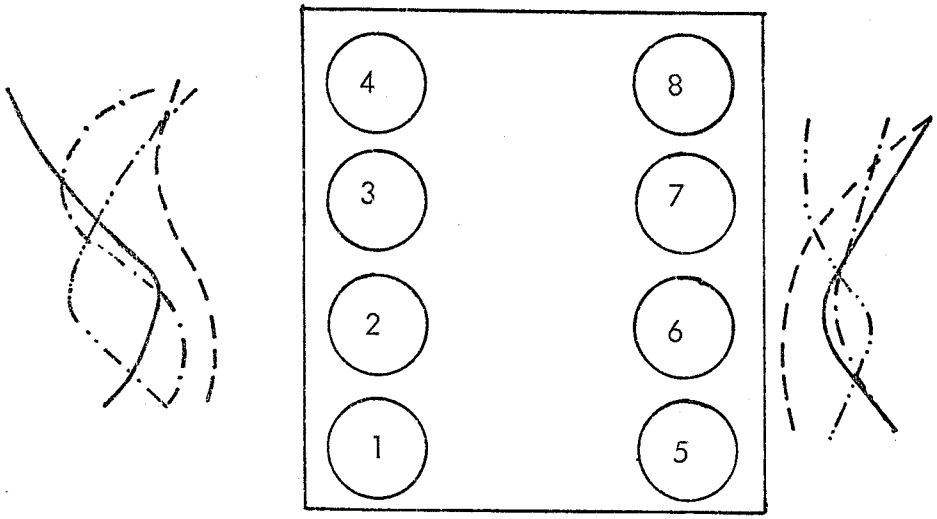

Cl_3 Firing

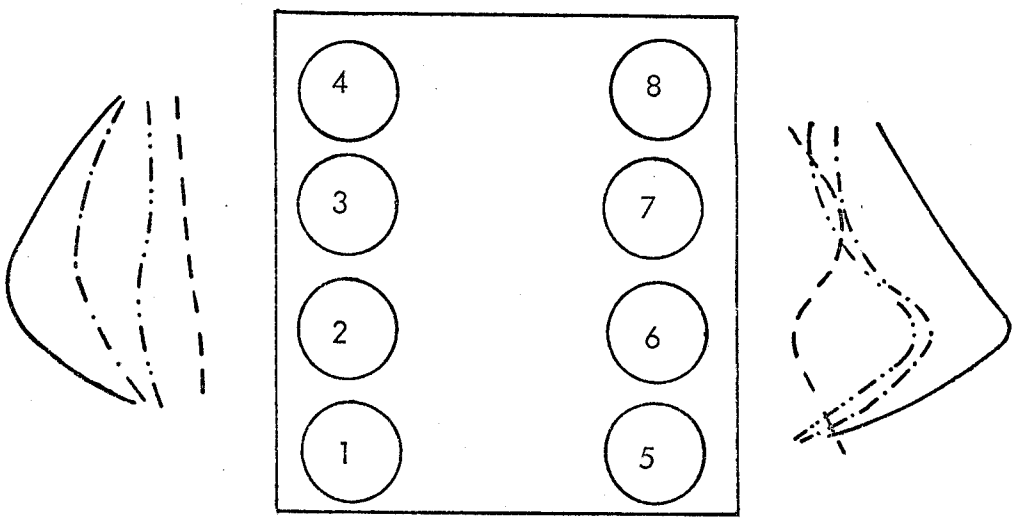

Cl_7 Firing

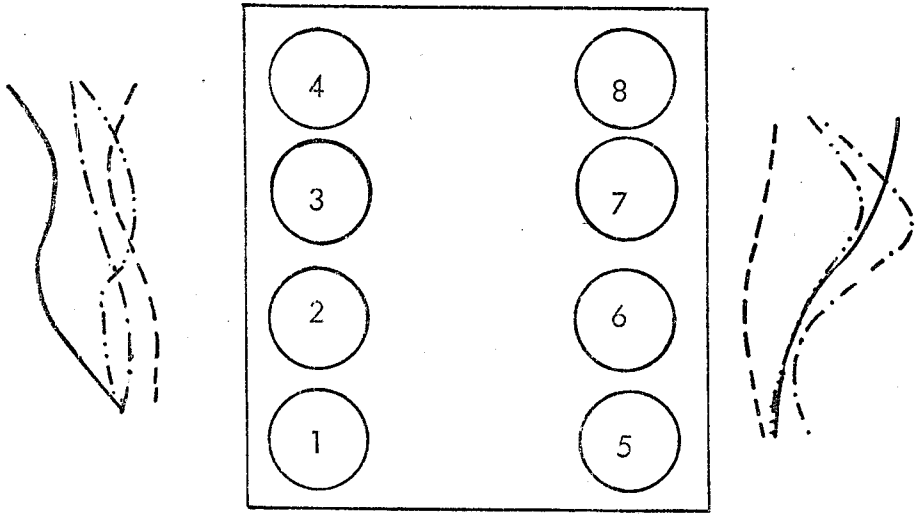

Cl_4 Firing

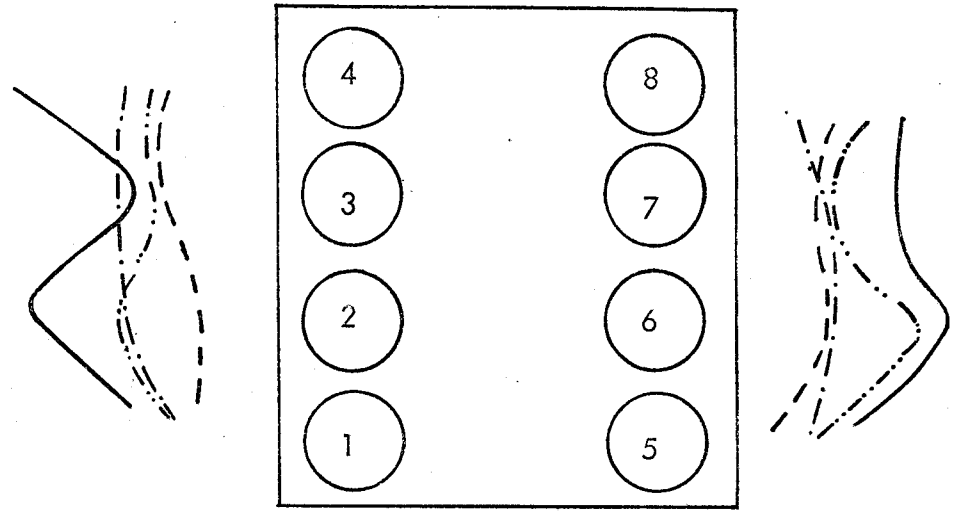

Cl_8 Firing

FIG. 4.18 MAXIMUM VIBRATION AMPLITUDES SA ENGINE STANDARD @ 3000 r.p.m.

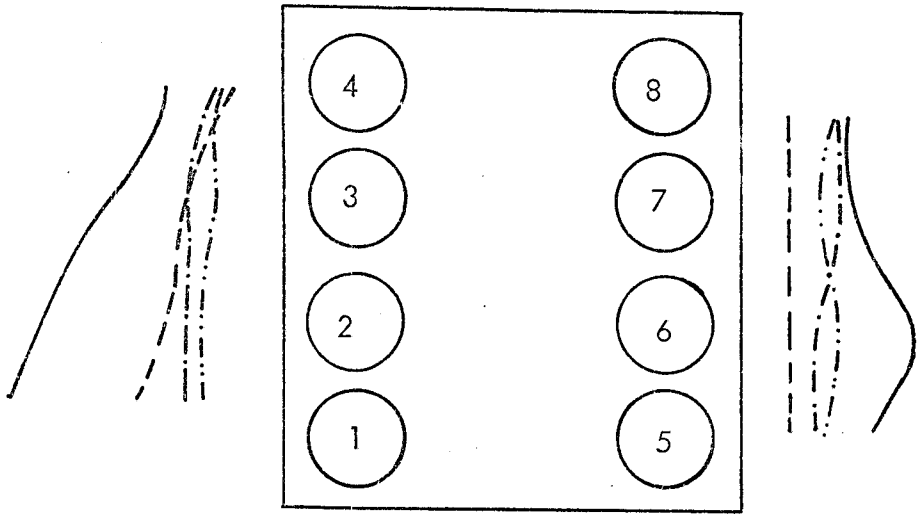

Cl_1 Firing

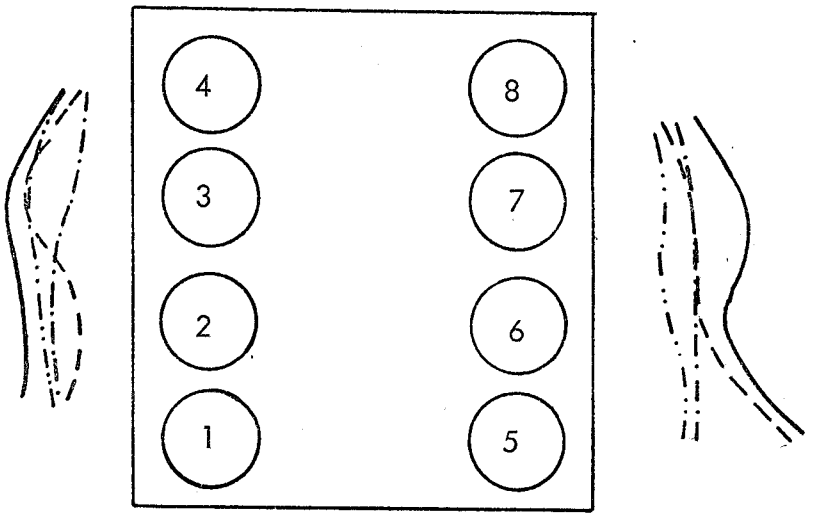

Cl_5 Firing

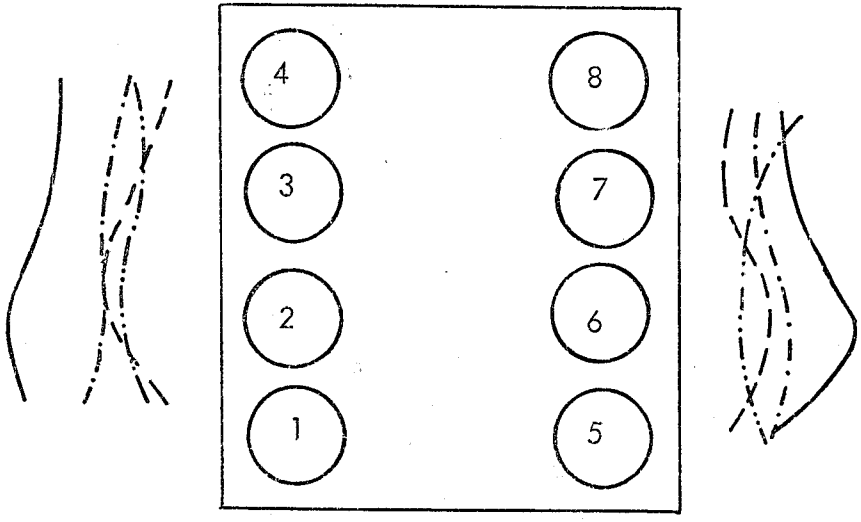

Cl_2 Firing

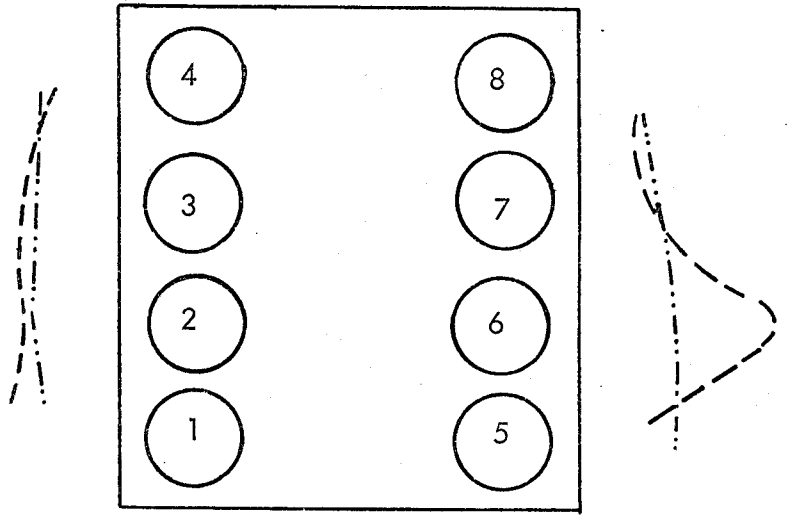

Cl_6 Firing

FIG. 4.19 MAXIMUM VIBRATION AMPLITUDES FOR SA ENGINE MAHLE @ 3000 r.p.m.

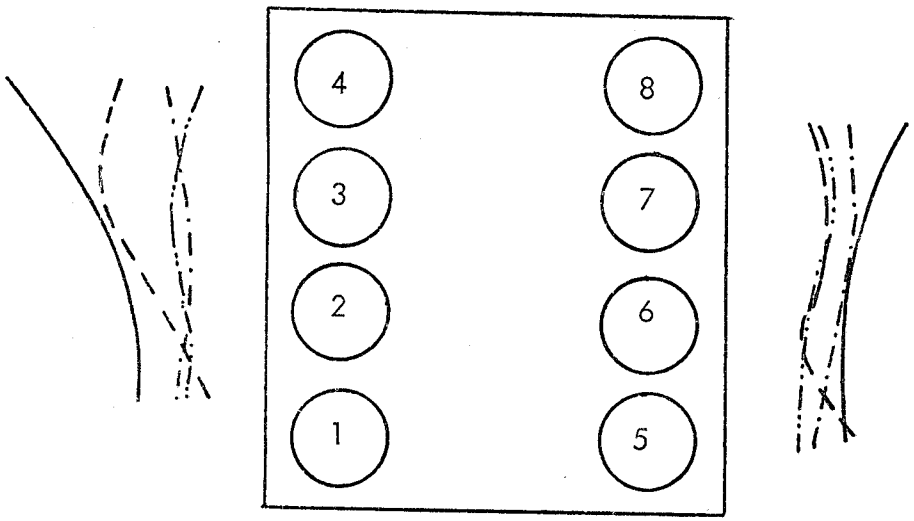

Cl_3 Firing

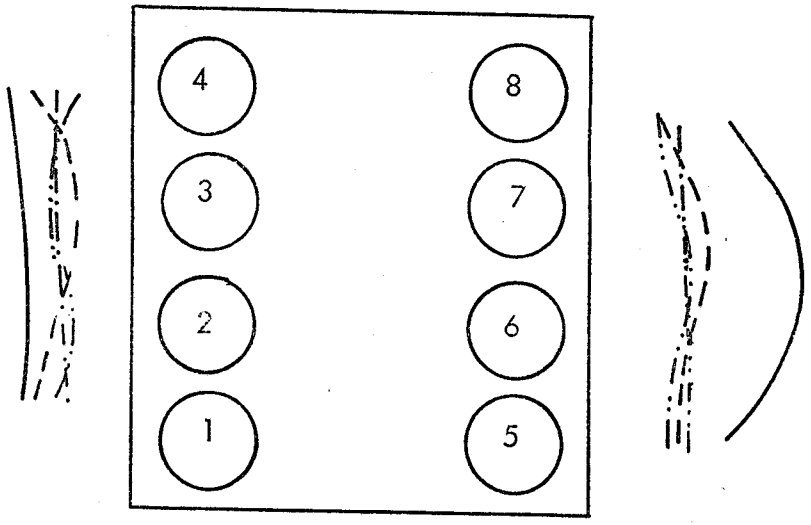

Cl_7 Firing

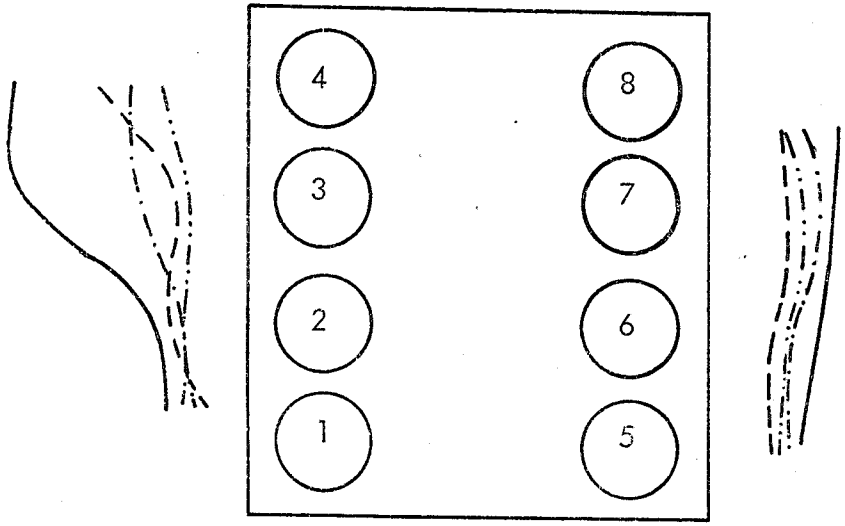

Cl_4 Firing

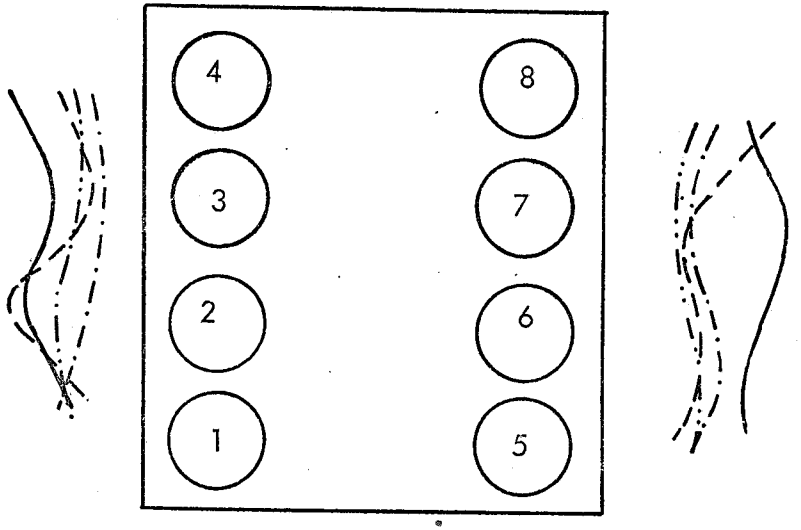

Cl_8 Firing

FIG. 4.20 MAXIMUM VIBRATION AMPLITUDES FOR SA ENGINE MAHLE @ 3000 r.p.m.

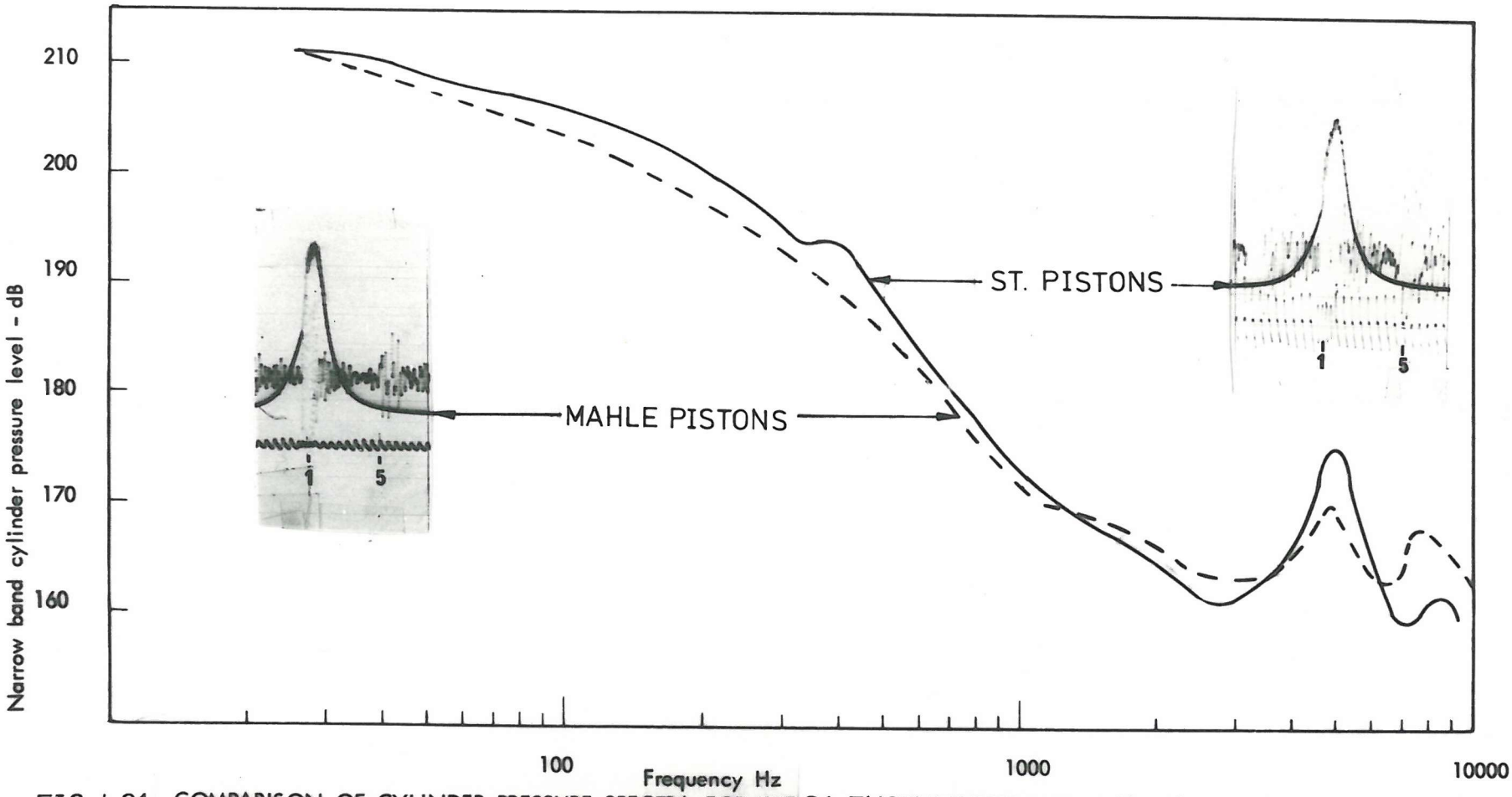

FIG. 4.21 COMPARISON OF CYLINDER PRESSURE SPECTRA FOR THE SA ENGINE FITTED WITH STANDARD AND MAHLE PISTONS @ 3000 r.p.m. FULL LOAD.

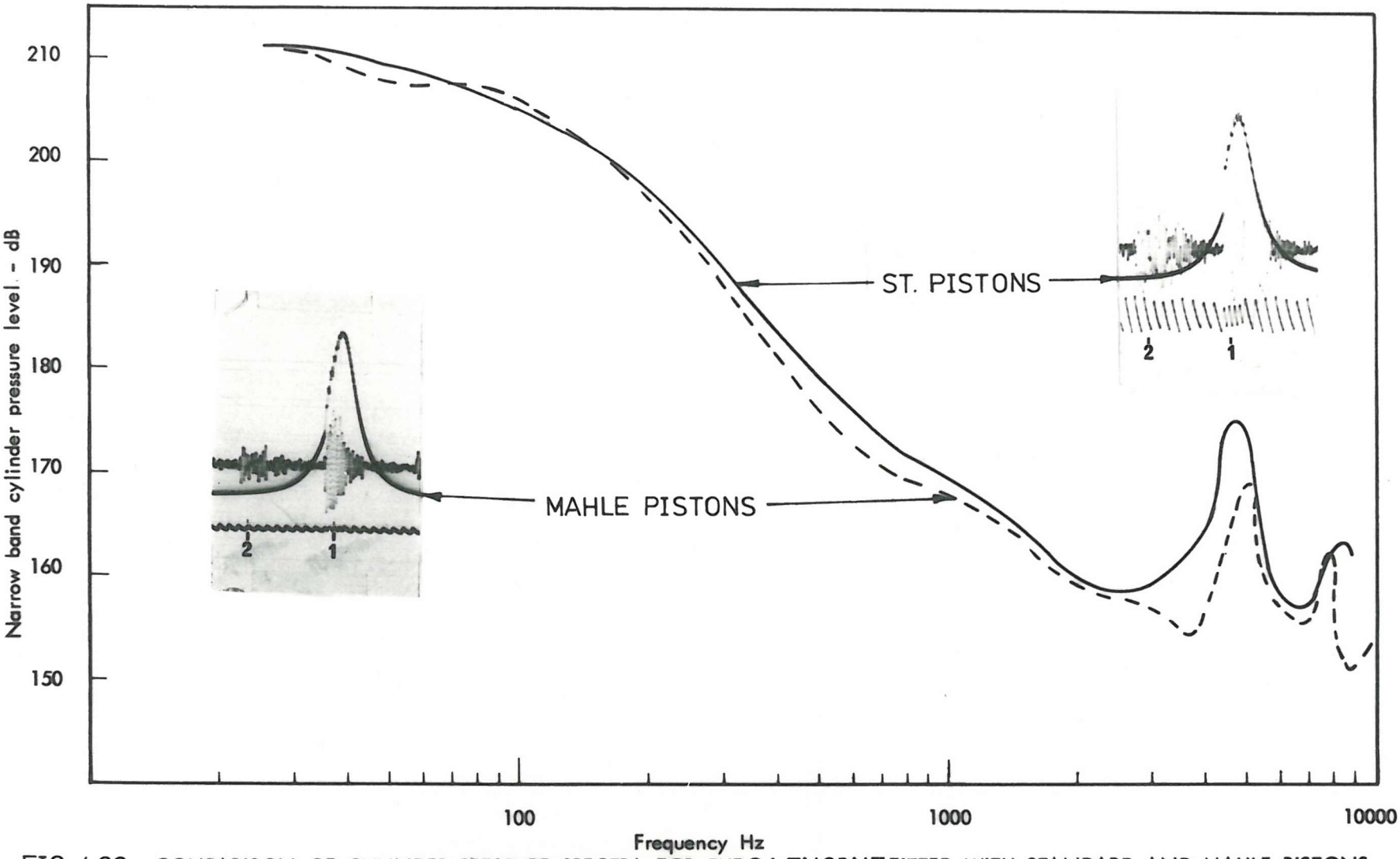

FIG. 4.22 COMPARISON OF CYLINDER PRESSURE SPECTRA FOR THE SA ENGINE FITTED WITH STANDARD AND MAHLE PISTONS @ 2000 r.p.m. FULL LOAD.

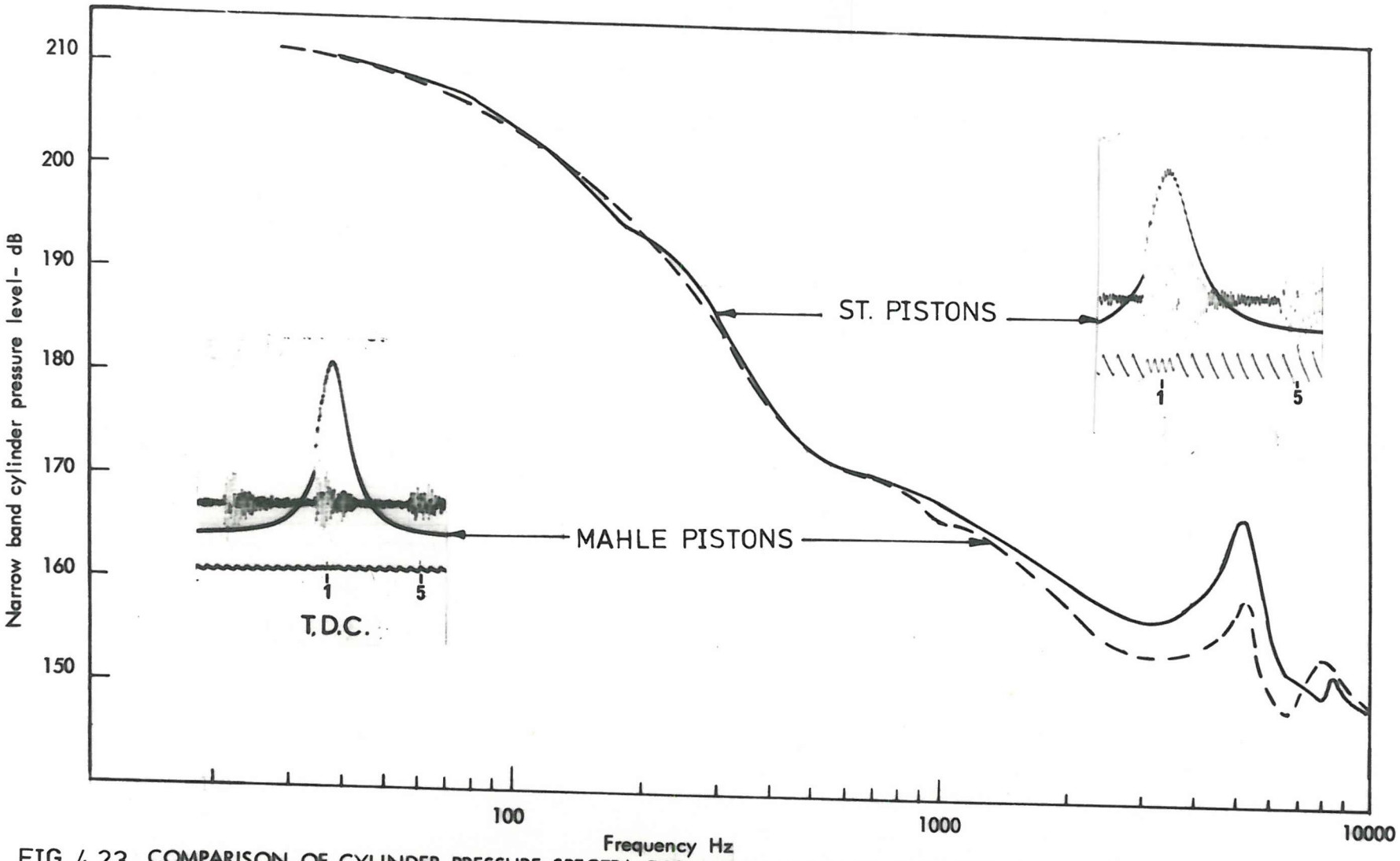

FIG. 4.23 COMPARISON OF CYLINDER PRESSURE SPECTRA FOR THE SA ENGINE FITTED WITH STANDARD AND MAHLE PISTONS @ 1500 r.p.m. FULL LOAD.

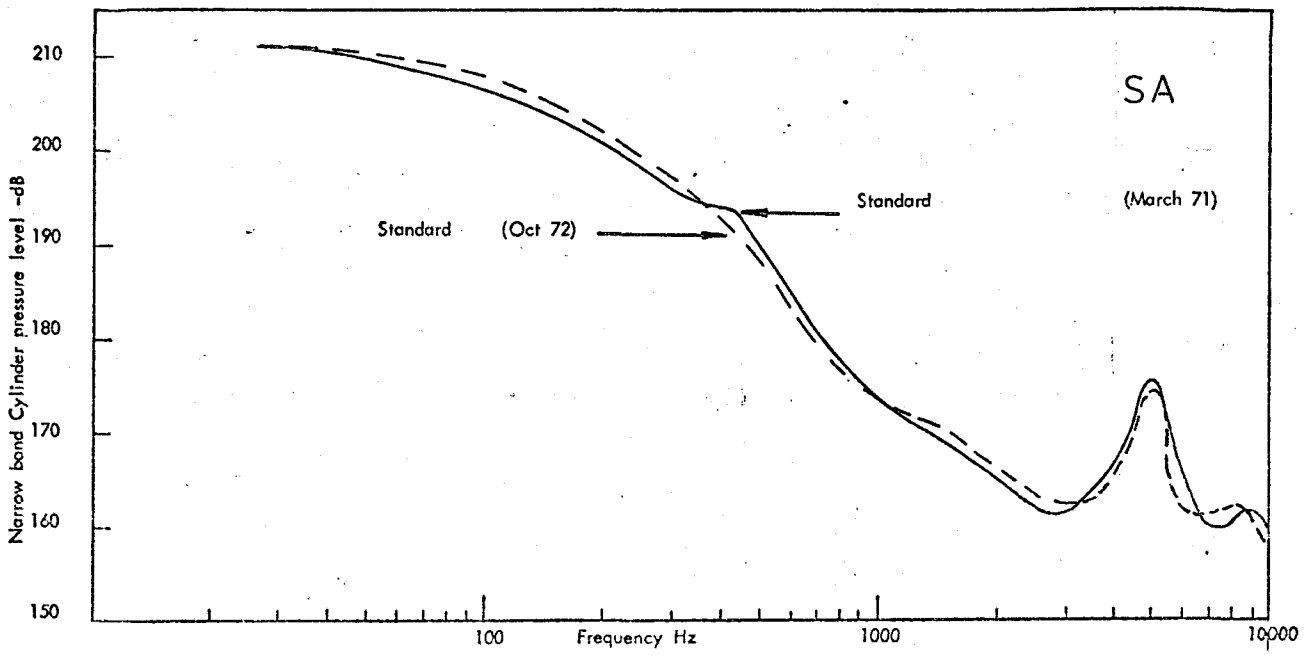

FIG. 4.24 COMPARISON OF CYLINDER PRESSURE SPECTRA FOR THE SAME MAKE AND TYPE OF ENGINE TESTED UNDER NEARLY IDENTICAL CONDITIONS @ 3000 r.p.m. FULL LOAD.

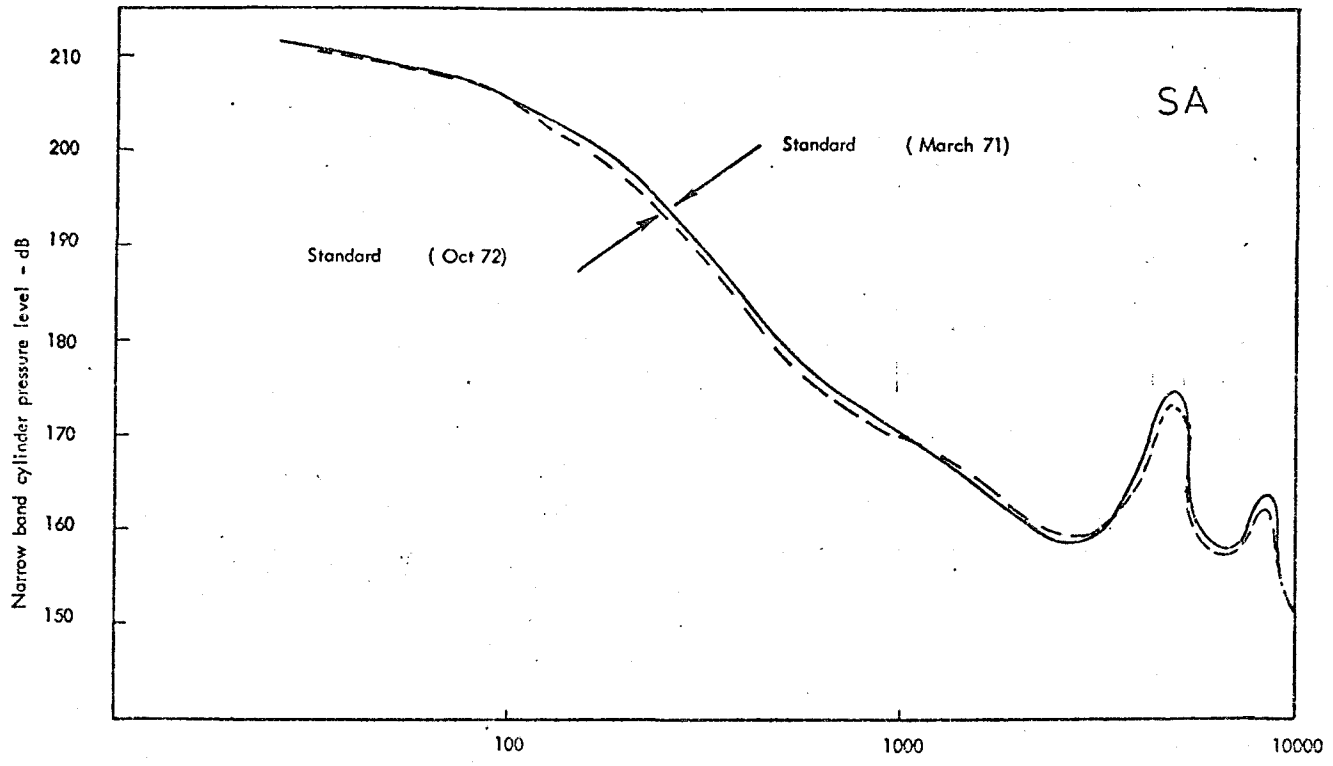

FIG. 4.25 COMPARISON OF CYLINDER PRESSURE SPECTRA FOR THE SAME MAKE AND TYPE OF ENGINE TESTED UNDER NEARLY IDENTICAL CONDITIONS @ 2000 r.p.m. FULL LOAD.

CHAPTER 5

SIMULATION OF PISTON SLAP IN NON-RUNNING DIESEL ENGINES

5.1 Introduction

As already discussed in the previous chapter, the identification and investigation of the various parameters which control piston slap in the running engine present considerable difficulties because of the presence of other exciting forces and their induced vibration in the engine structure. For that reason it was considered essential to develop a technique where realistic piston slap could be simulated in a non-running engine and thus studied in isolation from other sources.

It was found that simulation of piston slap is possible since the piston sideways force can be calculated for a particular engine as the sum of the resultants of all the forces acting through the gudgeon pin along a line perpendicular to the liner and this can be reproduced by commercially available force generators.

5.2 Development of Piston Slap Simulation Technique and Instrumentation Using an Electrodynamic Force Generator

Theoretical deductions indicated that the already known information about the piston slap event should be sufficient to develop a simulation technique. The first step was to test this experimentally. Ideally the force should be applied through the centre of the gudgeon pin. This is only possible by cutting a slot through the block and liner to accommodate the force transmitter, therefore altering the structural response of the engine. An in-line engine of which noise and vibration results were available was chosen for the preliminary tests.

One piston was made to slap the liner using a small electrodynamic vibration generator via a rod connected to an extension block fitted to the

top of the piston crown. The force in the rod was measured as near as possible to the piston using a Kistler 902A load washer. In this arrangement the piston was given an extraneous moment and therefore a correction had to be applied to arrive at the correct side force actually acting through the gudgeon pin. Piston movement was monitored using a Wayne Kerr capacitive probe "C". Liner vibration, block vibration and noise were recorded for various forces and repetition rates.

The photograph, fig. 5.1, shows this piston slap rig and the method of applying and measuring the side force, piston movement, liner and block vibration.

Figure 5.2 shows the layout of the instrumentation used for the study of piston slap simulation on this engine. In these tests it was intended to simulate the major slap around T.D.C. although other minor slaps are equally possible to simulate.

Starting with known cylinder pressure diagrams and physical parameters of the engine the side force at every condition was calculated using the following formula (see ref. 3.1)

$$\text{Side force} = A \sin\theta \frac{Pr}{\ell} + B \sin\theta \left| (M + m_p)\omega^2 r \frac{r^2}{2\ell^2} + m(k^2 - ab) \frac{\omega^2 r}{\ell^2} \right| - B \sin 2\theta \left| (M + m_p) \frac{\omega^2 r^2}{2\ell} \right| - B \sin 3\theta \left| (M + m_p) \frac{\omega^2 r^3}{2\ell^2} \right| \quad (5.1)$$

where A = piston area in (in^2)

B = constant $= \pi^2/900 \times 386$

m = mass of con rod (lb)

M = mass of piston (lb)

m_p = equivalent mass of con. rod at small end (lb)

r = crank radius (in)

ℓ = connecting rod length (in)

ω = angular speed of crankshaft (rev./min)

k^2 = (radius of gyration of con. rod)^2 in (in^2)

θ = crank angle in degrees

P = gas pressure corresponding to θ (in psi)

a = distance of C. of G. of con. rod from big end (in)

b = distance of C. of G. of con. rod from small end (in).

Figure 5.3 shows a typical calculated side force using this formula for the engine at 1000 r.p.m. full load. To translate this case to the piston slap rig simulation, the following points were considered:

(a) The major slap was taken to apply around T.D.C. at the rotational frequency corresponding to the engine speed (ex. 1000 rpm ≡ 16.7 Hz) and so the vibrator simulating this side force was made to vibrate at this frequency.

(b) It can be observed that the side force around T.D.C. is very similar to a sawtooth waveform but for the purposes of the preliminary tests on this rig it was approximated to a sinusoidal force. For sinusoidal excitation a B & K Beat Frequency Oscillator type 1022 was used.

(c) From the oscillographic study conducted on running engines it could be deduced that at any instant the contribution of piston slap can be identified from a specific cylinder. Therefore exciting one piston in the engine was considered sufficient.

It was found that the small capacity of the vibration generator (maximum force of 50 lbf) made it difficult to obtain the correct rate of rise of piston sideways force (K) shown in Figure 5.3. Figure 5.4 shows a typical piston side force variation which was possible using this set up at a repetition rate of 16.7 Hz corresponding to an engine speed of 1000 revs/min. It can

be observed that the 'slap' did not occur at the thrust side. By increasing the input force to the maximum available it was just possible to simulate the slap around T.D.C. as shown in figure 5.5, for a repetition rate of 33.3 Hz corresponding to an engine speed of 2000 revs/min. Despite the various shortcomings of this simulation rig, many useful tests were carried out to establish some of the following important information related to piston slap as a source of noise and vibration.

(a) The vibration response on the block resembles that on the running engine in relative frequency content as shown in figure 5.6 at a repetition rate of 46.7 Hz corresponding to engine speed of 2800 revs/min.

(b) The vibration response is greatest at the top of the block coinciding with the centre line of the impacting piston.

(c) The introduction of an oil film in the piston to bore clearance alters the engine block vibration response.

(d) Liner vibrations are transmitted to the whole engine block and crankcase which subsequently radiate the noise.

One of the disadvantages of this system was that the applied force was distorted due to back e.m.f. in the electrodynamic vibration generator. Therefore, it was concluded that a larger force generator was needed with minimum feedback.

5.3 Piston Slap Simulation using a Hydraulic Force Generator

A new piston slap simulation rig was built using a 1250 lbf hydraulic force generator. In this instance a Vee engine, which already was used for piston slap study by oscillographic method, was employed and mounted rigidly on a frame as shown in figure 5.7. The hydraulic vibration generator was mounted on a specially fabricated beam support so that its central axis is perpendicular to the centre line of No. 3 cylinder. The sideways force on the piston was applied through twin back-to-back connecting rods as shown in figure 5.8. In this arrangement the crankshaft acts as a

pivot transferring the applied force equal and opposite to the centre of the gudgeon pin. The force was measured using a Kistler 9331 force transducer mounted to the connecting rod as shown in figure 5.9. The big end bearings of the crankshaft were packed with grease to prevent distortion of the applied force due to possible impacts which may occur in the plain bearings.

This system therefore offers close approximation to actual conditions in the engine. Theoretical and experimental analyses were conducted to show that the inertia of the back-to-back system of connecting rods has little effect in modifying the force and therefore no correction was necessary (see Appendix A).

Certain difficulties were experienced during the initial tests. Since the vibrator consists of a double acting hydraulic jack controlled by an electrically driven valve, in conjunction with a displacement transducer, the operation tends to be sluggish and drifts occur as shown in figure 5.10. It was necessary to design the force transducer fixing bolt to break before damaging the transducer itself. The original system of the generator and the driving electronics had a specially fitted force transducer with a feedback system ensuring the application and balance of a constant force. In this instance it was necessary to adjust the equilibrium of the vibration generator manually through careful observation of a specially fitted pointer as shown in Figure 5.10. In addition, considerable effort was made towards improving the sensitivity of the driving electronics.

Figure 5.11 shows some of the instrumentation used with this piston slap rig while figure 5.12 shows a general layout of the instrumentation and circuit diagram. The piston skirt was fitted with two movement transducers (T4 proximity gauges) and a pressure transducer (Kistler 601A) as shown in figure 5.8.

5.4 Test Results

The calculated side forces were obtained for the V8 engine for various conditions using equation 5.1 . Figure 5.13a shows a typical side force for the Vee engine at 1000 revs/min full load. Initially, a sinusoidal approximation was used. However, it was found that to obtain the correct rate of rise of force with sinusoidal excitation, excessive peak forces were necessary which in some cases were beyond the full capacity of the force generator (see Appendix B).

An attempt was made to simulate electronically the sideways force waveform as shown by the dotted line in figure 5.13b. Figure 5.14 shows the circuit diagram of the oscillator capable of producing this idealised force waveform. This oscillator was originally designed by Dr. White of ISVR (ref. 5.1). It was slightly modified to enable certain adjustments to the resultant waveform to be made, that is VR4 to vary the symmetry while VR6 adjusts the converter input. The type of waveform obtained with this is shown in figure 5.13c.

Only one piston (Piston no. 3) was excited at T.D.C. and vibration response measured at the top of the block centre line of no. 3 cylinder (position $C\ell_3$). This is considered adequate since the instantaneous response at position $C\ell_3$ has been found to be due to the T.D.C. slap of no. 3 piston. At higher engine speeds there is some interference from the adjacent cylinders and therefore it would be preferable that two adjacent cylinders were excited, but this was found impossible in this case because of the non-availability of another force generator and the driving electronics.

5.4.1 Comparison of running engine vibration response with the simulated response

Using the special oscillator it was found difficult to simulate all engine conditions of speed and load using the hydraulic vibration generator. The orders of magnitude obtained, however, were within the practical range. This enabled the confirmation and correlation of the piston slap induced

vibration on the rig with that on the running engine.

In the process of this study, 1/3 octave analyses of force and response were made. Also photographs of these were taken from a storage oscilloscope to obtain the detailed information of the events. Figure 5.15 is a typical oscillogram showing:

(a) Force waveform where the rate of force rise (K), rates of fall and maximum peak values can be estimated. It is also observed that the force waveform is somewhat distorted because of the back-to-back system resonance.

(b) Upper and lower piston skirt movements. As mentioned earlier, two inductive gauges were mounted in the piston skirt (thrust side) to record piston movement.

(c) Vibration amplitude on the cylinder block (position $C\ell_3$) using dBA weighting network of the B & K equipment. This enables one to relate maximum instantaneous amplitudes and structure response frequency to compare with that on the running engine.

In the first instance it was necessary to establish the controlling parameters of the sideways force affecting piston slap response. In the running engine it is impossible, for example, to tailor the piston sideways force but the rig offers this facility. Tests were carried out to compare the vibration response with varying rate of rise of piston side force, rate of fall and peak values. It was found that the rate of force rise (K) is the most important controlling parameter affecting piston slap response. Therefore the effect of rate of side force was investigated in detail at repetition rates corresponding to engine speeds of 1000, 1500, 2000 and 3000 rpm with rates of side force ranging from 10 to 500 lbf/msec; a range of 50:1. In some cases even higher rates of force rise were used for short periods to record maximum instantaneous vibration amplitudes at position $C\ell_3$ and to compare with the running engine conditions. The actual rates of side force in the running engine at no load are 190-500 lbf/msec and at full load are

500-1200 lbf/msec. At higher rates beyond 500 lb/msec, the system was becoming dangerously unstable due to difficulties in the manual control of the force generator which made it unadvisable to leave it operating at those conditions for the duration required for on-line analysis. Tape recordings were also made as an alternative and were found useful for later analysis.

The effect of the rate of side force for the corresponding engine speed of 1500 revs/min is illustrated in figures 5.16-5.20 for K = 9, 18, 47, 60 and 90 lbf/msec. These tests were made with no oil film present in the piston to bore clearance. The figures also show the frequency analyses (1/3 octave using B & K equipment) of the force input which shows an approximate decay of force components by about 20 dB/decade. Also shown in these figures are the measured response spectra of the engine block at the position $C\ell_3$. The data from these measurements are summarised in Table 5.1, which also includes information obtained from the relevant oscillograms. Figures 5.21 and 5.22 show the plotted relationship between vibration response of the cylinder block with rate of rise of piston sideways force at individual third octave frequency bands. As can be seen, the vibration amplitude is proportional to the logarithm of the rate of side force which increases by about 20 dB per tenfold increase of the rate of side force (K). The following general relationship can be used for estimating the vibration response at a certain engine speed

$$V_R \propto \log K \qquad (5.2)$$

where V_R = engine vibration response of the cylinder block

K = rate of rise of piston sideways force - lbf/sec.

Since the calculated rates of sideforce (K) at full load and no load are known for the running engine (see Table 1B, Appendix B), it is possible by extrapolation of the data to obtain the vibration response at these

conditions for each 1/3 octave frequency band and so to derive the vibration levels that could be expected in the running engine. This was carried out for conditions corresponding to engine speeds of 1000, 1500, 2000, 3000 and 3300 revs/min. It is worth mentioning that at no load conditions it was possible to obtain on-line experimental vibration spectra which agree reasonably with the extrapolated data.

Figures 5.23a, b show simulated vibration spectra of the cylinder block compared with that measured on the running engine at 1500 rpm for full and no load respectively. The agreement is fairly good, especially when remembering that the measured spectra on the running engine include responses to other sources. A better agreement was obtained when comparing the simulated spectrum with the analysed spectrum derived from the pulses only due to piston slap determined from the vibration oscillograms taken on the running engine (see Appendix C).

Figures 5.24-5.26 show the spectra of block vibration from the running engine and derived spectra from the rig test at full load speeds of 1000, 2000 and 3000 revs/min respectively. The agreement is generally better at lower speed.

5.4.2 Effect of engine speed on piston slap induced vibration

Using the data obtained from the rig tests it is possible to establish the relation between piston slap induced vibration and engine speed in the absence of any other source. Typical results of this relationship are presented in third octave frequency bands for conditions corresponding to engine full load as shown in figure 5.27. The piston slap induced vibration in most frequency bands increases by about 20 dB per tenfold increase of engine speed.

In the running engine, the rate of side force (K) increases with engine speed as shown in figure 5.28. The log K factor increases by about 16 dB per tenfold increase of engine speed.

From the simulated rig results it is also possible to establish the effect of repetition frequency (engine speed) and vibration response when the rate of side force K is kept constant. Figure 5.29 illustrates this effect for values of K = 10, 100 and 1000 lbf/msec, at two typical 1/3 octave frequency bands. The repetition frequency has small effect on the vibration response at constant rate of side force (K). It amounts to about 3-5 dB per tenfold increase in repetition frequency or engine speed.

By taking both relationships into account it will be seen that in general it can be expected that piston slap induced vibration in the engine increases by about 20 to 22 dB per tenfold increase of engine speed thus confirming the results obtained in the running engine.

5.4.3 Effect of oil film on piston slap induced vibration

Lubricating oil and gas oil were mixed in order to achieve a viscosity similar to that of lubricating oil at operating temperatures in a running engine. This oil was injected continuously at the top of cylinder no. 3 through the injector hole. Sideways force, piston movement, and vibration response were measured for various conditions and compared with the corresponding data obtained for the dry case as shown in Figures 5.30a, b, c, d, e and f.

Some of the following observations can be made from these figures. The effect at 1000 revs/min is negligible. At 2000 revs/min, the oil film reduces the vibration response in the frequency range from 5000 Hz upwards. At higher speeds the reduction in vibration is seen in the frequency range from 800 Hz upwards.

Figure 5.31 shows typical oscillographs corresponding to engine speeds of 1000 and 3000 revs/min with and without the oil film present. These oscillographs show that the oil film has a marked effect on the piston movement. Generally it appears to delay the slap at the top of the skirt. At

some conditions it could also be observed to be capable of preventing contact with the liner. The bottom of the skirt appears to follow the same course as for the dry condition but rebound is somewhat attenuated.

With the oil film the shape of the input force is slightly smoothed. However, the 1/3 octave analyses of force shown in Figures 5.30a-f, show close similarity throughout the frequency range whether wet or dry.

The 1/3 octave analyses of the vibration response show that for the dry condition, the spectra exhibit marked peaks around 1250 Hz while for the wet condition the peaks appear both at 1250 Hz and 2500 Hz. The oscillographs of piston movement and block vibration response shown in figure 5.31 were analysed to determine the frequencies of piston rebound and block response. It can be seen that the rebound frequency of the piston lower skirt (800-1250 Hz) is of the same order as that of the first peak in the vibration response spectrum (≈ 1250 Hz). Also the peak at 2500 Hz is near the important natural frequency of the liner showing that the oil layer may act as a stiff film exciting the liner directly by hydraulic force (for calculated natural frequency of the liner, see Appendix D).

The oil film effect on the piston liner response may be explained in greater detail as follows:

For the Cantilevered Mode** the oil film acts as an auxiliary damper, as shown in Sketch 1, which tends to affect liner vibration around 2500-2900 Hz.

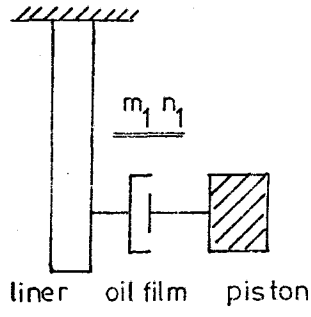

Sketch 1

** See next page

For the liner Ovalling Mode **
(≃ 1700 Hz) the oil film has a more direct effect as shown in Sketch 2.

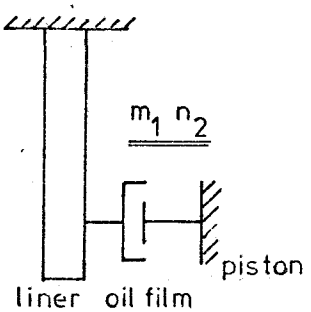

Sketch 2

This may explain the tendency for the components of the response spectrum to increase around 2500 Hz and decrease slightly around 1600 Hz since the oil film appears to have greater effect on damping the motion in the ovalling mode.

Effect of piston to bore clearance on piston slap induced vibration

All the previous tests on the rig have been conducted using standard pistons with average piston to bore clearance of .012". To investigate the ultimate effect of clearance, all tests were repeated using expansion controlled pistons (Mahle K.G. Ltd) which enable piston to bore clearance of .002" to be satisfactorily maintained in the running engine.

Figures 5.32a, b and c compare vibration response spectra at $C\ell_3$ for the expansion controlled pistons and standard pistons at the dry condition both excited with the same values and forms of piston sideways force at repetition rates of 16.7, 25 and 50 Hz per second respectively corresponding to engine speeds of 1000, 1500 and 3000 revs/min.

The expansion controlled pistons reduce the vibration response of the cylinder block by about 8 dB in the frequency range from 1000 Hz and upwards. The effect at frequencies below 1000 Hz is negligible. With

---

** 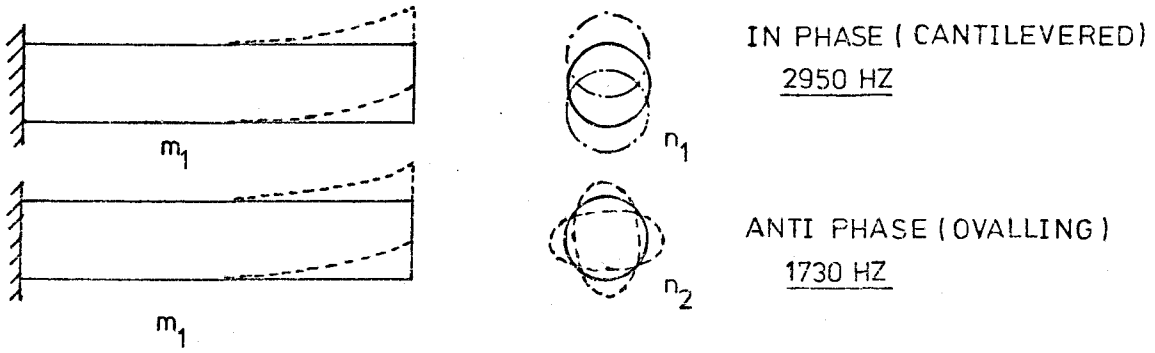

increasing engine speed the reduction becomes greater. The effect of oil film with these two pistons is illustrated in figures 5.33a, b and c, when excited by the same level and shape of side force at repetition rates of 16.7, 25 and 50 per sec respectively. The effect is only in the higher frequency range except at high speeds where the reduction in vibration response is somewhat smaller.

It is also of interest to compare the reduction in block vibration levels obtained by using the expansion controlled pistons on the rig with that on the running engine derived from the oscillographic study. This is by comparison in terms of the maximum instantaneous vibration amplitudes (in g) of the cylinder block for the two pistons. The following table 5.II summarises these values for the engine under no load conditions.

Table 5.II

Engine Speed Revs/ Min.	Running Engine: Maximum Instantaneous vib. amp. at $C\ell_3$ in (g)		Running Engine: Reduction in block vibration		Piston Slap Rig Dry: Max. Inst. Vibn. Amp. in g		Piston Slap Rig Dry: Reduction in vibn.		Piston Slap Rig Wet: Max. Inst. Vibn. Amp. in g		Piston Slap Rig Wet: Reduction in vibn.	
	St. Pistons	Mahle	in g	in dB	St.	Mahle	in g	in dB	St.	Mahle	in g	in dB
1500	27.2	12.8	14.4	6.6	37.2	10.5	16.7	11.3	23.5	10.2	13.3	7.5
2000	32	11.2	20.8	8.8	42.7	13.5	29.2	11.5	-	-	-	-
3000	38.4	14.4	24	9.2	52	14	31	11.6	35.5	12	23.5	9.8

Comparing the running engine case with the wet case in the rig, it can be seen that there is good agreement of vibration reduction resulting from the use of expansion controlled pistons. This conclusion is most important, indicating that piston development can be carried out on the rig and so an estimation may be made of the effect of piston slap in the running engine.

5.4.4 Effect of oil film viscosity

Figures 5.34a and b present force response spectra showing the effect of varying oil film viscosity on the V8 rig for the standard pistons at repetition rates of 16.7 and 25 Hz respectively. It can be seen that, for the less viscous oil, the vibration levels tend to increase in the higher frequency range while in the low and medium frequency ranges the effect is less marked. This aspect of the investigation can be extended to study the non linear behaviour of the oil film under various conditions.

5.4.5 Effect of piston mass

The mass of the piston was increased by 25% by the addition of plasticene underneath the piston crown. This modification tended to increase the block response possibly due to the change of the centre of gravity of the piston.

5.4.6 Effect of crank angle variation

The crank angle at which the main impact occurred was altered by small steps around T.D.C. and was found to have only marginal effect on the response.

5.4.7 Oil film pressure measurement on the rig

Since the oil in the piston-to-bore clearance was shown to alter the force and the vibration response, it was considered relevant to study the pressure development in the oil film. A preliminary investigation was made using a Kistler 601A pressure transducer fixed in the skirt of the piston through a special adaptor located at the centre line of the gudgeon pin and recessed by 0.005" from the curved surface to prevent damage to the transducer diaphragm at impact. Figure 5.35 presents typical oscillographs of the oil film pressure development obtained for one case using the set up. As can be seen, oil pressure of about 50 to 70 psi developed during piston

impact. No further study was made on the rig but the results indicated that it should be possible to measure the oil film pressure on a running engine.

5.5 Conclusions

(1) The technique of simulating piston slap in the non running engine using a force generator offers considerable advantage for the study of piston behaviour. The rig should help engine designers to study engine vibration and noise response at an early stage even before having to assemble and run the engine in a final form. It can also be a useful tool to both improve the design parameters of pistons and liners in current production engines. In particular, the piston slap contribution can be estimated using the rig technique to establish the relevant improvements needed to the piston-liner arrangement.

(2) Piston slap can be a contributory factor to the excitation of the bank to bank mode of a Vee engine (for the engine investigated the frequency of the bank to bank mode is 1250 Hz).

(3) The conical mode of a Vee engine (around 2500 Hz for the engine investigated) is accentuated in the presence of an oil film in the piston-to-bore clearance. This is influenced by the liner cantilevered natural frequency and so may be modified by careful choice of liner parameters and methods of fixing in the engine block.

(4) The rate of rise of piston sideways force, which is related to combustion, inertia and oil film pressure, is one of the most important parameters affecting piston slap induced engine vibration and noise. In general it is found that

$$\text{Vibration Level due to piston slap at block level (at constant speed)} \propto \log(\text{rate of rise of piston sideways force, } K)$$

with an average slope of 20 dB/decade.

Also, for constant K factor, the repetition rate or engine speed has small effect on cylinder block vibration response.

Reference

5.1 R.G. White "Measurement of Structural Frequency Response by Transient Excitation". ISVR Technical Report No. 12, January 1969.

TABLE 5.I

PISTON SLAP RIG VIBRATION RESPONSE. RESULTS AT 25 Hz ≡ 1500 rev/min. - DRY

RMS Lbf	26	45	106	140	190						
P.to P. Lbf	80	160	315	425	580			--Simulated--			
Force dBLin	104	112	119.5	122	125			Full load	No load		
Rate of rise Lbf/msec	9.1	18.7	47	60	90			706	290		
Log_{10} (Rate of rise)	.954	1.272	1.672	1.778	1.954			2.849	2.462		
Vib response in dB											
at 100 Hz	42	42	60	64	67			71	64.5		
125 Hz	46	52.5	62.5	64	61			84.5	76.5		
160 Hz	53.5	58	71	70	67.5			78	74.5		
200 Hz	38	49	59.5	63	63			85.5	76		
250 Hz	40	43	49	54	64			81	72		
315 Hz	36	37	44.5	52.5	63			67	60.5		
400 Hz	36	37.5	50	54	64.5			69	62.5		
500 Hz	35	44	49	56	65.5			83	73.5		
630 Hz	44	51	51	58	66			77.5	70		
800 Hz	40	50	55.5	58	65			79	72		
1000 Hz	46.5	54	61	60	70			86	78		
1250 Hz	45	52.5	62.5	63	71			88	79.5		
1600 Hz	48	55	63.5	64	69			90.5	81.5		
2000 Hz	46.5	54	63.5	66	69			88.5	80		
2500 Hz	48	57.5	65	66	70			90	82		
3150 Hz	47	54.5	62.5	63	68			88	79		
4000 Hz	50	57.5	64	69	72			92.5	84		
5000 Hz	45.5	57	63	65.5	70.5			95	85		
6300 Hz	37	48	59.5	62	63			88.5	78.5		
8000 Hz	42	54	63	64.5	70			92.5	82.5		
10000 Hz	44.5	58	69	73	75			100	89.5		
dBA	56.5	64	74	76	80.5			103.5	95		

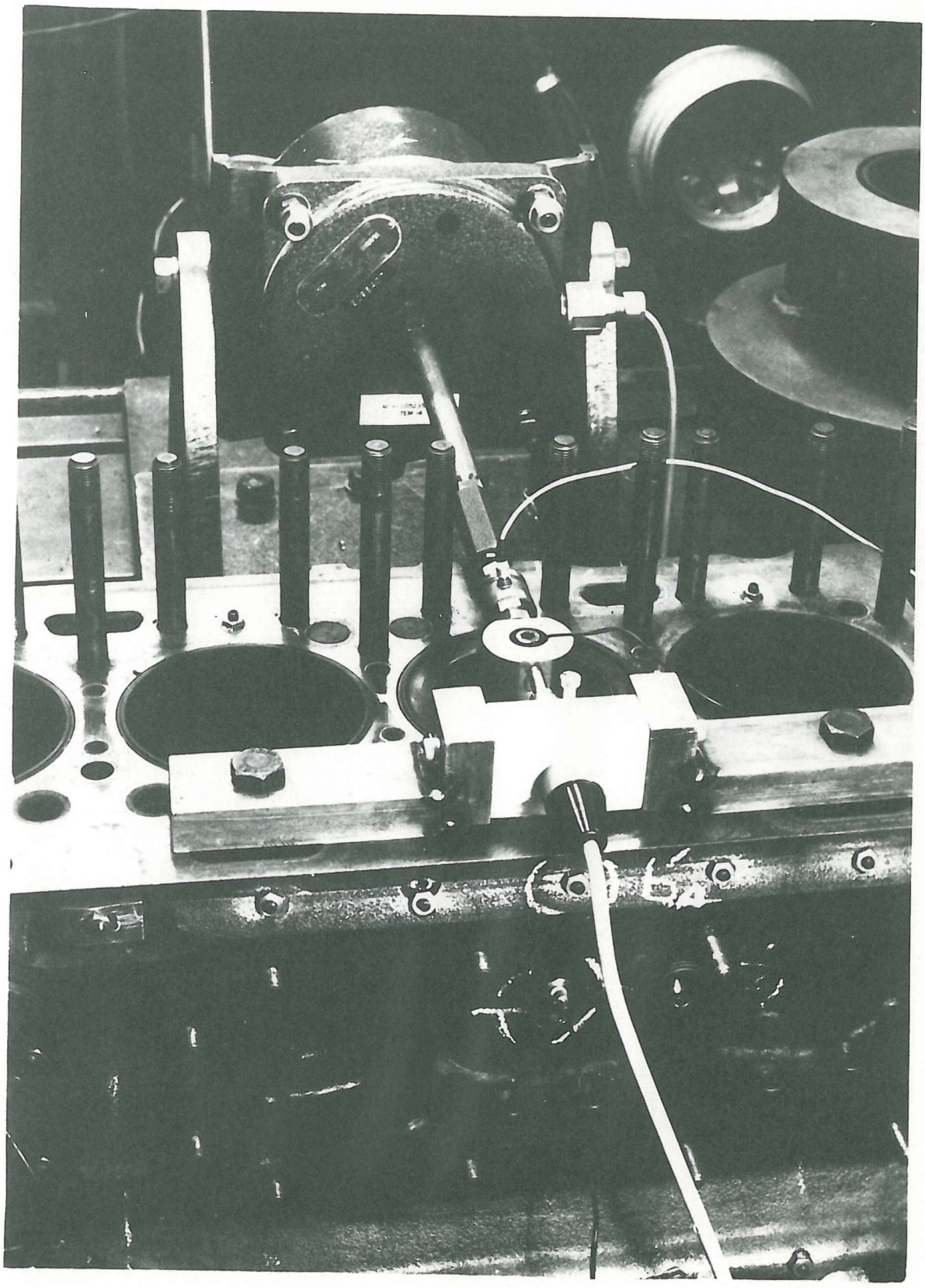

Close up of the InLine 6 Piston Slap Rig.

FIG. 5.1

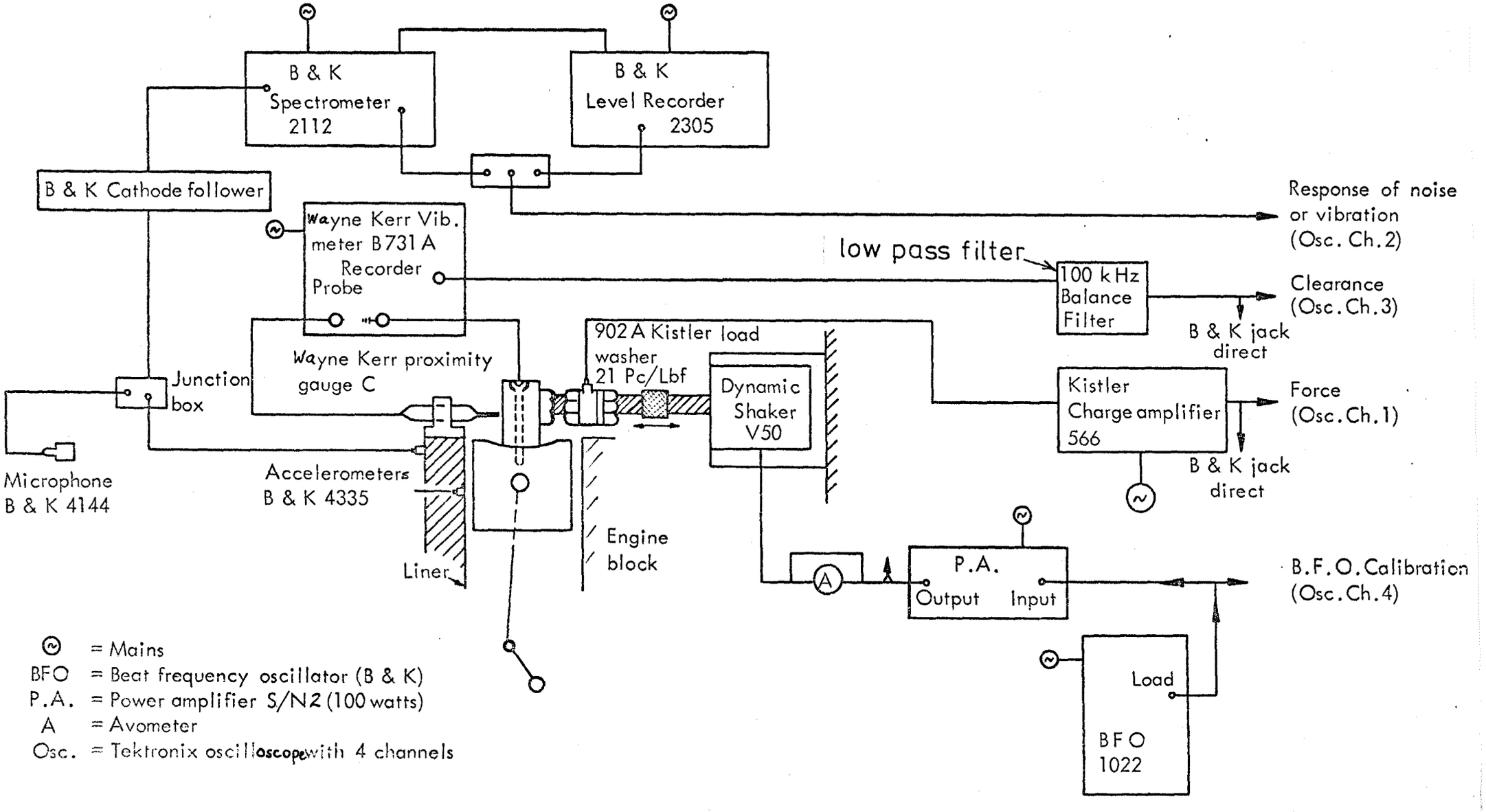

FIG. 5.2 LAYOUT OF INSTRUMENTATION AND CIRCUIT DIAGRAM FOR THE STUDY OF PISTON SLAP SIMULATION ON A SIX CYLINDER IN-LINE DIESEL ENGINE

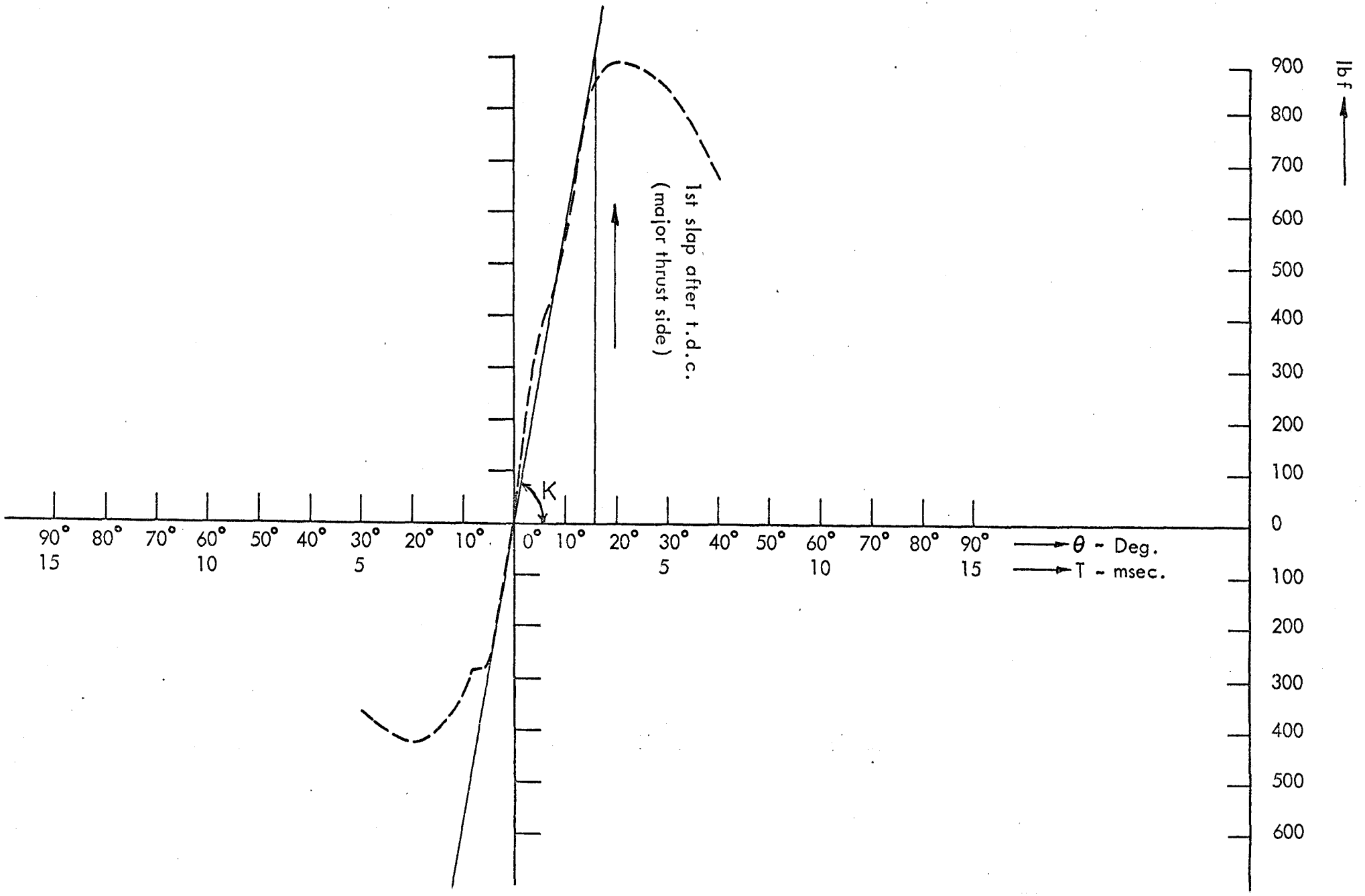

FIG. 5.3 CALCULATED PISTON SIDE FORCE OF ENGINE AT 1000 r.p.m. FULL LOAD

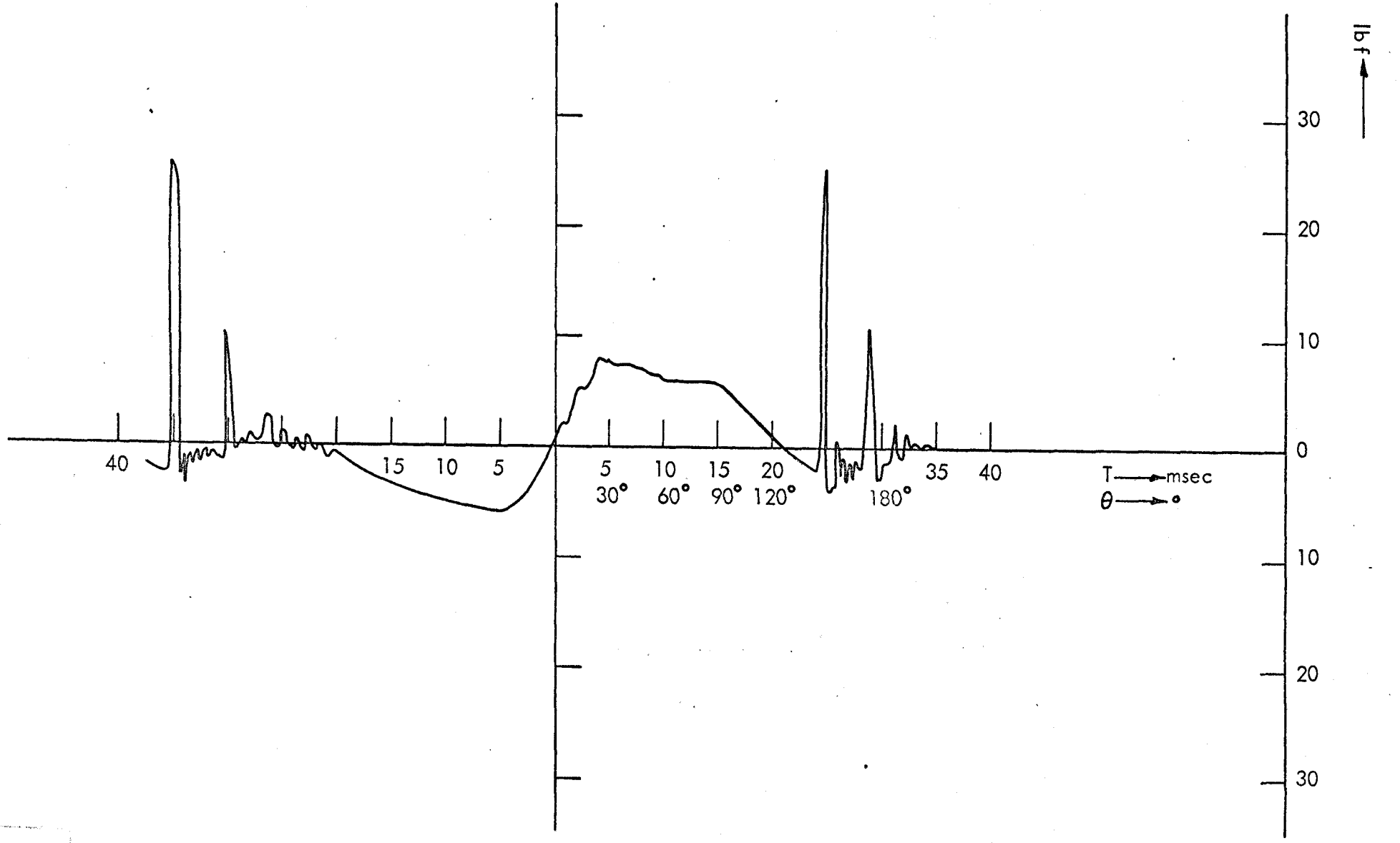

FIG. 5.4 ACTUAL PISTON SIDE FORCE USED TO SIMULATE PISTON SLAP AT 16·7 Hz.

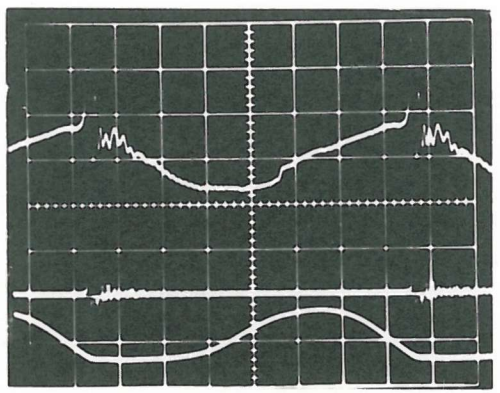

Force 23 Lbf RMS (.2 v/div)

'dBA'

Vibration response at $L'4$ (5 v/div)

Piston movement (.05 v/div)

Dry

4 msec

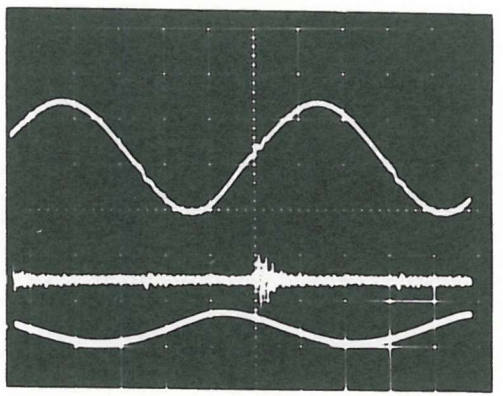

Force 40 Lbf RMS (.5 v/div)

'dBA'

Vibration response at $L'4$ (1 v/div)

Piston movement (.05 v/div)

Wet

5 msec

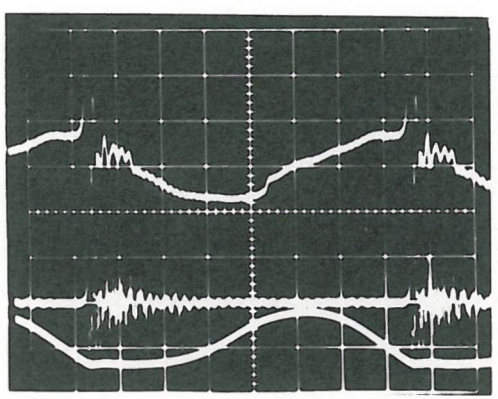

Force 23 Lbf RMS (.2 v/div)

'dBA'

Vibration response at $b'4$ (10 v/div)

Piston movement (.05 v/div)

Dry

4 msec

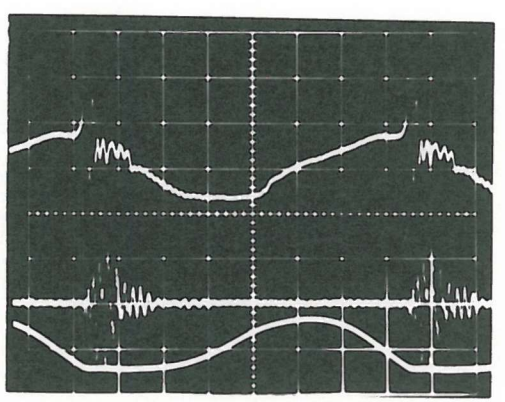

Force 23 LbfRMS (.2 v/div)

'dBA'

Vibration Response on bearing cap of con rod '2' (10 v/div)

Piston movement (.05 v/div)

Dry

4 msec

FIG. 5.5 TYPICAL OSCILLOGRAPHS SHOWING FORCE, VIBRATION RESPONSE AND PISTON MOVEMENT ON THE SIX CYLINDER INLINE PISTON SLAP RIG SHOWING EFFECT WITH STRUCTURE LOCATION AND OIL FILM AT 33.3 Hz ≡ 2000 r.p.m.

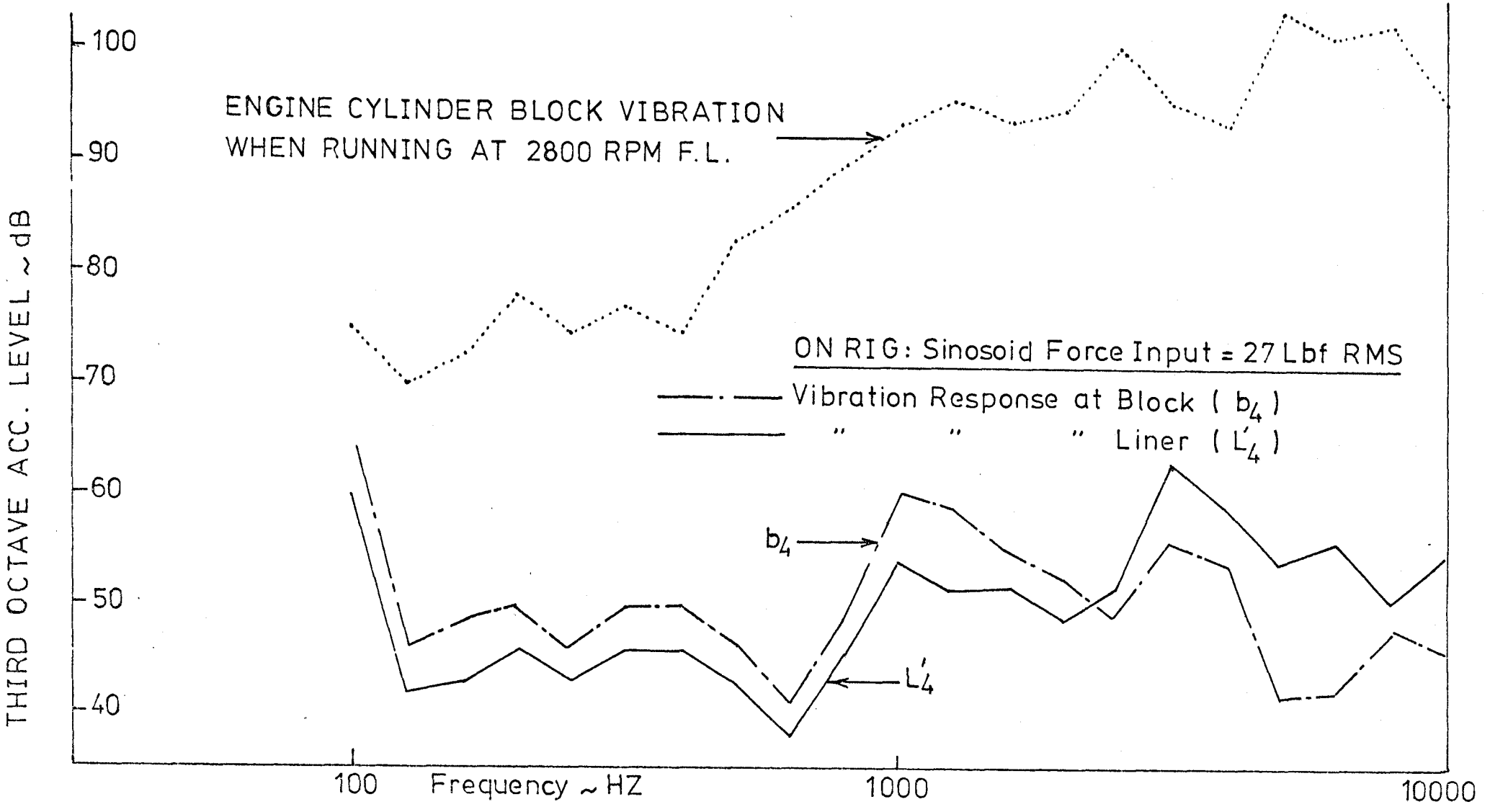

FIG. 5.6 COMPARISON OF CYLINDER BLOCK VIBRATION ON THE RUNNING ENGINE AND THE IN LINE RIG AT REPETITION RATE 46.7 per sec. ≡ 2800 RPM

(SR)

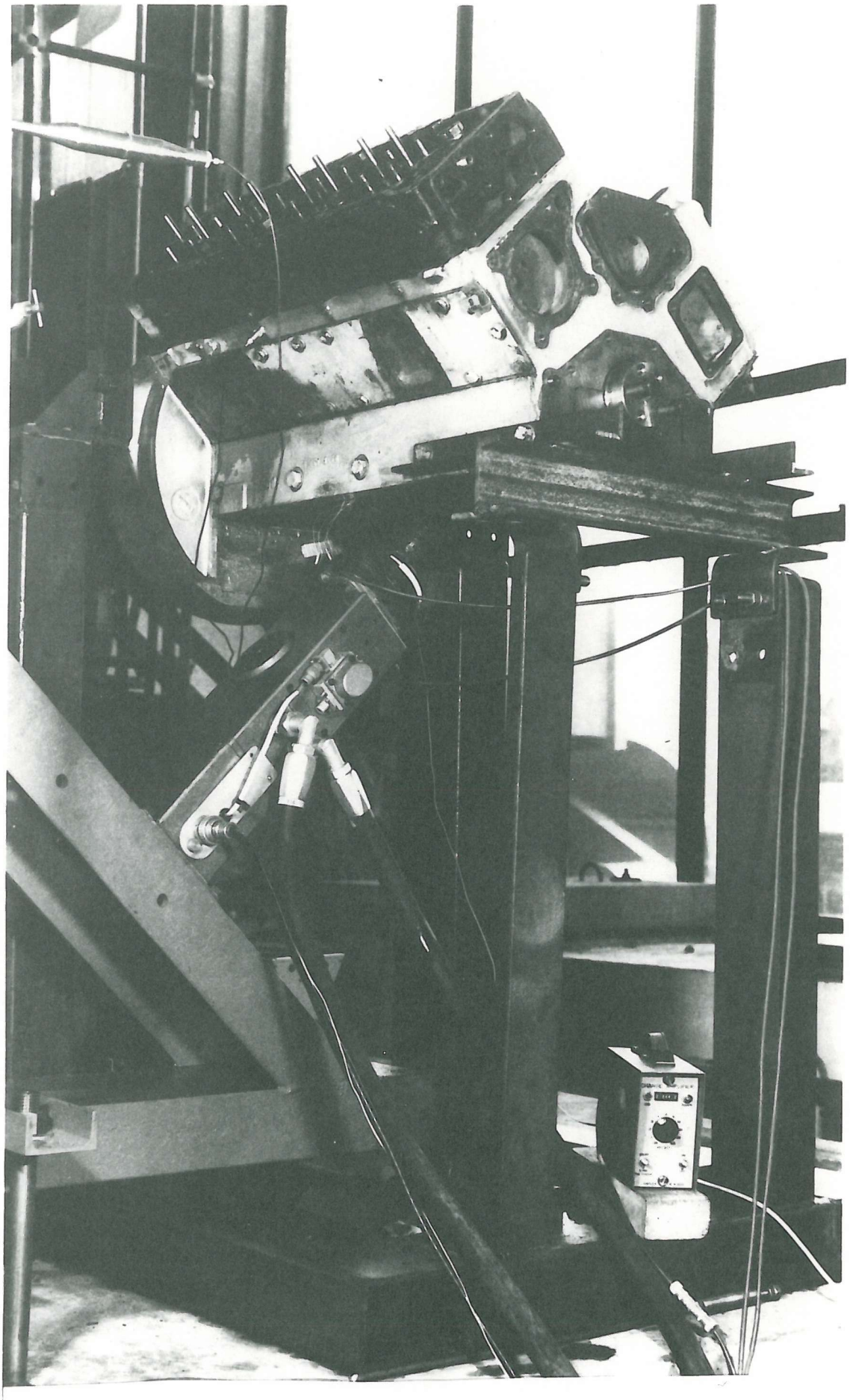

FIG. 5.7 GENERAL ARRANGEMENT OF THE PISTON SLAP RIG AS ASSEMBLED FOR TESTING

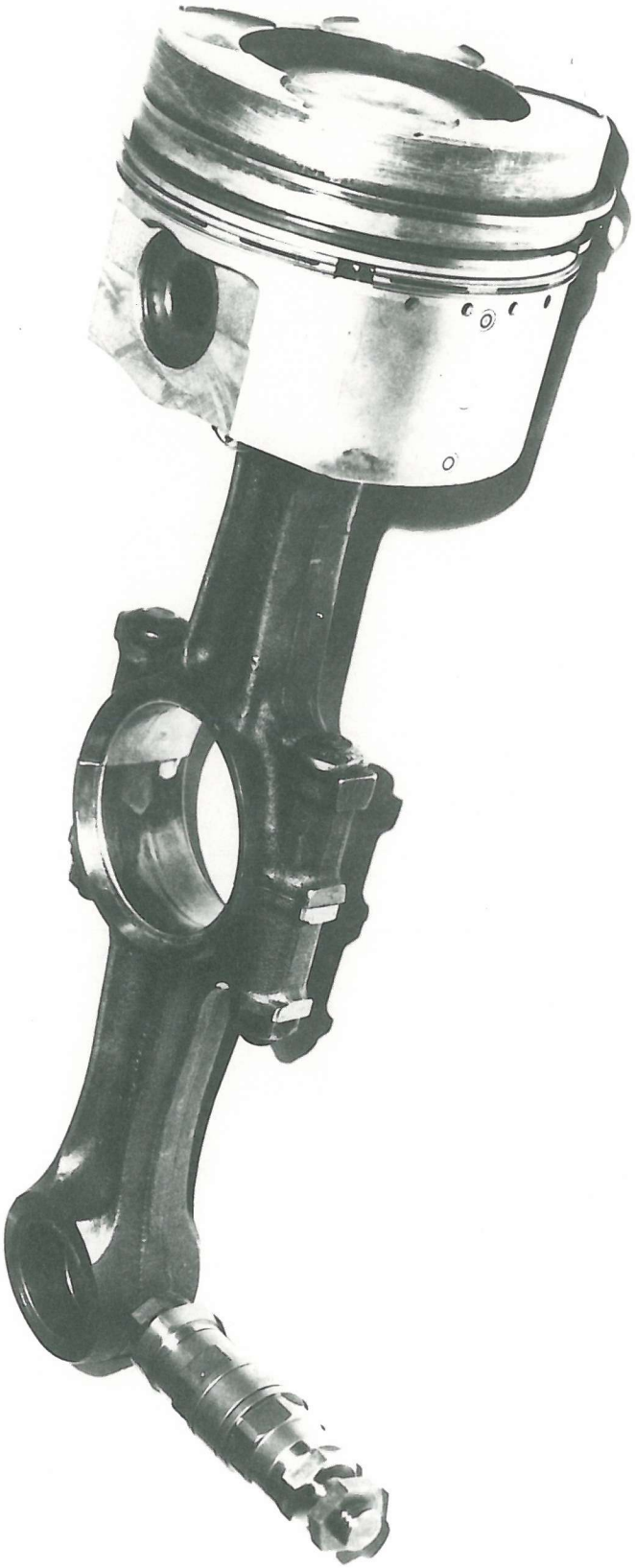

FIG. 5.8 METHOD OF APPLYING THE PISTON SIDE FORCE THROUGH BACK TO BACK CON RODS IN THE V8 PISTON SLAP RIG

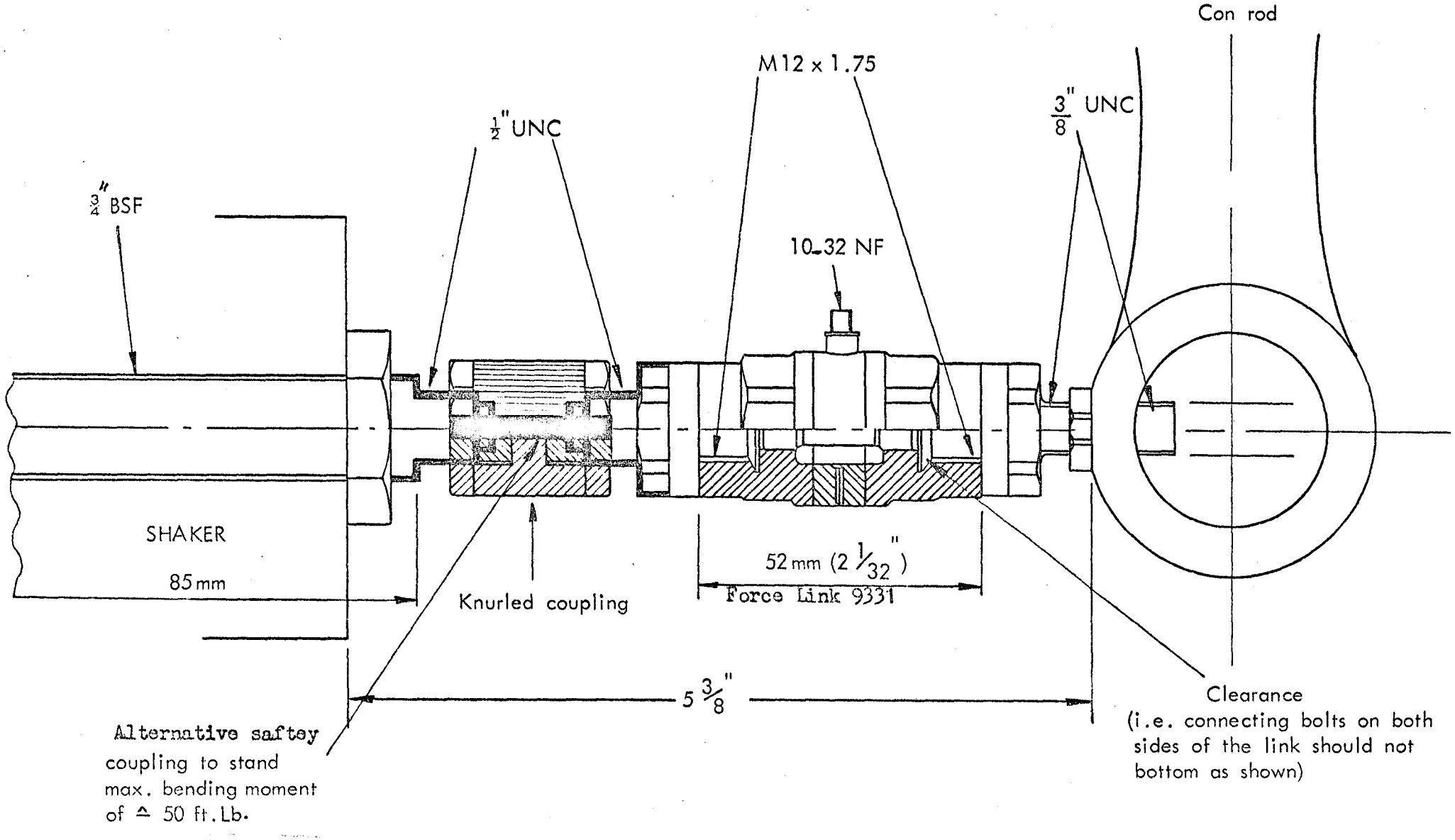

FIG. 5.9 DETAILS OF FORCE TRANSDUCER AND METHOD OF CONNECTION TO MEASURE THE APPLIED FORCE IN THE V8 PISTON SLAP RIG.

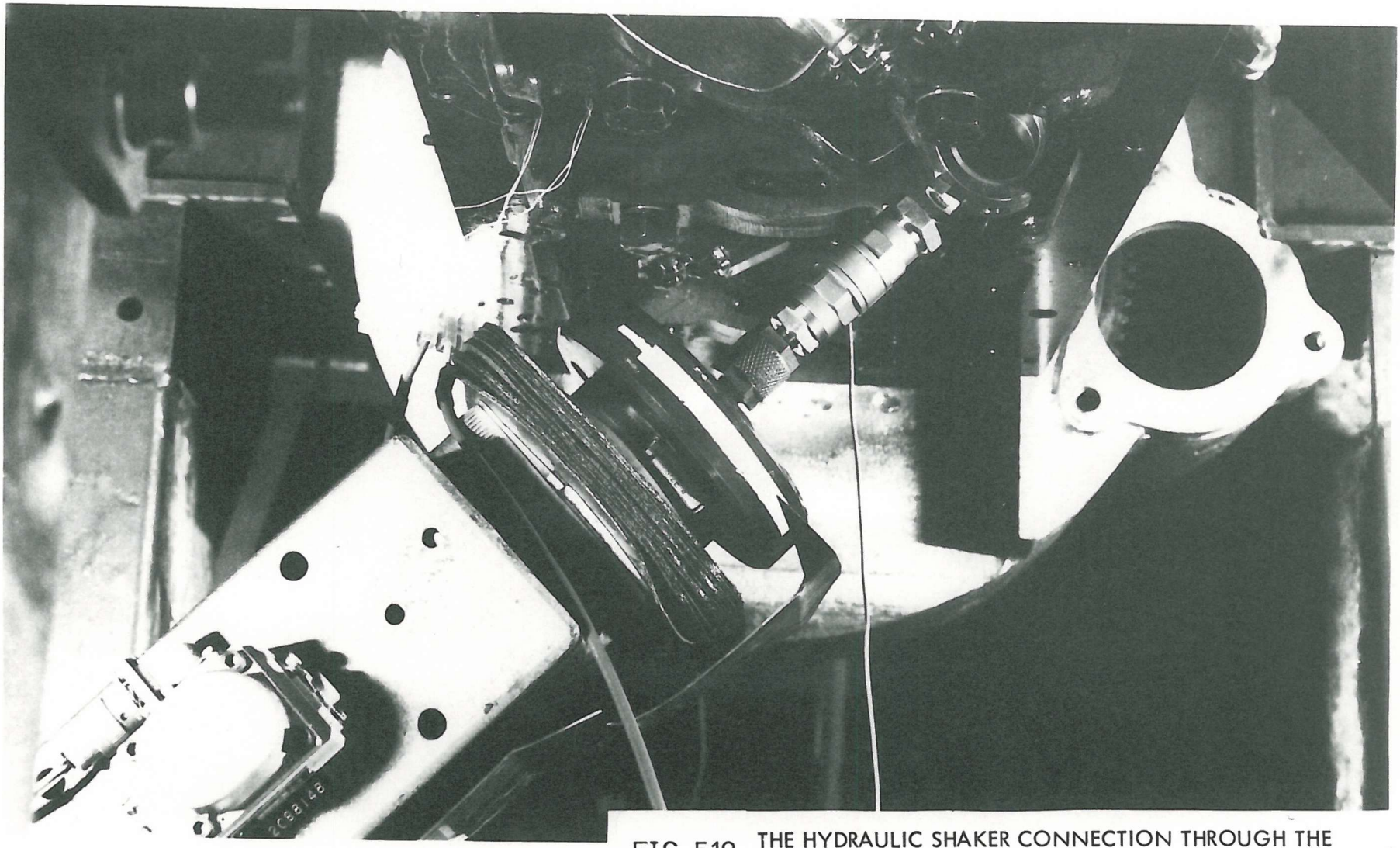

FIG. 5.10 THE HYDRAULIC SHAKER CONNECTION THROUGH THE BACK TO BACK CON RODS SHOWING A CASE OF BOLT BREAKAGE DUE TO DRIFT

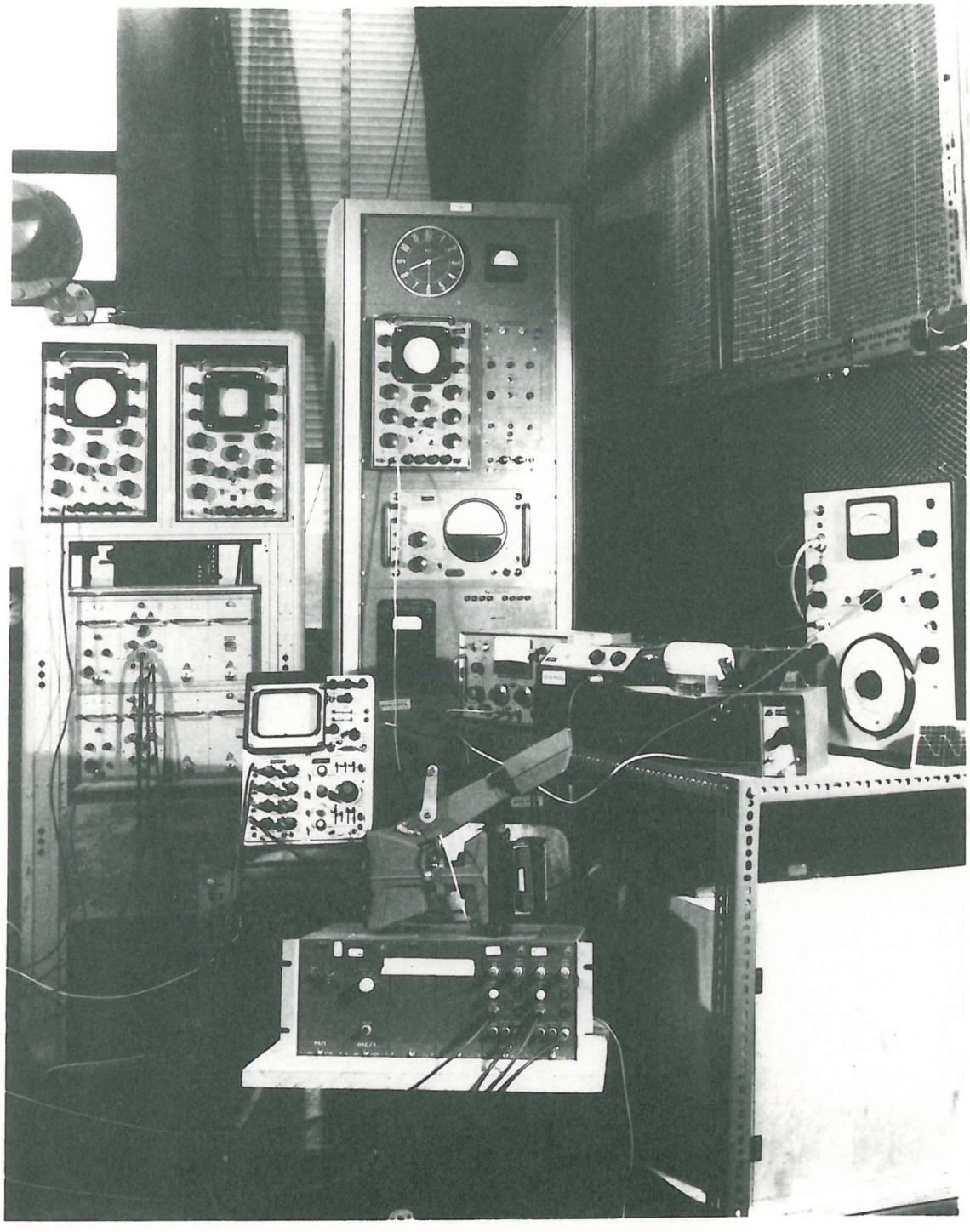

Some of the instrumentation used with the V8 Piston Slap Rig.

FIG. 5.11

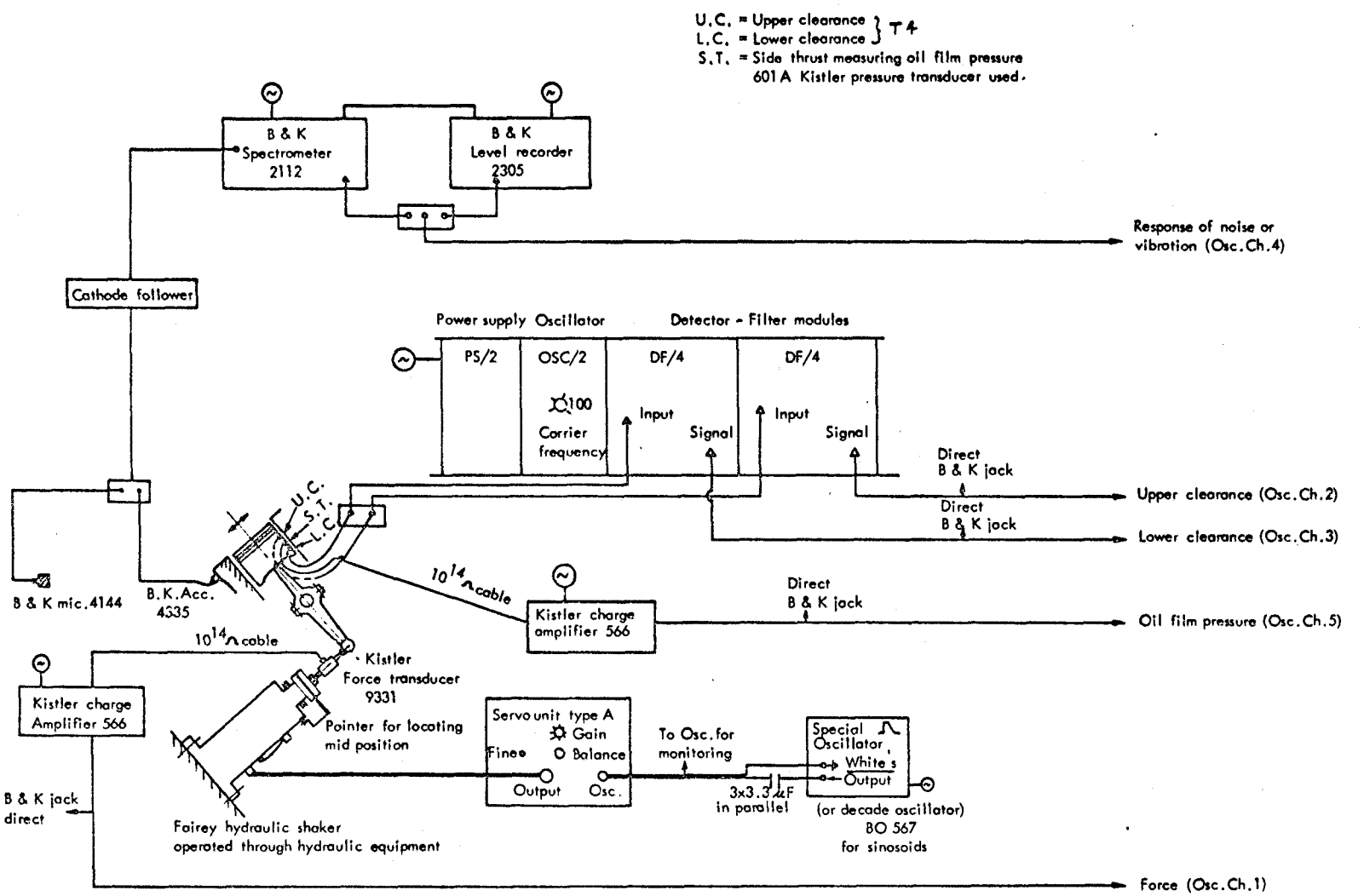

FIG. 5.12 LAYOUT OF INSTRUMENTATION AND CIRCUIT DIAGRAM FOR THE STUDY OF PISTON SLAP SIMULATION ON THE V8-470 DIESEL ENGINE

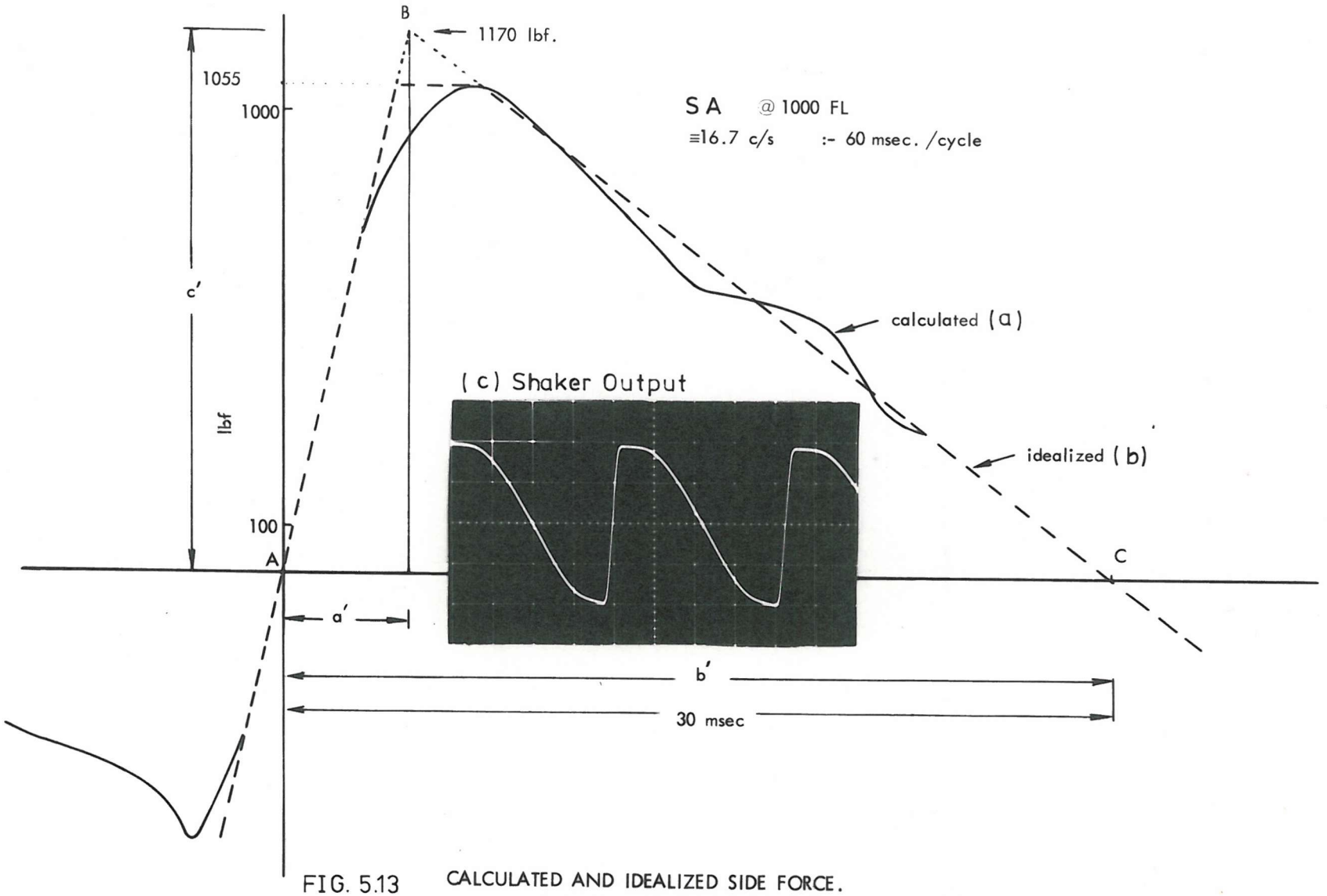

FIG. 5.13 CALCULATED AND IDEALIZED SIDE FORCE.

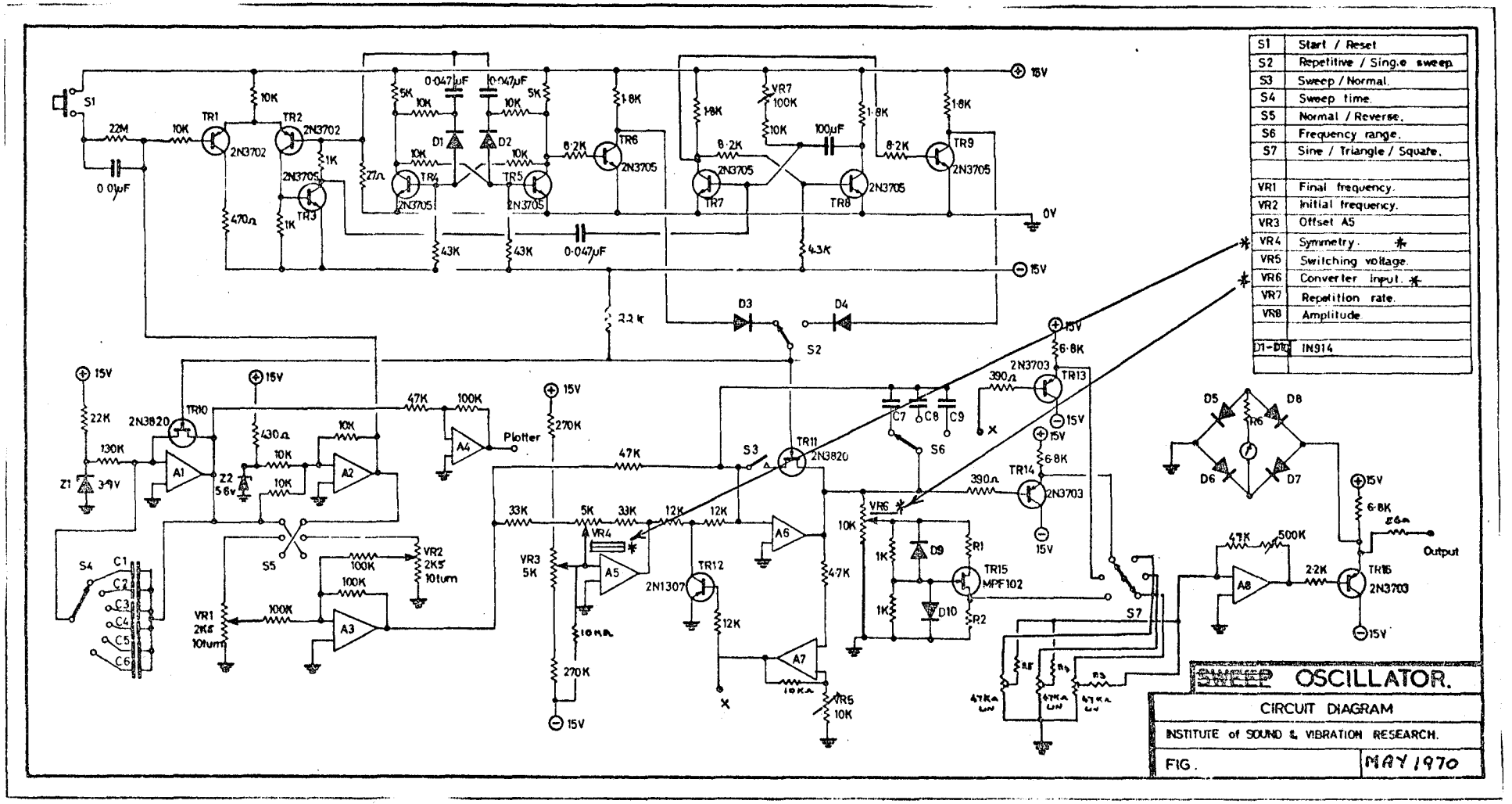

FIG. 5.14 CIRCUIT DIAGRAM OF THE SPECIAL OSCILLATOR USED TO SIMULATE PISTON SIDEWAYS FORCE ON THE VEE PISTON SLAP RIG —— ENGINE SA

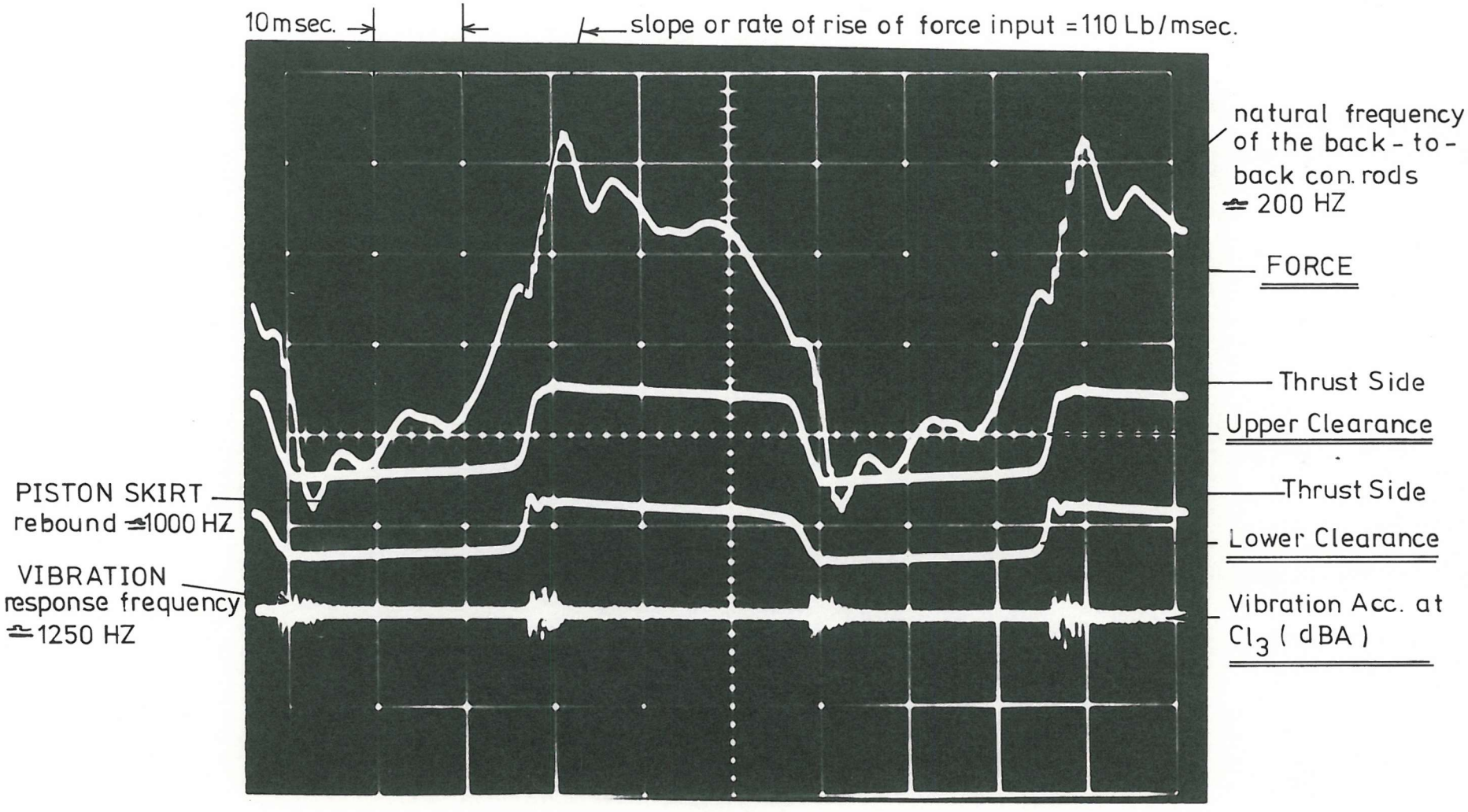

FIG. 5.15 TYPICAL OSCILLOGRAPH FOR THE VEE PISTON SLAP RIG AT REPETITION RATE 16.7 per sec. ≡ 1000 RPM (DRY CASE)

CHARLES WELL — Graph Data Ref. 5535 — Log 3 Cycles x 10th, ½ and 1 Inch

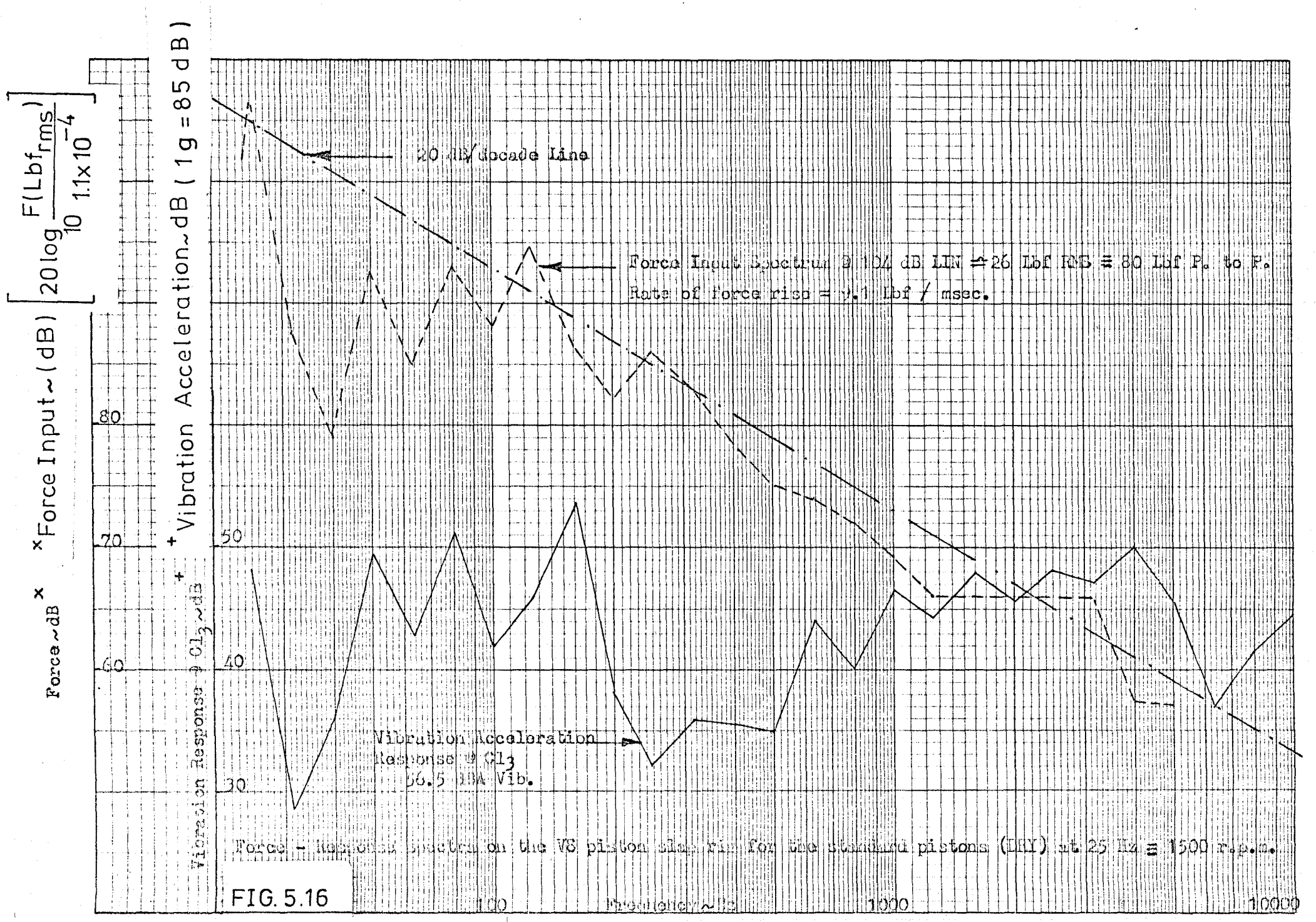

Force ~ Input Spectrum on the VS piston slap rig for the standard pistons (DHY) at 25 Hz ≡ 1500 r.p.m.

FIG. 5.16

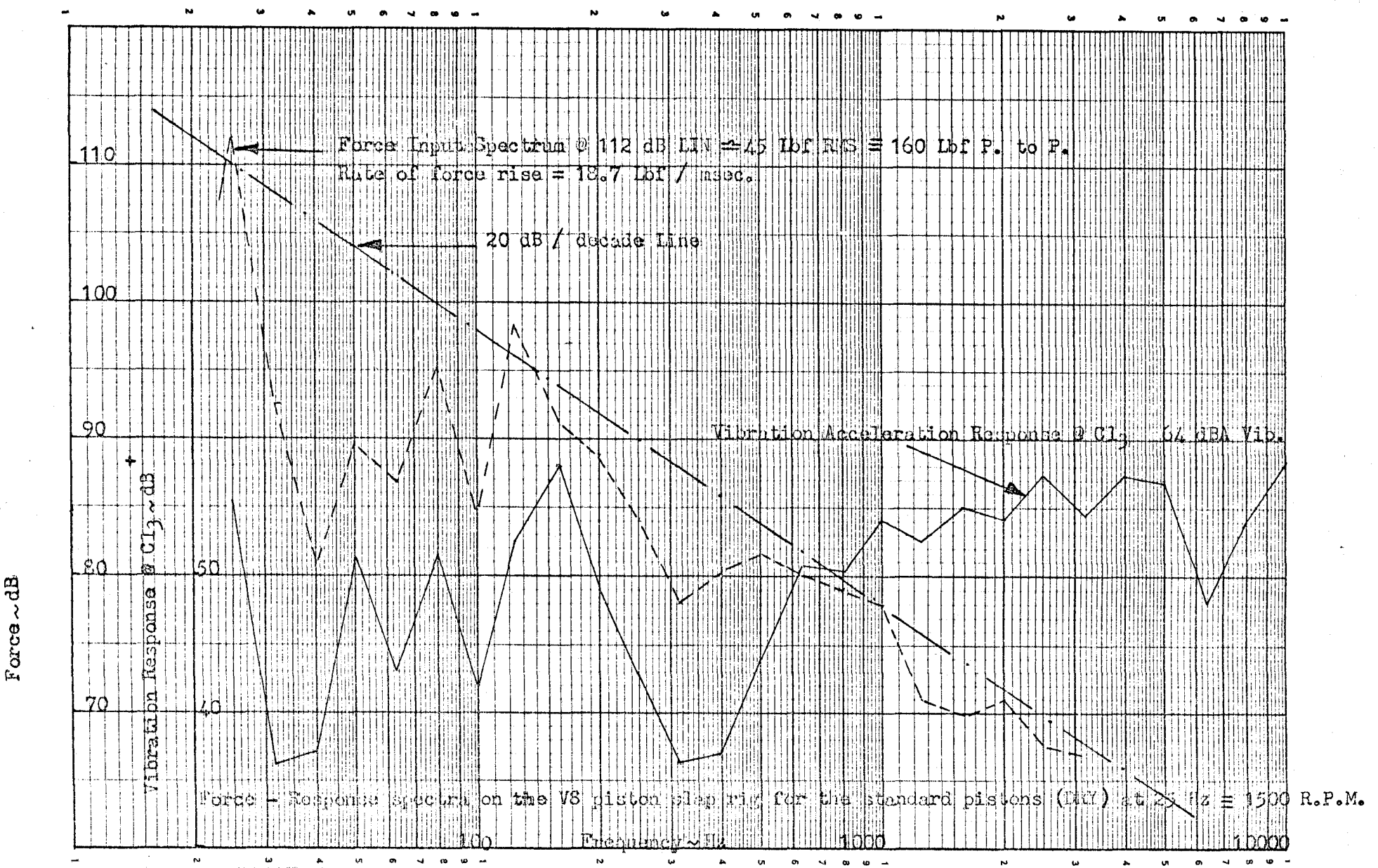

Force ~ Response spectrum on the V8 piston slap rig for the standard pistons (LHY) at 25 Hz = 1500 R.P.M.

FIG. 5.17

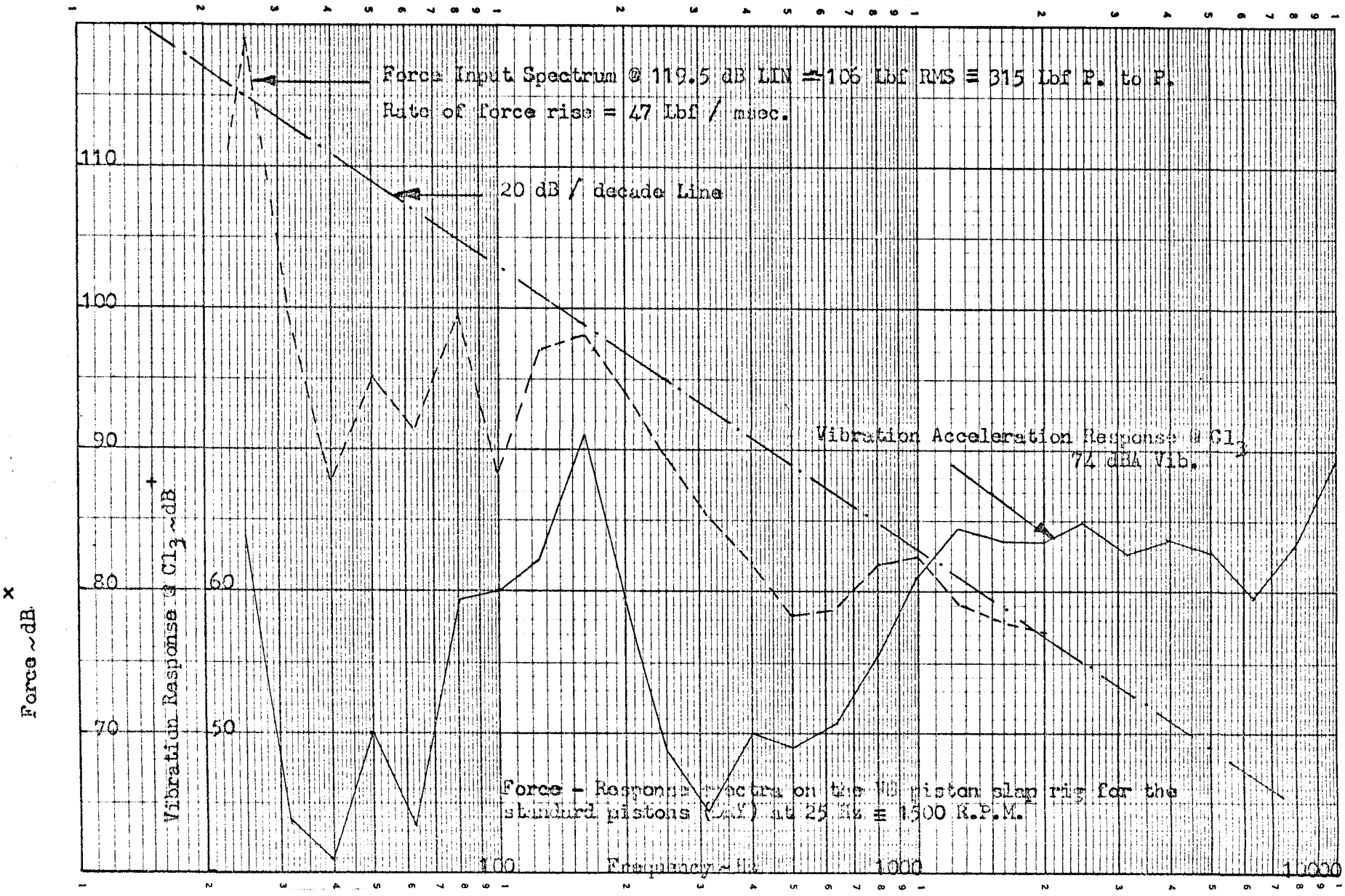
Force Input Spectrum @ 119.5 dB LIN ≒ 106 Lbf RMS ≡ 315 Lbf P. to P.
Rate of force rise = 47 Lbf / msec.
20 dB / decade Line
Vibration Acceleration Response @ Cl3
74 dBA Vib.
Force - Response spectra on the [illegible] piston slap rig for the standard pistons (Cast) at 25 Hz ≡ 1500 R.P.M.
Force ~dB
Vibration Response @ Cl3 ~dB
Frequency ~Hz
110
100
90
80
70
60
50
100
1000
1,000

FIG. 5.18

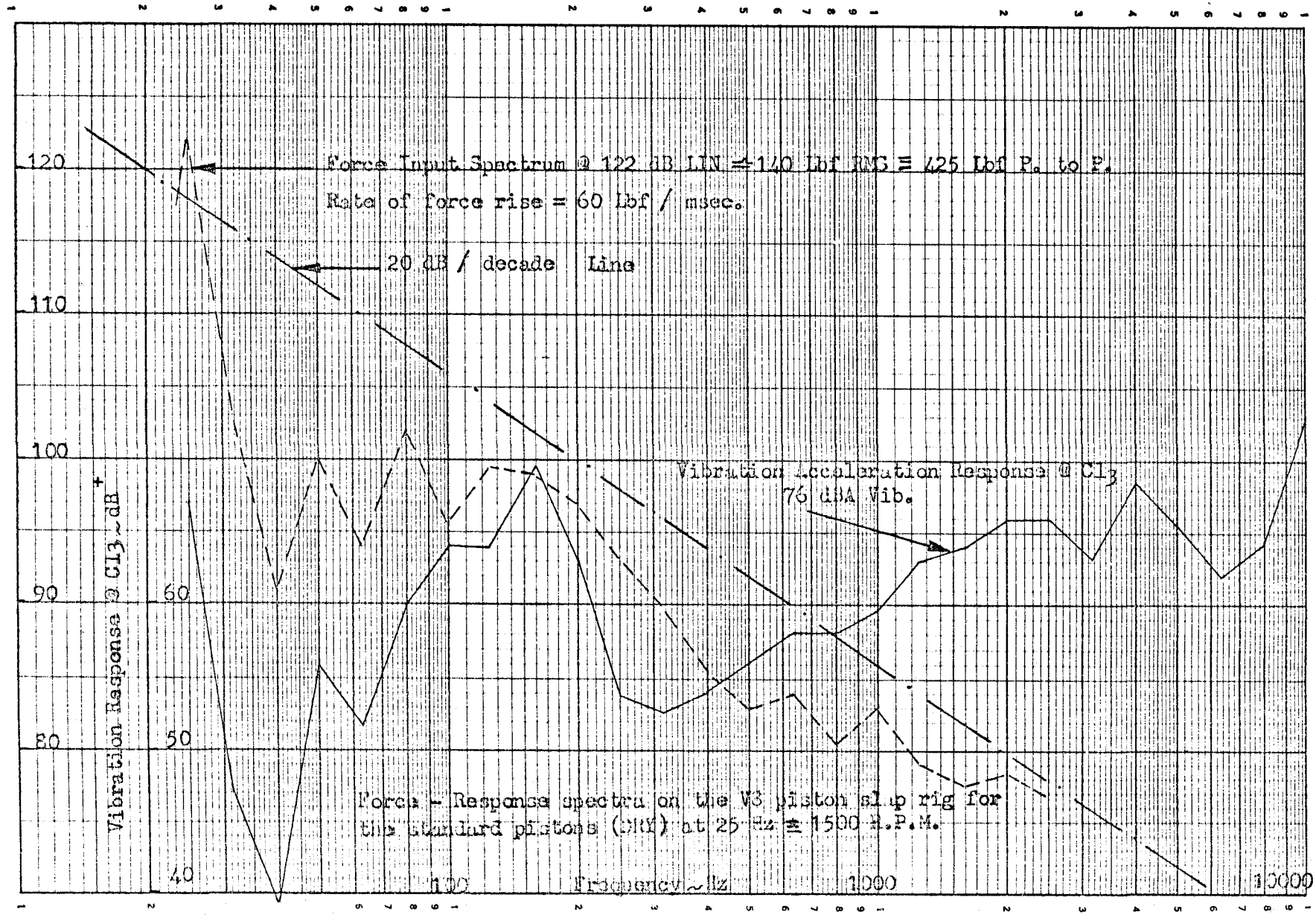
Force Input Spectrum @ 122 dB LIN ≡ 140 Lbf RMS ≡ 425 Lbf P. to P.
Rate of force rise = 60 Lbf / msec.
20 dB / decade Line
Vibration Acceleration Response @ CL3
76 dBA Vib.
Force - Response spectrum on the V8 piston slap rig for the standard pistons (DTM) at 25 Hz ≡ 1500 R.P.M.
Force ~ dB
Vibration Response @ CL3 ~ dB
Frequency ~ Hz
120
110
100
90
80
60
50
40
100
1000
10000

FIG. 5.19

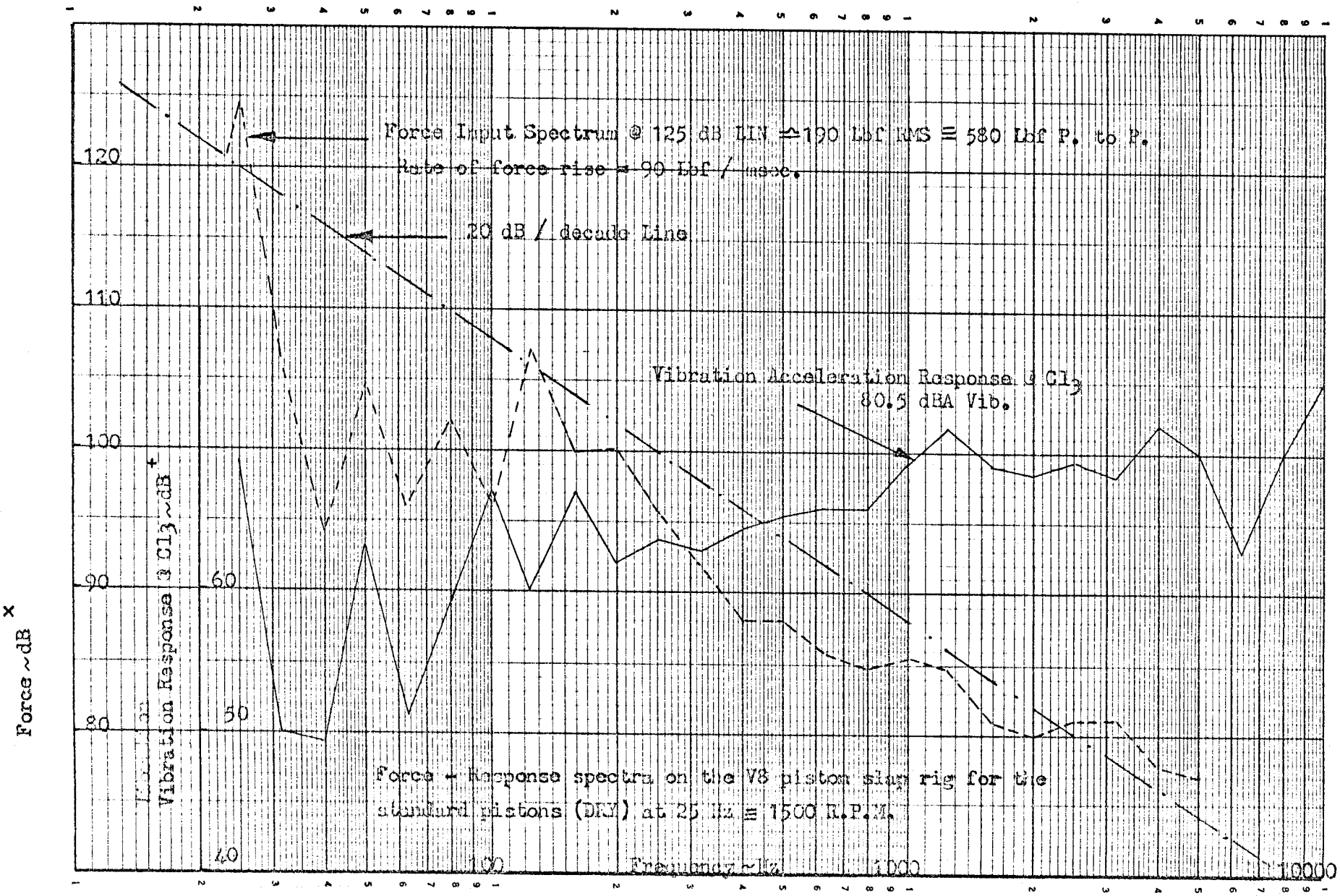
Force Input Spectrum @ 125 dB LIN ≏190 Lbf RMS ≡ 580 Lbf P. to P.
Rate of force rise = 90 Lbf / msec.
20 dB / decade Line
Vibration Acceleration Response @ Cl3
80.5 dBA Vib.
Force ~dB
Vibration Response @ Cl3 ~dB
120
110
100
90
80
60
50
40
100
1000
10000
Frequency ~Hz
Force - Response spectra on the V8 piston slap rig for the standard pistons (DKM) at 25 Hz ≡ 1500 R.P.M.

FIG. 5.20

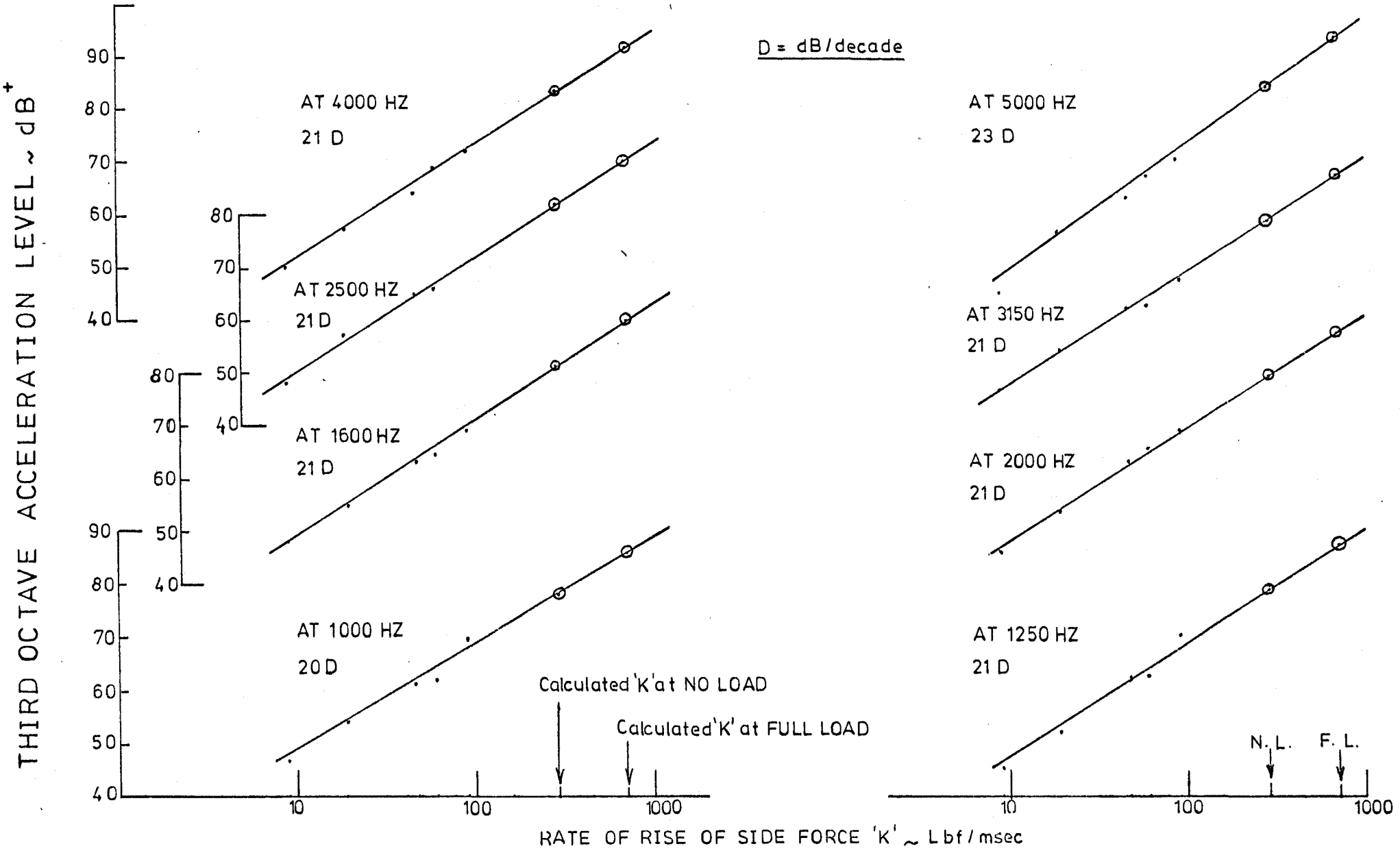

FIG. 5.21 RELATION BETWEEN VIBRATION RESPONSE AT Cl_3 AND 'K' FACTOR AT REPETITION RATE 25 per sec. ≡ 1500 RPM ENGINE SPEED (SA)

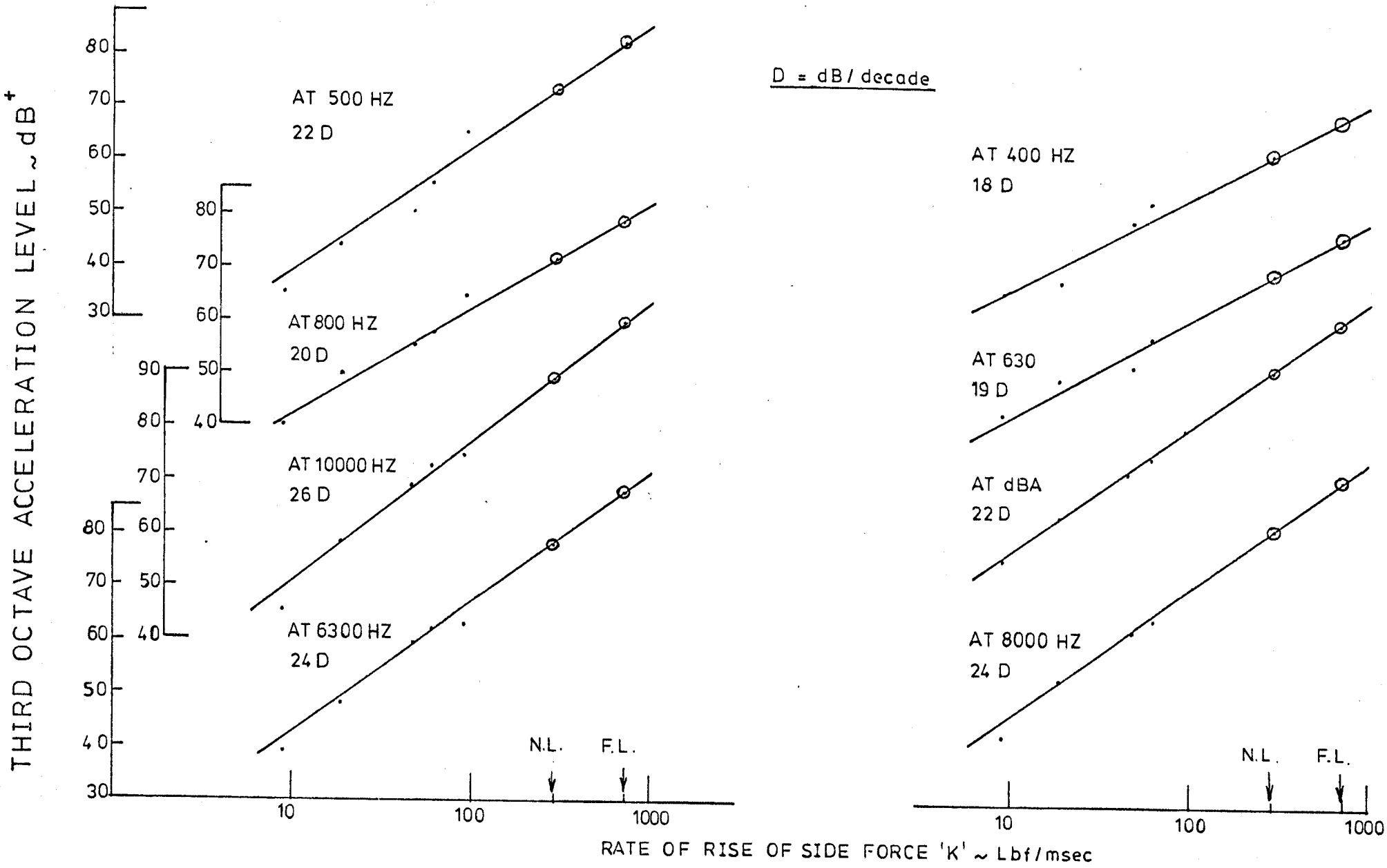

FIG. 5.22 RELATION BETWEEN VIBRATION RESPONSE AT Cl_3 AND K FACTOR AT REPETITION RATE 25 per sec. ≡ 1500 RPM ENGINE SPEED (SA)

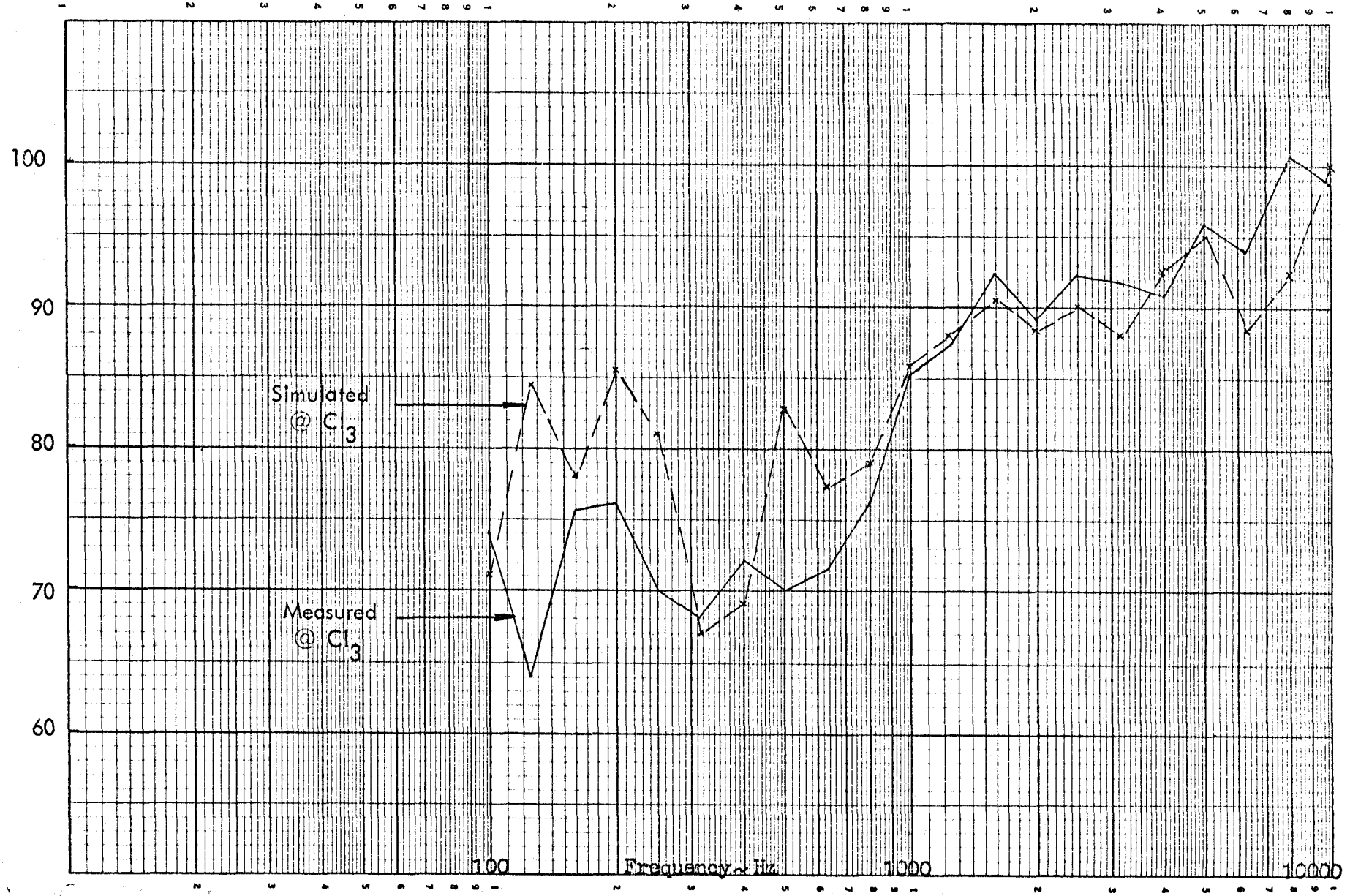

$\frac{1}{3}$ OCTAVE ACCELERATION LEVEL ~dB.

FIG. 5.23a COMPARISON OF MEASURED VIBRATION @ Cl_3 AND THAT SIMULATED THROUGH THE PISTON SLAP RIG. @ FULL LOAD 1500 r.p.m. ≡ 25 Hz. •••V8 RIG

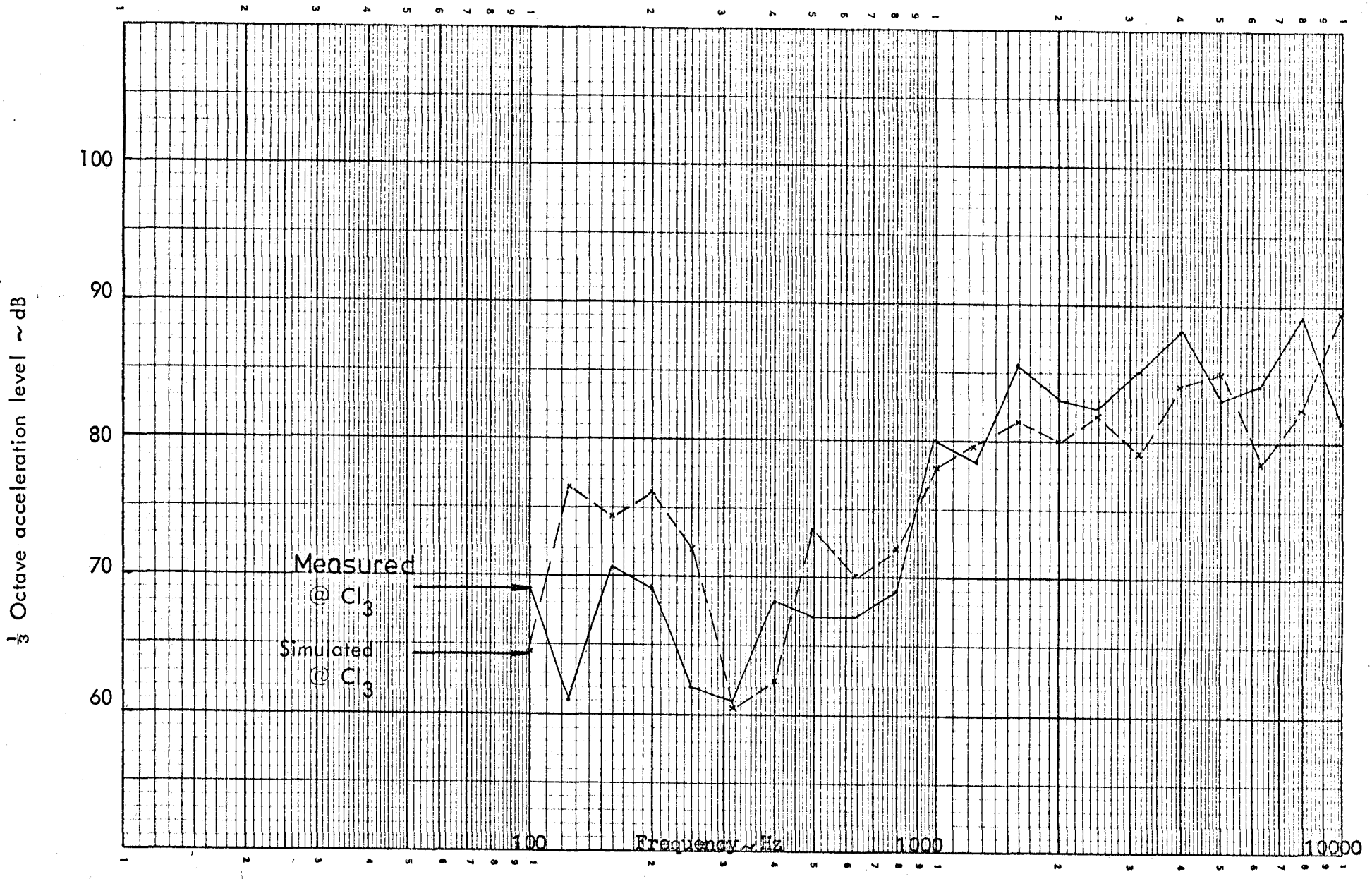

FIG. 5.23 b COMPARISON OF MEASURED VIBRATION @ Cl_3 AND THAT SIMULATED THROUGH THE PISTON SLAP RIG @ NO LOAD 1500 r.p.m. ≡ 25 HZ. .....V8 RIG

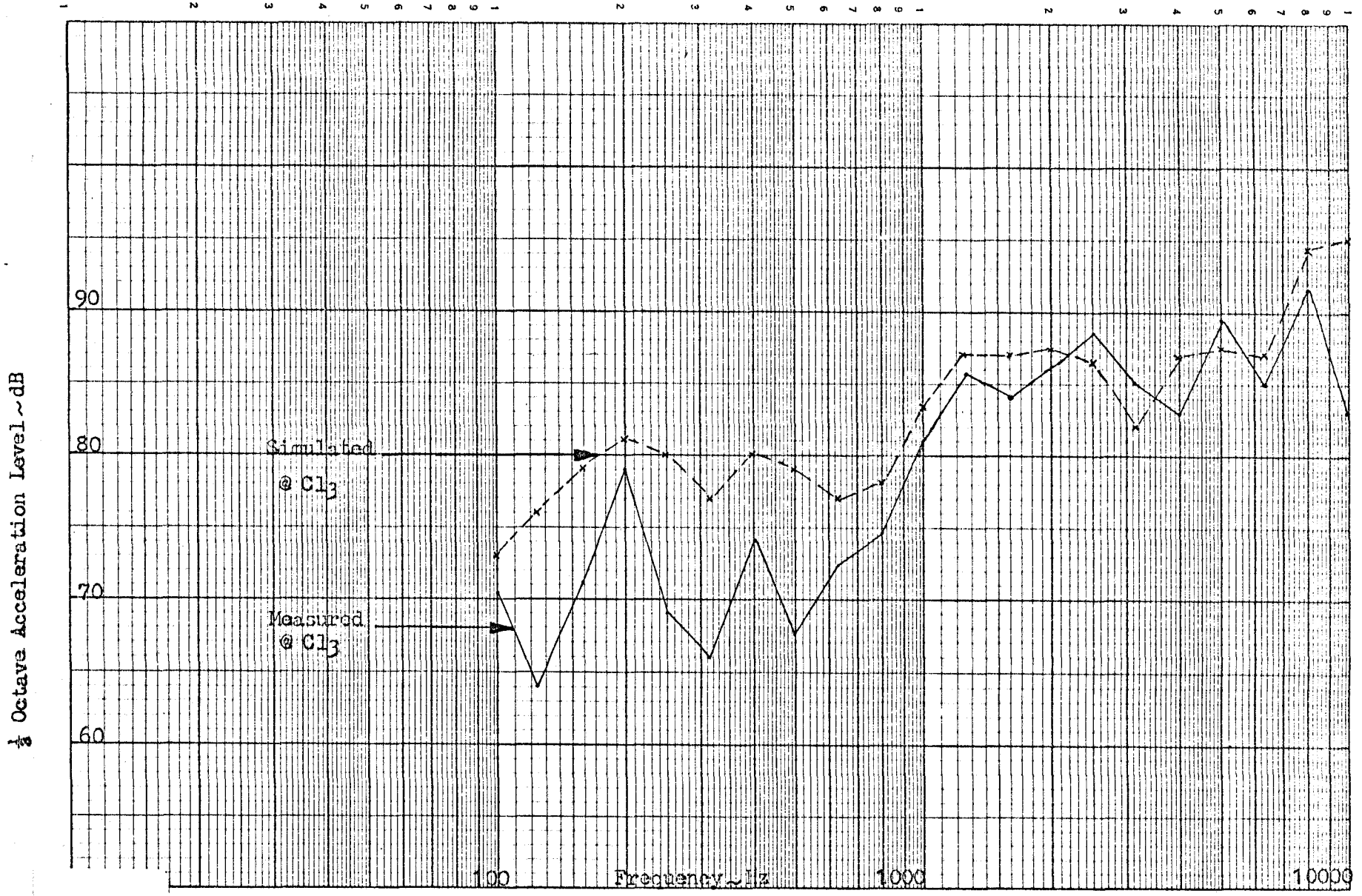

FIG. 5.24 Comparison of measured vibration @ Cl_3 and that simulated through the piston slap rig at Full Load

1000 R.P.M. ≡ 16.7 Hz ...., V8 RIG

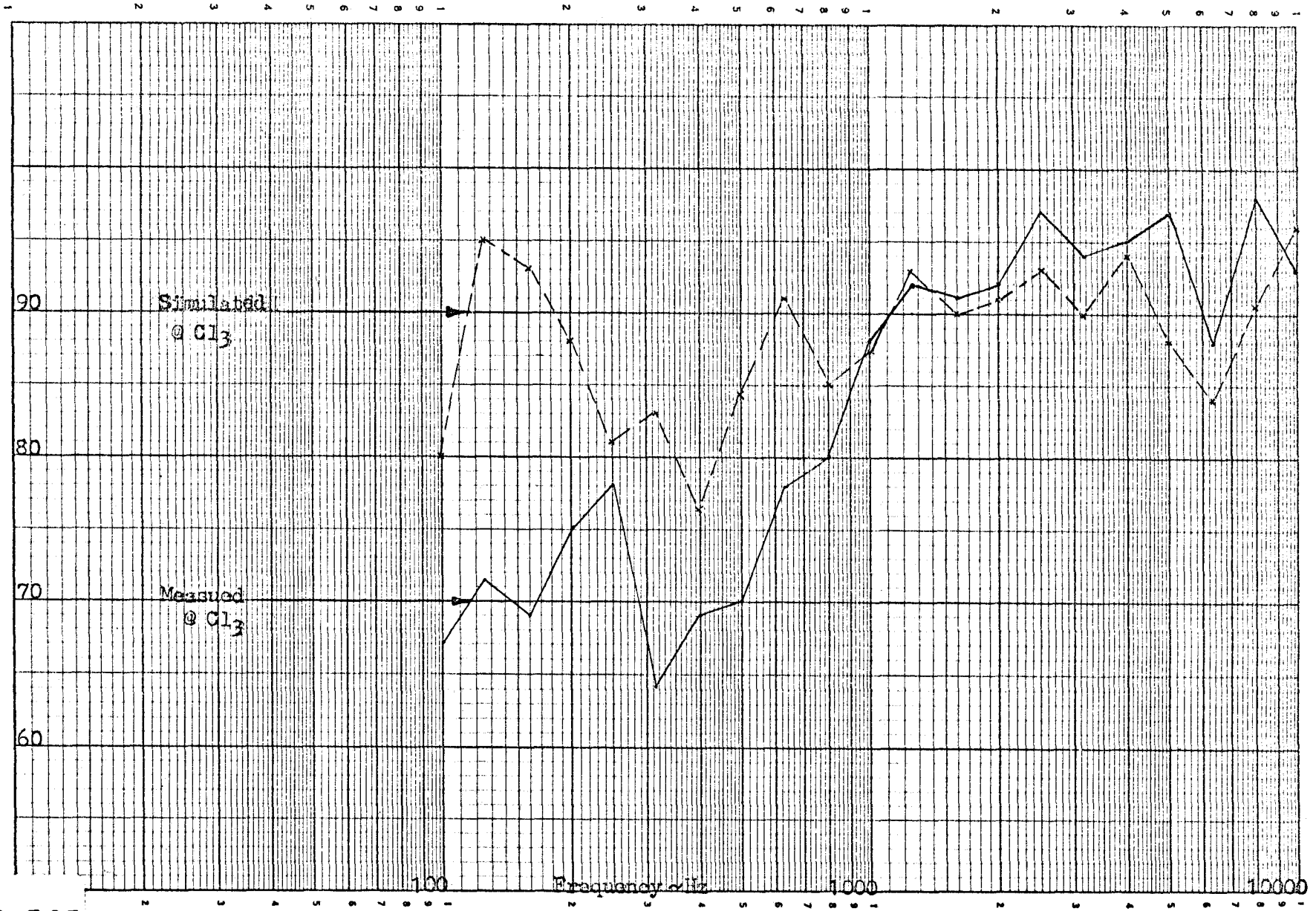

FIG. 5.25 Comparison of measured vibration @ Cl_3 and that simulated through the piston slap rig at Full Load 2000 R.P.M. ≡ 33.3 Hz .... V8 RIG

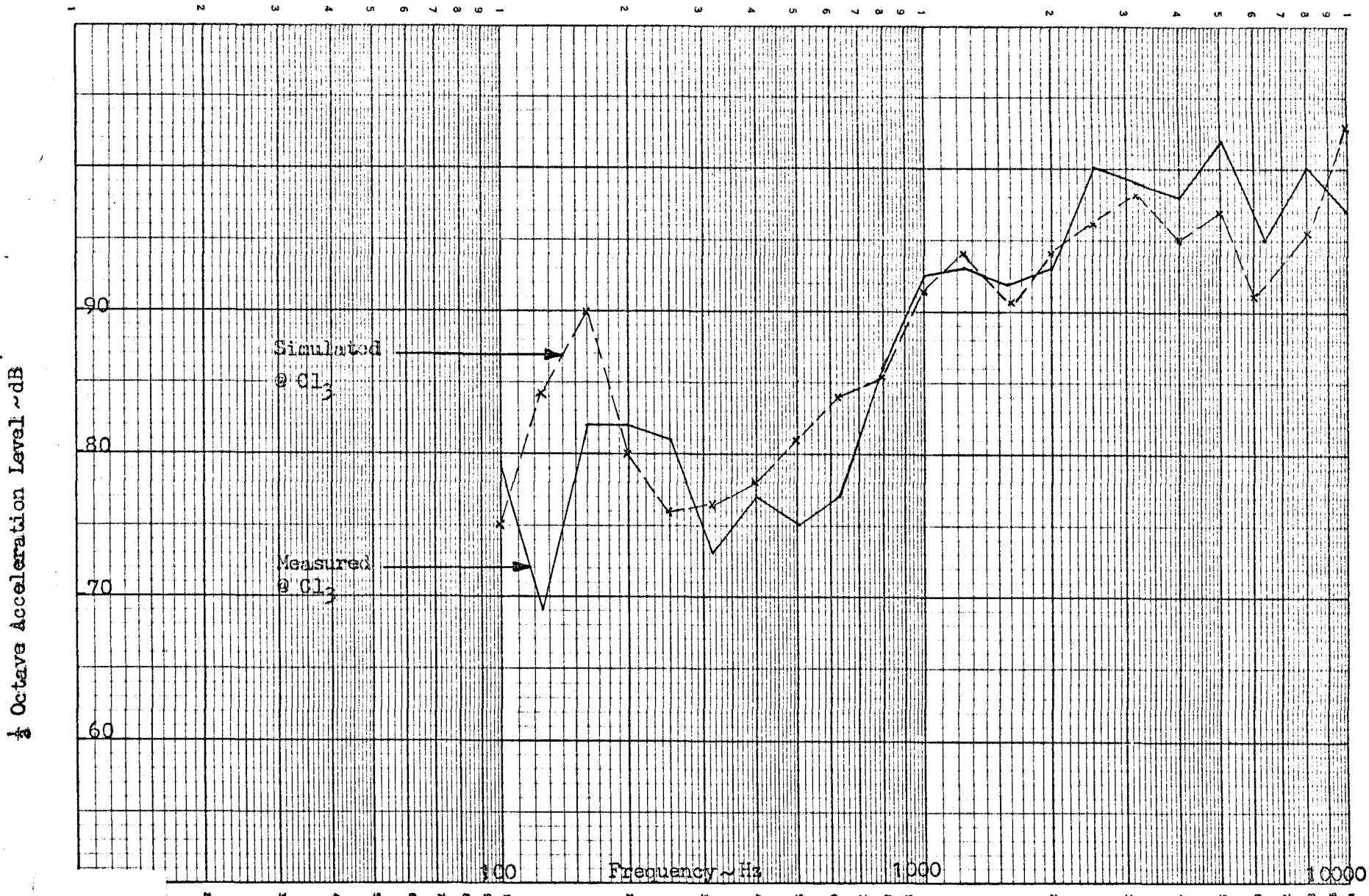

FIG. 5.26 Comparison of measured vibration @ Cl_3 and that simulated through the piston slap rig at Full Load 3000 R.P.M. ≡ 50 Hz ....V8 RIG

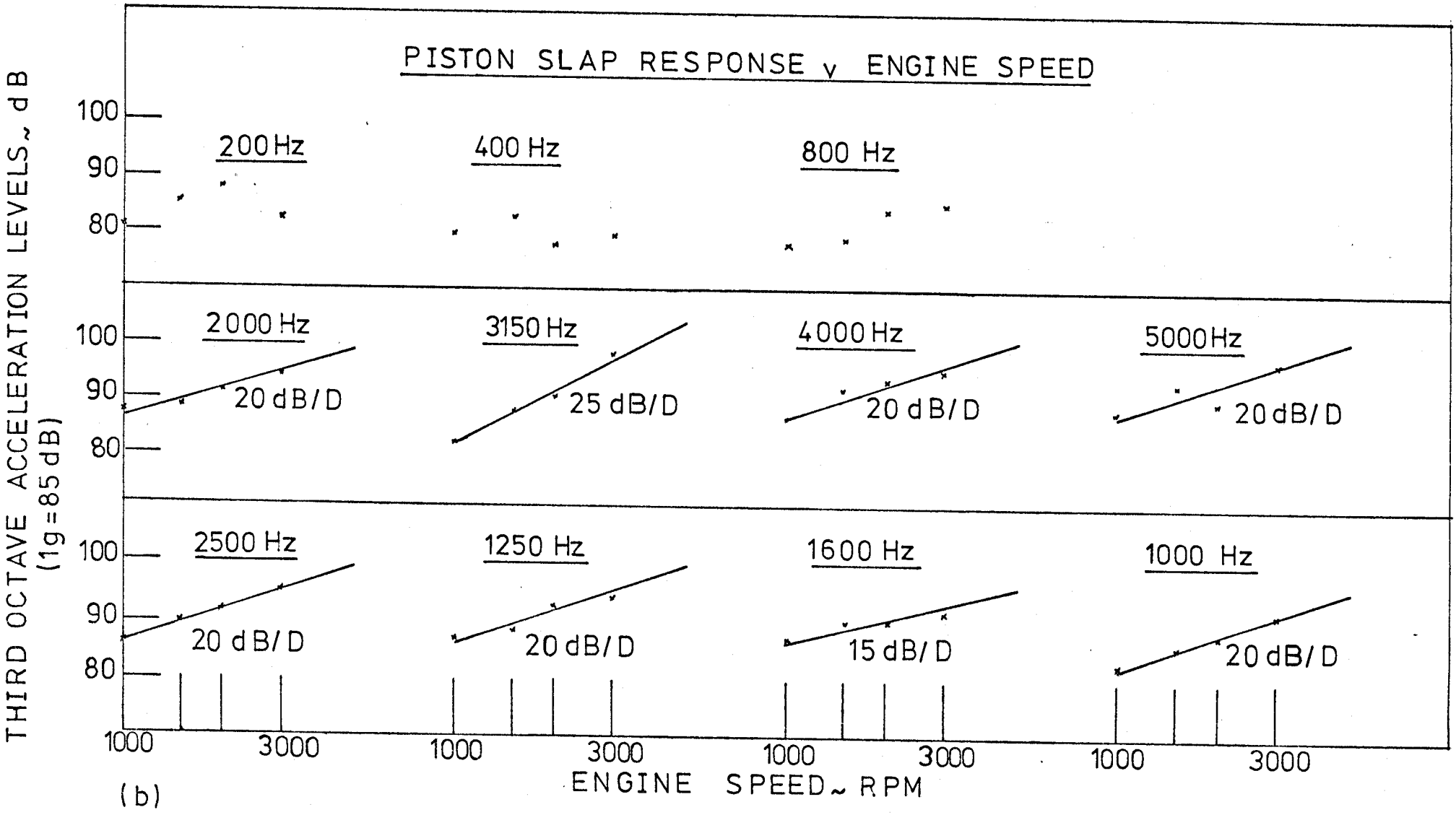

FIG. 5.27 CHARACTERISTICS OF PISTON SLAP INDUCED VIBRATION AND ITS RELATION WITH ENGINE SPEED — FULL LOAD

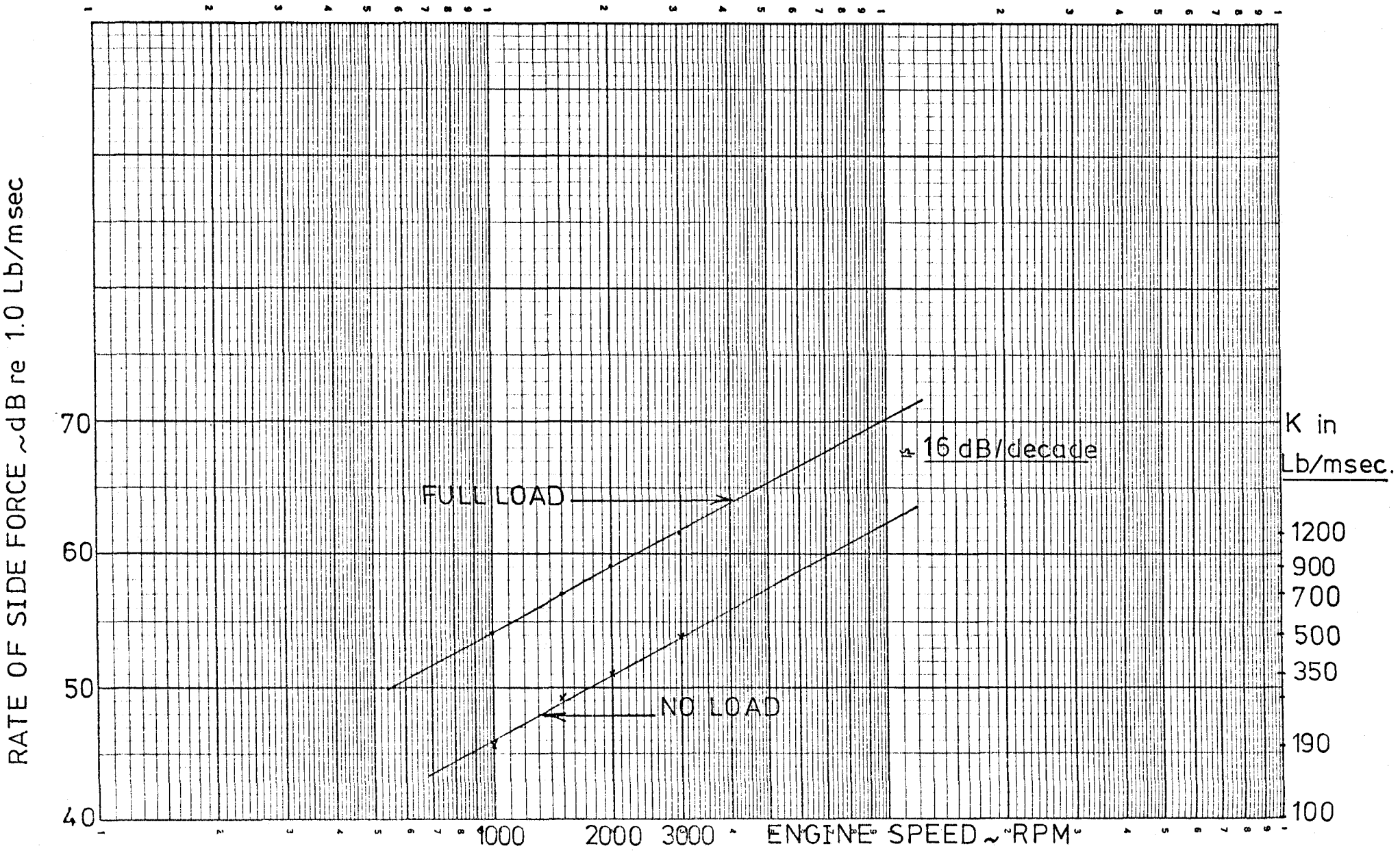

FIG. 5.28 RELATION BETWEEN 'K' FACTOR AND ENGINE SPEED – ENGINE SA

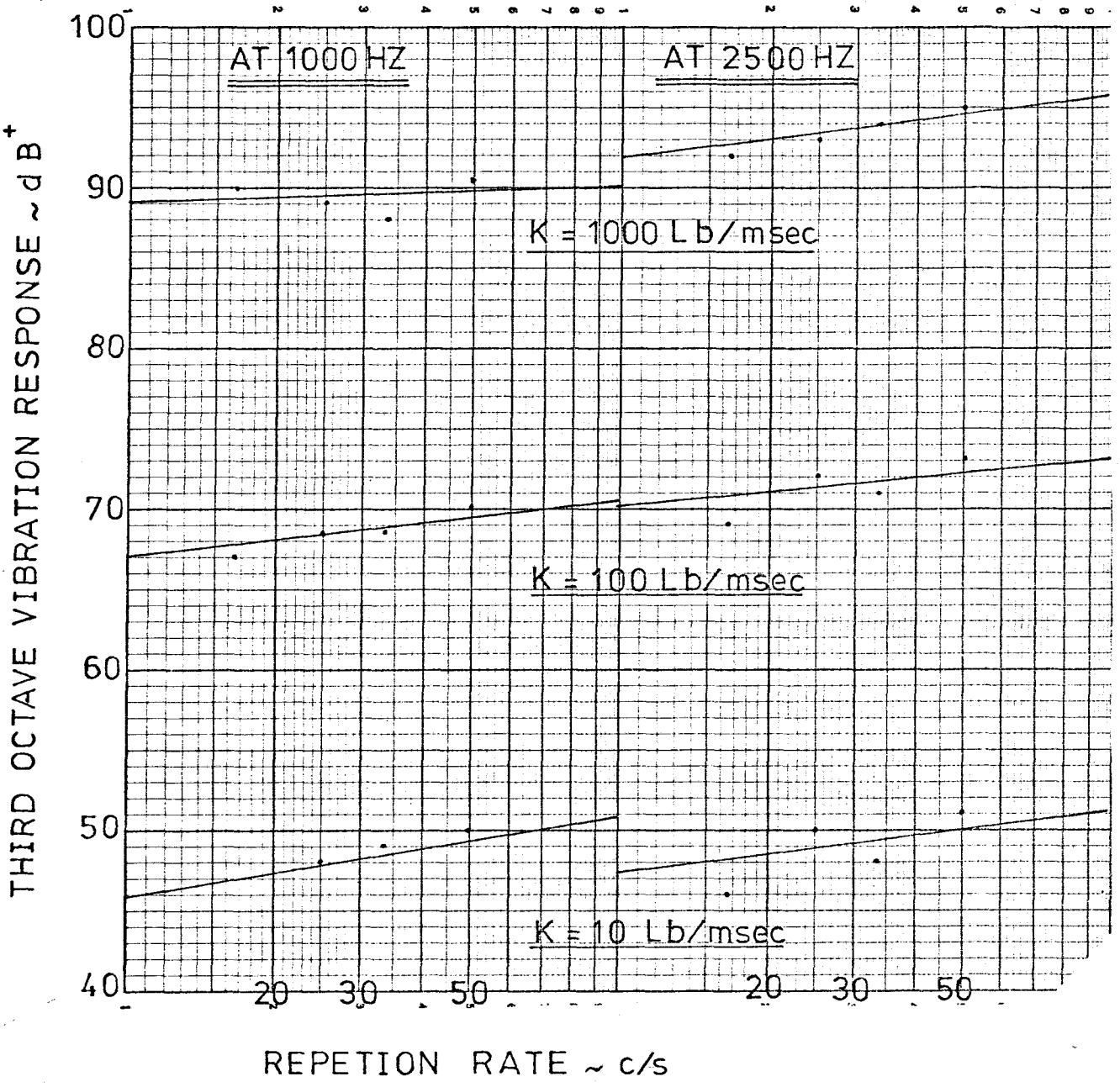

FIG. 5.29 RELATION BETWEEN VIBRATION RESPONSE AT Cl_3 AND PISTON SLAPPING RATE FOR CONSTANT K FACTORS AT TWO TYPICAL THIRD OCTAVE FREQUENCY BANDS

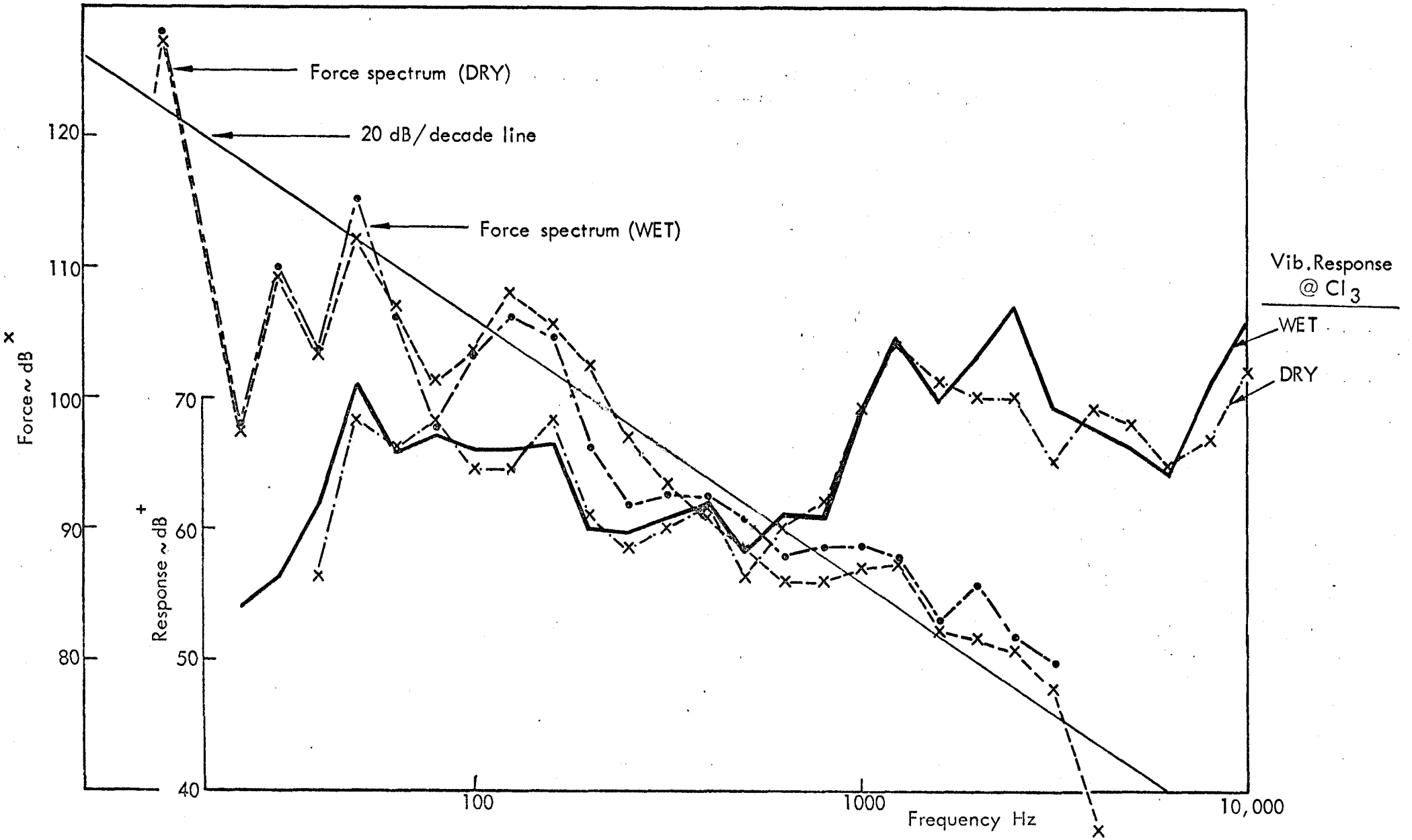

FIG. 5.30a TYPICAL EFFECT OF OF OIL FILM ON THE VEE RIG AT REPETITION RATE 16.7 per sec. – STANDARD PISTONS OF SA

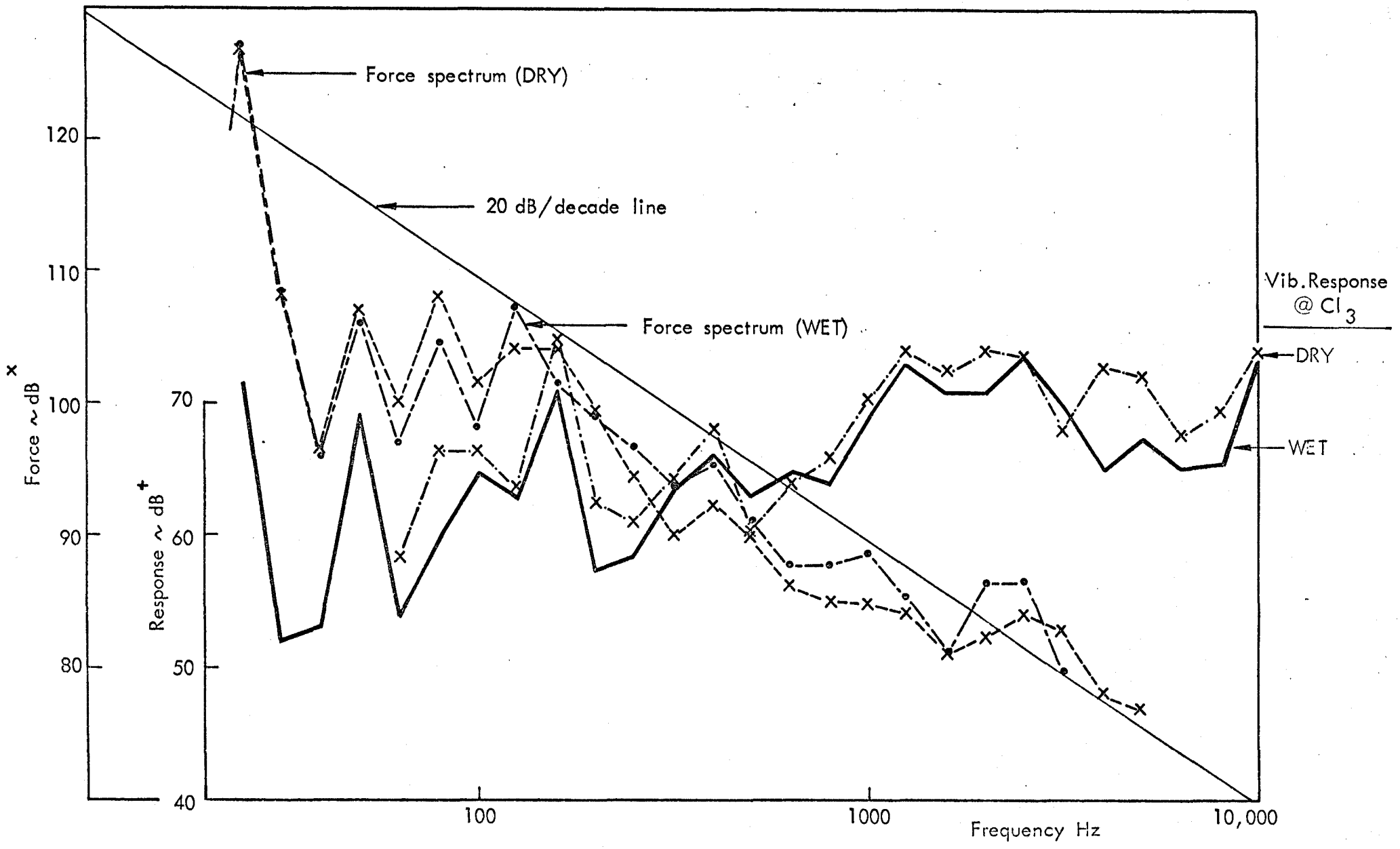

FIG. 5.30 b TYPICAL EFFECT OF OIL FILM ON THE VEE RIG AT REPETITION RATE 25 per sec. — STANDARD PISTONS OF SA

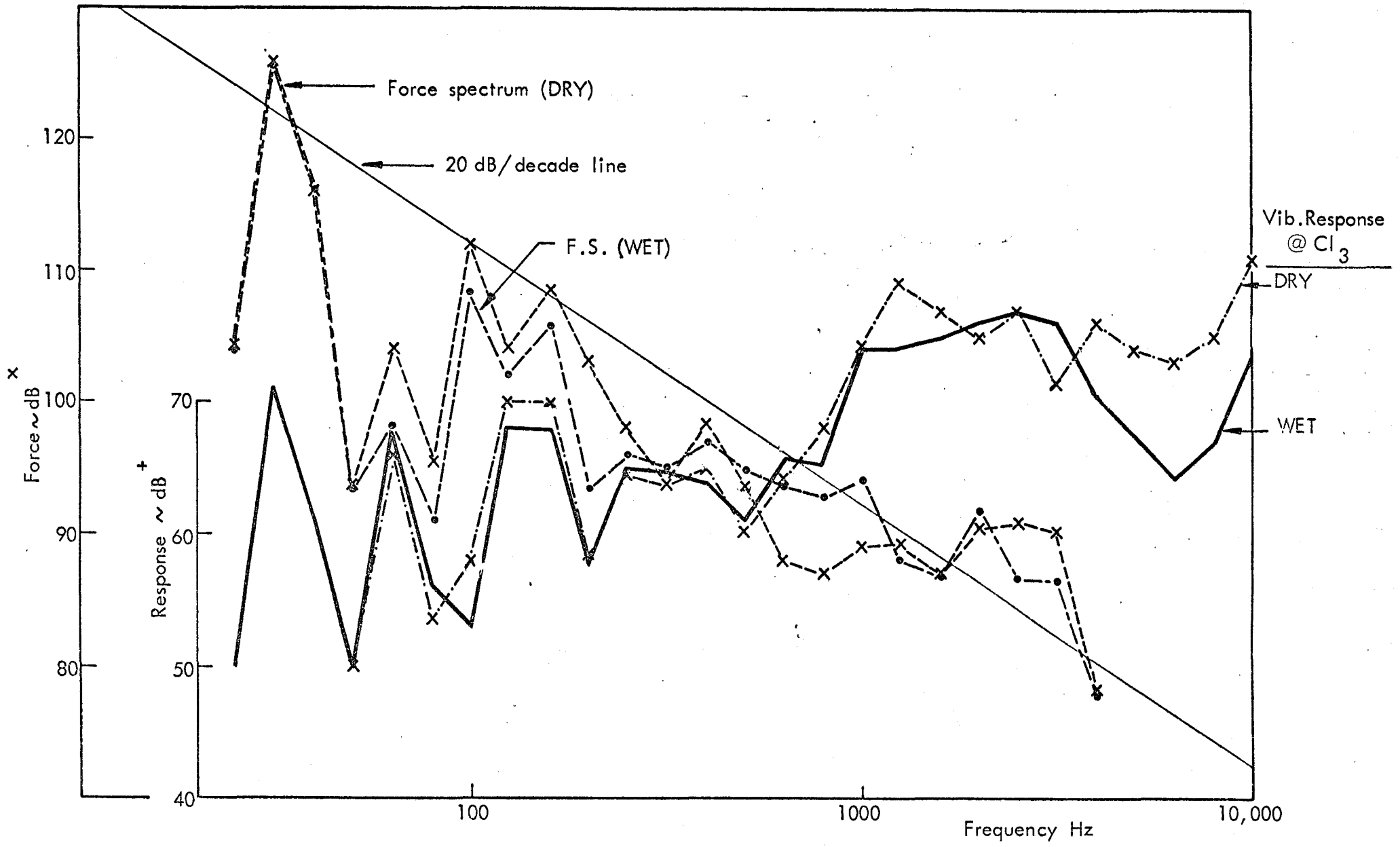

FIG. 5.30c TYPICAL EFFECT OF OIL FILM ON THE VEE RIG AT REPETITION RATE 33.3 per sec. — STANDARD PISTONS OF SA

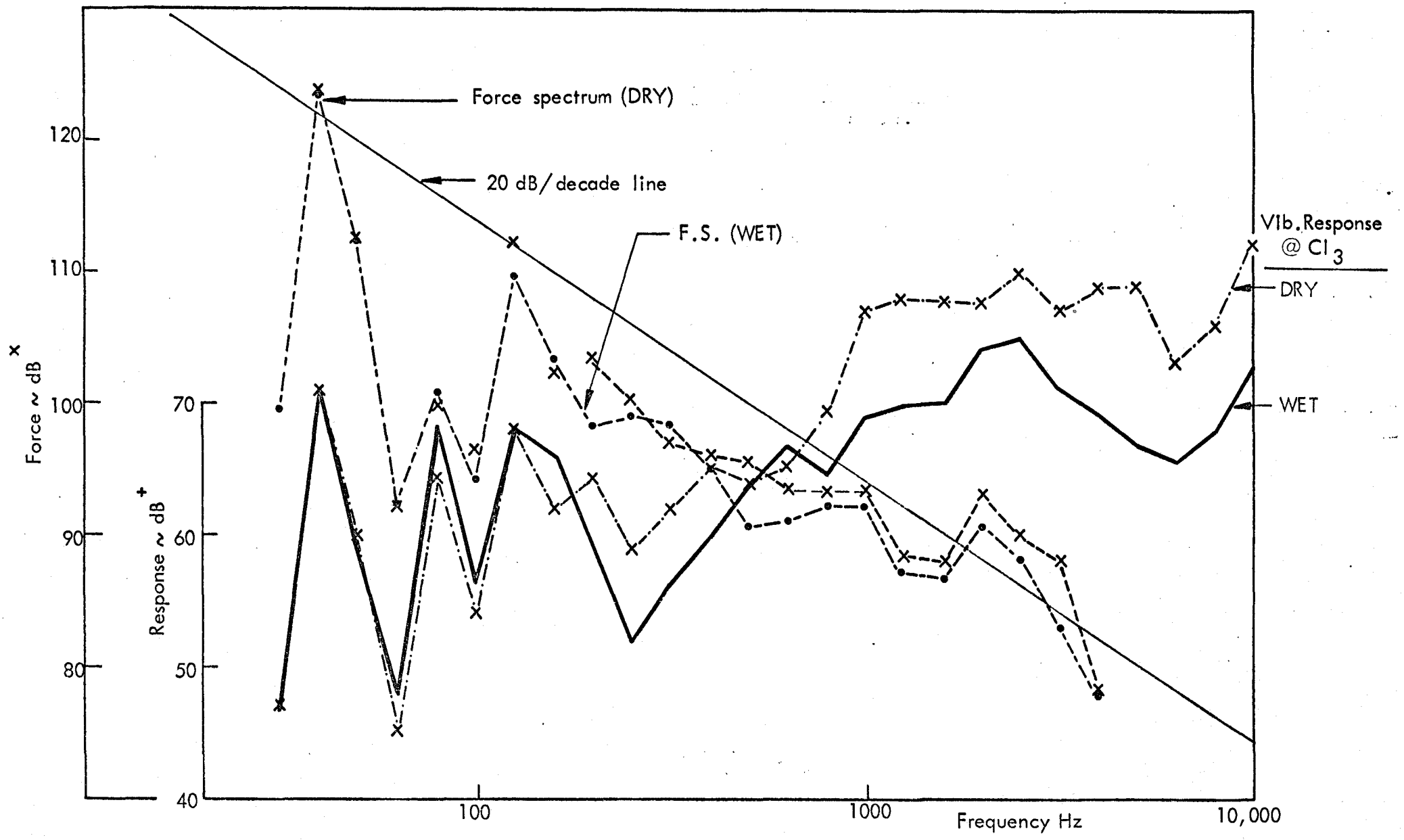

FIG. 5.30d TYPICA EFFECT OF OIL FILM ON THE VEE RIG AT REPETITION RATE 41.7 per sec. — STANDARD PISTONS OF SA

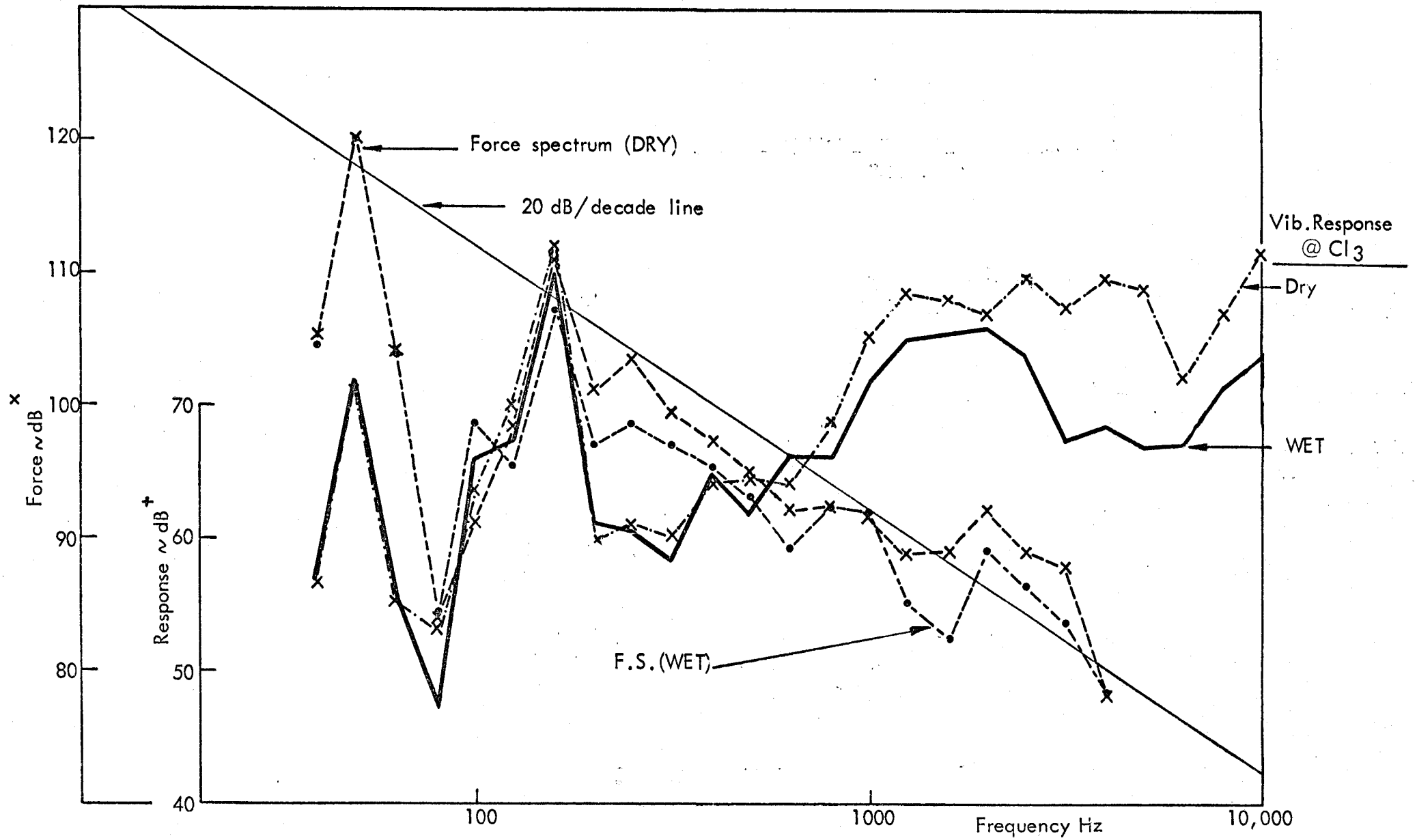

FIG. 5.30e TYPICAL EFFECT OF OIL FILM ON THE RIG AT REPETITION RATE 50 per sec. — STANDARD PISTONS OF SA

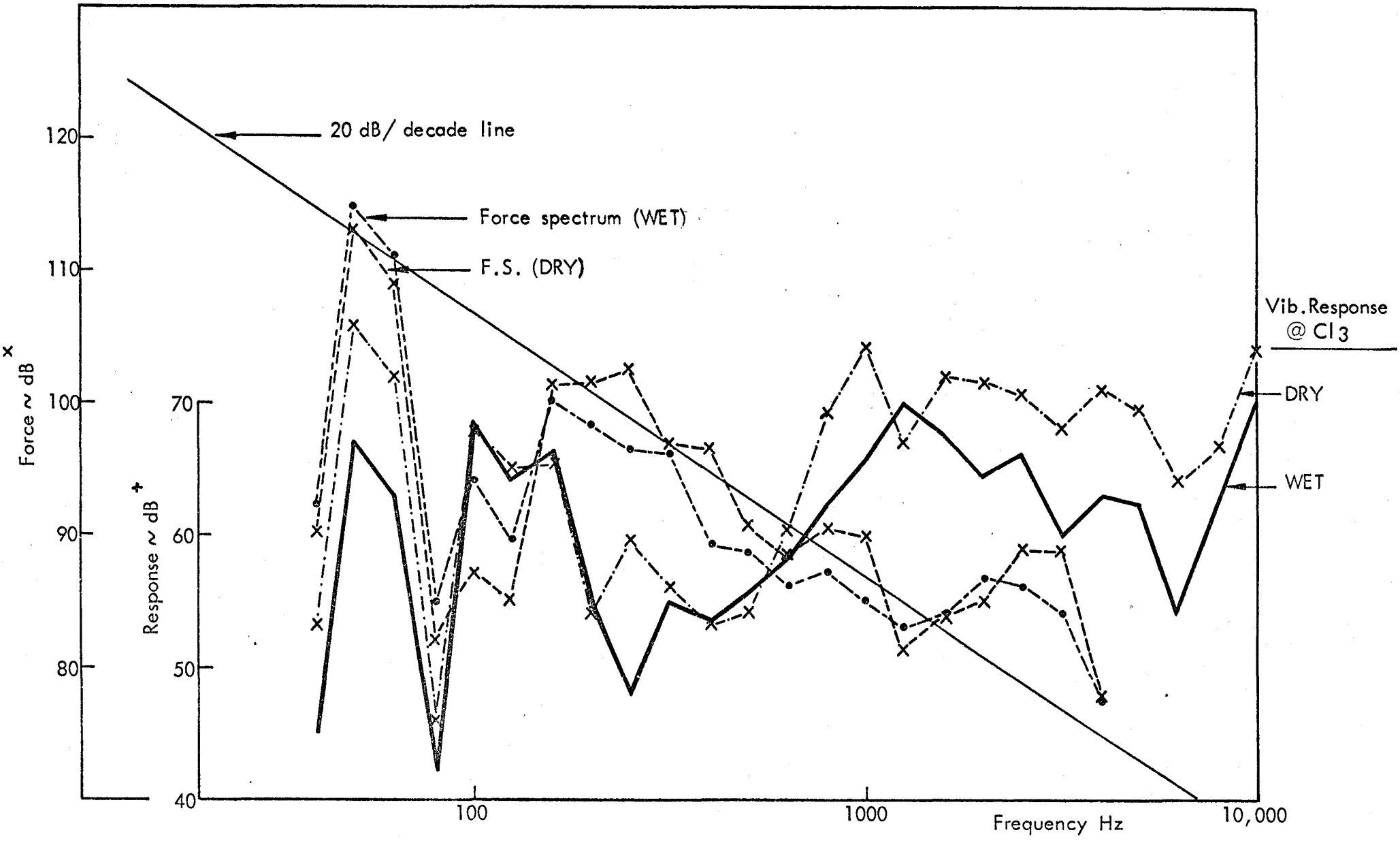

FIG. 5.30f TYPICAL EFFECT OF OIL FILM ON THE VEE RIG AT REPETITION RATE 55 per sec. — STANDARD PISTONS OF SA

DRY

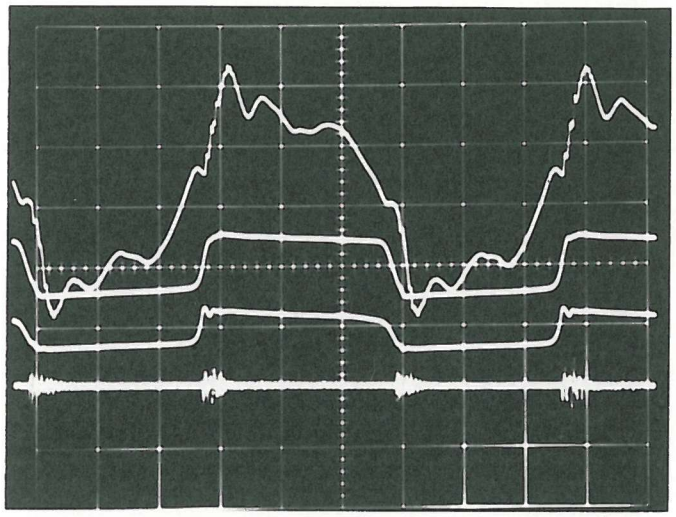

—FORCE — 2 v./d.

_U.C. — 2 v./d.

_L.C. — 2 v./d.

_VIB. at Cl_3 (dBA)
16 g/div.

WET

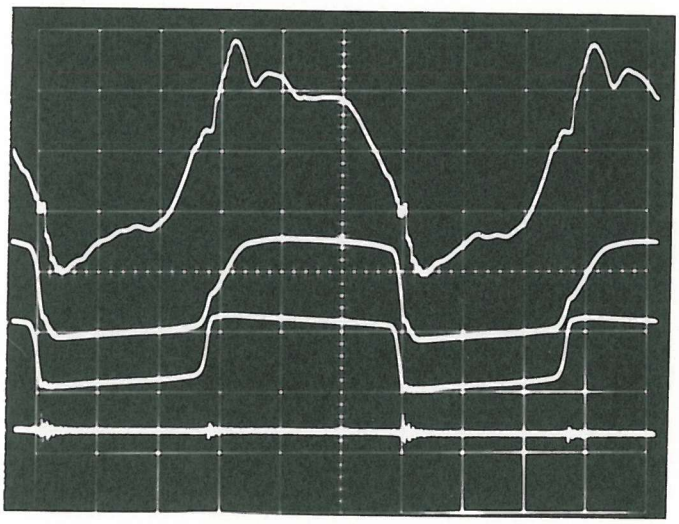

— 2 v./d.

— 1 v./d.

— 1 v./d.

–16 g/div.

FIG. 5.31a TYPICAL EFFECT OF OIL FILM ON PISTON MOVEMENT AND CYLINDER BLOCK VIBRATION DUE TO THE APPLICATION OF THE SAME FORCE AT REPETITION RATE 16.7 per sec. ≡ 1000 RPM—ST. PISTONS... ENGINE SA RIG

DRY

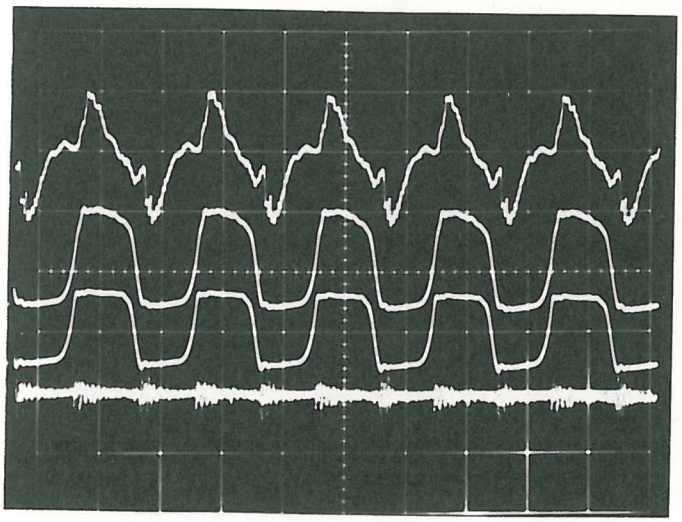

— FORCE — 2 v./d.

— U.C. — 1 v./d.

— L.C. — 1 v./d.

— VIB. at Cl_3 (dBA)
16 g/div.

WET

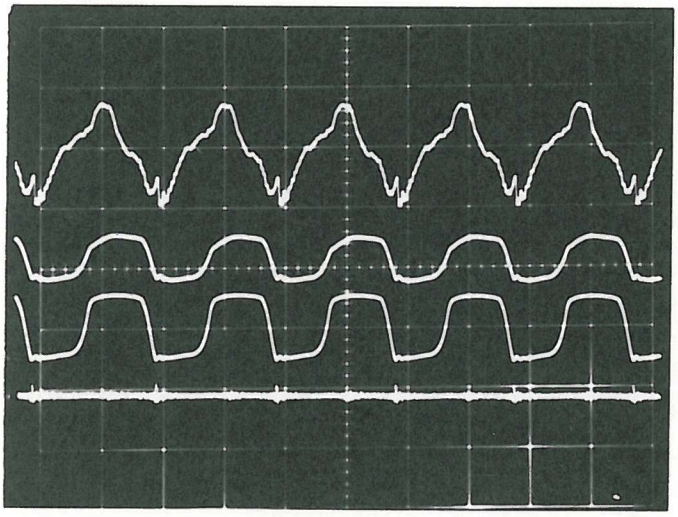

— 2 v./d.

— 1 v./d.

— 1 v./d.

— 32 g/div.

FIG. 5.31b TYPICAL EFFECT OF OIL FILM ON PISTON MOVEMENT AND CYLINDER BLOCK VIBRATION DUE TO THE APPLICATION OF THE SAME FORCE AT REPETITION RATE 50 per sec. ≡ 3000 RPM — ST. PISTONS — ENGINE SA RIG

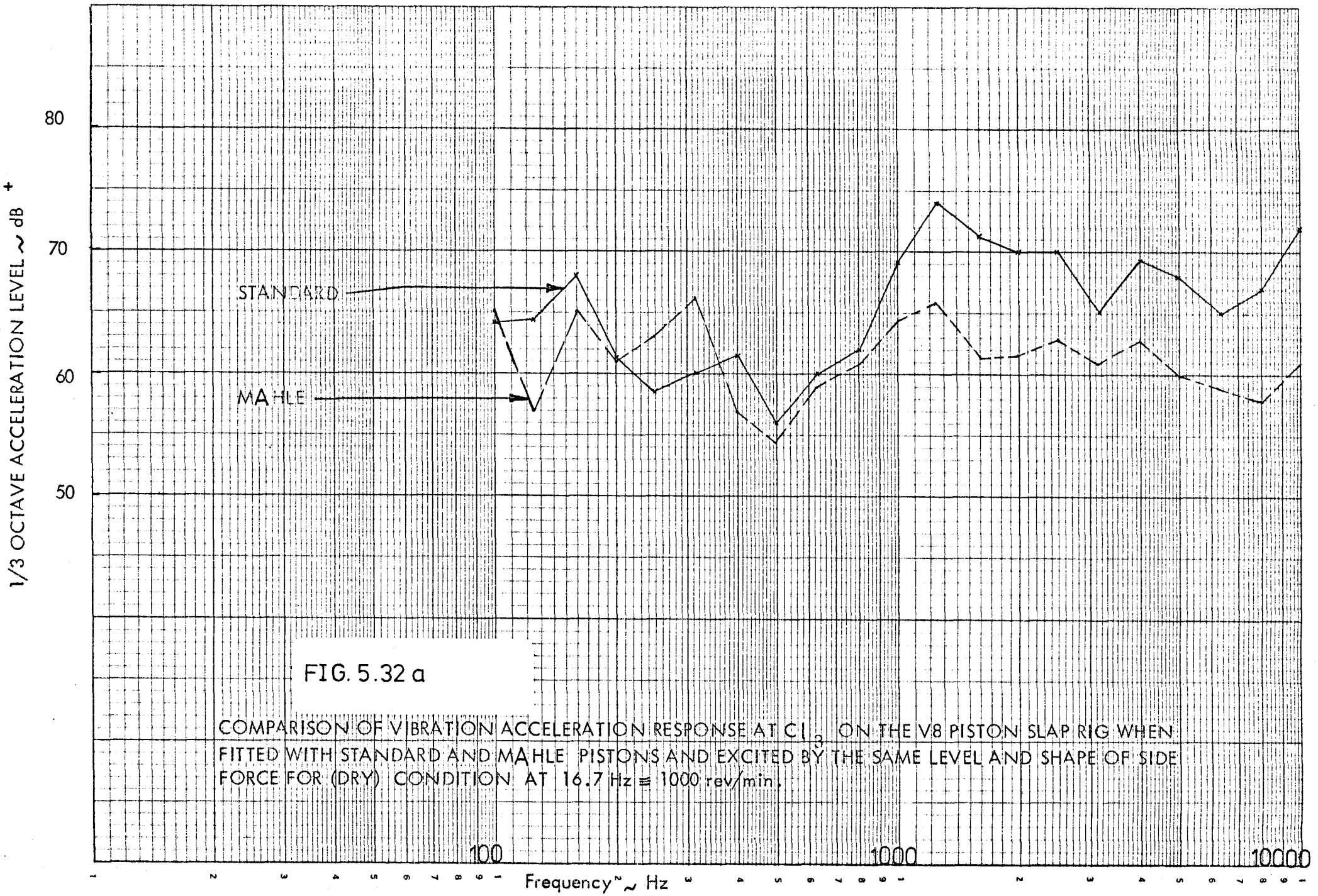

FIG. 5.32 a

COMPARISON OF VIBRATION ACCELERATION RESPONSE AT CI_3 ON THE V8 PISTON SLAP RIG WHEN FITTED WITH STANDARD AND MAHLE PISTONS AND EXCITED BY THE SAME LEVEL AND SHAPE OF SIDE FORCE FOR (DRY) CONDITION AT 16.7 Hz ≡ 1000 rev/min.

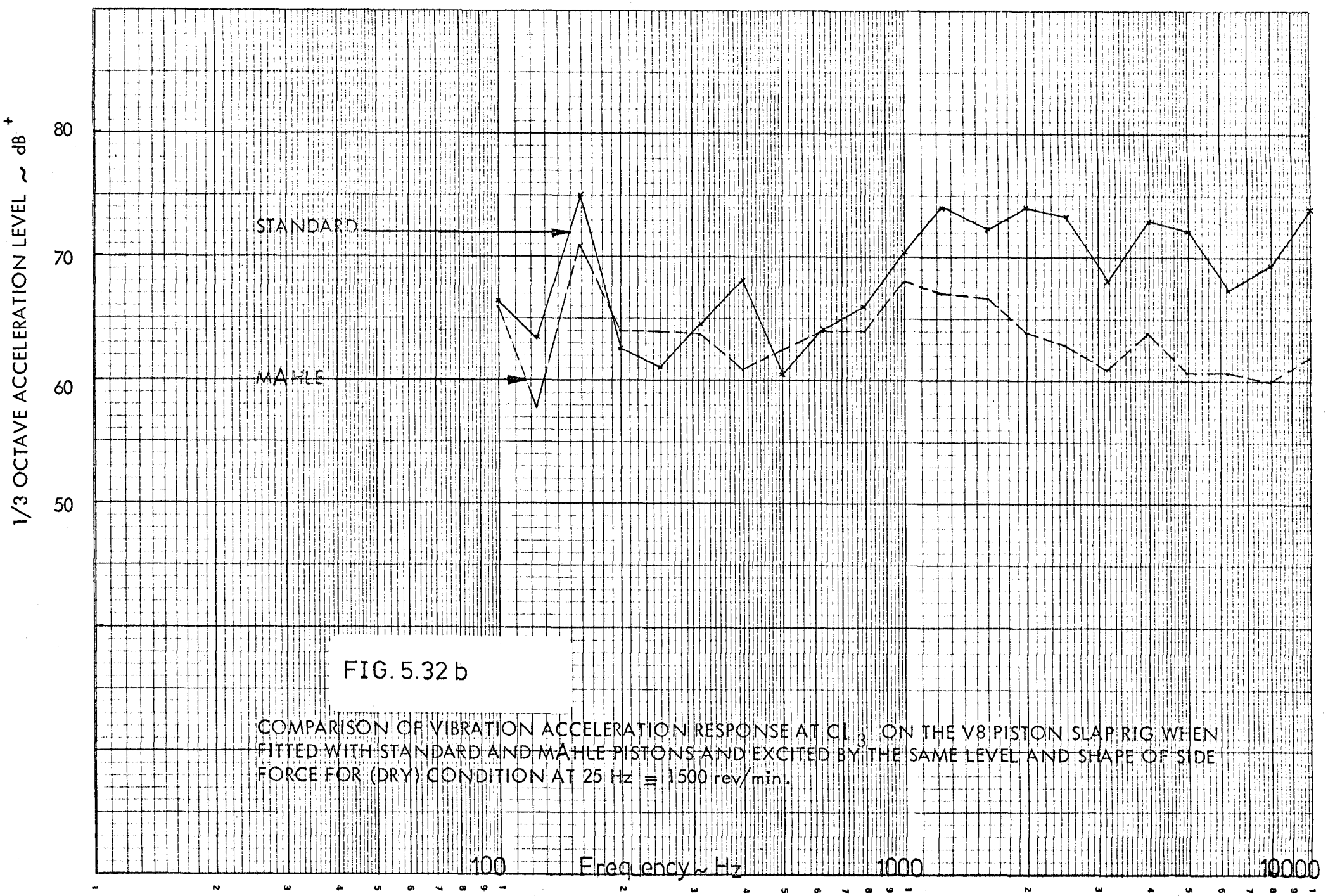

FIG. 5.32 b

COMPARISON OF VIBRATION ACCELERATION RESPONSE AT Cl_3 ON THE V8 PISTON SLAP RIG WHEN FITTED WITH STANDARD AND MAHLE PISTONS AND EXCITED BY THE SAME LEVEL AND SHAPE OF SIDE FORCE FOR (DRY) CONDITION AT 25 Hz ≡ 1500 rev/min.

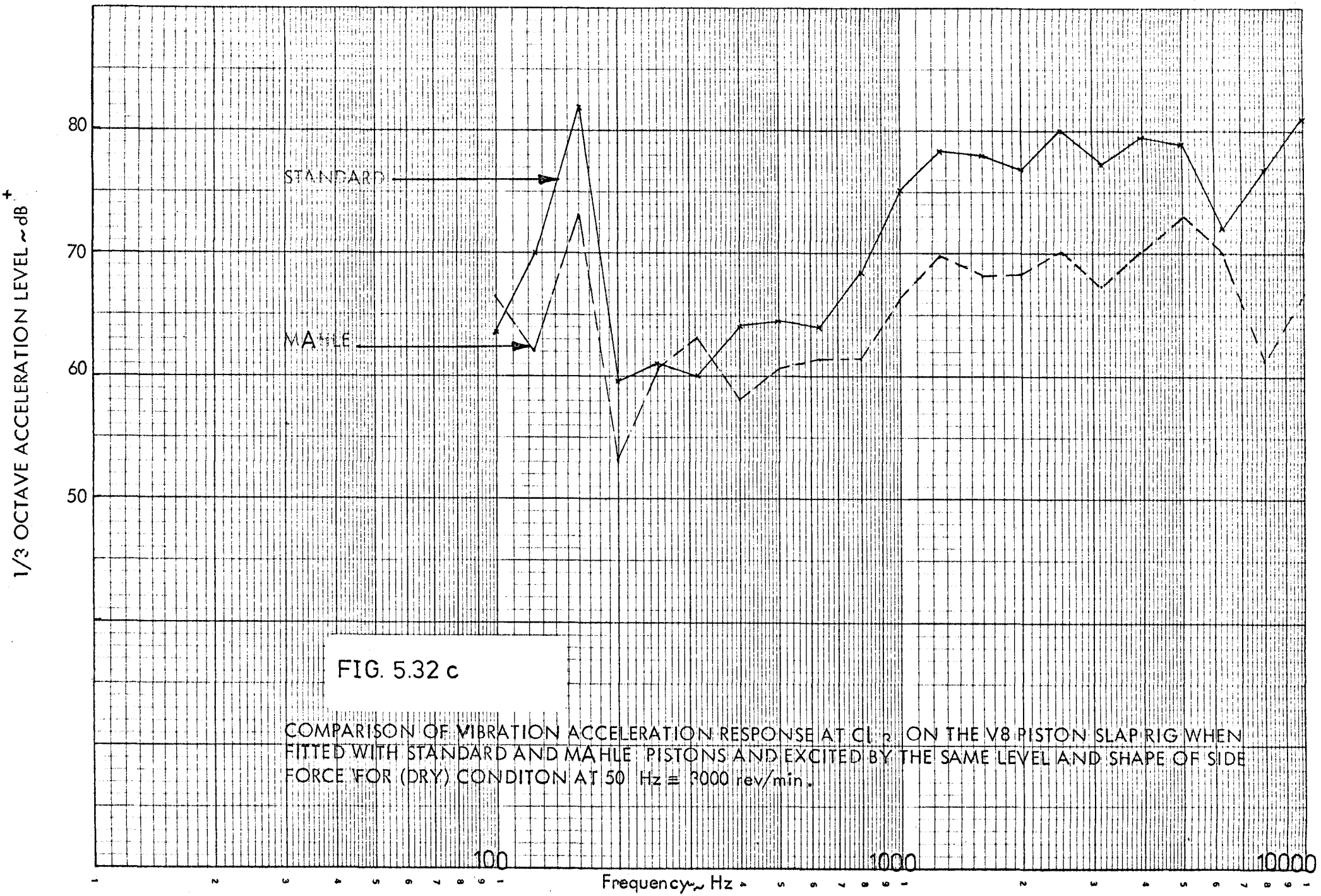

FIG. 5.32 c

COMPARISON OF VIBRATION ACCELERATION RESPONSE AT Cl 2 ON THE V8 PISTON SLAP RIG WHEN FITTED WITH STANDARD AND MAHLE PISTONS AND EXCITED BY THE SAME LEVEL AND SHAPE OF SIDE FORCE FOR (DRY) CONDITON AT 50 Hz ≡ 3000 rev/min.

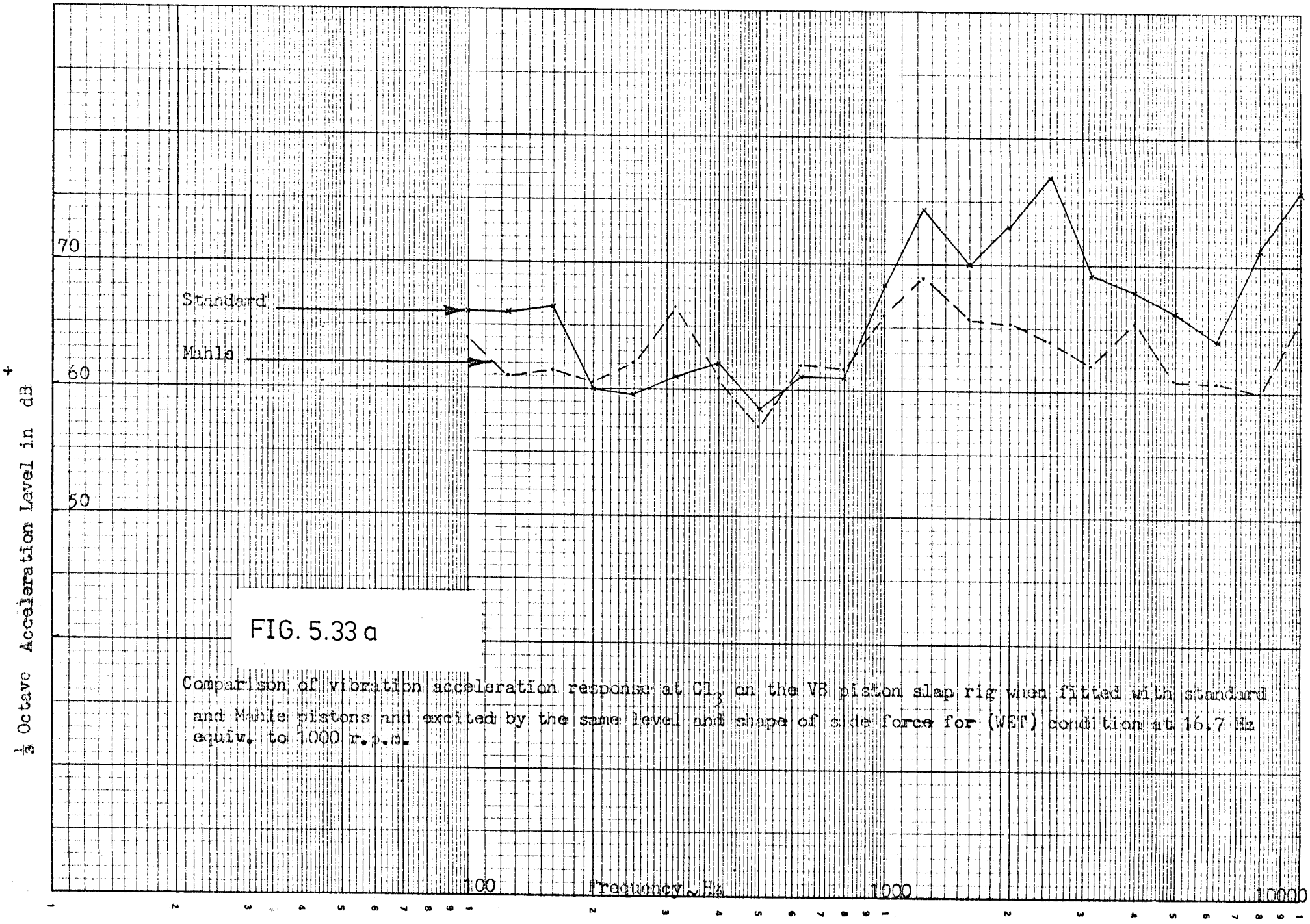

FIG. 5.33 a

Comparison of vibration acceleration response at Cl_2 on the V8 piston slap rig when fitted with standard and Mahle pistons and excited by the same level and shape of side force for (WET) condition at 16.7 Hz equiv. to 1000 r.p.m.

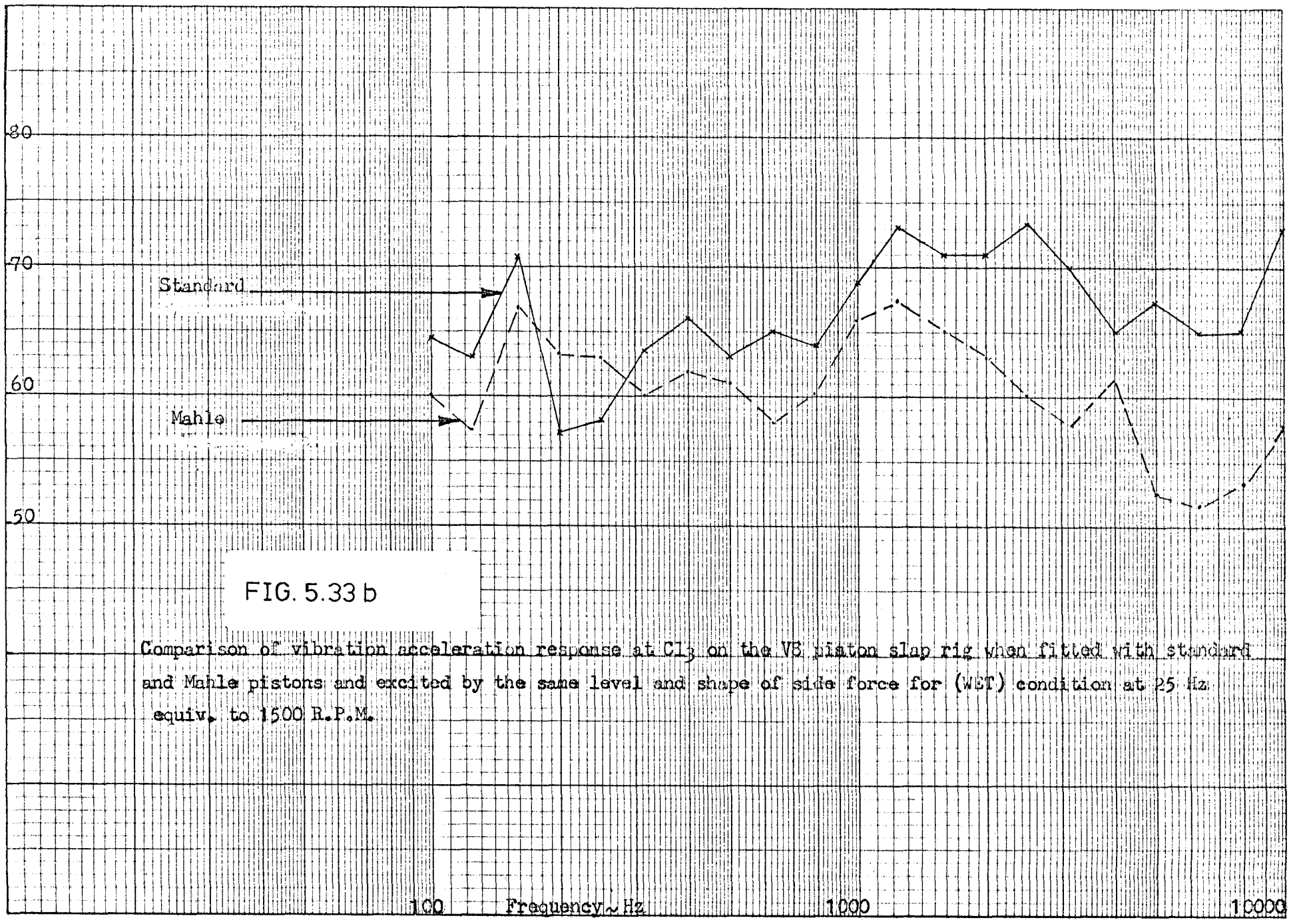

FIG. 5.33 b

Comparison of vibration acceleration response at $C1_3$ on the V8 piston slap rig when fitted with standard and Mahle pistons and excited by the same level and shape of side force for (WET) condition at 25 Hz equiv. to 1500 R.P.M.

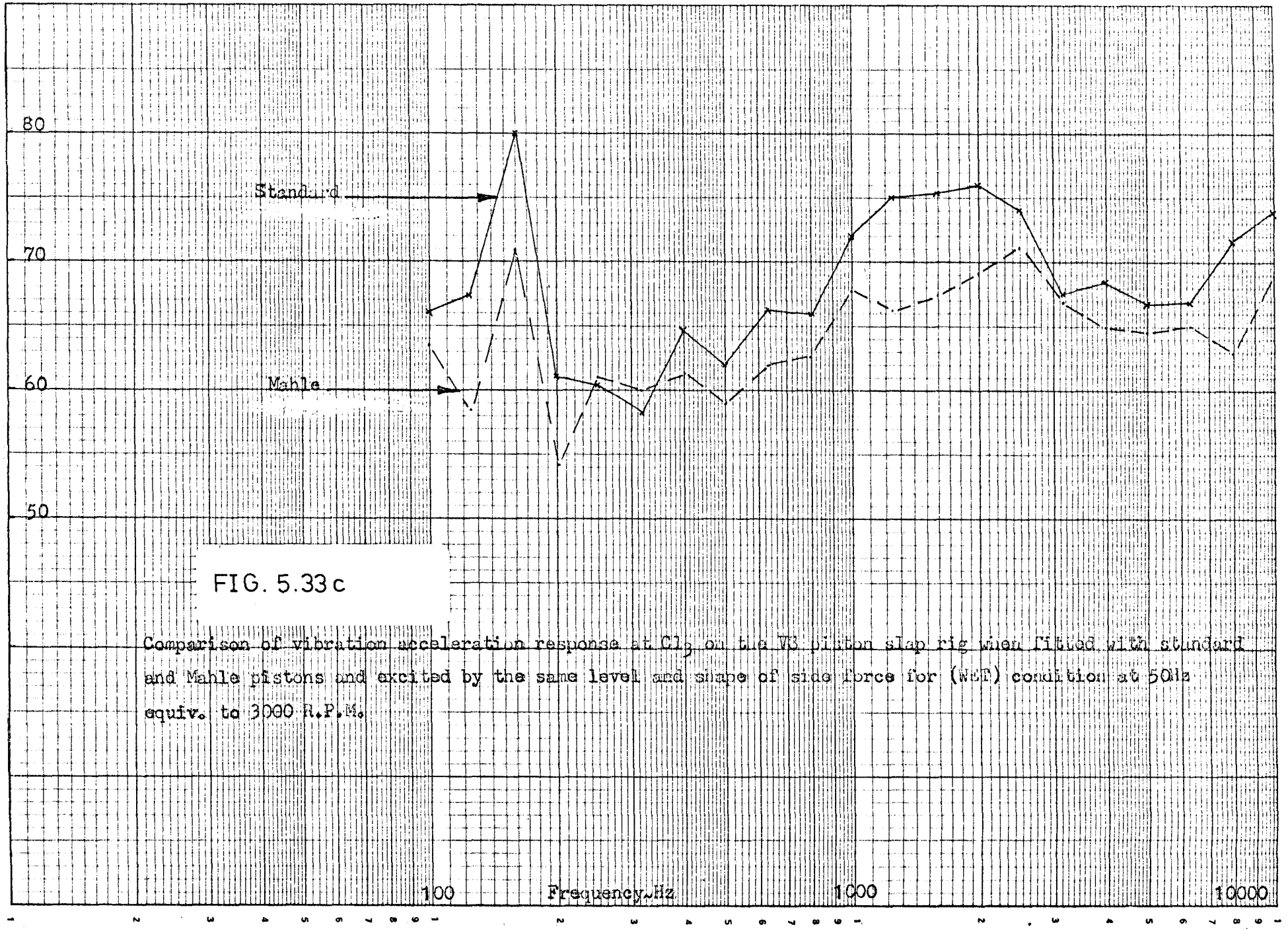

FIG. 5.33 c

Comparison of vibration acceleration response at Cl_3 on the V8 piston slap rig when fitted with standard and Mahle pistons and excited by the same level and shape of side force for (WOT) condition at 50Hz equiv. to 3000 R.P.M.

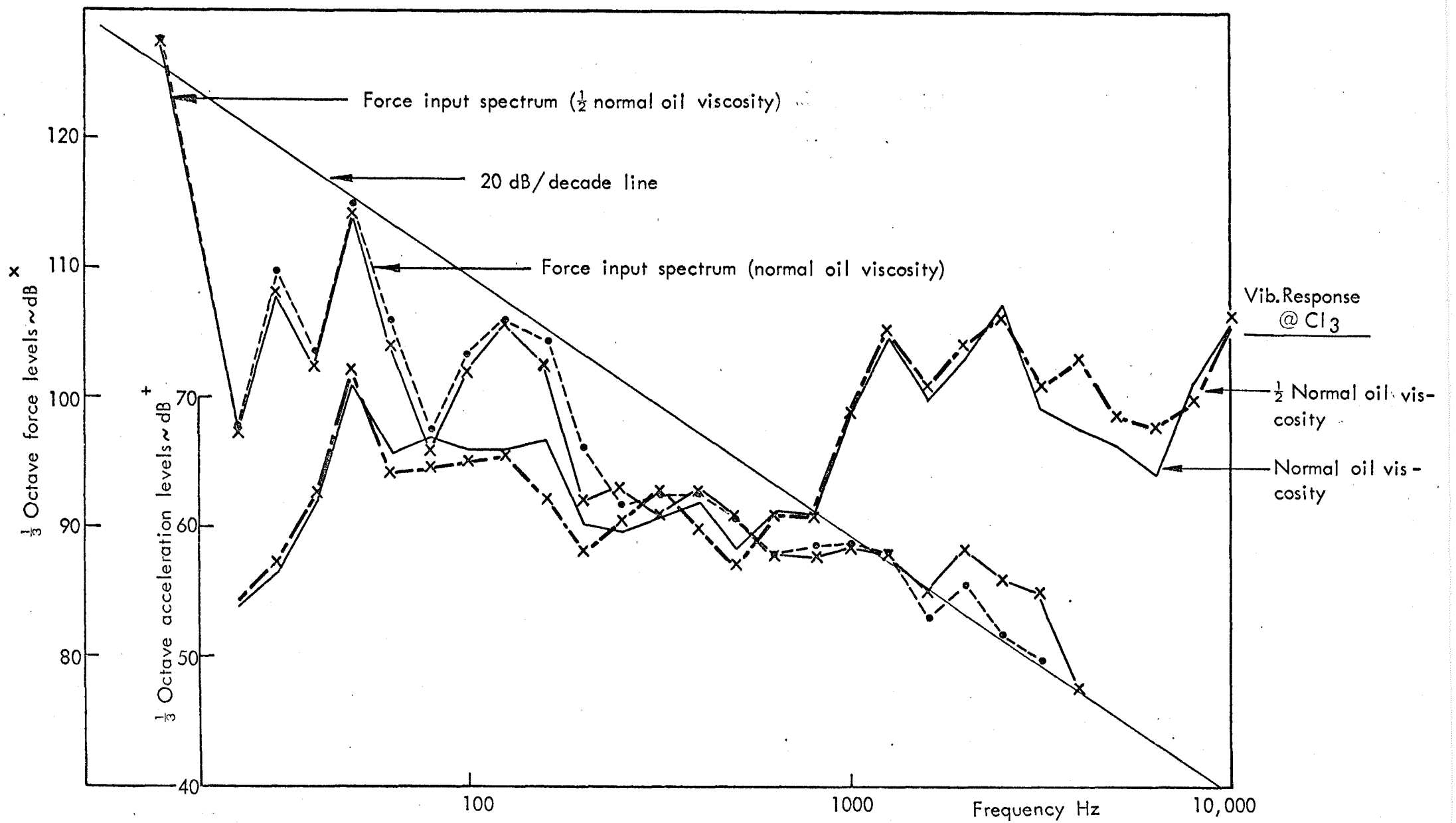

FIG. 5.34a FORCE RESPONSE SPECTRA SHOWING EFFECT OF VARYING OIL FILM VISCOSITY ON THE V8 PISTON SLAP RIG FOR THE STANDARD PISTON AT 16.7 Hz ≡ 1000 RPM

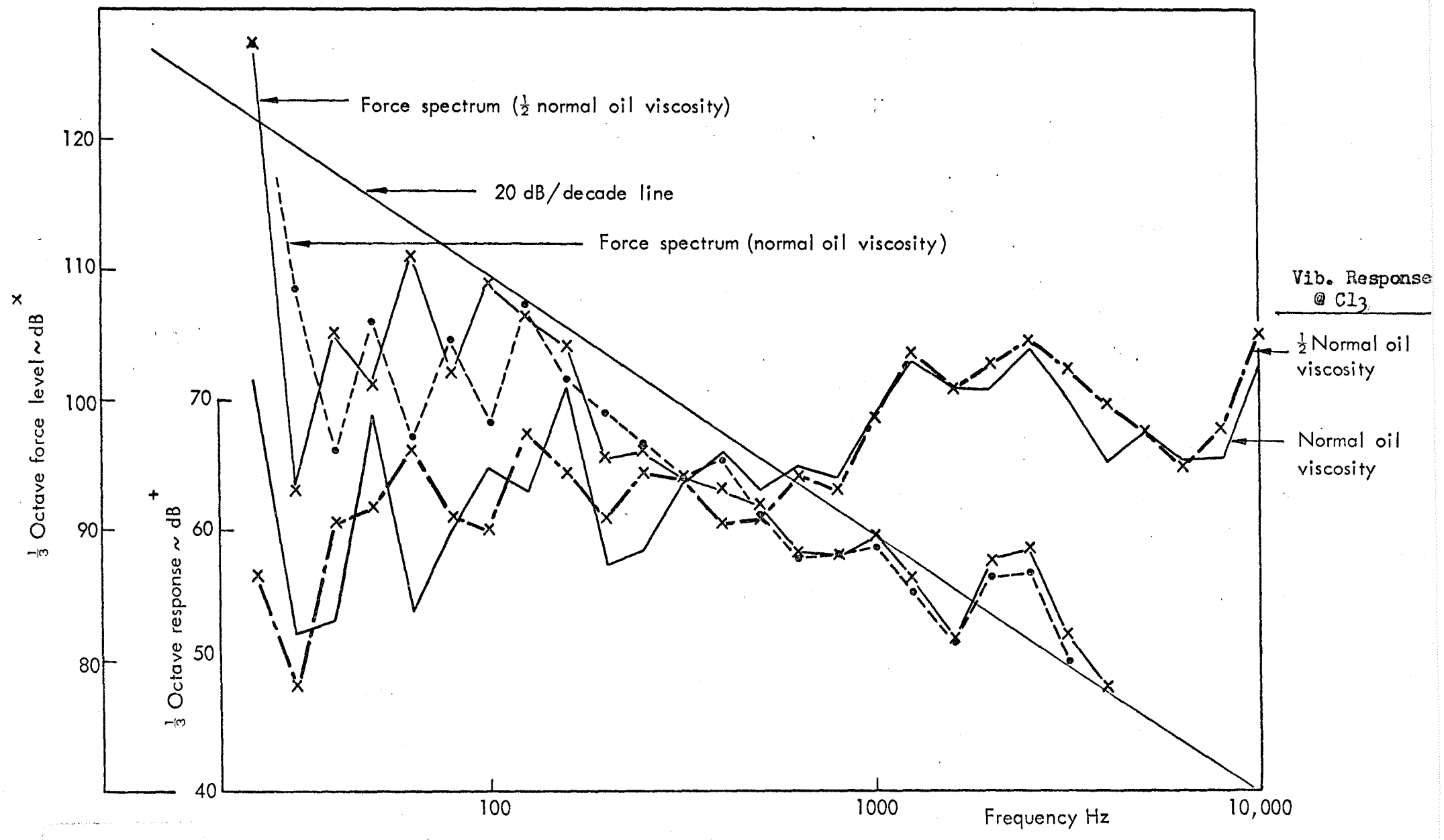

FIG. 5.34 b FORCE RESPONSE SPECTRA SHOWING EFFECT OF VARYING OIL FILM VISCOSITY ON THE V8 PISTON SLAP RIG FOR THE STANDARD PISTONS AT 25 Hz ≡ 1500 R.P.M.

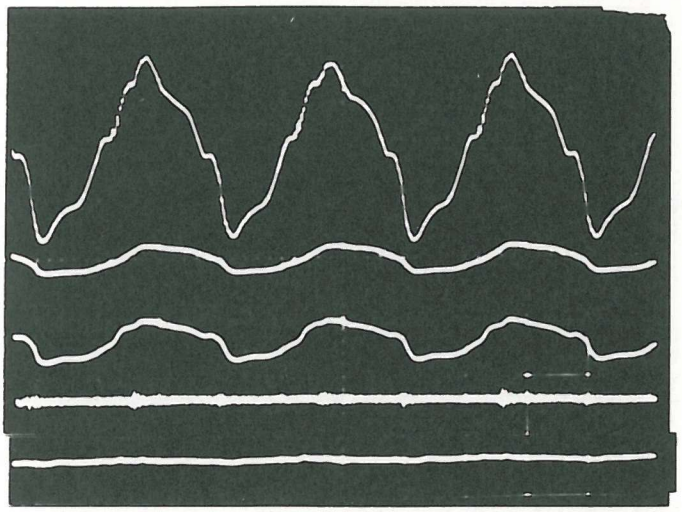

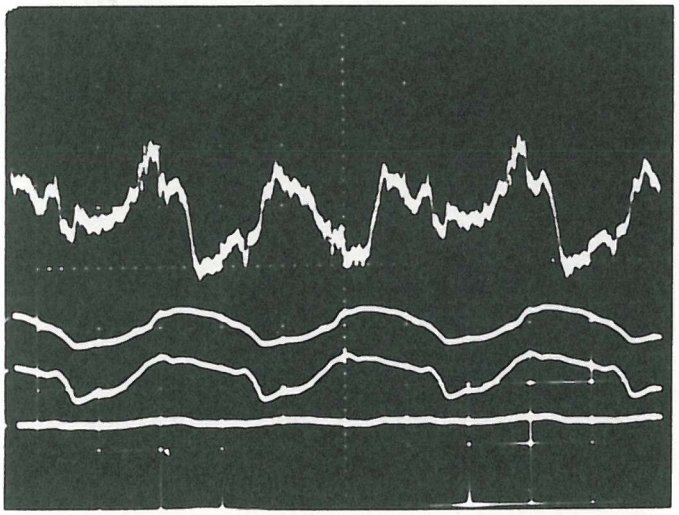

FIG. 5.35

TYPICAL OSCILLOGRAPHS SHOWING THE ATTEMPT AT MEASURING THE OIL FILM PRESSURE ENTRAPPED BETWEEN THE PISTON AND LINER IN THE V8 ENGINE PISTON SLAP RIG AT 33.3 Hz ≡ 2000 r.p.m.

CHAPTER 6

ANALOGUE SIMULATION OF PISTON SLAP

The analogue computer offers a convenient approach for the solution of problems where the basic equations of motion are known. It can be considered that piston behaviour can be described realistically by analytical equations. The analogue computer will therefore present the solutions which are visually displayed and therefore allowing observations to be made while changing the various parameters controlling the process. The analogue computer is also more economical and faster than the digital computer for solutions of second order differential equations and is therefore particularly suitable to solutions of the piston slap problem.

6.1 The analogue simulation as an alternative to the experimental simulation rig

At an early stage of the development of the experimental piston slap rig described in Chapter 5, many difficulties were experienced especially in the control of the driving electronics associated with the hydraulic force generator causing drifts and damage to the rig. Since it was considered that this problem may have been difficult to overcome, it was decided also to formulate the basic equations and to set up on the analogue computer a programme to investigate the effects of the parameters controlling piston slap. Although it was realised that the analogue computer cannot be regarded as an absolute replacement for the experimental rig, it would offer some of the following advantages.

(a) No interaction between the exciter and the system, since the force in the analogue computer is applied through either a built-in oscillator or an external force generator. In both cases, the system is not affected by the operation of the force generator. In the experimental rig, interaction

is bound to interfere whatever care is taken.

(b) The analogue computer is considerably faster, since the relevant values can be readily changed.

In order to obtain realistic solutions the equations describing piston slap must be fully representative in the physical sense. The perfection of the analogue circuit may be achieved through parallel comparison with experimental solutions of the problem. When the experimental piston slap rig was made to operate reliably, the analogue circuit was continuously improved. The exercise of developing this method is therefore presented in this chapter to show its merits and possible future use.

6.2 Analysis of the Transverse Motion of the Piston Across the Clearance

Initially a simple model was considered where only the transverse motion of the piston across the clearance around top dead centre (T.D.C.) is used.

The piston can be considered to be a rigid mass, m_p, capable of one translation y and the liner (or cylinder) as two rigid masses, m_c, on springs and dampers, capable of motion in two degrees of freedom x_1 and x_2. If the total piston to bore clearance = 2δ, the model is as shown in sketch (1):

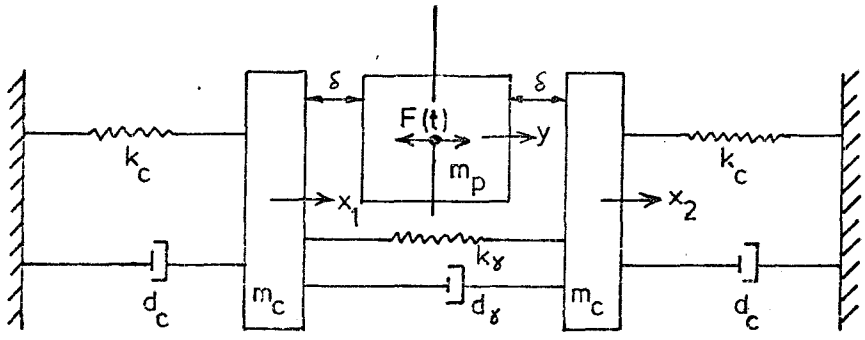

SKETCH (1). Simple Model of Piston-liner Movement Around TDC.

Let $F(t)$ be the force applied to piston. The following equations may be written.

(i) Piston $\quad m_p \ddot{y} = F(t) \qquad (6.1)$

(ii) Liner

$$\begin{vmatrix} m_c & 0 \\ 0 & m_c \end{vmatrix} \begin{vmatrix} \ddot{x}_1 \\ \ddot{x}_2 \end{vmatrix} + \begin{vmatrix} d_c + d_\gamma & -d_\gamma \\ -d_\gamma & d_c + d_\gamma \end{vmatrix} \begin{vmatrix} \dot{x}_1 \\ \dot{x}_2 \end{vmatrix}$$

$$+ \begin{vmatrix} k_c + k_\gamma & -k_\gamma \\ -k_\gamma & k_c + k_\gamma \end{vmatrix} \begin{vmatrix} x_1 \\ x_2 \end{vmatrix} = 0 \qquad (6.2)$$

where

$\begin{vmatrix} m_c & 0 \\ 0 & m_c \end{vmatrix}$ is the inertia matrix

$\begin{vmatrix} d_c + d_\gamma & -d_\gamma \\ -d_\gamma & d_c + d_\gamma \end{vmatrix}$ is the damping matrix

and

$\begin{vmatrix} k_c + k_\gamma & -k_\gamma \\ -k_\gamma & k_c + k_\gamma \end{vmatrix}$ is the stiffness matrix

(iii) Impact relation

Let e be the coefficient of restitution of m_c to m_p.

$$\bar{m}_p = m_p/(m_p + m_c)$$

and

$$\bar{m}_c = m_c/(m_p + m_c).$$

Then for impact on the left

$$\begin{vmatrix} \dot{y} \\ \dot{x}_1 \end{vmatrix}_{\text{after}} = \begin{vmatrix} \bar{m}_p - e\bar{m}_c & \bar{m}_c(1 + e) \\ \bar{m}_p(1 + e) & \bar{m}_c - e\bar{m}_p \end{vmatrix} \begin{vmatrix} \dot{y} \\ \dot{x}_1 \end{vmatrix}_{\text{before}}$$

and on the right (6.3)

$$\begin{vmatrix} \dot{y} \\ \dot{x}_2 \end{vmatrix}_{after} = \begin{vmatrix} \bar{m}_p - e\bar{m}_c & \bar{m}_c(1+e) \\ \bar{m}_p(1+e) & \bar{m}_c - e\bar{m}_p \end{vmatrix} \begin{vmatrix} \dot{y} \\ \dot{x}_2 \end{vmatrix}_{before}$$

Equations (6.1), (6.2) and (6.3) may be written as follows:

$$m_p\ddot{y} = F(t) \tag{6.4}$$

$$m_c\ddot{x}_1 + (d_c + d_\gamma)\dot{x}_1 - d_\gamma\dot{x}_2 + (k_c + k_\gamma)x_1 - k_\gamma x_2 = 0 \tag{6.5}$$

$$m_c\ddot{x}_2 - d_\gamma\dot{x}_1 + (d_c + d_\gamma)\dot{x}_2 - k_\gamma x_1 + (k_c + k_\gamma)x_2 = 0 \tag{6.6}$$

$$\dot{y}_f = \alpha\dot{y}_i + \beta\dot{x}_{1i} \tag{6.7}$$

$$\dot{x}_{1f} = \phi\dot{y}_i + \gamma\dot{x}_{1i} \tag{6.8}$$

$$\dot{y}_f = \alpha\dot{y}_i + \beta\dot{x}_{2i} \tag{6.9}$$

$$\dot{x}_{2f} = \phi\dot{y}_i + \gamma\dot{x}_{2i} \tag{6.10}$$

where i = initial

f = final

and

$$\alpha = \frac{m_p - em_c}{m_p + m_c} \qquad \beta = \frac{(1+e)m_c}{m_p + m_c}$$

$$\phi = \frac{(1+e)m_p}{m_p + m_c} \qquad \gamma = \frac{m_c - em_p}{m_p + m_c}$$

Equations (6.4) to (6.10) may be represented on the analogue computer for the engine under investigation but the coefficients of the variables must be calculated.

F(t) = piston sideways force where a built in or external oscillator may be used

m_p = 4.54 lb = .140 slugs

m_c = 3.095 lb = .096 slugs.

It has been estimated that $e \simeq 0.4$ for the piston-liner impact, therefore other values are as follows:

$$\alpha = .432$$

$$\beta = .565$$

$$\phi = .830$$

$$\gamma = .168$$

To calculate k_c, k_γ, d_c and d_γ, impact tests were made on the engine described in Appendix E. As the liner equations (6.5) and (6.6) have been treated as a system with two degrees of freedom, two basic modes have to be considered. These are:

ω_{o_1} = 1250 Hz = liner bodily motion which induces the bank to bank mode of the engine vibration

ω_{o_2} = 2950 Hz = liner cantilever motion.

For such a system

$$\omega_{o_1} = \sqrt{\frac{k_c}{m_c}} \tag{6.11}$$

and

$$\omega_{o_2} = \omega_{o_1}\sqrt{1 + 2a} \qquad \text{(ref. 6.1)} \tag{6.12}$$

where $$a = k_\gamma/k_c \tag{6.13}$$

Substituting in (6.11)

$$k_c = 85 \times 10^6 \text{ N/m} = 5.8 \times 10^6 \text{ lb/ft.}$$

Substituting in (6.12)

$$a = 2.3.$$

Therefore from (6.13) $k_\gamma = 195.5 \times 10^6$ N/m $= 13.3 \times 10^6$ lb/ft.

From Appendix E the average damping ratios obtained are as follows:

Average $z_c = .028$

Average $z_\gamma = .010$

$$\therefore \quad d = 2z\sqrt{km} \tag{6.14}$$

Therefore

$$d_c = 2z_c\sqrt{k_c m_c} = 41.7 \text{ lb.sec/ft.} = 3.5 \text{ lb.sec/in} \quad (Q_c = 18)$$

and

$$d_\gamma = 2z_\gamma\sqrt{k_\gamma m_c} = 22.6 \text{ lb.sec./ft.} = 1.9 \text{ lb.sec/in} \quad (Q = 50)$$

Therefore

$$d_c + d_\gamma = 64.3 \text{ lb.sec./ft.} = 5.4 \text{ lb.sec./in.}$$

Therefore, equations (6.4) to (6.10) may now be written for the two liner modes as follows:

$$\ddot{y} - 85F(t) = 0 \tag{6.15}$$

$$\ddot{x}_1 + 692\dot{x}_1 - 244\dot{x}_2 + 200 \times 10^6 x_1 - 139 \times 10^6 x_2 = 0 \tag{6.16}$$

$$\ddot{x}_2 - 244\dot{x}_1 + 692\dot{x}_2 - 139 \times 10^6 x_1 + 200 \times 10^6 x_2 = 0 \tag{6.17}$$

$$\dot{y}_f = .432\dot{y}_i + .565\dot{x}_{1i} \tag{6.18}$$

$$\dot{x}_{1f} = .83\dot{y}_i + .168\dot{x}_{1i} \tag{6.19}$$

$$\dot{x}_{2f} = .83\dot{y}_i + .168\dot{x}_{2i} \tag{6.20}$$

$$\dot{y}_f = .432\dot{y}_i + .565\dot{x}_{2i} \tag{6.21}$$

where y, x_1 and x_2 are in inches

$\dot{y}$, $\dot{x}_1$ and $\dot{x}_2$ are in inches/sec.

$\ddot{y}$, $\ddot{x}_1$ and $\ddot{x}_2$ are in inches/sec^2.

6.3 Development of the Piston Slap Simulation Analogue Circuit

The independent variable of the piston slap simulation equations is represented on the analogue computer in terms of time; the dependent variables and their derivatives with respect to time are represented by voltages. These signal voltages should never exceed the maximum allowable value of one machine unit (usually $\pm$ 10 volts). Other limitations and instructions are documented in ref. (6.2).

(a) Amplitude Scaling

Amplitude scale factor = 1/estimated maximum of variable.

Problem variable	Max. Expected Value	Scale Factor	Computer Variable	m.u.
y and x	.010 inches	$\frac{1}{.01} = 10^2$	$10^2 y$ and	$10^2 x$
$\dot{y}$ and $\dot{x}$	100 in/sec	$\frac{1}{100} = 10^{-2}$	$10^{-2}\dot{y}$ and	$10^{-2}\dot{x}$
$\ddot{y}$ and $\ddot{x}$	10^6 in/sec^2	$\frac{1}{10^6} = 10^{-6}$	$10^{-6}\ddot{y}$ and	$10^{-6}\ddot{x}$
F_{max}	500 lbf.	$\frac{1}{5000} = 2 \times 10^{-4}$	$2 \times 10^{-4} F_{max}$	

(b) Time Scaling

If t = time required for a solution in the physical problem

and τ = time required for the same solution on the computer

and β = dimensionless time scale factor

then $\tau = \beta t$.

In the present case the time is slowed down by a factor of 100 so that visual display can be readily observed.

From information in (a) and (b), equations (6.15) to (6.21) may be scaled as follows:

$$10^{-6}\ddot{y} - 10^{-6}.85F(t) = 0 \qquad \therefore \quad P_2 = \underline{\text{Pot*}(01)} = \underline{.425}$$

$$10^{-6}\ddot{y} - (P_2).2 \times 10^{-4} F(t) = 0$$

$$10^{-6}\ddot{x}_1 + 10^{-6}(692)\dot{x}_1 - 10^{-6}(244)\dot{x}_2 + 10^{-6}(200.10^6)x_1 - 10^{-6}(139.10^6)x_2 = 0$$

$$10^{-6}\ddot{x}_1 + 10^{-2}(P_6)\dot{x}_1 - 10^{-2}(P_9)\dot{x}_2 + 10^{2}(P_{10})x_1 - 10^{2}(P_7)x_2 = 0$$

Therefore,

$$P_6 = \underline{\text{Pot}(05)} = \underline{.0692}$$

$$P_7 = \underline{\text{Pot}(06)} = 1.39 = \underline{.139 \text{ x Gain } 10}$$

$$P_9 = \underline{\text{Pot}(07)} = \underline{.0244}$$

$$P_{10} = \underline{\text{Pot}(08)} = 2 = \underline{.2 \text{ x Gain } 10}$$

*Pot = Potentiometer

$$10^{-6}\ddot{x}_2 - 10^{-6}(244)\dot{x}_1 + 10^{-6}(692)\dot{x}_2 - 10^{-6}(139.10^6)x_1 + 10^{-6}(200.10^6)x_2 = 0$$

$$10^{-6}\ddot{x}_2 - 10^{-2}(P_{14})\dot{x}_1 + 10^{-2}(P_{11})\dot{x}_2 - 10^{2}(P_{12})x_1 + 10^{2}(P_{15})x_2 = 0$$

Therefore

$$P_{11} = \underline{\text{Pot(35)}} = \underline{.0692}$$

$$P_{12} = \underline{\text{Pot(36)}} = 1.39 = \underline{.139 \text{ x Gain } 10}$$

$$P_{14} = \underline{\text{Pot(37)}} = \underline{.0244}$$

$$P_{15} = \underline{\text{Pot(38)}} = 2 = \underline{.2 \text{ x Gain } 10}$$

$$\alpha = \underline{\text{Pot(31)}} = \underline{.432}$$

$$\beta = \underline{\text{Pot(32)}} = \underline{.565}$$

$$\phi = \underline{\text{Pot(41)}} = \underline{.83}$$

$$\gamma = \underline{\text{Pot(40)}} = \underline{.168}$$

The analogue circuit for equations (6.15) to (6.21) is drawn and built on the PACE TR 48 analogue computer as shown in drawing 6.TR48 (enclosed in pocket at end of thesis) with potentiometers set to the values shown above. This drawing presents the final circuit which was obtained after some development and incorporates the following features:

(1) Liner impact detectors

Comparator relays were used for the purpose of detecting the instant when the piston impacted on the liner so that the piston could be instructed to recommence the motion with a certain initial velocity. These relays give logic statements to feed the amplifiers with instructions to operate or reset as required.

(2) Initial condition computation

Electronic comparators are used here in the 'Track/Hold' mode to calculate the immediate initial conditions after each impact. These are fed with logic supplied from comparator B_2 and scaled down from -25V (Relay Volts) to 5 Volts being the acceptable input to the 'track holds' relays.

(3) Initial condition selector

This is a relay used to select the initial condition as appropriate.

(4) Restart system

This system consists of two integrators and two potentiometers as shown in the drawing. It was introduced to instruct the computer to recommence computing when new initial conditions have been reset following an impact with the liner. Without this system the circuit will remain in the hold/reset state indefinitely after impact.

(5) Force on piston (input)

The excitation force driving the piston towards the liner may be provided by means of internal or external inputs. For the internal input, a circuit may be built within the analogue computer to provide a step force, sinusoidal or any other shape forcing input to the piston. For the external input a separate oscillator may be employed to provide any shape of forcing waveform.

6.4 Discussion of Some Typical Results

The circuit shown in drawing 6.TR48 was constructed and operated on the Pace TR48.

Some typical piston-liner movement results were recorded using a four channel chart recorder. In each case, the recordings exhibited four signals namely:

1 - Piston movement

2 - Movement of Left Hand Side of liner x_1

3 - Movement of Right Hand Side of liner x_2

4 - Logic signal

The last signal is most helpful in locating the incidence of impact. Without it, it is extremely difficult at times to locate the impact event.

It may be seen from the chart recordings of figures 6.1-6.7 that certain regions are hatched to identify the times where the computer is not operating. These hatched regions commence at the instant that collision takes place and last for a period which is sufficient for the computer to calculate and set up the initial conditions for subsequent motion. The duration of this period is not related in any way to the piston/liner motion.

It is unfortunate that the TR48 computer has no mechanism for dealing with the situation when the piston is continuously in contact with a liner, e.g., sliding smoothly in continuous contact. In these circumstances, the computer will spend most of its time in the non-operating mode, modelling the situation as a series of minute impacts.

Therefore, and for the purpose of interpreting the chart records, the hatched regions are omitted to obtain modified piston-liner movements as shown in figure 6.8.

Because of sluggish operation of the relays, repetitive application of force on the piston may saturate the computer. Therefore, to display the initial motion and subsequent impacts a step force was employed to send the piston travelling towards one side of the liner, to impact, bounce and leave towards the other side of the liner.

Figure 6.1 shows typical piston/liner movement due to the application of a step force on the piston. It is seen that the amplitudes of vibration of the liners are exaggerated relative to that of the piston. When these are drawn to the same scale and the hatched regions omitted, figure 6.8a is obtained. It can be seen from this figure that, while the liner is still oscillating with small amplitudes (resulting from previous impact) the piston impacts on one side of the liner, pushing it further to a relatively large amplitude after which it bounces and moves in harmony with the liner.

The other side of the liner can be seen to move also, but with different

amplitude characteristics. This is because of interaction of the liner modes. Figure 6.8a also shows that three impacts may occur in this case before the piston leaves the left hand side of the liner. When the piston leaves one side of the liner, the whole liner is set in oscillation, exhibiting its natural modes.

Figure 6.2 shows amplified liner vibration response to facilitate a more accurate calculation of the liner natural frequencies. This is also employed to check that the circuit of the liner vibration equations are set correctly. It can be calculated from this figure that the natural frequencies of the liner are 1250 Hz and 3000 Hz. This is in very good agreement with the assumed natural frequencies of 1250 Hz and 2950 Hz. Figure 6.2 also shows the liner response characteristics due to piston impact.

Figure 6.3 shows the effect of the application of a step force to the piston but reversing it momentarily before impacting one side of the liner. Figure 6.8b shows the redrawn picture without the hatched parts. This is seen to produce a greater number of impacts than in fig. 6.8a. This is due to the phasing of the initial impact with respect to the residual oscillation of the liner. Head-on collision in fig. 6.8(a) leads to considerable loss of piston momentum and causes the second impact also to be head-on. Thereby, few impacts cause reversal of piston movement. In fig. 6.8(b) the initial impact is gentle, as are the subsequent ones, thereby requiring numerous impacts to reverse the piston movement.

Figure 6.4 shows the effect of making the stiffness and damping of the left hand side of the liner greater than the right hand side of the liner. This action tends to reduce the relative amplitudes of the two sides of the liner with subsequent alteration in impact behaviour. Also, the stiffer-damper side of the liner tends to resist bulging or deformation while the other side responds to impact more readily.

Figure 6.5 shows the effect of increasing the mass of the whole liner so as to affect the impact only. The natural frequencies of the liners were left unchanged. In this case the liner amplitudes become appreciably smaller and the piston tends to show less bouncing and leaves each side of the liner quickly, even when the initial impact is gentle.

Although there is no, or little, damping and stiffness between the piston and the block, these were introduced in the intermediate model of SKETCH (2),

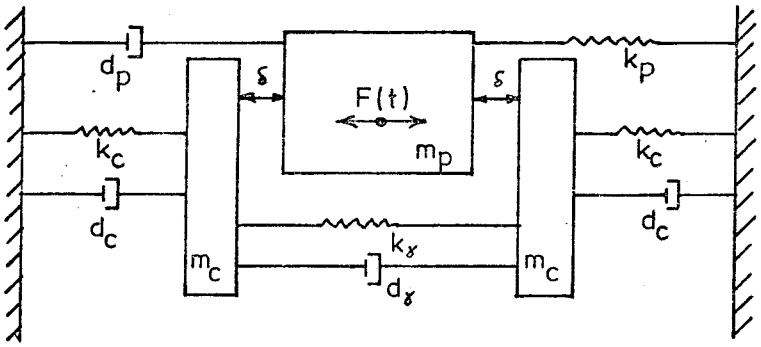

SKETCH (2)

where equation (6.1) is generalised to equation (6.22).

The solution of this model gives some interesting hypothetical results which are shown in figures 6.6 and 6.7. It may be seen that there exist some critical values of damping and stiffness (piston to block) that can prevent the piston from hitting the two sides of the liner. The application of such an arrangement may be difficult to achieve in practice, though the model of SKETCH (3) presents a possibility, where d_p and k_p are optimised

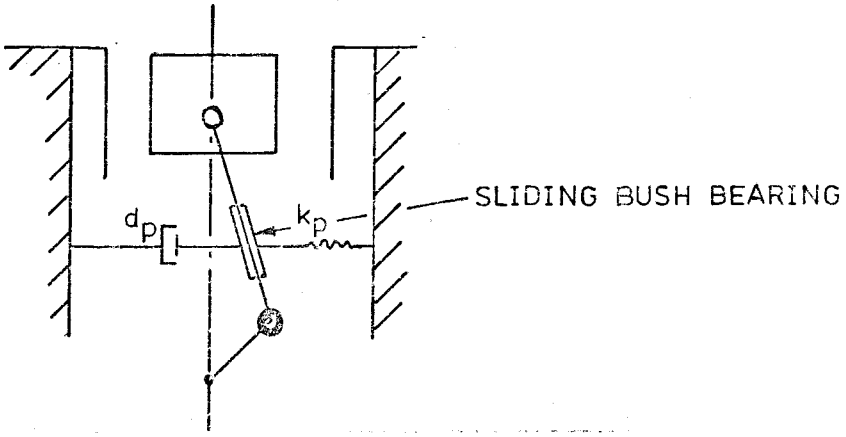

SKETCH (3)

for the system considered. The difficulty arises in assembling such a system to be durable, reliable and not to interfere with the operation of the crank mechanism.

This example shows to some extent an advantage of the analogue system, since it provides the possibility of changing any parameter (alteration of potentiometer values). With no practical difficulties, a solution may emerge which may be very difficult and complicated to test in the physical case. The solution presented in the above model is similar to the crosshead piston designs which are known to minimise sideways impacts in engines.

Although a relatively simple model has been used to obtain the typical results presented, the piston liner movements show reasonable agreement with those obtained on the physical piston slap rig simulation dealt with in the previous chapter. Therefore the analogue circuit may be improved through feedback from the rig testing.

6.5 Possible Analogue Circuit Improvements to Obtain Better Agreement with the Rig Tests

In this section an attempt is made to introduce additional controlling parameters to improve the analogue circuit solutions. It is envisaged that by doing so, certain tests may be conducted through the analogue which are difficult to carry out experimentally:-

(a) to find the generalised masses of the piston and liner for more accurate mode evaluation.

(b) to introduce further parameters into the model and to study the effect of their variation on dynamic response.

(c) to determine the effect of force modifications.

The analogue circuit shown in drawing 6.TR48 may be regarded as an intermediate circuit which was operated and found to give solutions agreeing closely with the data from the physical rig. Additional equations are

presented below to incorporate other equally important parameters. Some of these additions can be accommodated on the TR48 existing board. However, a larger computer will be needed to incorporate all equations.

The proposed new model is shown in SKETCH (4) and has the following features:-

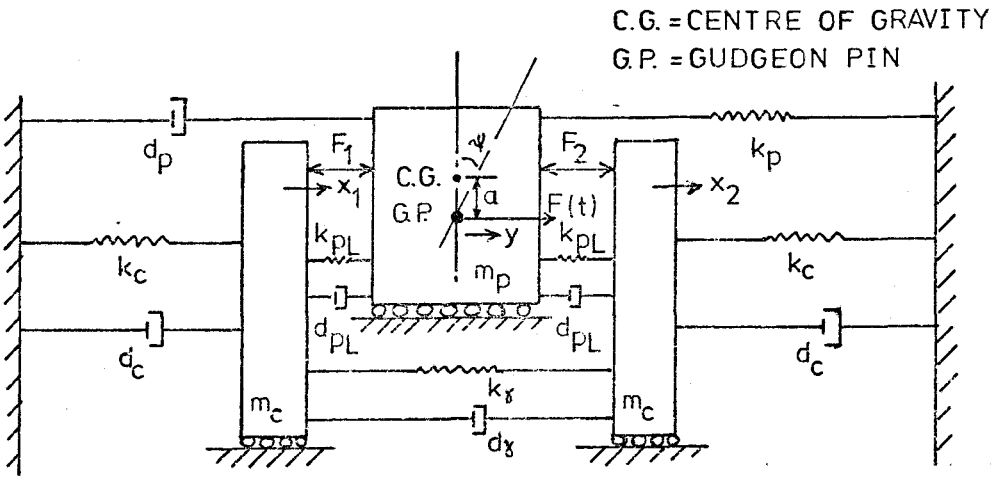

SKETCH (4)

(i) The piston may have a small amount of stiffness (k_p) and damping (d_p) relative to the structure, and allowing for interaction forces F_1 and F_2 between the piston and cylinder, the equations of motion may be written as follows:

<u>Piston</u> $$m_p\ddot{y} + d_p\dot{y} + k_p y = F(t) - F_1 - F_2 \qquad (6.22)$$

<u>Liner</u>
$$\begin{vmatrix} m_c & 0 \\ 0 & m_c \end{vmatrix} \begin{vmatrix} \ddot{x}_1 \\ \ddot{x}_2 \end{vmatrix} + \begin{vmatrix} d_c + d_\gamma & -d_\gamma \\ -d_\gamma & d_c + d_\gamma \end{vmatrix} \begin{vmatrix} \dot{x}_1 \\ \dot{x}_2 \end{vmatrix}$$

$$+ \begin{vmatrix} k_c + k_\gamma & -k_\gamma \\ -k_\gamma & k_c + k_\gamma \end{vmatrix} \begin{vmatrix} x_1 \\ x_2 \end{vmatrix} = \begin{vmatrix} F_1 \\ F_2 \end{vmatrix} \qquad (6.23)$$

(ii) Considering the cocking motion of the piston as shown in the sketch above, the following equation may be added:

$$I_G\ddot{\psi} = F(t).a - d_p'\dot{\psi} - k_p'\psi \qquad (6.24)$$

where ψ = cocking angle = $\tan^{-1}$ y/a

a = vertical distance from gudgeon pin to centre of gravigy

d_p' = torsional damping = $c_1 d_p$

k_p' = torsional stiffness = $c_2 k_p$

(iii) Oil film effect:

$$F_1 = k_{PL}(x_1 - y) + d_{PL}(\dot{x}_1 - \dot{y})$$
$$F_2 = k_{PL}(x_2 - y) + d_{PL}(\dot{x}_2 - \dot{y}) \qquad (6.25)$$

where

k_{PL} = stiffness of oil film

d_{PL} = damping of oil film

Only when all the above effects are taken into account will the simulation become realistic. At that stage the variation of many piston-liner parameters may be altered simply by changing the values of the relevant potentiometers. Some of these parameters are:

(a) effect of changing the coefficient of restitution

(b) effect of clearance

(c) effect of mass change

(d) effect of stiffness and damping

(e) liner-piston separations

6.6 Conclusions

(1) Analogue simulation of the piston-liner system of an engine can be built to give reasonable representation of the physical problem and therefore offers a convenient tool to investigate the effect of changing the numerous controlling parameters. In some cases, unpredicted solutions are obtained which, if advantageous, may be made feasible in practice. However, the analogue computer has some limitations.

(2) It is basically difficult to set exact analytical treatment for complicated systems with clearance because of the inherent non linearity. Parallel feedback from the physical model should serve to improve the analogue circuit, and thus reduce the number of experimental rig tests necessary. However, the experimental rig will always be needed to check the validity of the analogue results, especially to check the resultant vibration and noise of a certain optimum condition.

References

6.1 W.T. Thomson. "Vibration Theory and Application". Publishers: George Allen and Unwin Ltd., 1966.

6.2 PACE TR48 Analogue Computer Manual and Reference Handbook.

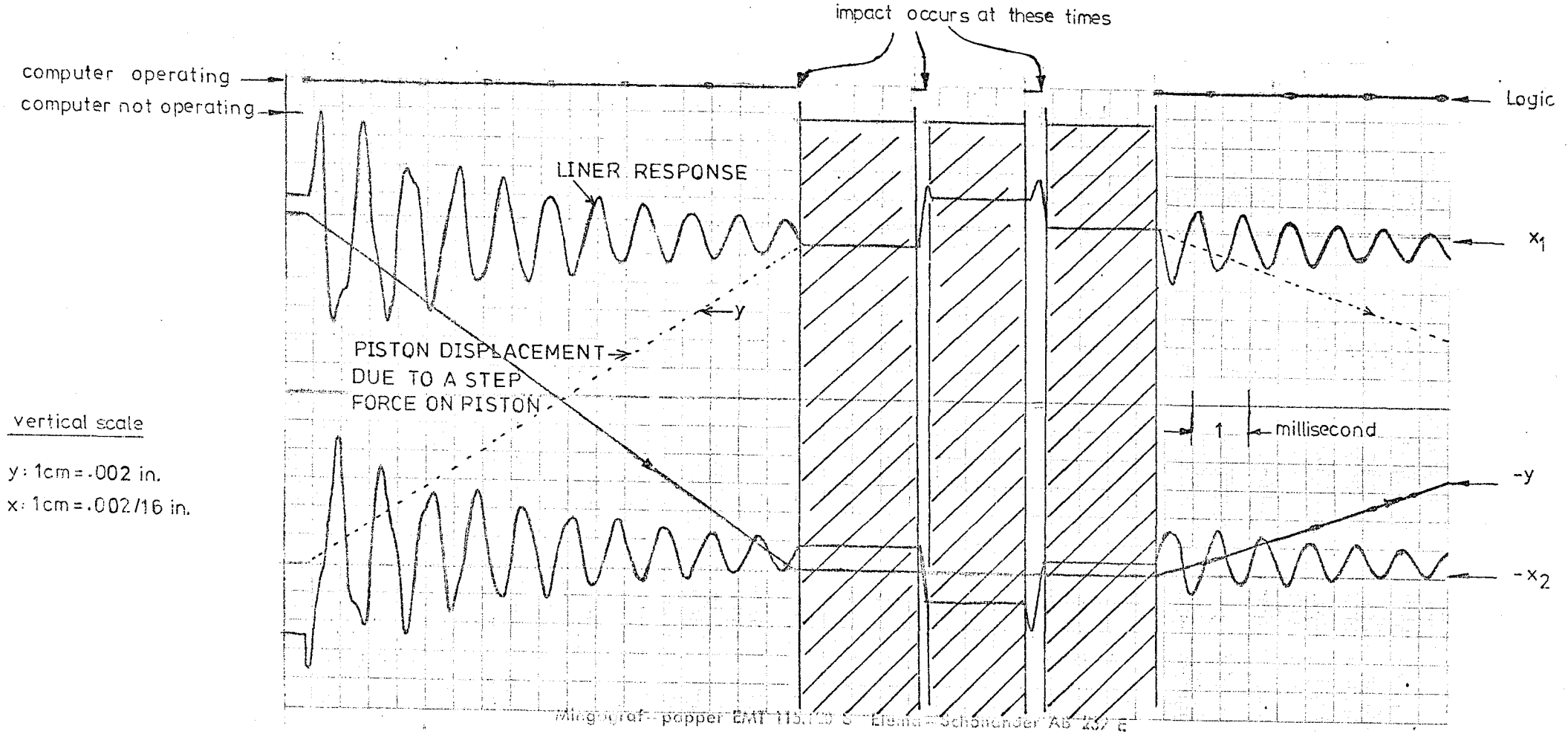

FIG. 6.1 Typical piston-liner movement due to the application of a step force on piston (Analogue TR-48)

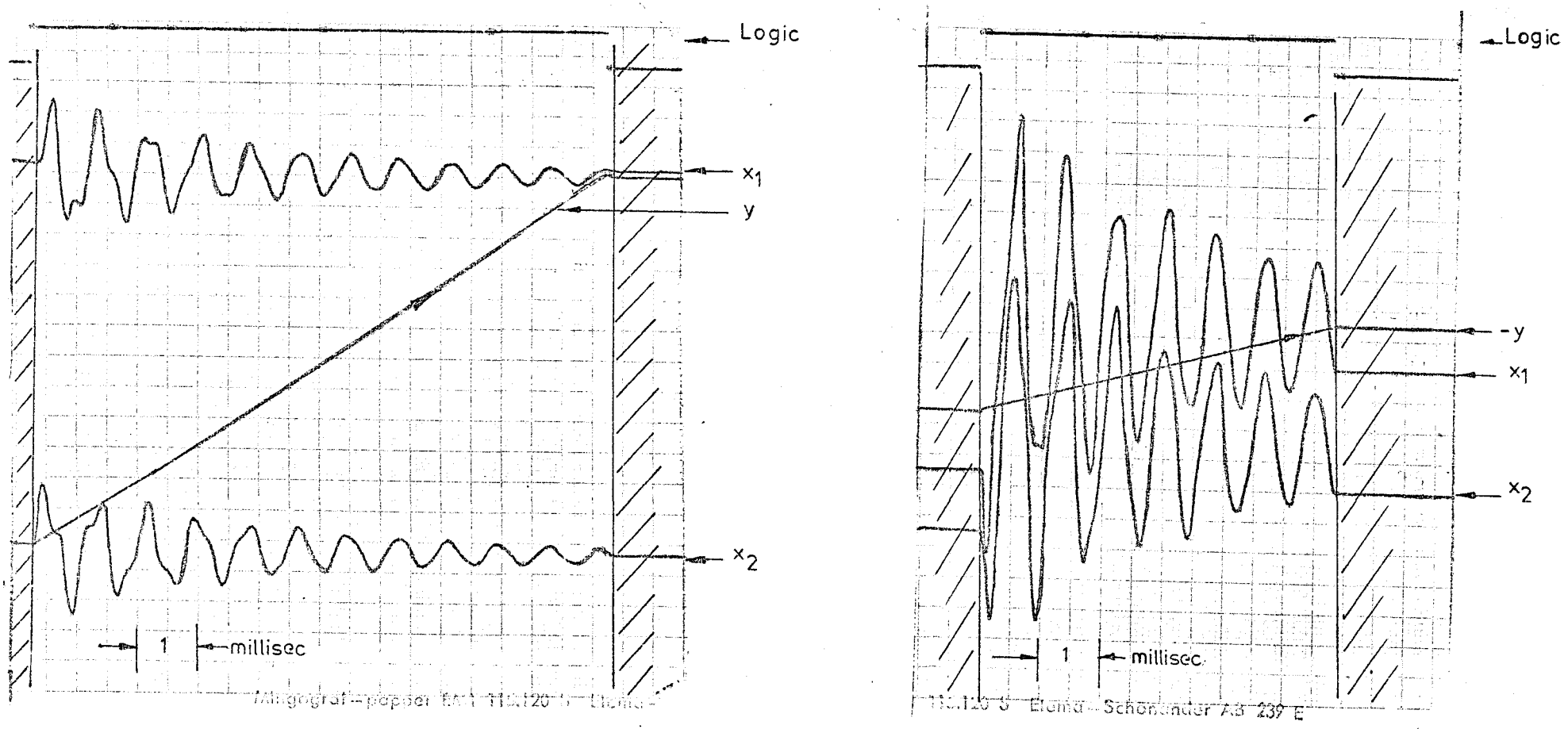

FIG. 6.2 Amplified liner vibration response for the calculation of liner natural frequencies

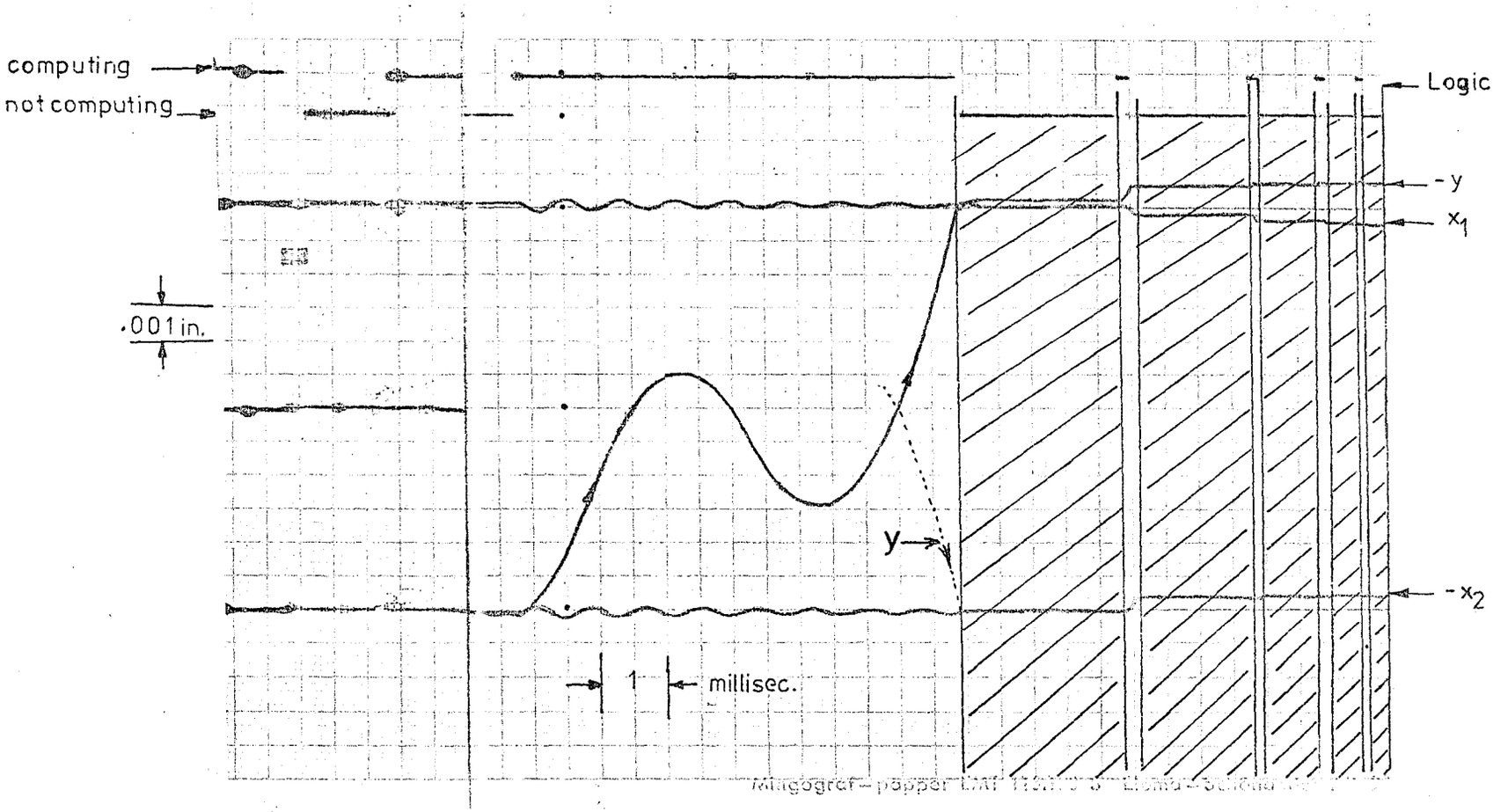

FIG. 6.3 Effect of step force on piston when reversed momentarily

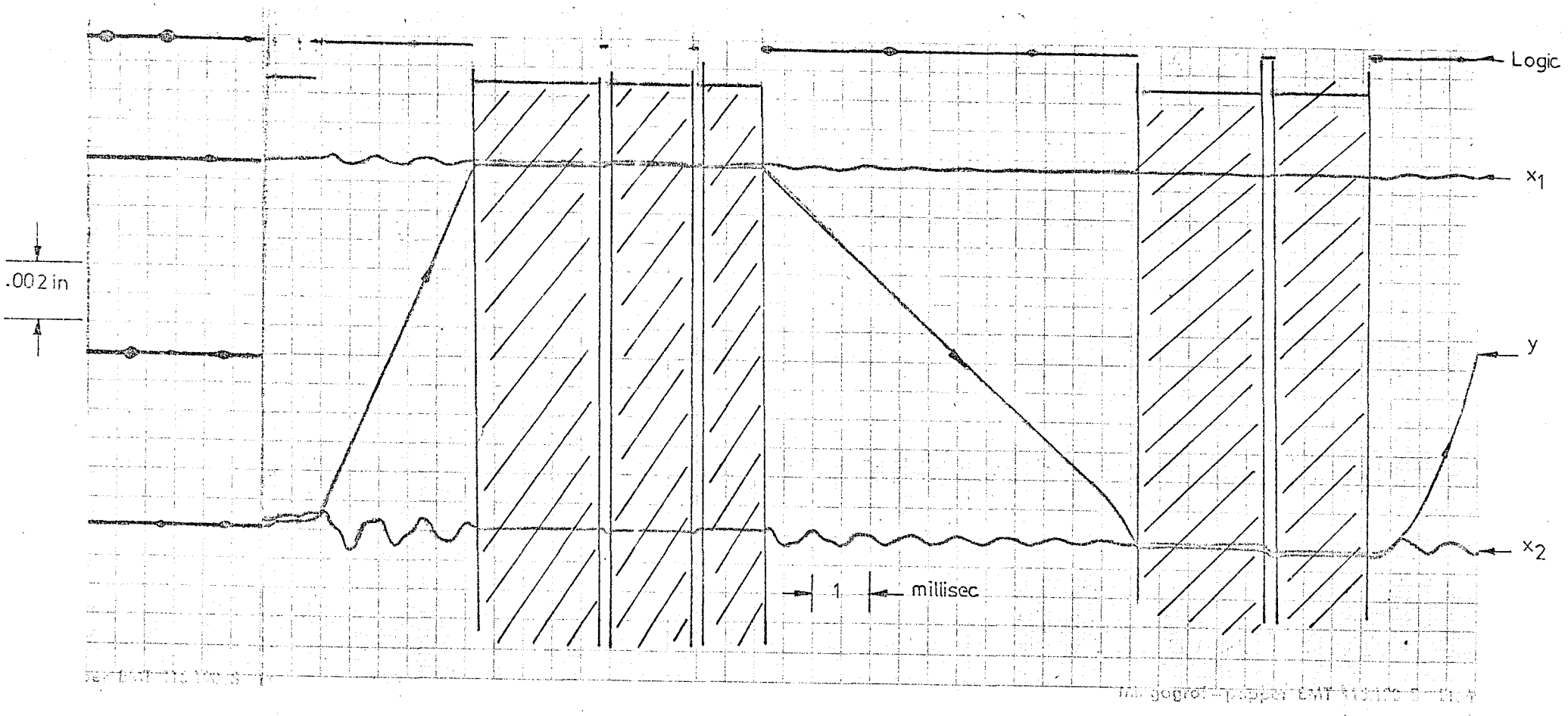

FIG. 6.4 Effect of increased stiffness and damping of x_1 side of liner

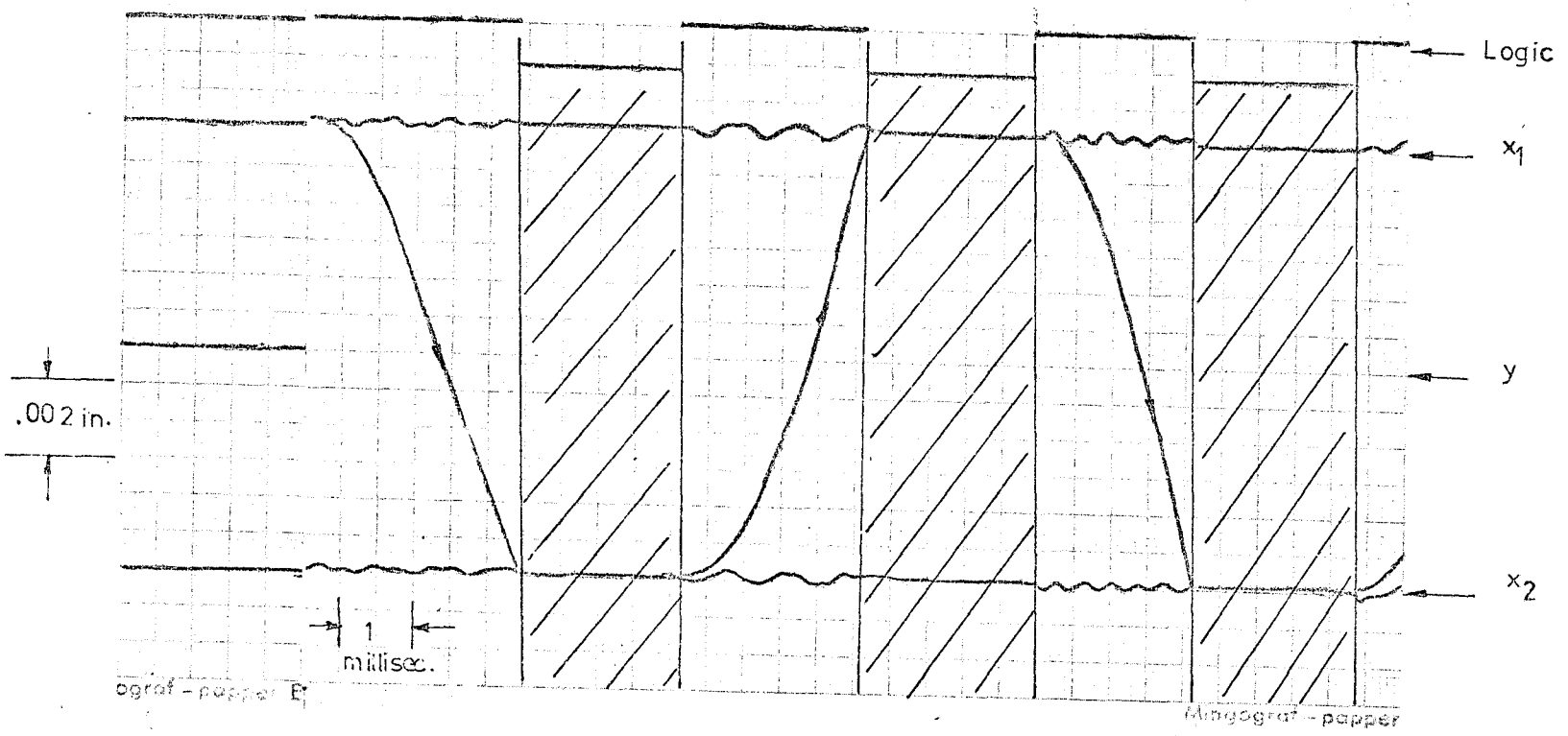

FIG. 6.5 Effect of increased mass of liner ($m_c > m_p$)

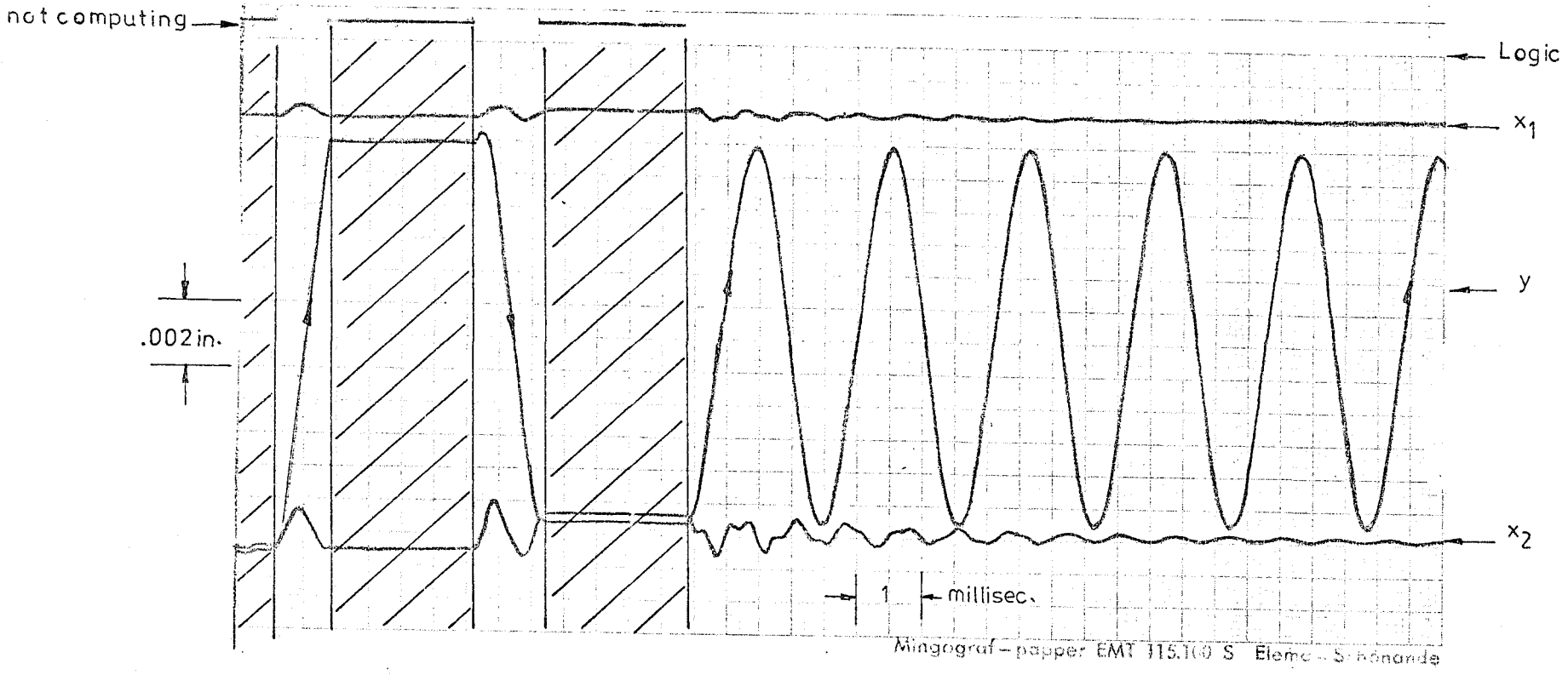

FIG. 6.6 Effect of introducing piston to block stiffness (artificial)

Pot.(03) = .095

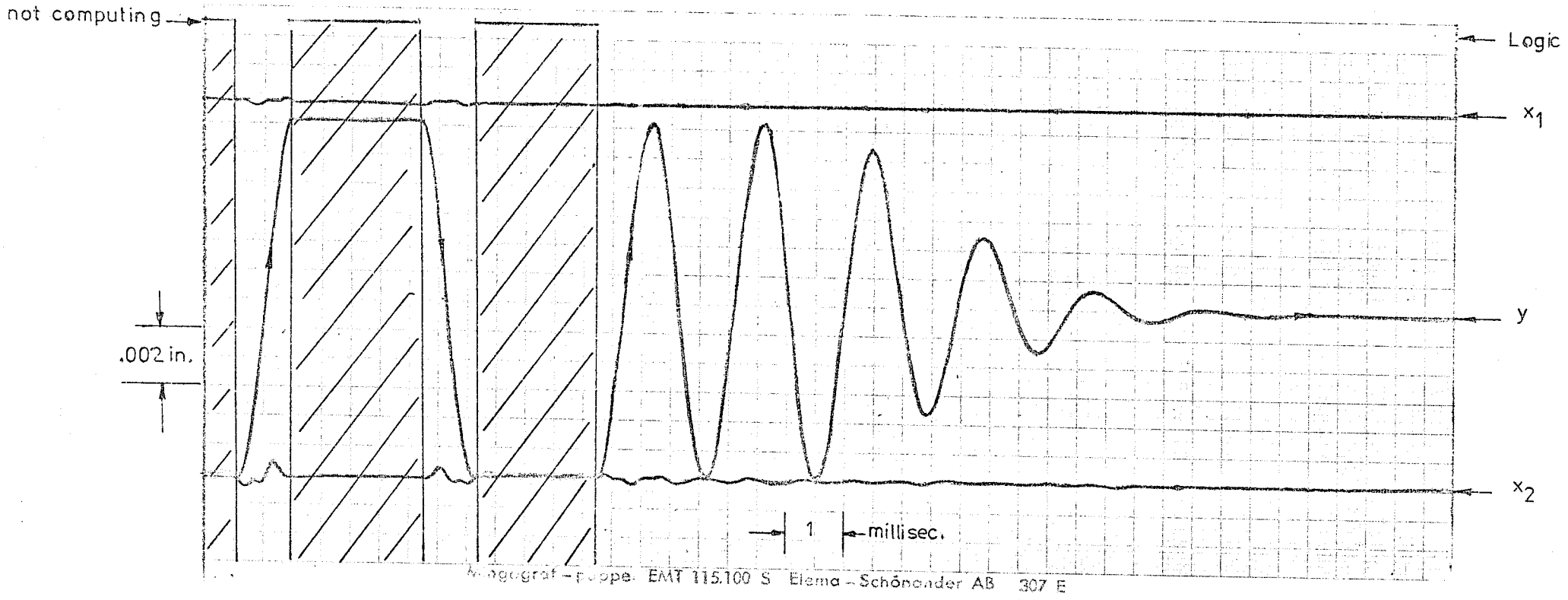

FIG. 6.7 Effect of introducing piston to block damping (artificial)

Pot.(00) = .345

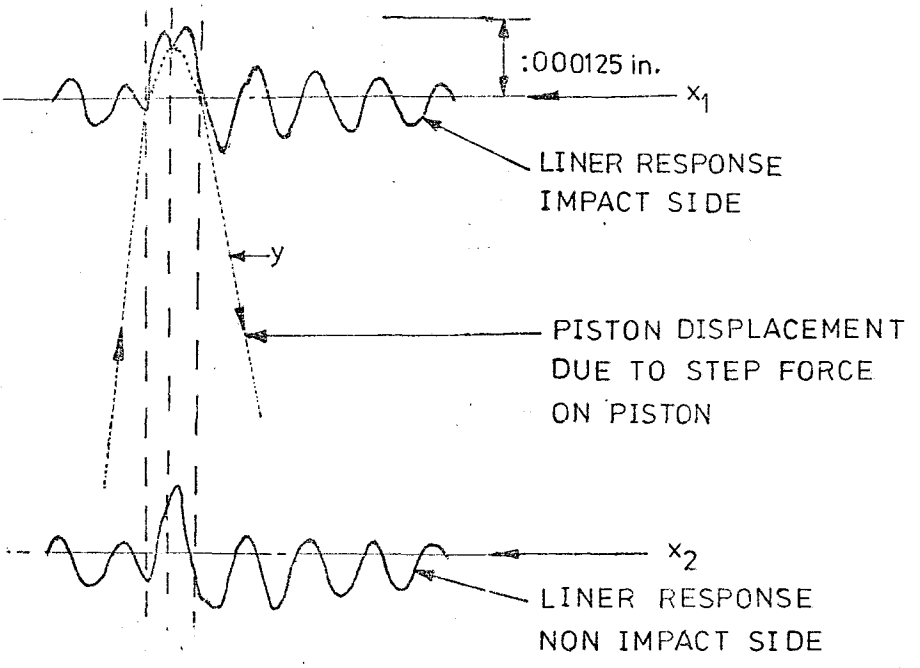

(extracted from fig. 1) ..... (a)

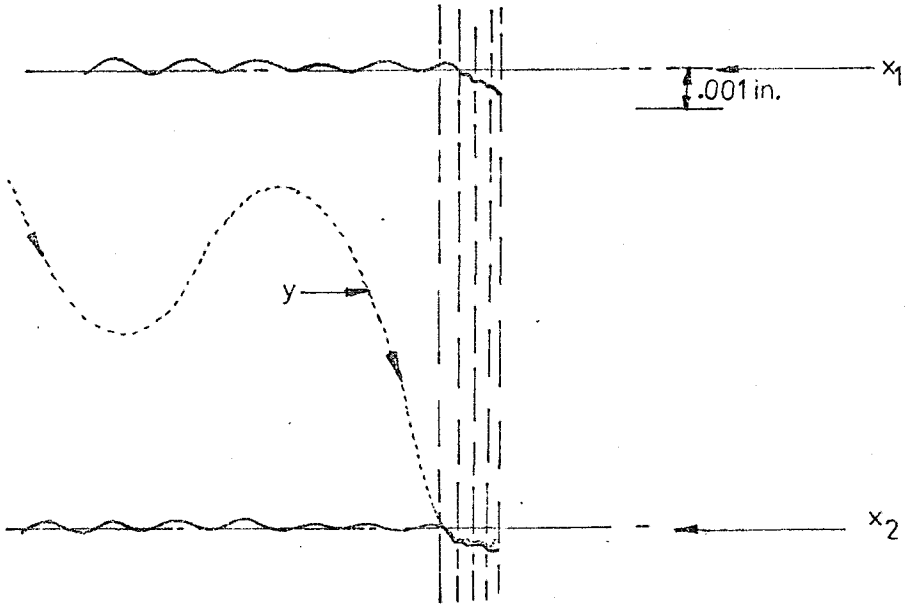

(extracted from fig. 3) ..... (b)

FIG. 6.8 Typical piston-liner movement due to the application of a step force on piston (by omitting the hatched parts of chart records i.e. computer not operating)

CHAPTER 7

Study of Piston Behaviour in a Running Engine to Identify Piston Slap Characteristics

7.1 Introduction

Oscillographic studies, simulation on the test rig and experimental investigations of various parameters, indicated the important contribution that piston slap can give to the resultant engine block vibration and noise. These various studies also made possible the establishment of the magnitude of the piston slap contribution relative to combustion and other sources. To understand fully the characteristics of piston slap, a better knowledge of the piston-liner behaviour in the running engine is needed. In other words, what is required is the instantaneous information from the actual running piston during the whole working cycle. This is made possible by telemetry techniques.

7.2 Survey of Available Telemetry Techniques

For long term progress in piston design, manufacturing methods and performance testing, piston manufacturers found it necessary to acquire a deeper knowledge of the behaviour of a piston which is subjected to a complex environmental condition. The study of a working piston can be satisfactorily accomplished only with specialised instrumentation and this includes not only development of the relevant transducers and electrical circuitry, but also the means by which the information can be transmitted to the outside world. Over the years, many systems have been developed for this purpose, but most of these have had severe limitations (ref. 2.11). They fall into four categories: (1) systems which use an arrangement in which a brief contact is made at the bottom of each stroke. Such a system was developed at Ricardo. It

consists of a berrillium-copper spring leaf fixed inside the sump and making contact with a terminal on the piston. This is only suitable for the measurement of phenomena which change at a slow rate compared with the engine cycle such as the mean piston temperature.

(2) Systems using slip rings (ref. 7.1) to provide a continuous contact. These require one set of slip rings at the small end bearing, and one at the big end bearing and a third set at one of the main bearings. This system has practical limitations in modern high speed engines, resulting in poor electrical contact.

(3) Systems which use radio methods of transmitting information from the piston to a stationary aerial fixed inside the engine (ref. 7.2). These have been found attractive because they require minimum modification to the engine and its components. The transmitter can be made of small physical size which can accept a sufficiently wide range of transducer inputs and thus cope with a number of channels of information. There is, however, the possibility of interference arising from the severe oil sump environment.

(4) Linkage systems which use a direct wire arrangement of some form that can flex with the reciprocating motion of the piston-rod assembly at one end and with a rigidly attached terminal at the engine crankcase. These have been successfully developed and are attractive especially if the modifications to the crankcase and oil sump are minimal. Many such linkages have been developed in the past, particularly in Germany and Japan, but only for relatively low speed engines. At AED-Cawston-UK., development over a decade has successfully produced a linkage system design which can operate for long periods at high speed with good reliability.

7.3 The AED Two Beam Linkage and Associated Instrumentation

The AED system is a two beam linkage connected to one of the big end bearings. This was considered as the most appropriate for the present investigation. Figure 7.1 shows a drawing of the linkage assembly for the engine investigated. Figure 7.2 shows a photograph of the linkage as it is connected to the piston and connecting rod. It consists of a light-weight two-arm mechanism of aluminium alloy connected to the big end of the connecting rod and terminating at a bracket mounted on the engine crankcase. The total system comprises four pivot points. The three pivot bearings, except for the small end in the piston, are of proprietary self-aligning spherical seat type which are manufactured to a high strength aircraft specification. The sump of the engine was modified to accommodate the stationary end of the linkage housing the output terminals. At the piston gudgeon pin four flexible leads are carried over both sides by an insulated spring and guide system, as shown in Fig. 7.2(c). All wiring on the system is PTFE insulated and it is finally fixed along its length by epoxy resin adhesive. Two Sangamo T4 proximity gauges were installed in the thrust side of No. 1 piston of the engine under investigation. These were connected to two unscreened channels. A screened channel was used to transmit the signal from a Kistler 601A pressure transducer installed in the piston skirt (thrust side) between the proximity gauges in level with the gudgeon pin centre line, as shown in figure 7.39(b). The installation of the three gauges is the same as that used on the piston slap rig. Many types of screened channels were tried in the past but have generally failed. Since the oil film pressure measurement was considered of great importance in the present study, it was decided to explore the possibility of using the best available technique. This consists of a flexible bowden tube fixed at the piston which carries a special screened transducer cable. Figure 7.2(b) shows the connection of this cable across the big end. Figure 7.3 shows the complete linkage assembly in the engine with the oil sump removed.

7.4 Test Results

In addition to the two movement gauges and pressure transducer installed in the thrust side of No. 1 piston, a cylinder pressure transducer was also fitted together with a degree marker disc on the crankshaft. All the signals from the transducers were displayed on the screen of a Storage Oscilloscope and Polaroid photographs were taken for analysis of the results. It was possible to record measurements from the running engine up to conditions of 3000 revs/min no load but difficulty was experienced at 3000 revs/min full load due to repeated transducer failure.

7.4.1 Relation between piston-to-bore oil film pressure, piston velocity and piston sideways force

The measured piston-to-bore oil film pressures (No. 1 thrust side) are shown in figures 7.4-7.12, together with cylinder pressure diagrams and degree marks, for various engine speeds at full and no load conditions. It can be seen from these measurements that the lubricating oil film pressures must play a very important part in controlling the attitude of the piston in the bore and the resultant structure vibration due to impacts or sudden pressure pulses. The development of oil film pressure between the moving piston and the stationary liner agrees in principle with the well known lubrication theory. Piston sideways force and sliding velocity must influence the formation of this oil film pressure and may be studied with relation to figures 7.13 to 7.15 which present typical relationships with side force and engine speed.

The oil film pressure increases with increasing downward piston velocity during the induction stroke. As the piston velocity decreases towards the end of the induction stroke, velocity becomes zero (piston stationary) resulting in a rapid drop of oil film pressure. A gradual increase of oil pressure will be noted also during the upward compression stroke until an abrupt pressure rise is produced by the main slap of the piston due to the

large sideways force resulting from combustion. This second peak is markedly wider than the peak observed during the induction stroke but it is probable that the second part is produced in a similar way to that of the induction stroke and is superimposed on the slap pressure rise, as suggested by the dotted lines in the figures. Assuming that the oil film pressure is acting over an area of about 10 in^2 it can be deduced that the hydraulic side force is of a magnitude of some 1000 lbf in the induction stroke while the side force resulting from inertia forces is of the order of 200 lbf. This clearly suggests that this pulse is due to hydrodynamic wedge action and not due to a minor slap occurring in that region. A minor pressure pulse starting at about 60^{o} BTDC (exhaust stroke) is also seen where a minor piston slap is expected to occur. It is observed that hydrodynamic pulses are formed when the piston approaches its maximum velocity and when the piston is moving towards the thrust side. No such pulses are seen when the piston approaches the non thrust side, but they would be expected to appear if oil film measurements were also made for the non thrust side.

7.4.2 Effect of engine speed and load on the piston-to-bore oil film pressure

Figures 7.14 and 7.15 show the effect of engine load and speed on the shape of the oil film pressure. In general the hydraulic oil pressures increase with engine speed. Some of the following observations may be made:
(1) The hydrodynamic pressure pulses (shown hatched) increase rapidly with engine speed. At no load conditions they achieve higher peak pressures compared with the corresponding speeds at full load. At full load, it is expected that because of higher temperatures, the oil viscosity in the clearnace becomes lower than for the no load case and therefore will produce lower hydrodynamic pressures.

(2) The initial rate of pressure rise and timing of the oil film pressure pulse due to the major piston slap around TDC is little affected by variation of speed and load. The part of the pulse immediately following the initial rise could be partly due to the form of the side force at different operating conditions. Figures 7.16 and 7.17 present the calculated piston sideways forces showing the variations with load and speed. It can be seen that there is little difference in side force with speed for the major slap around TDC. On the other hand, the peak side forces around TDC are considerably higher at full load than at no load, which suggests that the oil film pressure pulse due to the major slap should increase in magnitude with increasing load. However, this effect may be masked because of lower oil viscosity at full load conditions.

(3) A definite oil film pressure pulse is also observed starting at about 60° BTDC. Its magnitude tends to increase with speed but is unaffected by variation of load. Comparison with the relevant piston sideways forces will show that this pulse is due to a minor piston slap with a smoother rate of rise due to the smaller sideways force. It can also be seen that the effect of other minor slaps could be masked by the greater effect of hydrodynamic pressure pulses since they occur around the same timing as that of the maximum piston velocities.

7.4.3 Piston-to-bore oil film pressure as an important source of excitation in the engine

To quantify the exciting propensities of the oil film pressure, a frequency spectrum of the waveform is obtained (see Appendix G). Figures 7.18 and 7.19 show the Fourier spectra of the oil film pressures obtained which illustrate the effect of speed and load. Because of the sharp "major slap" oil pressure front, the spectra decay with an average rate of 20 dB/decade.

Figures 7.20 to 7.22 compare spectra of the oil film pressures and combustion at 1000, 2000 and 3000 revs/min no load and figures 7.23 to 7.25 show the same comparison at 1000, 2000 and 2500 revs/min full load. At no load, it can be seen that the oil film pressure controls the response throughout the frequency range from 500 Hz upwards. At full load, the oil film excitation may predominate in the frequency range from 125^{0} Hz upwards. Also it is seen that the increase of engine speed tends to reduce the significance of the oil film pressure, but in general the oil film pressures may be considered as one of the major sources of engine structure excitation. In order to reduce the levels of the oil film pressure spectra to below those of combustion, a smooth oil film waveform needs to be achieved. This may be attained in some of the following ways:

(1) oil cushioning: that is creating higher levels of residual hydrodynamic pressures to cushion any sudden rise in pressure.

(2) Tilt the piston permanently in such a way as to create the sufficient hydrodynamic pressures to mask the effect of impulsive pulses.

The impulsive oil film pressures must distort the liners, setting them in oscillation and subsequently vibrating the whole engine structure. This liner response may be considered as an exciting force in its own right. Appendix H shows analytically how this source of excitation can predominate over the combustion source.

7.4.4 Piston movements and approach velocities

Piston movements for the thrust side were also recorded at both the top and bottom of the skirt. Figures 7.26 to 7.29 present photographs of these measurements at 1000, 2000 and 2500 revs/min full and no load conditions.

The movement traces were enlarged and transferred on to transparent calibrated paper. Since the proximity gauges are non linear, the traces had to be converted into actual displacement in inches, using the relevant

calibration curves (see Appendix F). Figure 7.30 shows an example of correlation of all the events which take place in the cylinder of the running engine at 1000 revs/min no load. Some observation can be made. Around TDC (firing) the bottom of the piston skirt approaches the thrust side of the liner before the top of the skirt. After impact, the bottom of the skirt bounces. This could be due to liner deformation or its oscillation at the impact. The frequency of this bouncing is of the same order of magnitude as that of the first overtone of the liner natural frequency and corresponds to the bank to bank frequency in the engine ($\simeq$ 1250 Hz). It is also seen that the sudden piston movement around TDC generates an impulsive oil film pressure pulse.

The lower piston skirt tends to remain separated from the thrust side of the engine, except when the skirt slaps the liner thrust side after TDC in the next expansion stroke.

Figures 7.31 to 7.38 show the compensated measured movements of both the top and bottom of piston skirt at 1000, 1500, 2000 and 2500 revs/min for no and full load conditions. These figures also show the calculated movements using AED - Wellworthy programmes (ref. 7.3). Assuming that the piston skirt does not deform, it will be seen from the measured movements that the piston is nearly always adopting a tilted attitude. Comparison of these measured movements with those calculated show considerable difference which must be due to the effect of the oil film pressure developments which have not been taken into account in the calculations. At certain parts of the engine cycle and at some running conditions it was observed that there is a tendency for the top of the skirt to approach the liner before the bottom. A typical example is shown in figure 7.39(a). A possible explanation is that the gudgeon pin may develop high frictional force, with the piston boss, and thus influence the movements.

It is interesting to note here that the calculated piston movements shown in the figures agree closely with the corresponding movements obtained on the piston slap simulation rig (dry case), while the measured movements resemble those obtained on the rig (wet case). This illustrates that the simulation has been realistic.

In some cases the piston appears to travel beyond the cold clearance limits, suggesting liner deformation. Therefore, monitoring the liner distortion together with that of the piston, should give a better understanding of the piston-liner behaviour.

Piston impact or approach velocities after TDC can be estimated from the calculated and measured piston movements. Tables 7.I and 7.II summarise these values for engine speeds of 1000, 2000 and 3000 revs/min.

Table 7.I

Piston Approach Velocities using AED Programme ∿ in/sec.

Engine Speed RPM	Full load			No load		
	Upper clearance velocity	Lower clearance Velocity	Average skirt velocity	U.C.	L.C.	Av.
1000	19	27	23	15	21	18
2000	26	39	33	19	30	25
3000	33	51	42	25	39	32

Table 7.II

Piston Approach Velocities - Estimated from Measured Movements ∿ in/sec.

Engine Speed RPM	Full Load				No Load			
	U.C.	L.C.	Av.	Measured block vib'n. g	UC	L.C.	Av.	Measured block vib'n g
1000	10	14	12	28	6	13	95	20
2000	18	28	23	43	14	22	18	32
3000	24	32	28	40	18	27	23	39

As can be seen, the measured piston impact or approach velocities are about half of the calculated values. The incidence of approach is also markedly different. This must be due to the effect of the hydraulic pressures developed in the piston to bore clearance. Figure 7.40(a) shows the relationship between average piston skirt approach velocities and K factor. The average slope is about 20 dB/decade. Table 7.II also shows the measured block vibration acceleration in g.

A typical relationship between measured block vibration and piston approach velocities can be shown in figure 7.40(b) with near linear relationship. Therefore, it may be concluded that block vibration increases by about 20 dB per tenfold increase in K factor which is similar to that obtained on the simulation test rig.

7.5 Possible Improvements to Piston Slap Theory

In the present investigation, the piston side forces have been calculated using equation 5.1 (Chapter 5) by means of a computer programme shown in figure 7.41. Figure 7.42 compares piston side forces around TDC using the above programme and the AED programme. As can be seen there is close agreement between the two programmes. This figure also shows the effect of inertia on the side forces which can be neglected for low engine speeds. Another relatively important factor is that of offsetting the gudgeon pin and Figure 7.43 shows this effect on the side forces, and also on the calculated piston approach velocities after TDC (ref. 7.3).

None of the methods for calculating piston behaviour and side forces has considered the effect of the oil film which has clearly been shown to affect piston movements and attitudes. The form and magnitudes of the oil film pressures also suggest the development of appreciable shear and compressive forces. With better understanding of the oil film behaviour it is suggested that general lubrication theory (ref. 7.4) could be employed in the analysis

to yield a more accurate evaluation of the force distribution along the piston skirt. The following general equation may be used:

$$\frac{\partial}{\partial x}\left(h^3 \frac{\partial p}{\partial x}\right) + \frac{\partial}{\partial y}\left(h^3 \frac{\partial p}{\partial y}\right) = 6\eta \left\{u \frac{dh}{dx} + 2 \frac{dh}{dt}\right\}$$

where h = oil film thickness

η = absolute viscosity

p = pressure

x = coordinate in direction U

y = coordinate in direction V

u = surface velocity in x direction

The dh/dt term is known as the "squeeze film" term (ref. 7.5). The greatest problem in lubrication theory is the solution of the pressure integral term. The only way to predict the oil film effect for a real situation is to relate the theoretical treatment to the relevant experimental data resulting in semi-empirical relationship. This same technique has been adopted by researchers of journal bearing lubrication, (refs. 7.6 and 7.7).

Since the piston movements (h) were measured, it was possible to estimate piston skirt velocities (dh/dt) by evaluating the instantaneous slopes. Using the equation the oil film pressures were then calculated and compared with those measured and a marked difference was observed. This could be due to the variation in the oil viscosity and the variable length/diameter ratio of the bearing land during the cycle. However, it should be possible to simplify the above equation to agree reasonably well with the measured oil film pressures to give a semi-empirical method for calculating the oil film forces.

The top and bottom of the piston skirt can also be influenced by gudgeon pin friction. To evaluate this effect the coefficient of friction (μ) during the cycle must be known. An approximate technique to do this is suggested here. The total oil film resistance (P) may be considered as the

horizontal force necessary to cause slipping to impend between the gudgeon pin and piston boss. If the vertical force through the gudgeon pin = W, then, as shown in the sketch below:

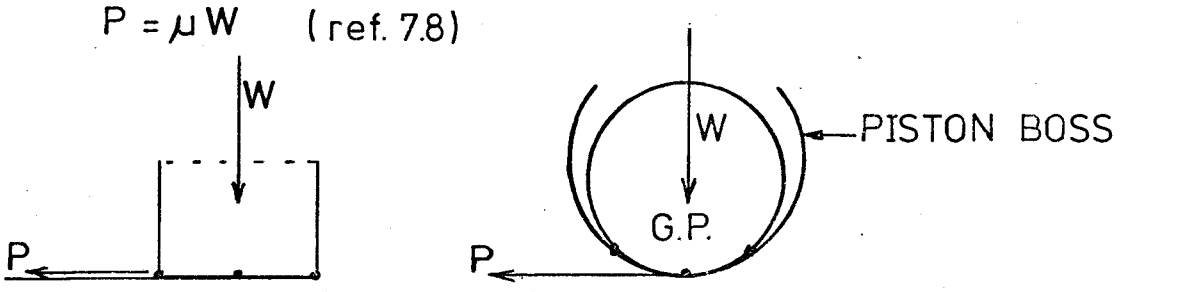

Finally, the strains on the gudgeon pin, piston and connecting rod may be measured and related to the forces in the system with the possibility of giving an accurately measured piston side force (top and bottom) taking into account the effect of all parameters.

7.6 Conclusions

1. The piston to bore oil film pressure development can be a major source of excitation in the diesel engine and can predominate over the combustion induced noise in the frequency range from 1000 Hz upwards. Its effect is more significant at no load conditions.
2. The oil film pressure can be described as having distinct regions of hydrodynamic and squeeze film effects. The former due to the piston sliding in the bore and the latter due to the sudden application of piston sideways force. The major slap at TDC produces a very impulsive sawtooth oil film pressure pulse which controls its frequency spectrum. Smoothing this impulsive front should reduce piston slap induced vibration and noise.
3. The impulsive oil pressures can deform the liner. The resultant liner response is shown to control the cylinder block vibration, indicating a possibility of vibration reduction by liner or structure design.

4. The frictional forces at the gudgeon pin appear to influence piston behaviour at certain parts of the cycle, suggesting the need for careful design of this part of the piston.

5. The piston side force calculations should take into account the effect of the oil film and gudgeon pin friction which are considered as important parameters affecting piston behaviour.

References

7.1 P.M. Heldt. "Effect of Piston Offset". Automotive Industries, 1953, pp. 28-31 and p.73.

7.2 M.K. Stark. "Short Range Telemetry". IEEE Transactions on Industrial Electronics and Control Instrumentation", 1965, pp. 29-33.

7.3 Private communications with AED and Wellworthy. "Computation of piston side forces, movements and velocities".

7.4 O. Reynold. Phil. Trans. (1886), Vol. 177, pp. 157-234.

7.5 A. Cameron. "Basic Lubrication Theory". Longman, 1971. Chapters 3 and 9.

7.6 J.F. Booker. "Dynamically loaded Journal bearings: mobility method of solution". Trans. ASME, J. Basic Engineering, 1965, No. 187.

7.7 H. Blok. "Fundamentals and application to design". Paper 2, Conference of lubrication and wear, Proc. I. Mech. E., 1967.

7.8 S. Timoshenko and D.H. Young. "Engineering Mechanics". McGraw-Hill Inc. 1951.

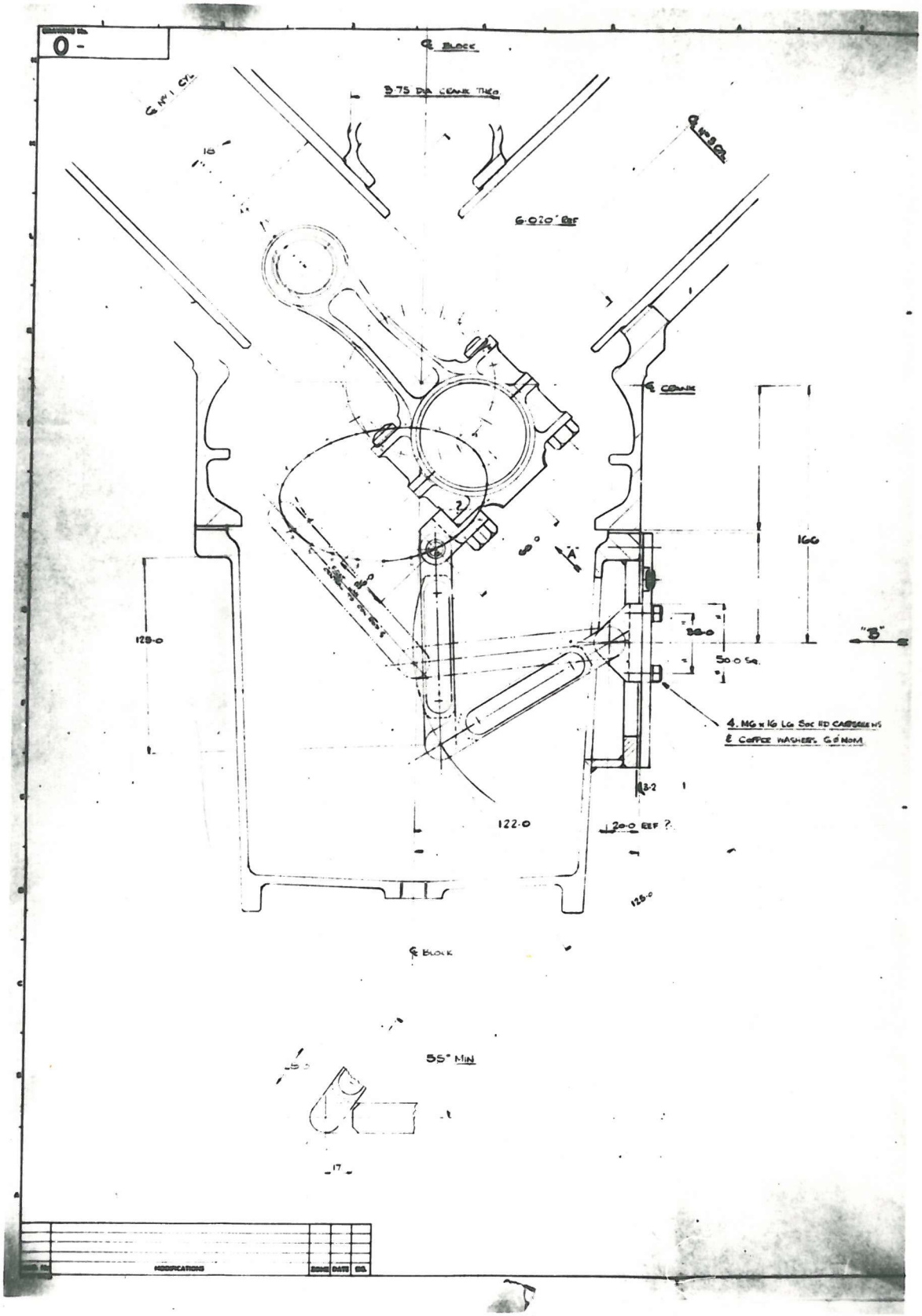

FIG. 7.1 DRAWING OF AED LINKAGE DESIGNED FOR ENGINE SA

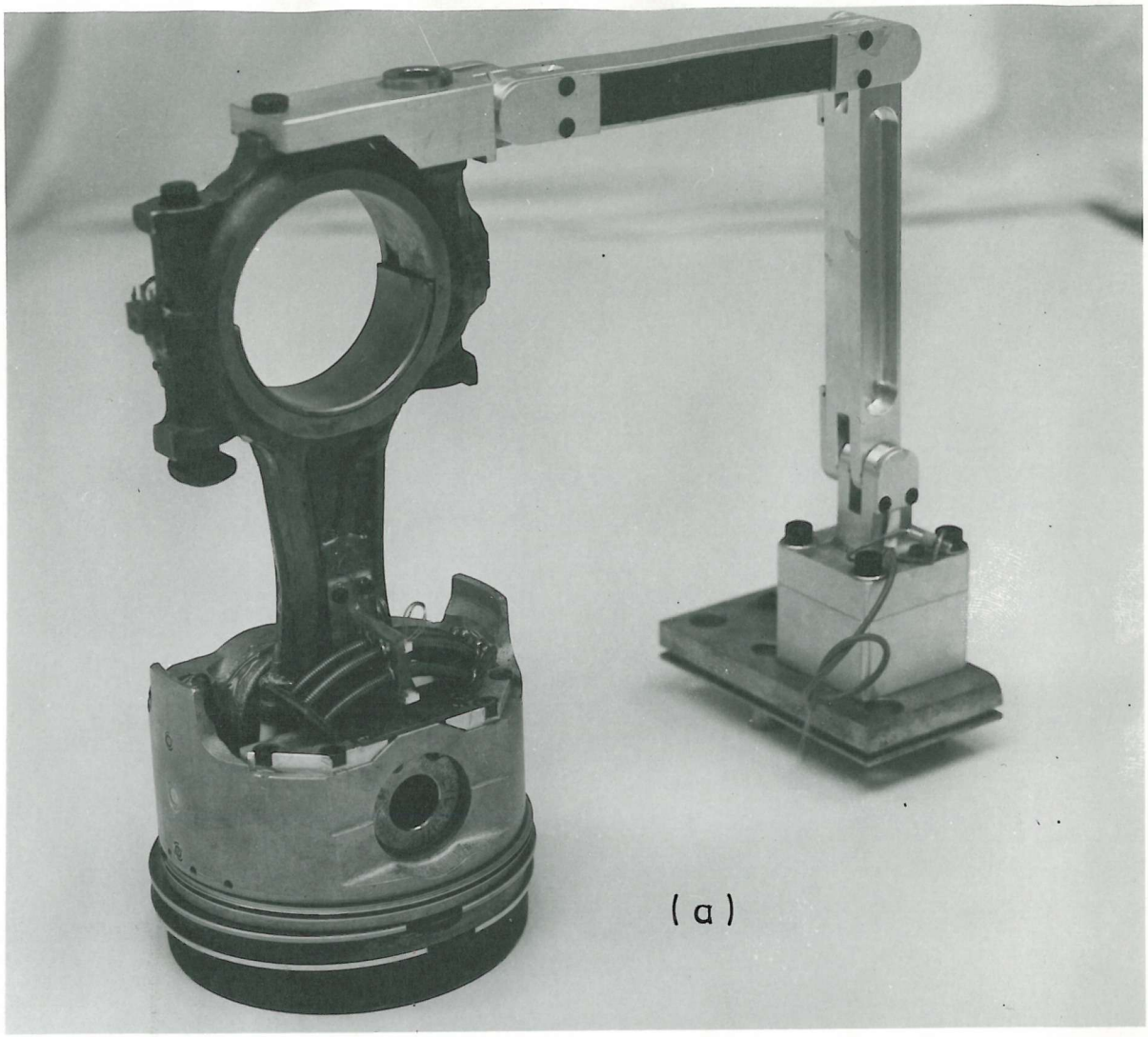

(b)

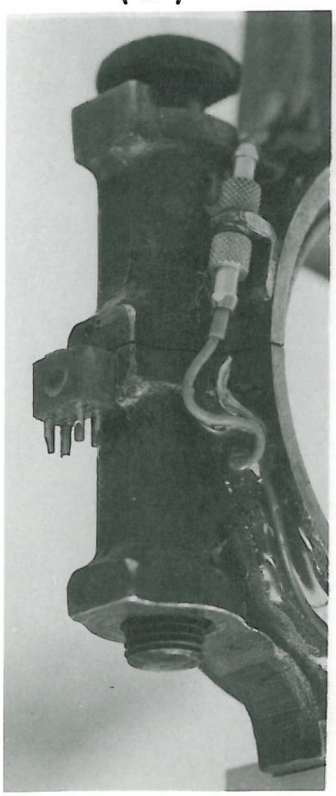

(c)

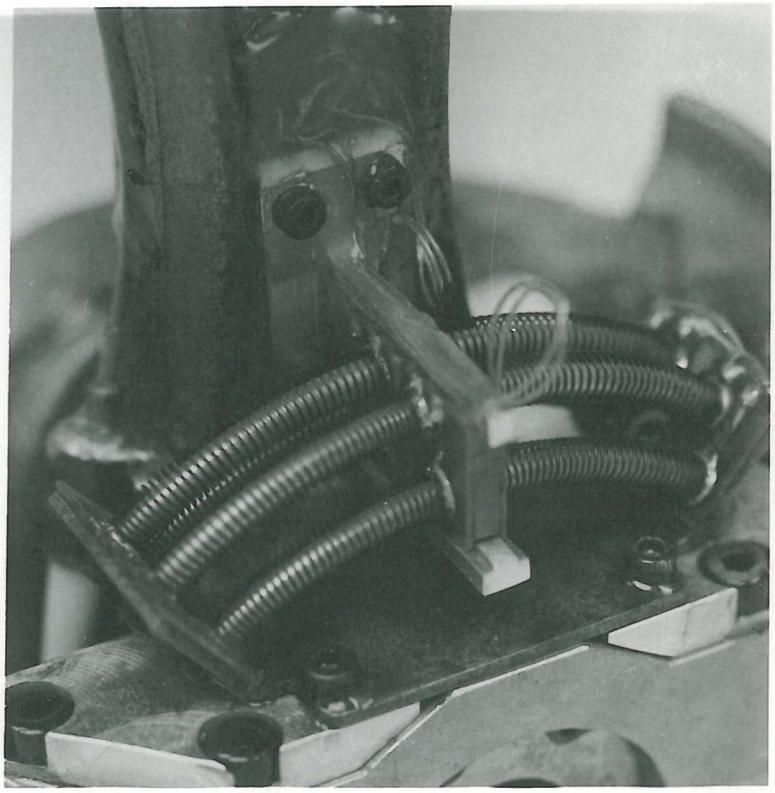

FIG. 7.2 DETAILS OF LINKAGE ASSEMBLLY

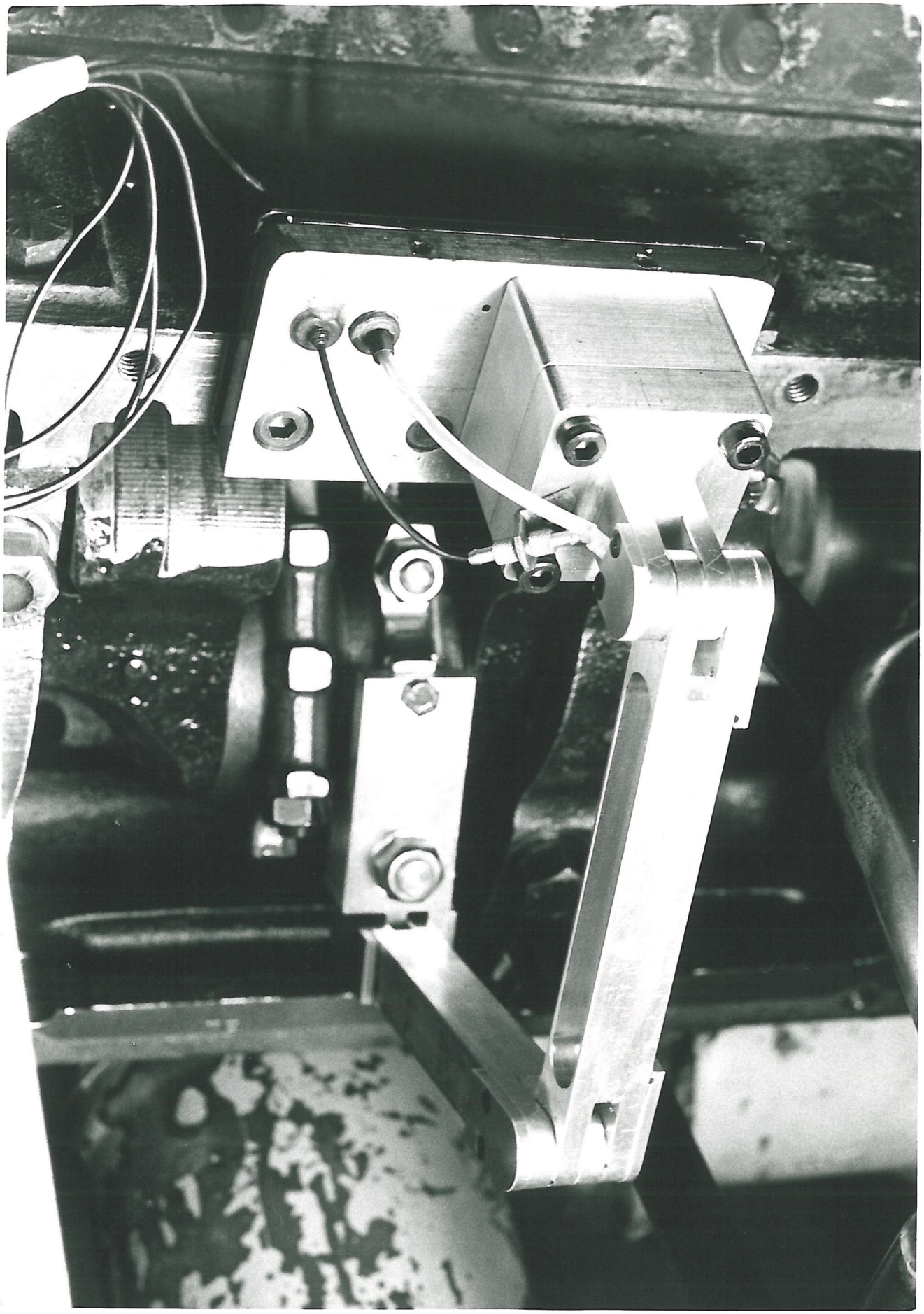

FIG. 7.3 LINKAGE AS FITTED IN ENGINE SA

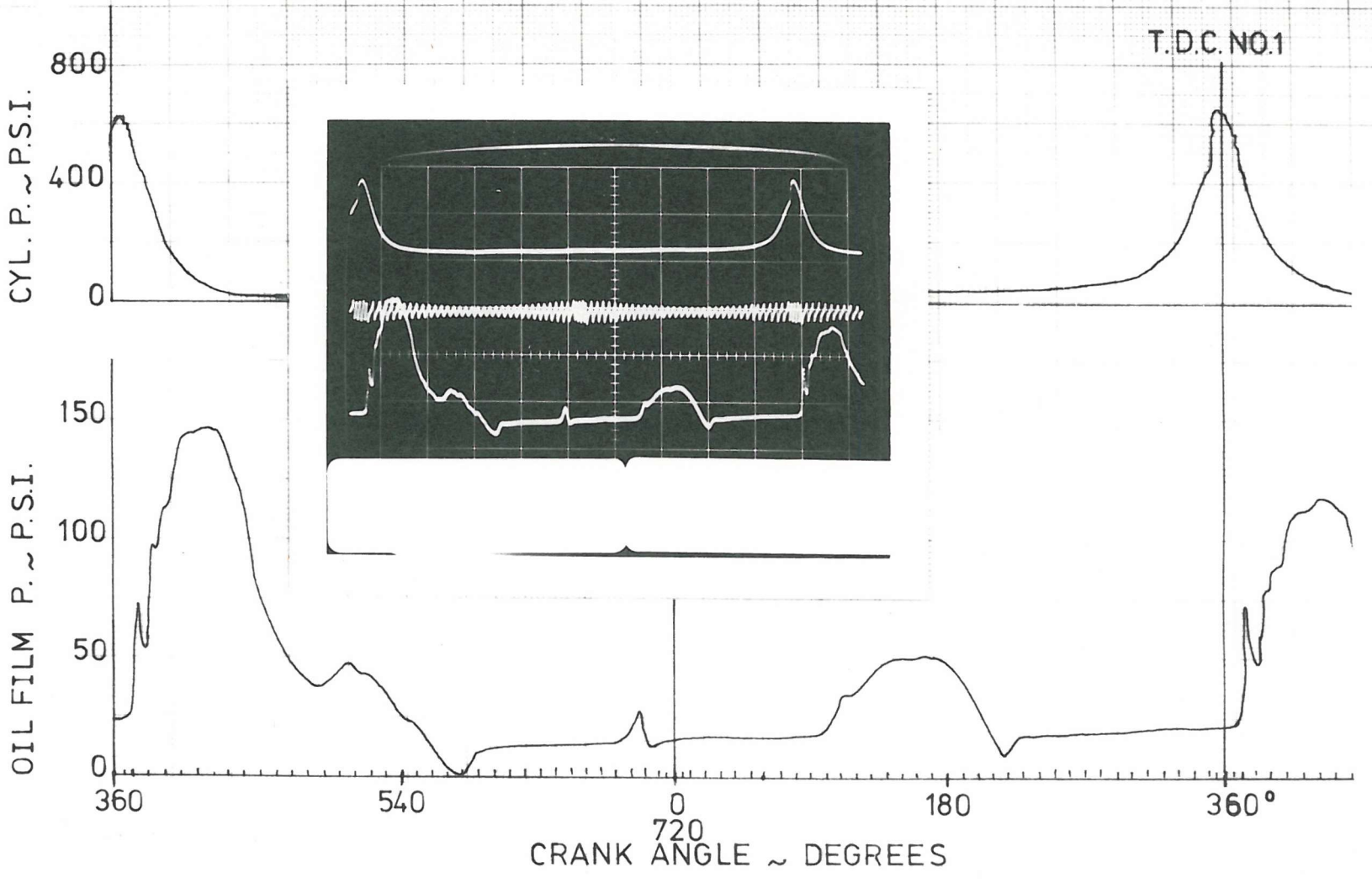

FIG. 7.4 CYLINDER PRESSURE AND PISTON TO BORE OIL FILM PRESSURE (THRUST SIDE) AT 1000 RPM NO LOAD - SA ENGINE

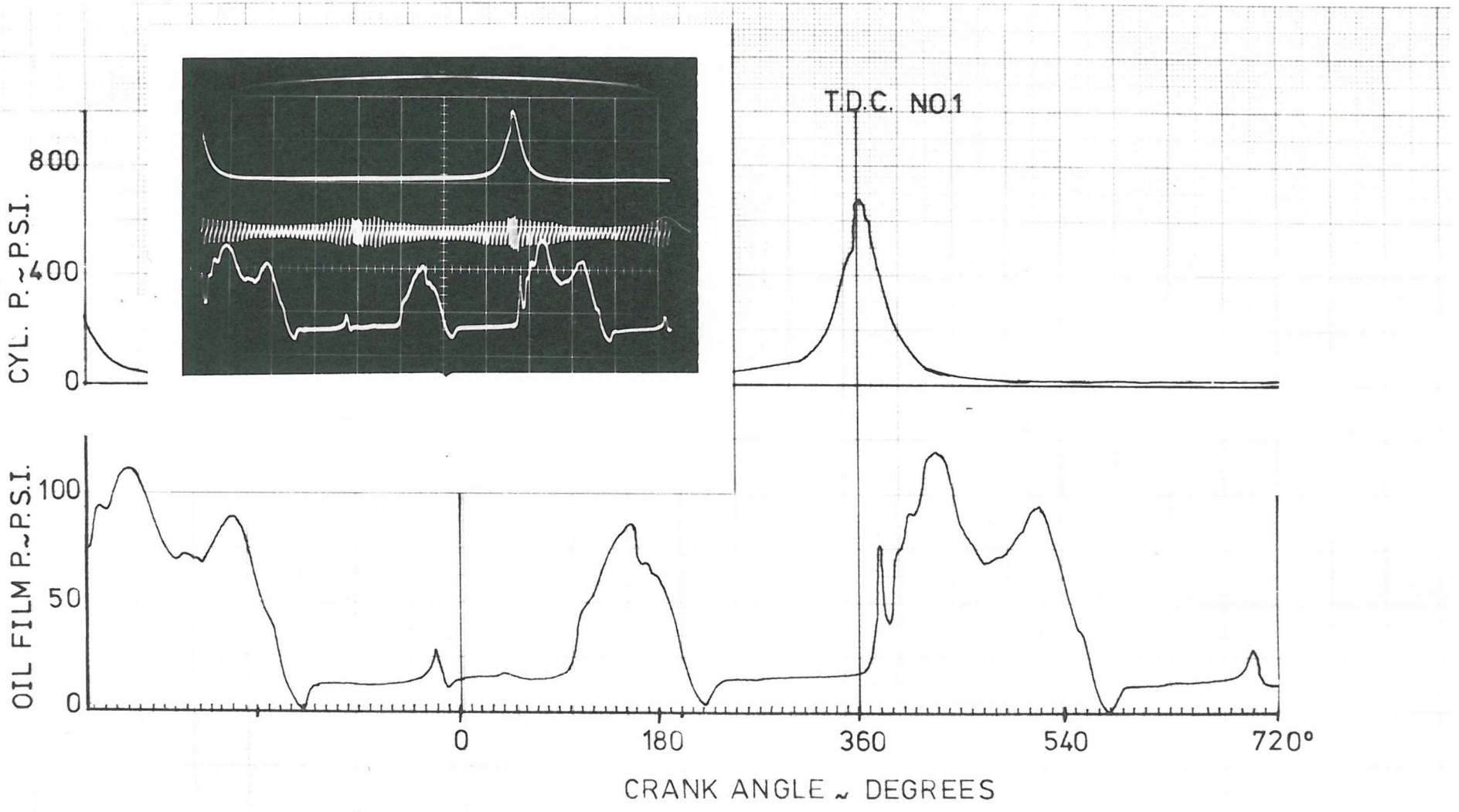

FIG. 7.5 CYLINDER PRESSURE AND PISTON TO BORE OIL FILM PRESSURE (THRUST SIDE) AT 1500 RPM NO LOAD - SA ENGINE

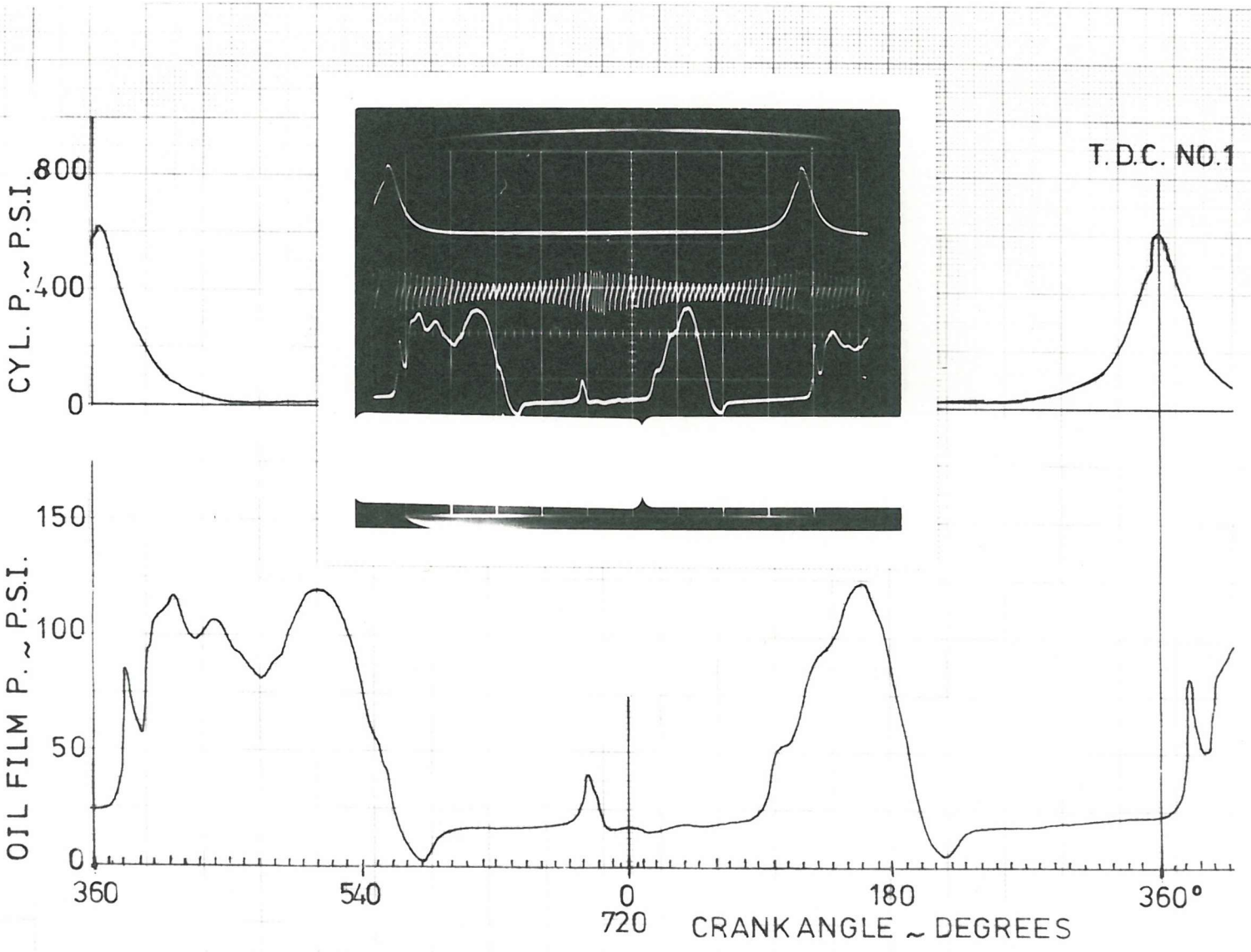

FIG. 7.6 CYLINDER PRESSURE AND PISTON TO BORE OIL FILM PRESSURE (THRUST SIDE) AT 2000 RPM NO LOAD - SA ENGINE

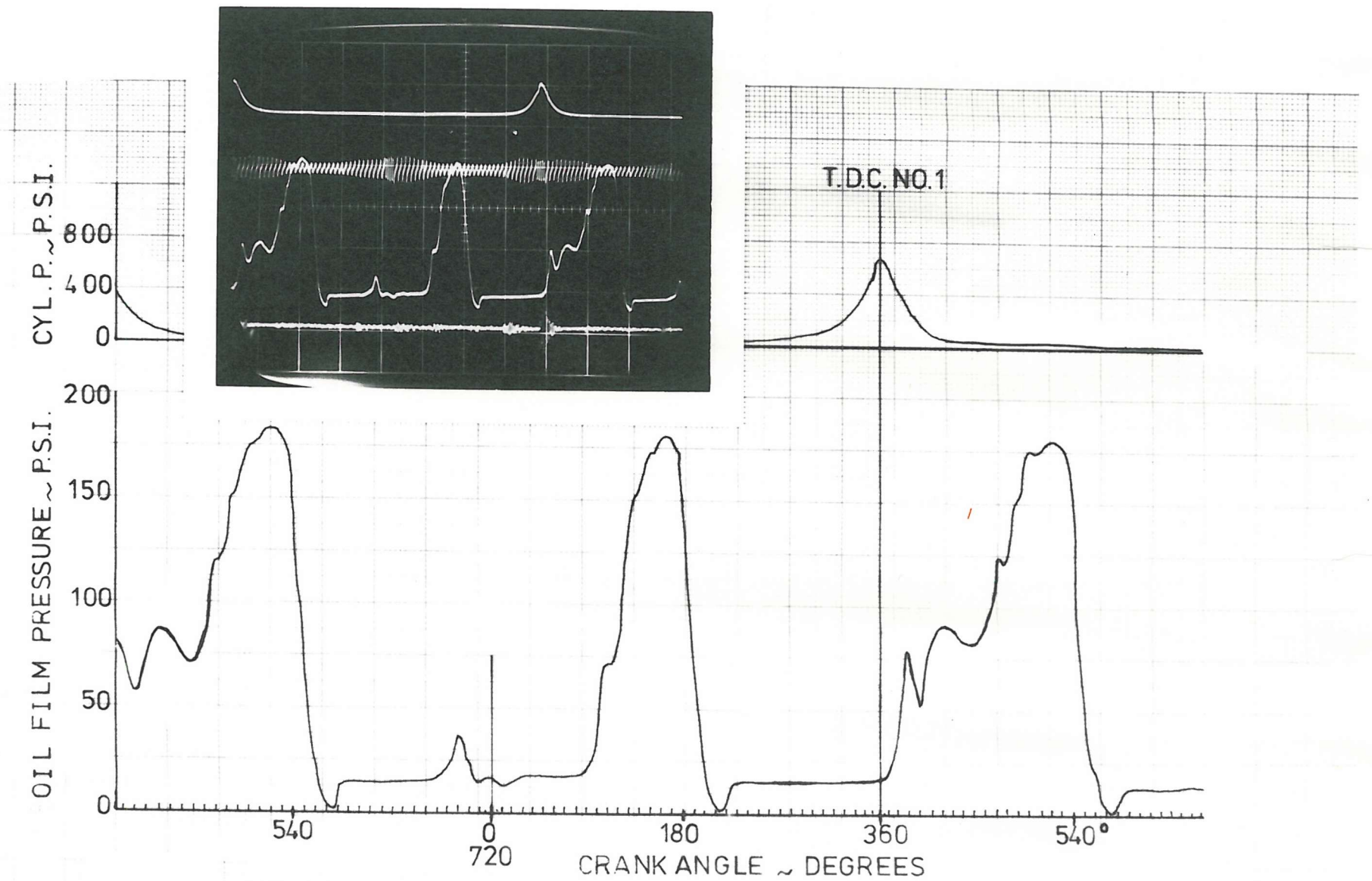

FIG. 7.7 CYLINDER PRESSURE AND PISTON TO BORE OIL FILM PRESSURE (T.S.) AT 2500 RPM NO LOAD - SA ENGINE

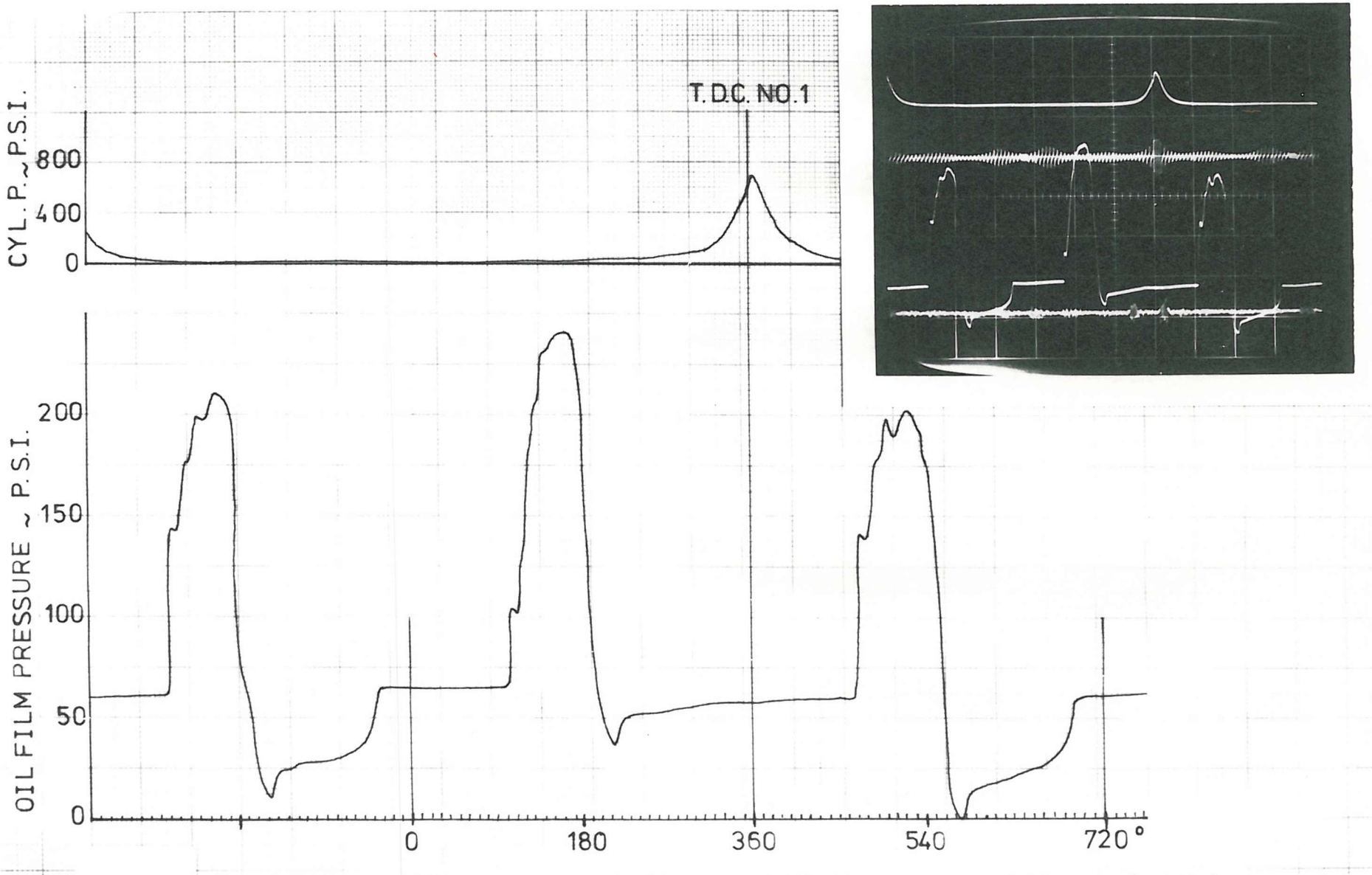

FIG. 7.8 CYLINDER PRESSURE AND PISTON TO BORE OIL FILM PRESSURE (T.S.) AT 3000 RPM NO LOAD - SA ENGINE

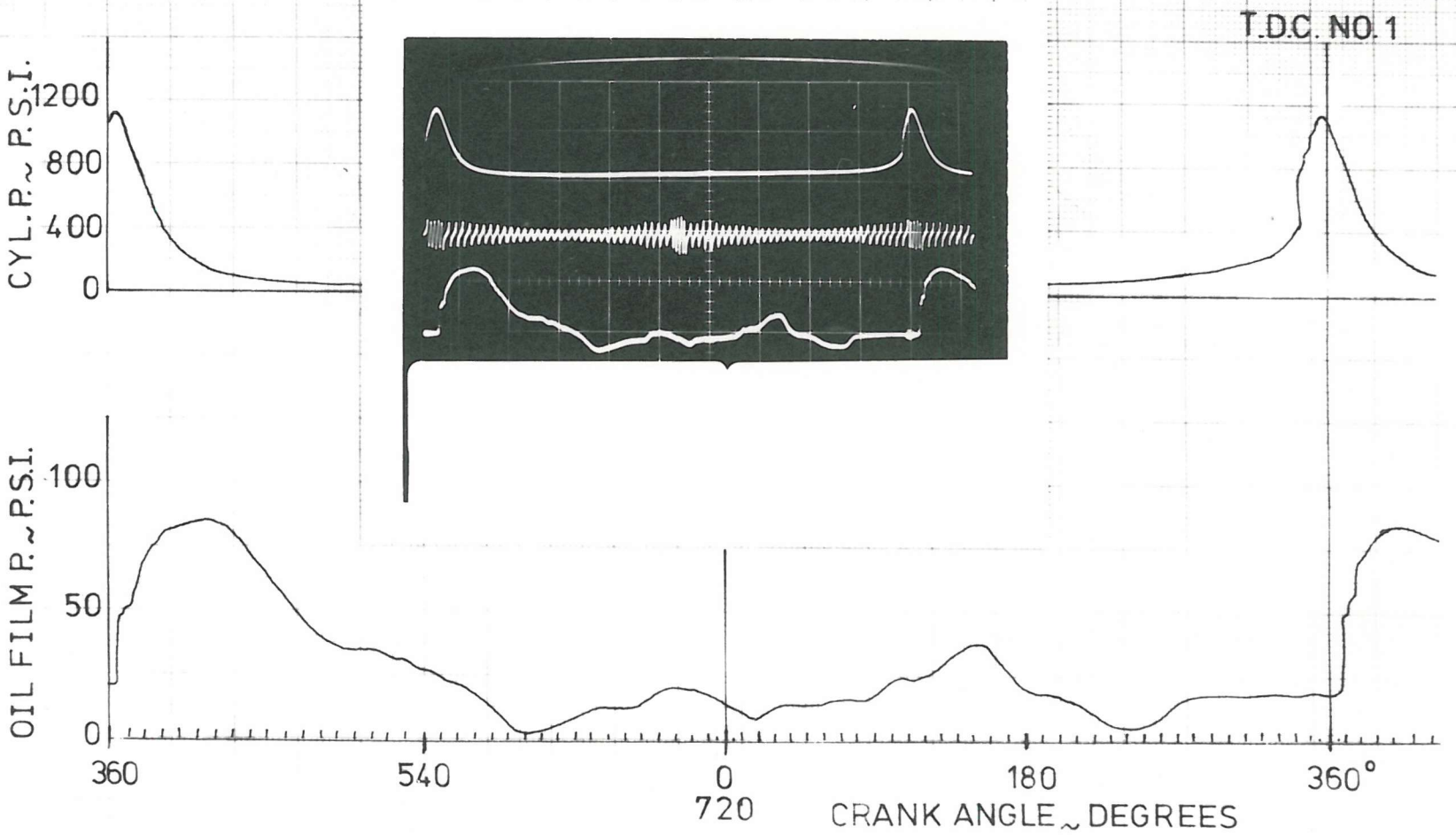

FIG. 7.9 CYLINDER PRESSURE AND PISTON TO BORE OIL FILM PRESSURE (T.S.) AT 1000 RPM FULL LOAD - SA ENGINE

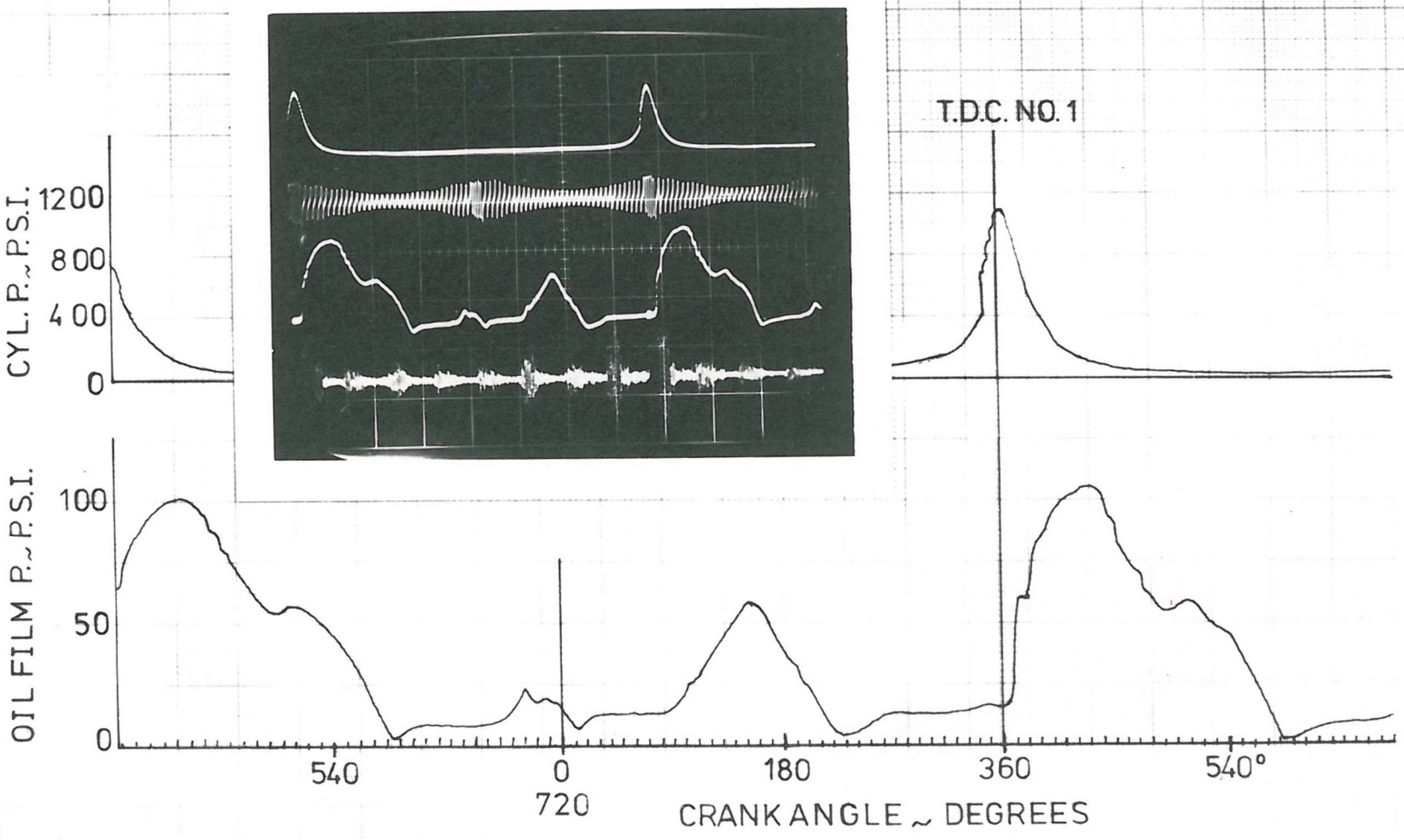

FIG. 7.10 CYLINDER PRESSURE AND PISTON TO BORE OIL FILM PRESSURE (T.S.) AT 1500 RPM FULL LOAD- SA ENGINE

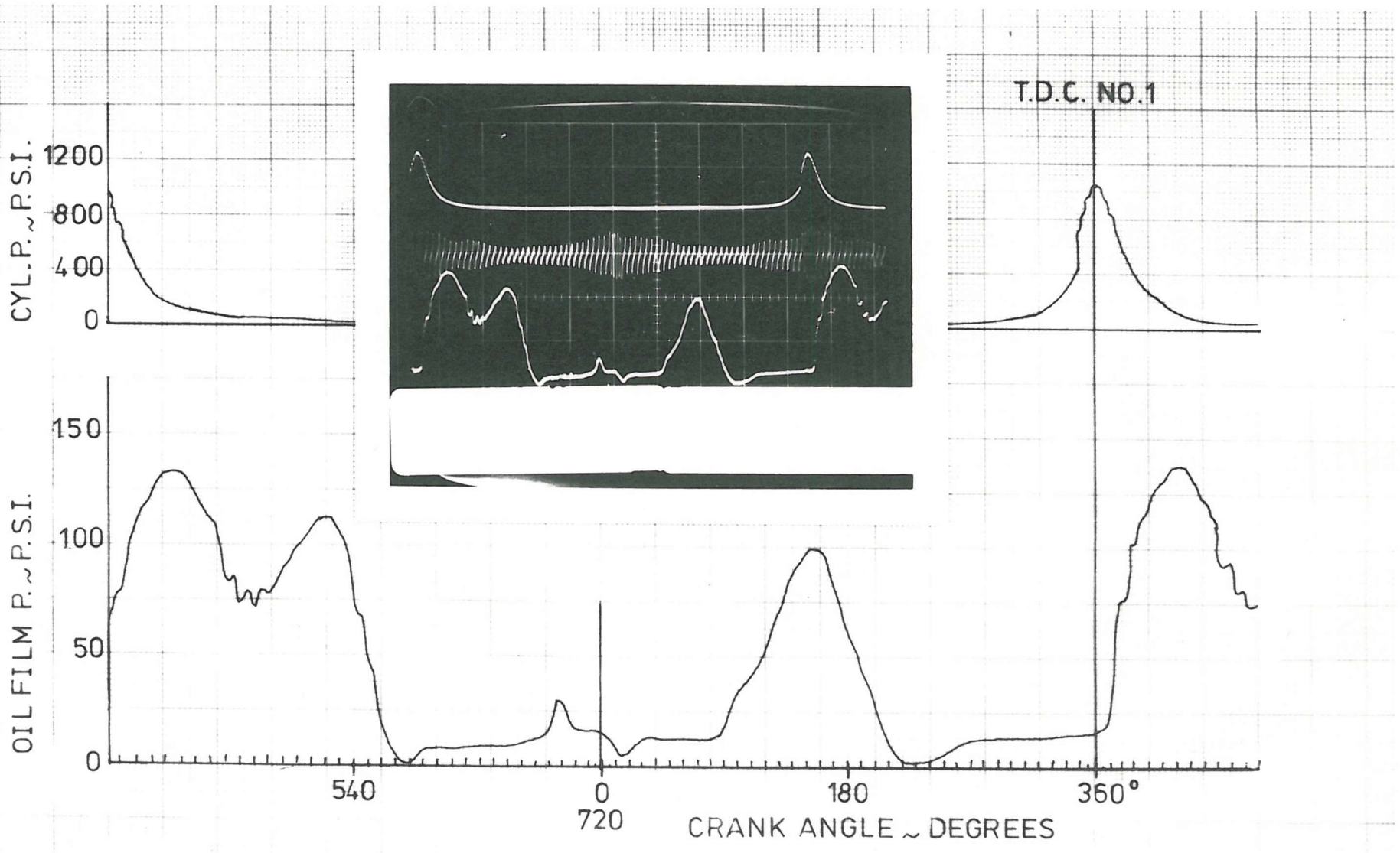

FIG. 7.11 CYLINDER PRESSURE AND PISTON TO BORE OIL FILM PRESSURE (T.S.) AT 2000 RPM FULL LOAD - SA ENGINE

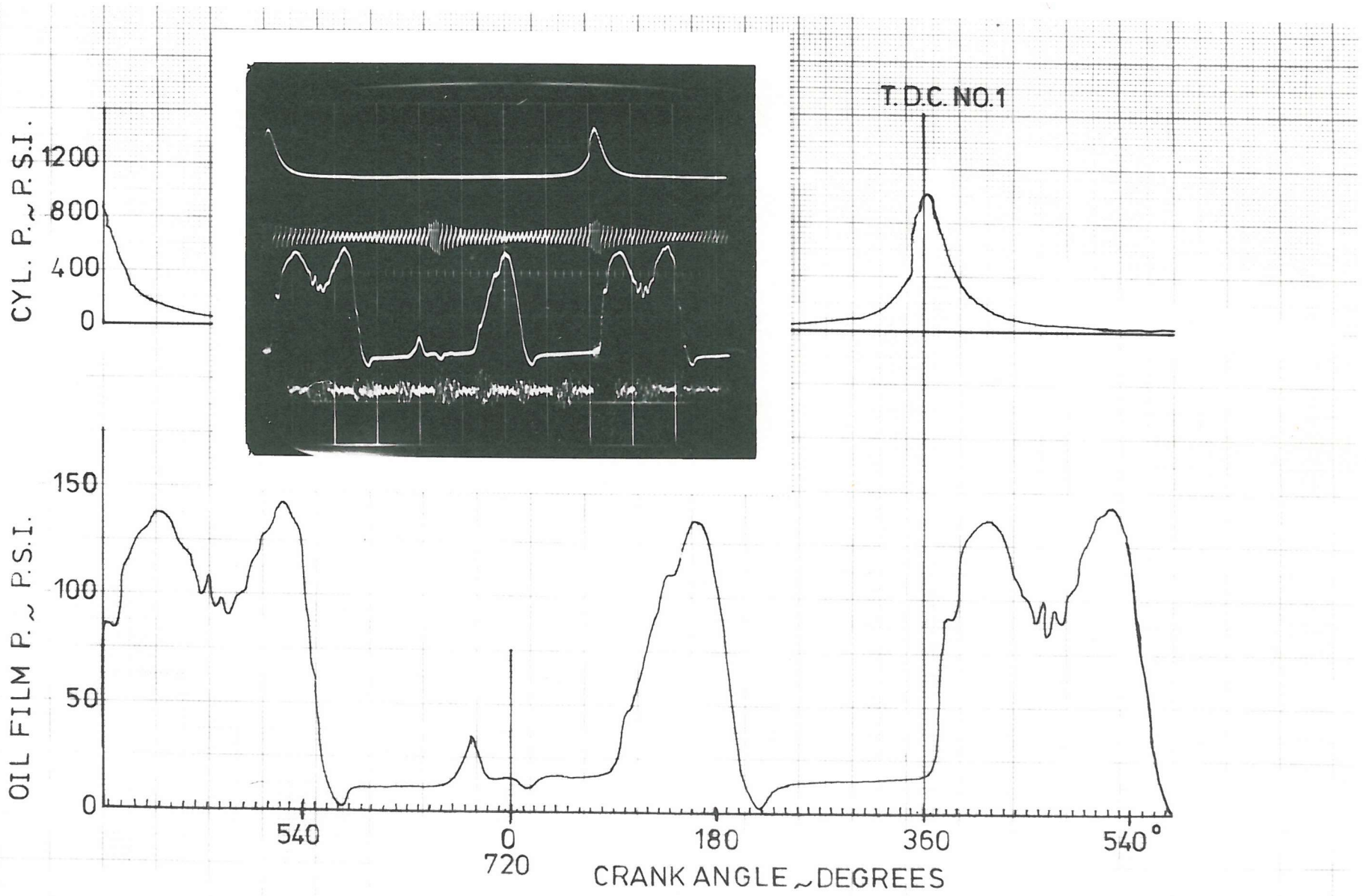

FIG. 7.12 CYLINDER PRESSURE AND PISTON TO BORE OIL FILM PRESSURE (T.S.) AT 2500 RPM FULL LOAD - SA ENGINE

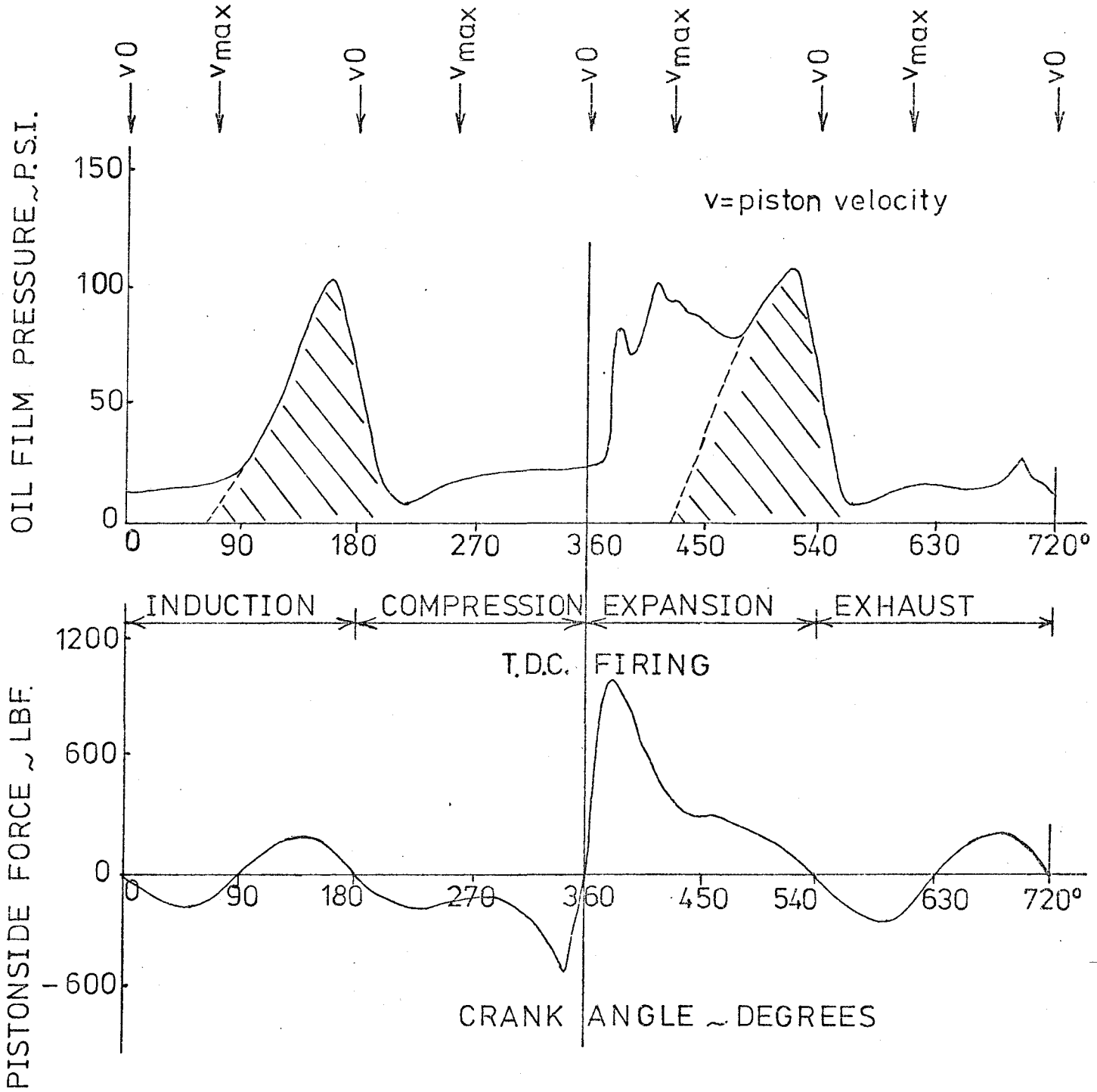

FIG. 7.13

RELATION BETWEEN PISTON TO BORE OIL FILM PRESSURE AND SIDEWAYS FORCE AT 2000 RPM NO LOAD . FOR ENGINE SA

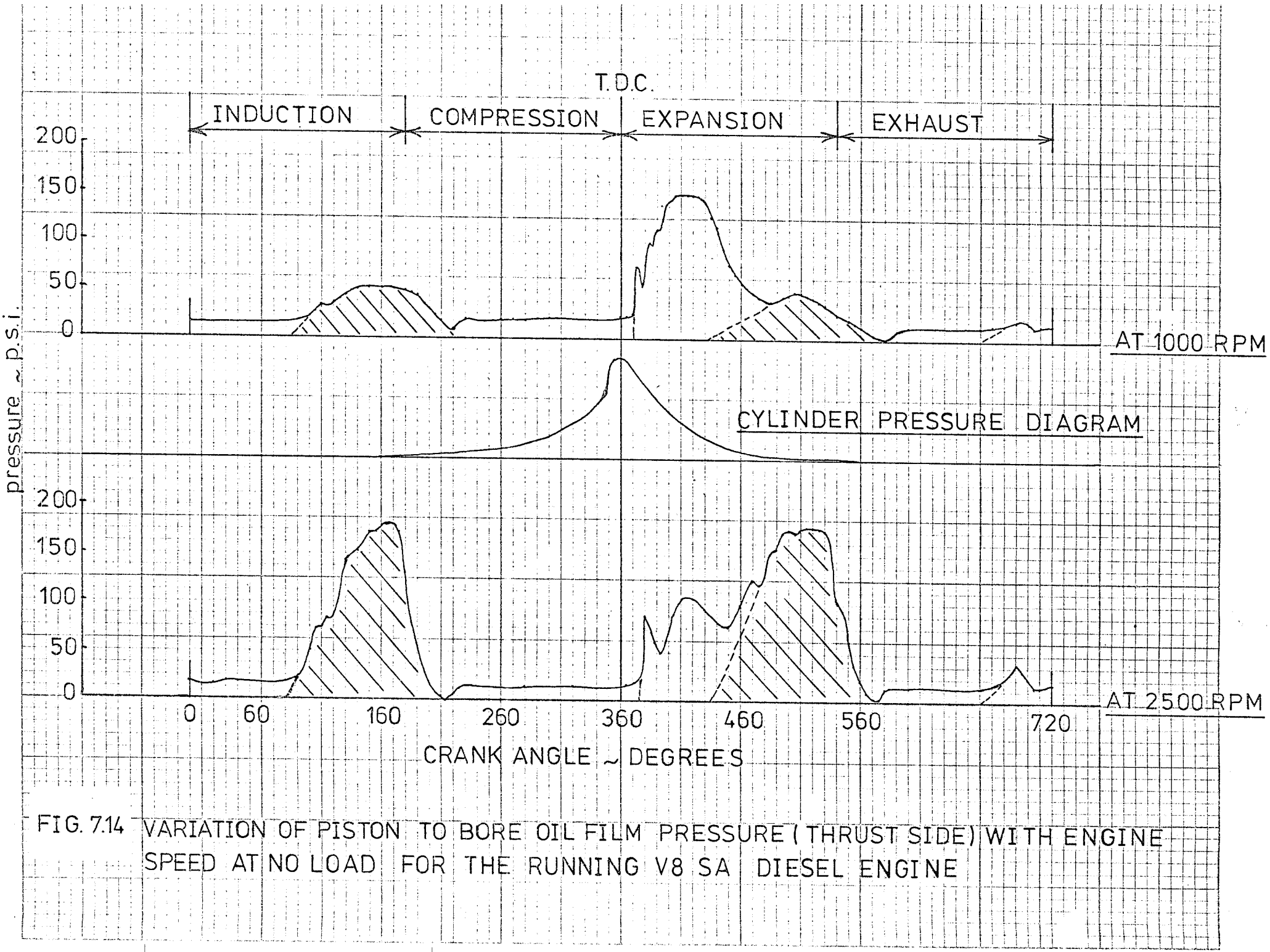

FIG. 7.14 VARIATION OF PISTON TO BORE OIL FILM PRESSURE (THRUST SIDE) WITH ENGINE SPEED AT NO LOAD FOR THE RUNNING V8 SA DIESEL ENGINE

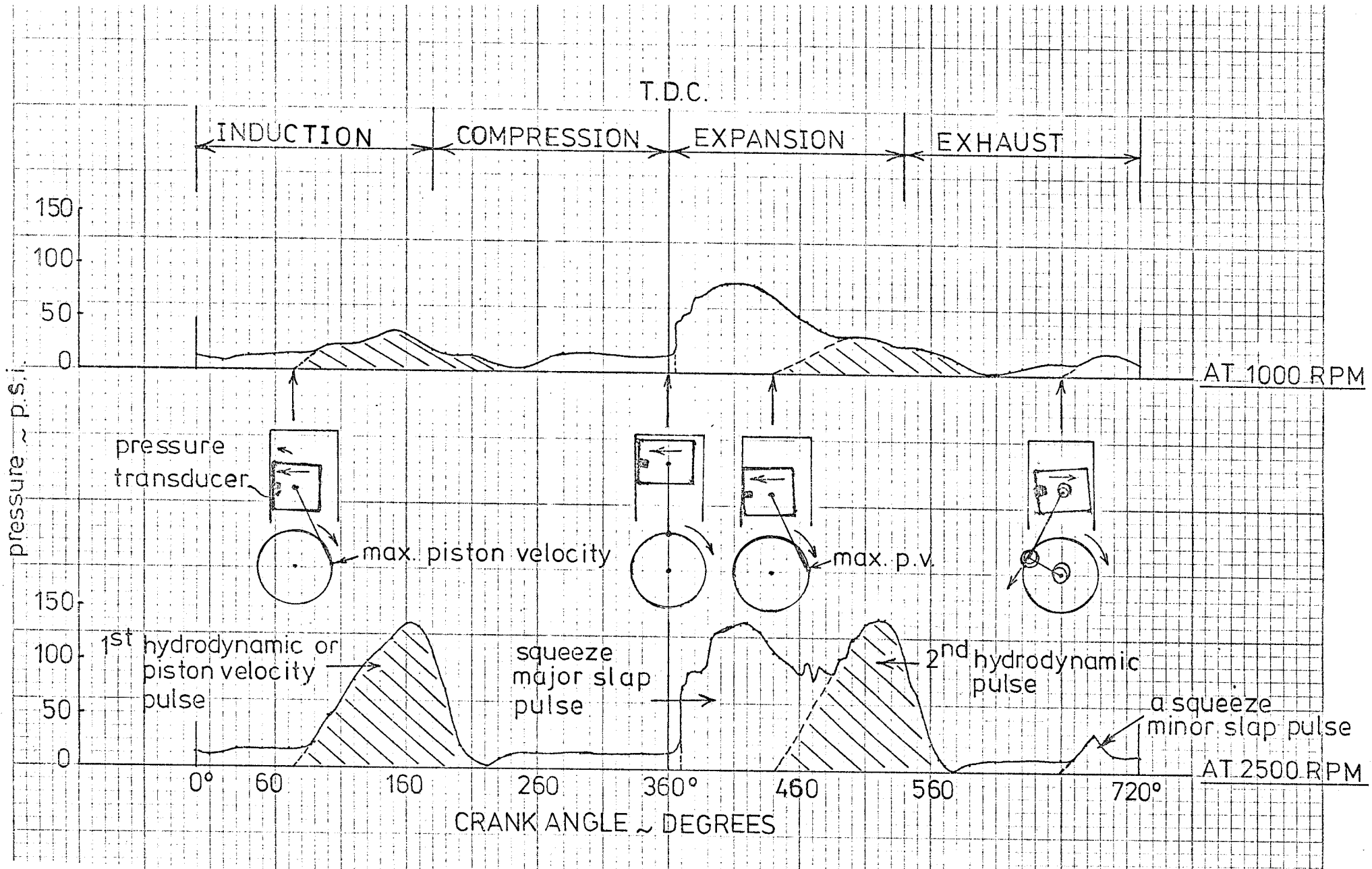

FIG. 7.15 VARIATION OF PISTON TO BORE OIL FILM PRESSURE (THRUST SIDE) WITH ENGINE SPEED AT FULL LOAD FOR THE RUNNING V8 SA DIESEL ENGINE

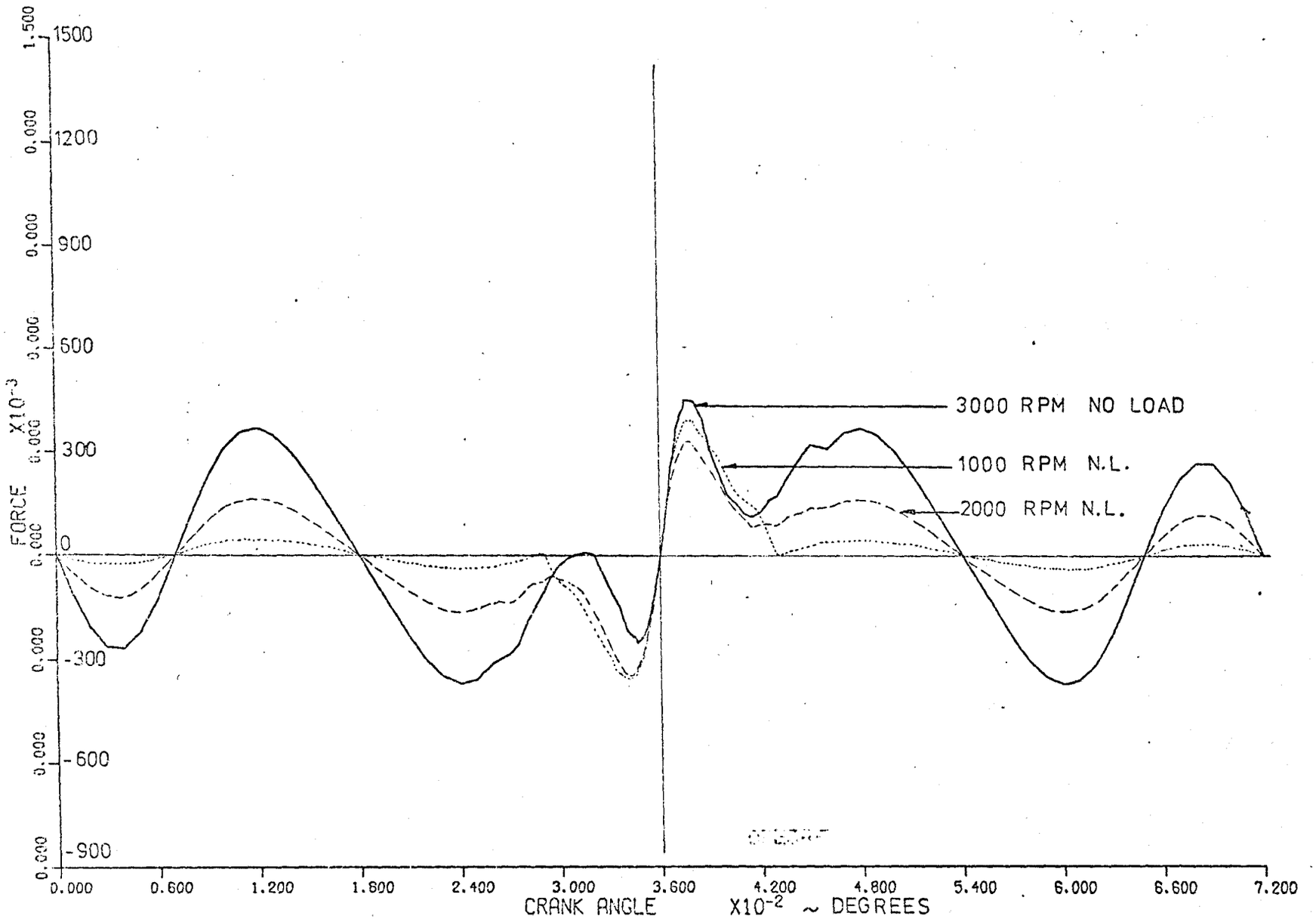

FIG. 7.16 PISTON SIDEWAYS FORCES FOR ENGINE SA

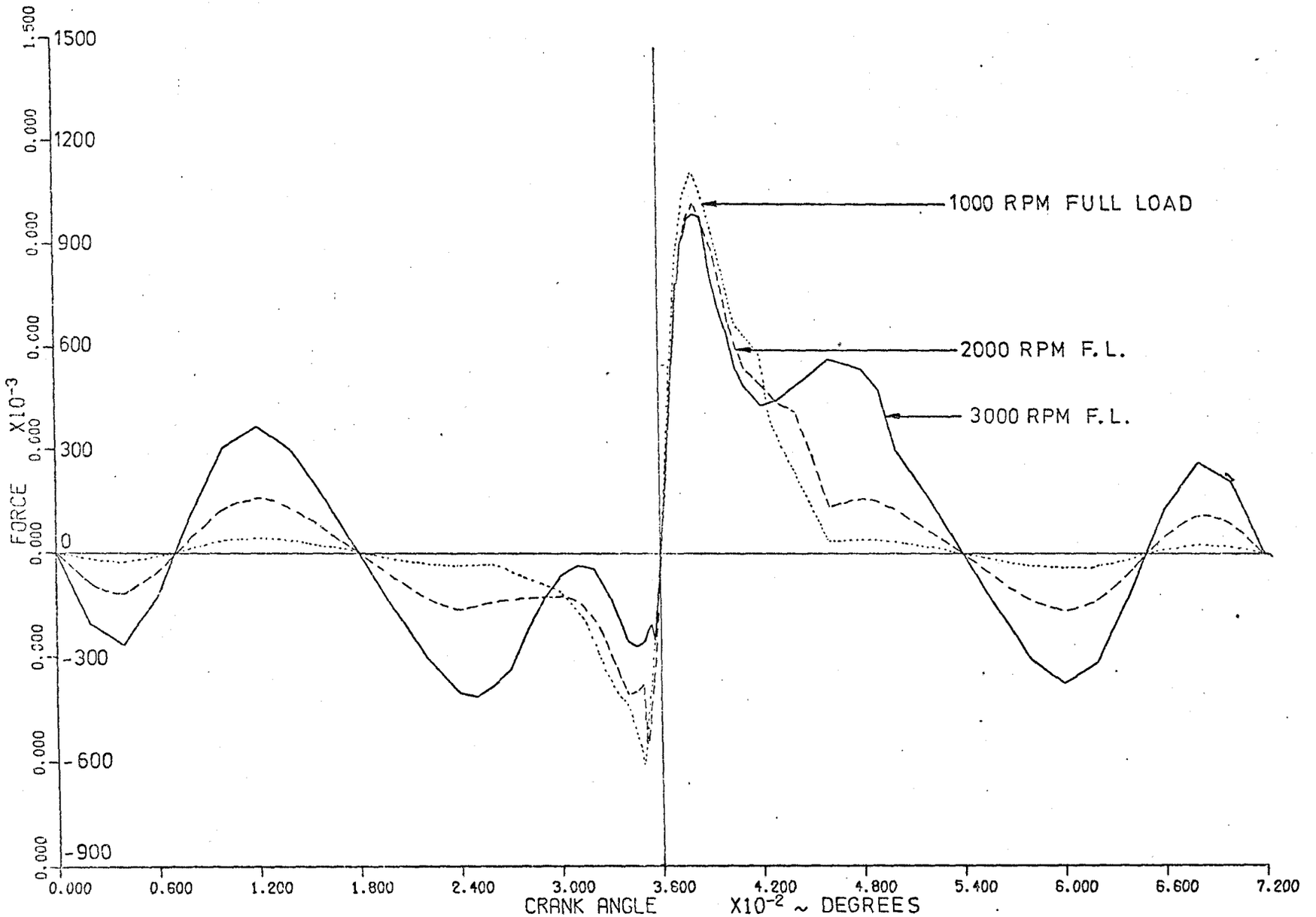

FIG. 7.17 PISTON SIDEWAYS FORCES FOR ENGINE SA

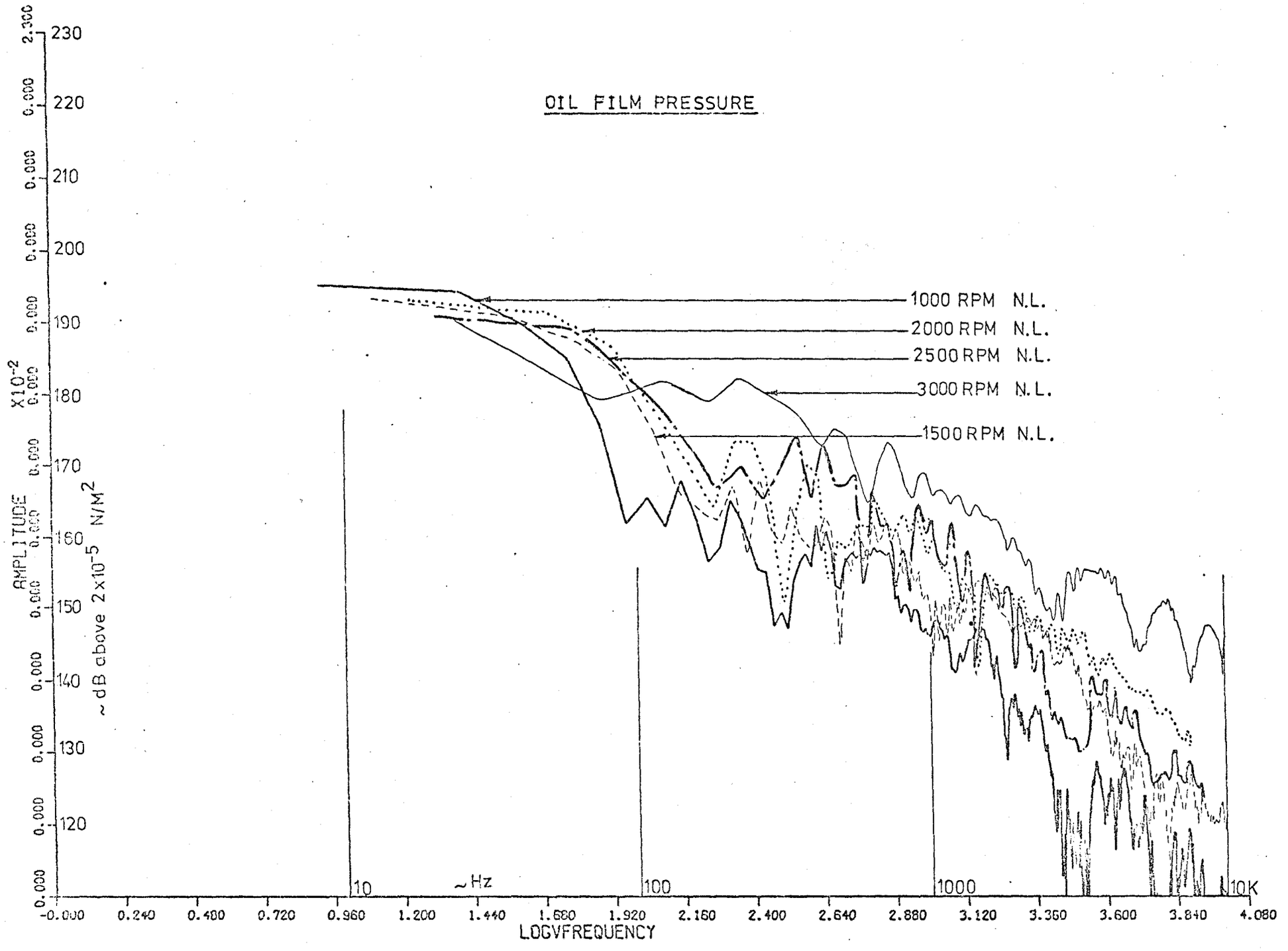

FIG. 7.18 NARROW BAND SPECTRA OF PISTON TO BORE OIL FILM PRESSURES - SA

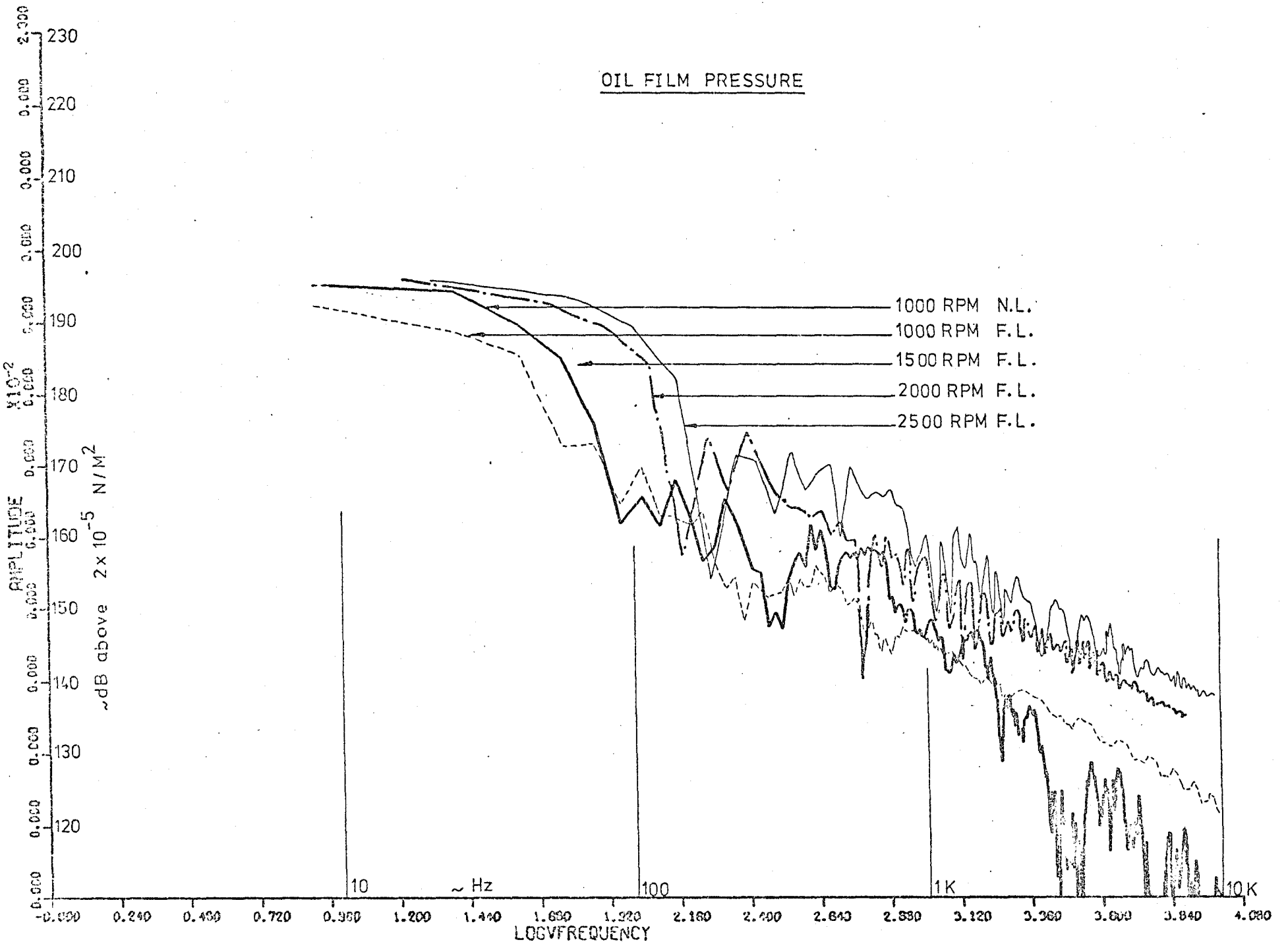

FIG. 7.19 NARROW BAND SPECTRA OF PISTON TO BORE OIL FILM PRESSURES - SA

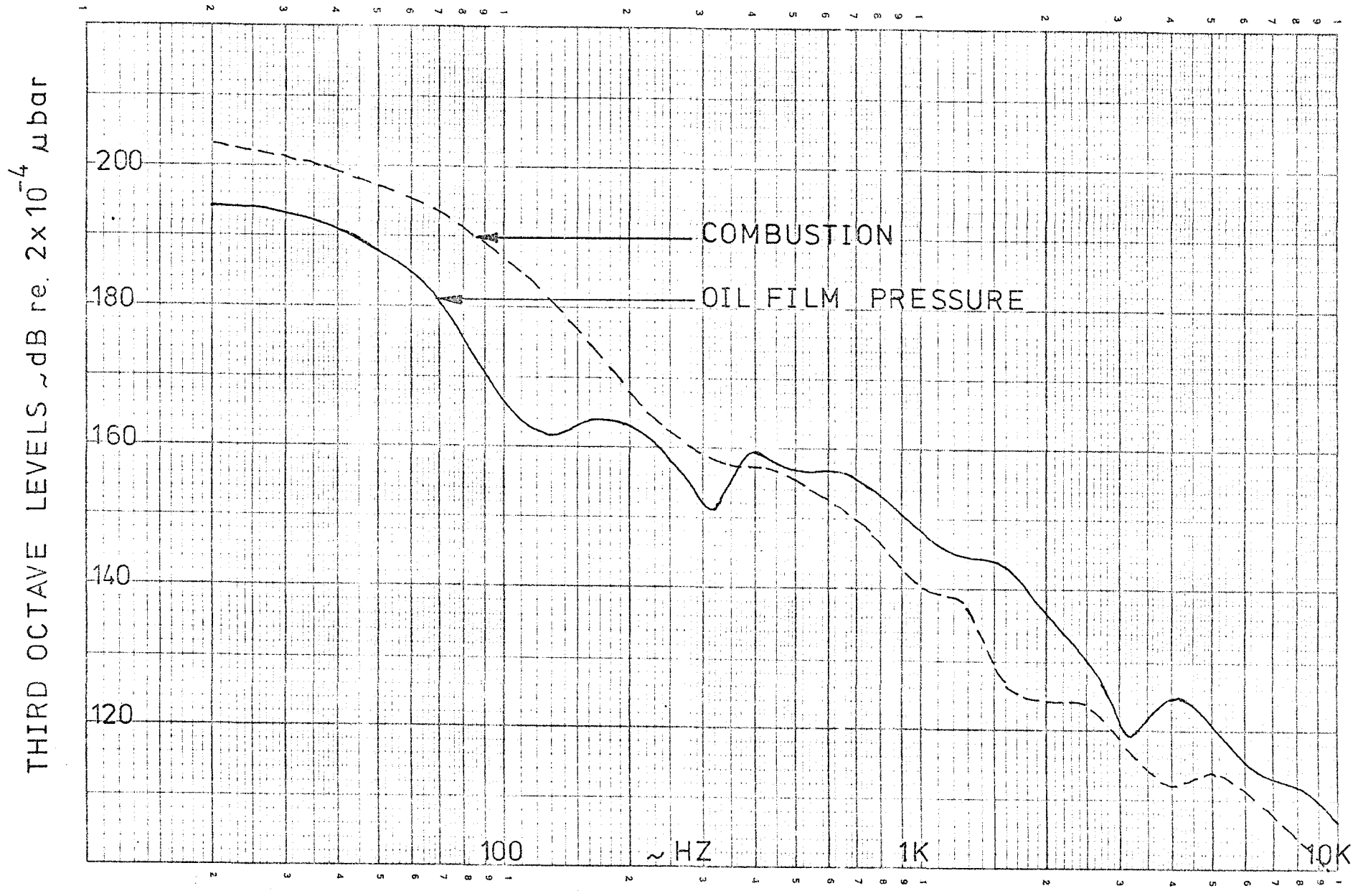

FIG. 7.20 SPECTRA OF PISTON TO BORE OIL FILM PRESSURE AND COMBUSTION FOR SA ENGINE AT 1000 RPM NO LOAD

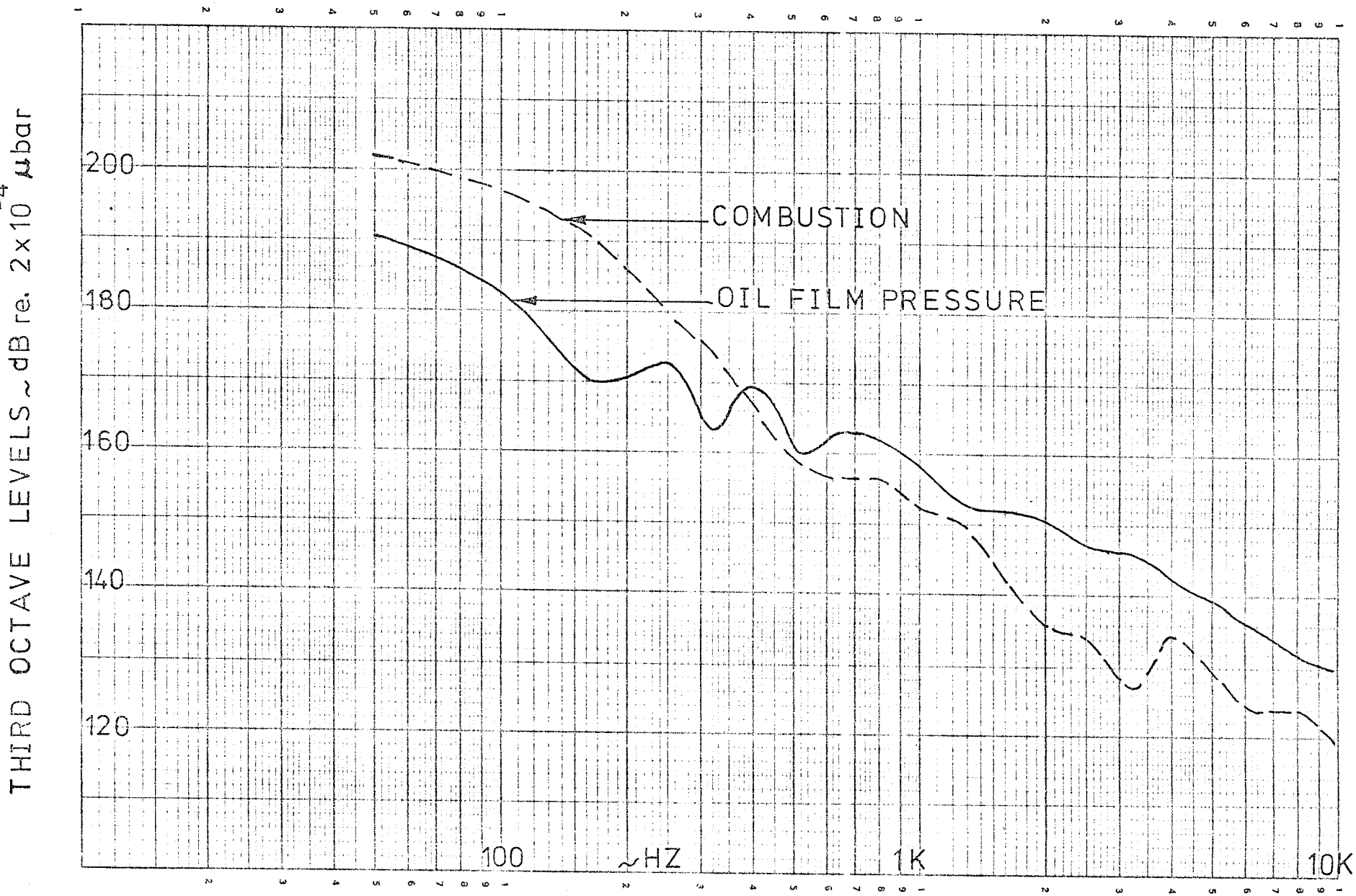

FIG. 7.21 SPECTRA OF PISTON TO BORE OIL FILM PRESSURE AND COMBUSTION FOR SA ENGINE AT 2000 RPM NO LOAD

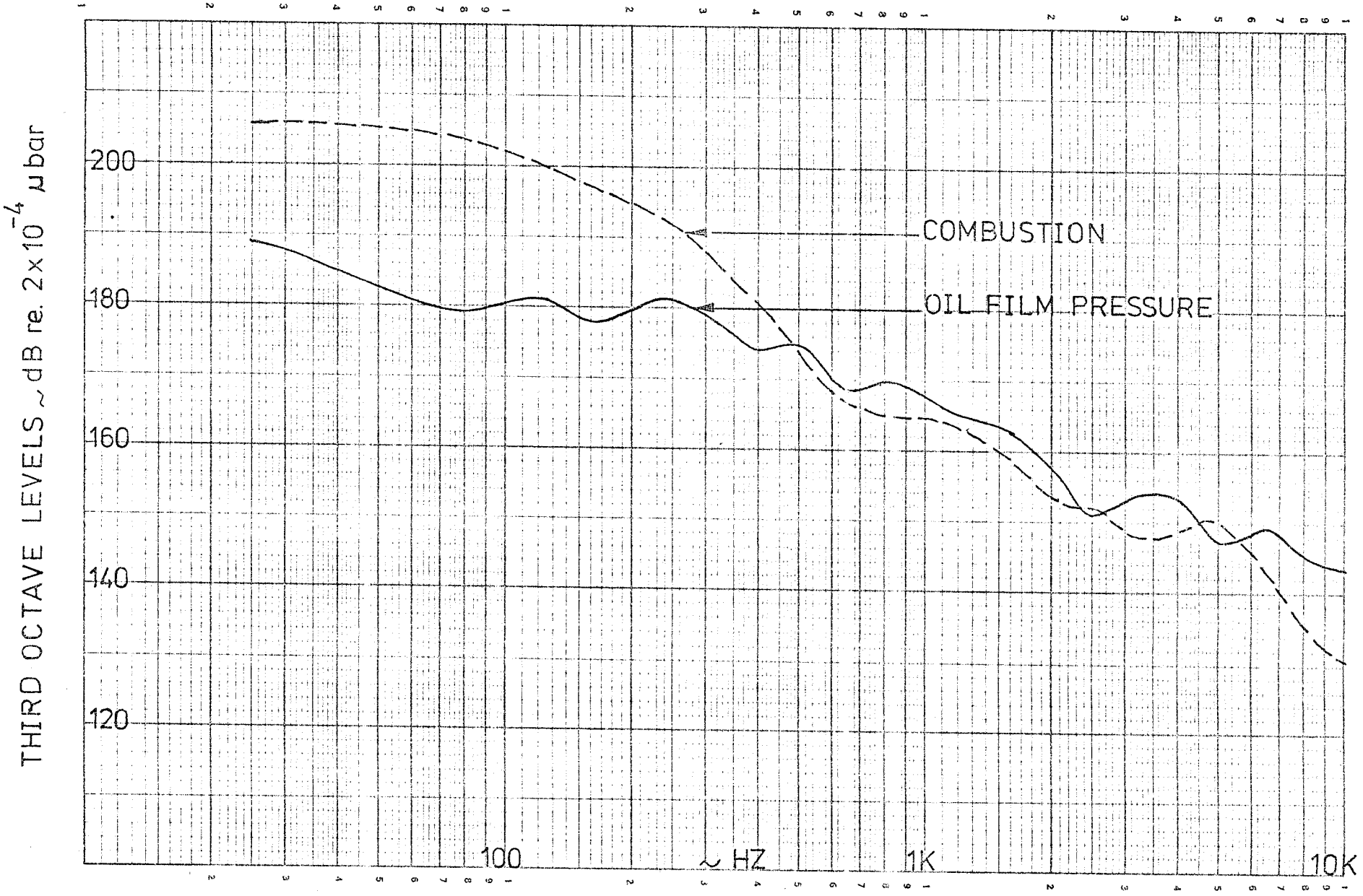

FIG. 7.22 SPECTRA OF PISTON TO BORE OIL FILM PRESSURE AND COMBUSTION FOR THE SA ENGINE AT 3000 RPM NO LOAD

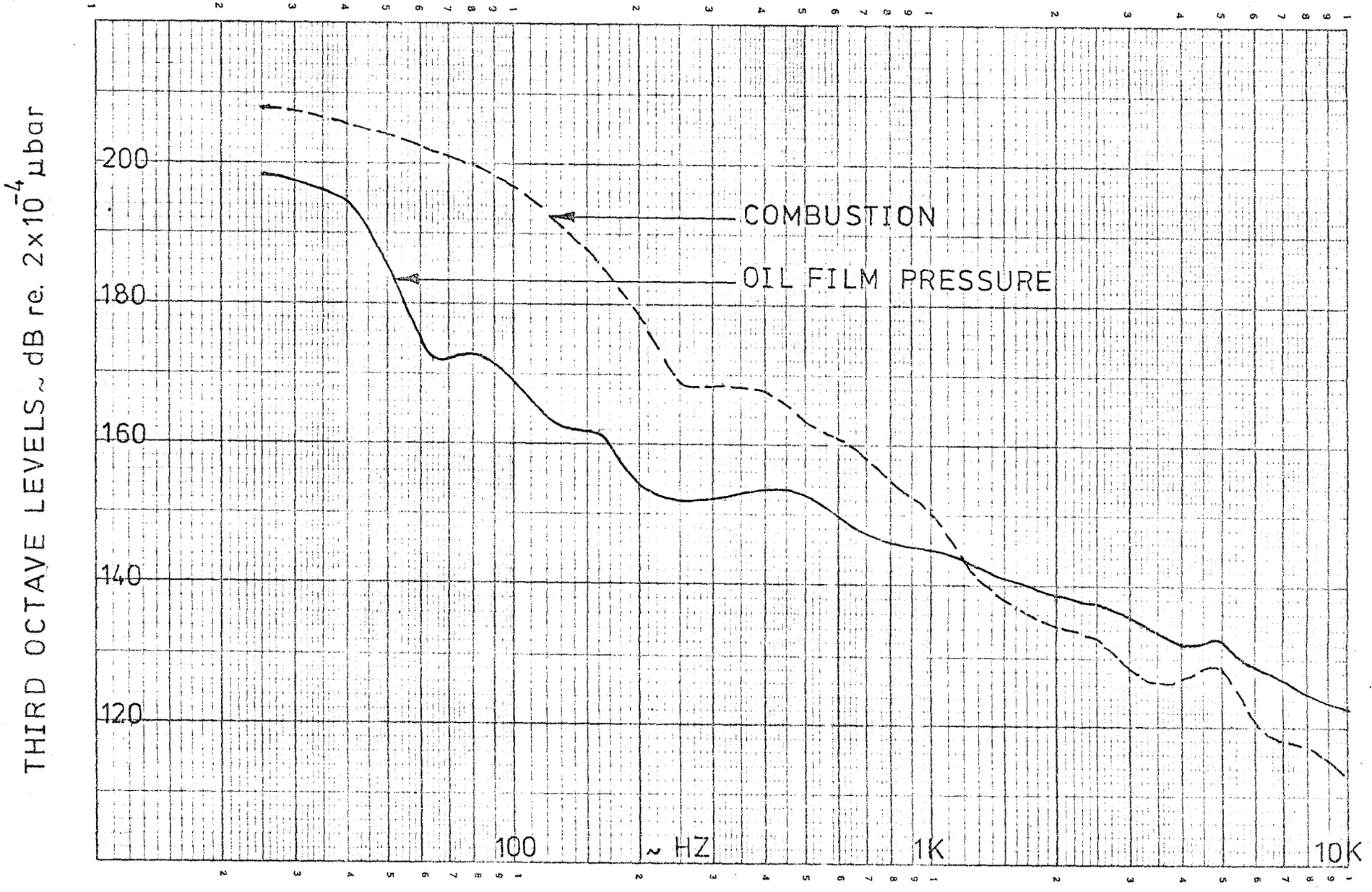

FIG. 7.23 SPECTRA OF PISTON TO BORE OIL FILM PRESSURE AND COMBUSTION FOR SA ENGINE AT 1000 RPM FULL LOAD

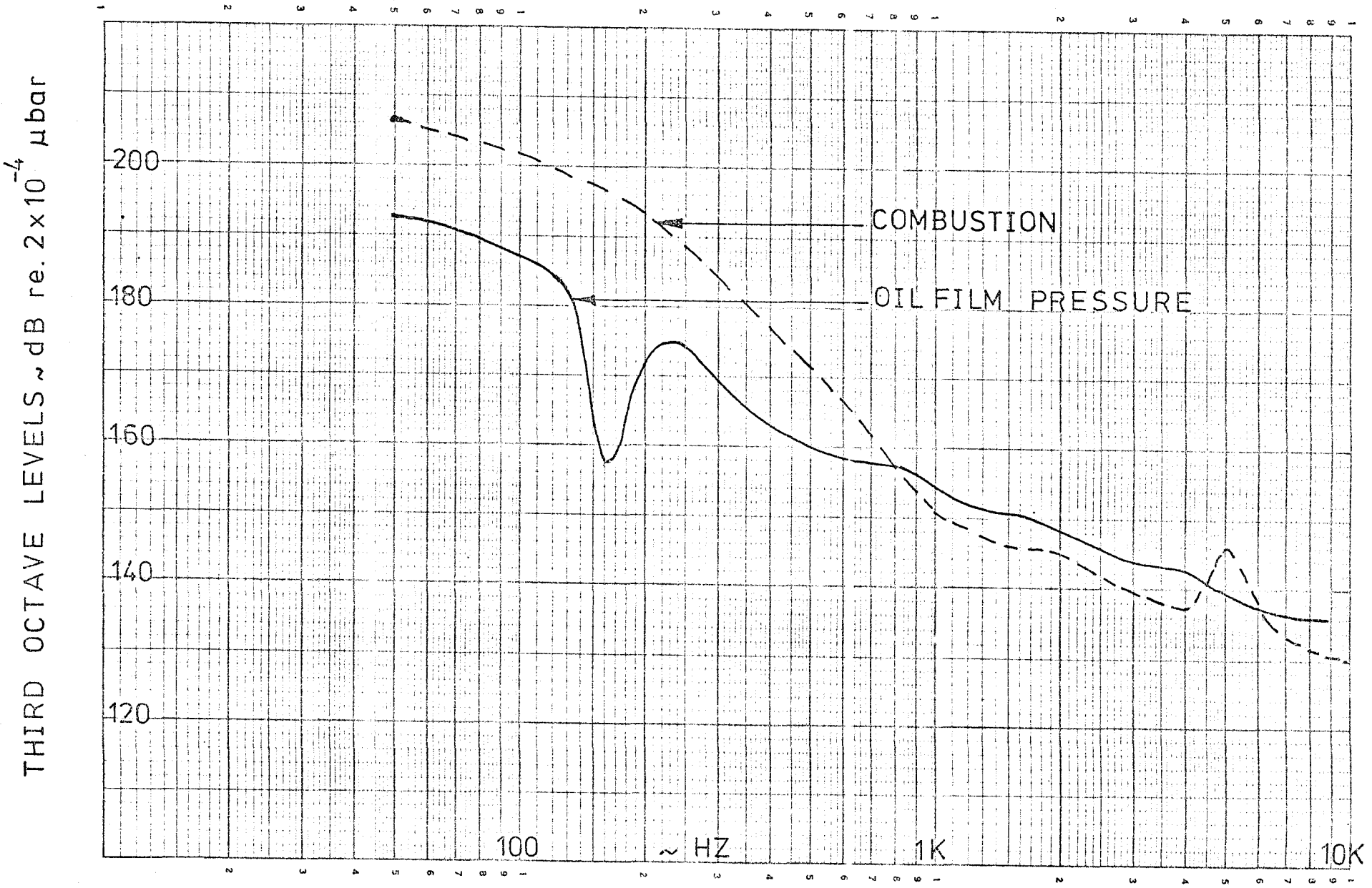

FIG. 7.24 SPECTRA OF PISTON TO BORE OIL FILM PRESSURE AND COMBUSTION FOR SA ENGINE AT 2000 RPM FULL LOAD

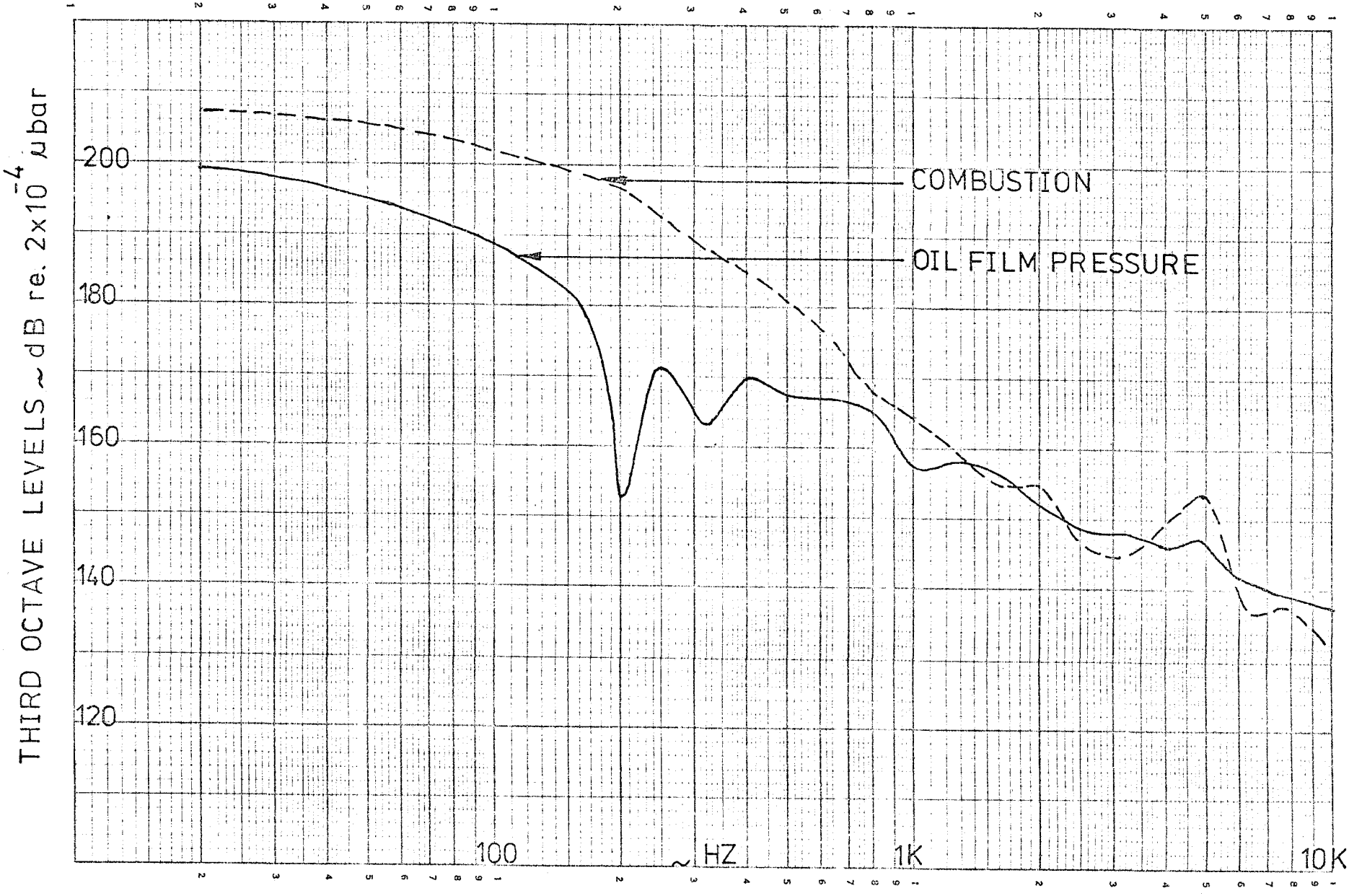

FIG. 7.25 SPECTRA OF PISTON TO BORE OIL FILM PRESSURE AND COMBUSTION FOR THE SA ENGINE AT 2500 RPM FULL LOAD

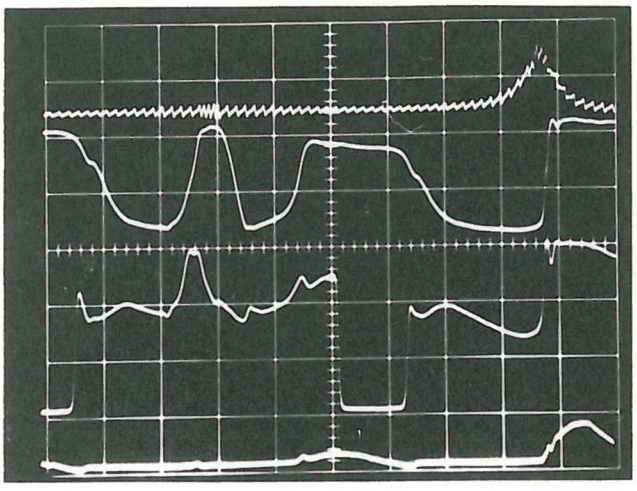

— C.P. + D.M.

— U.C. (0.5 v/div)

— L.C. " "

— OIL F. P. (0.1v/div)

NO LOAD

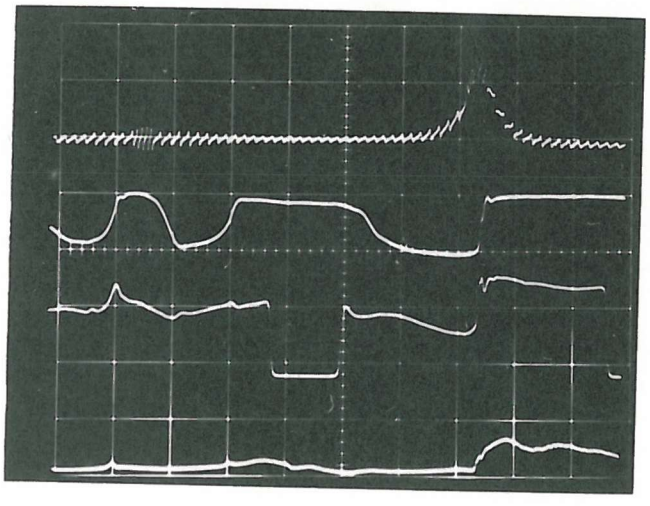

— C.P. + D.M.

— U.C. (1v/div)

— L.C. " "

— OIL F. P. (0.1v/div)

FULL LOAD

FIG. 7.26 PISTON MOVEMENT, CYLINDER PRESSURE AND OIL FILM PRESSURE IN NO 1 CYLINDER OF THE SA ENGINE RUNNING AT 1000 RPM

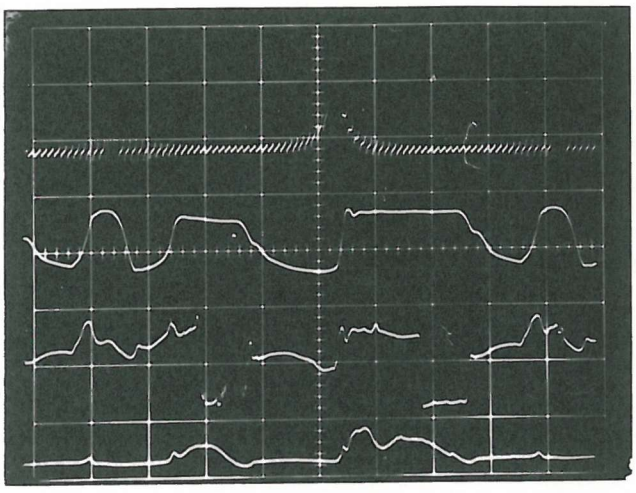

— C.P. + D.M.

— U.C. (1 v/div)

— L.C. " "

— OIL F.P. (0.1 v/div)

NO LOAD

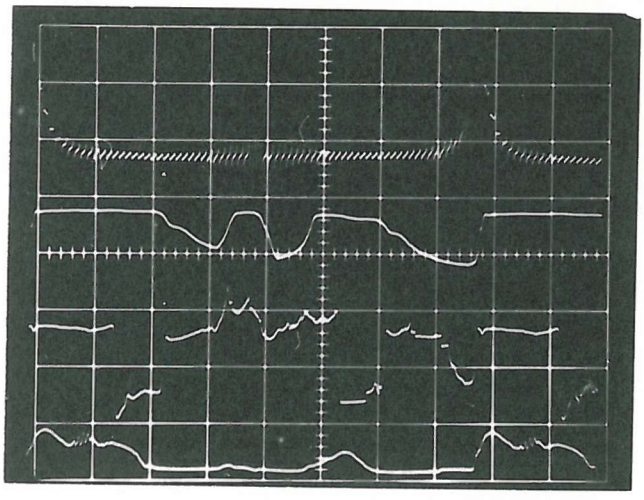

— C.P. + D.M.

— U.C. (1 v/div)

— L.C. " "

— OIL F.P. (0.1 v/div)

FULL LOAD

FIG. 7.27 PISTON MOVEMENT, CYLINDER PRESSURE AND OIL FILM PRESSURE IN NO 1 CYLINDER OF THE SA ENGINE RUNNING AT 1500 RPM

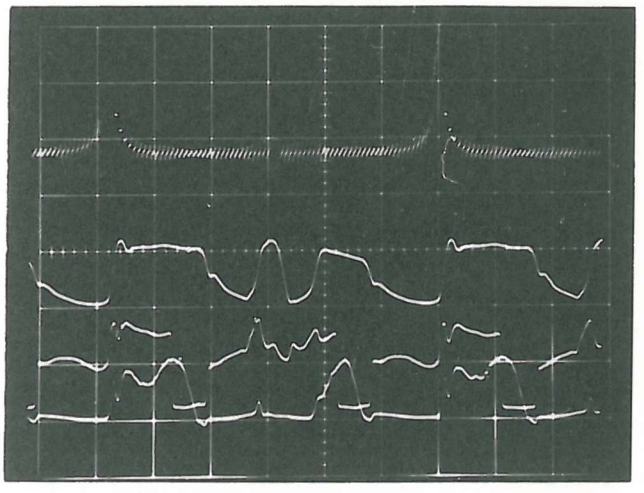

NO LOAD

FULL LOAD

FIG. 7.28 PISTON MOVEMENT, CYLINDER PRESSURE AND OIL FILM PRESSURE IN NO 1 CYLINDER OF THE SA ENGINE RUNNING AT 2000 RPM

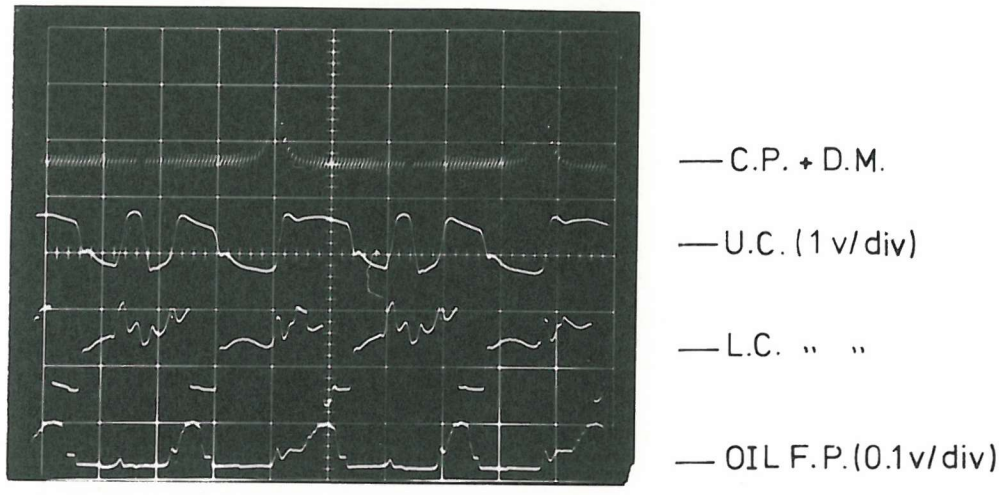

NO LOAD

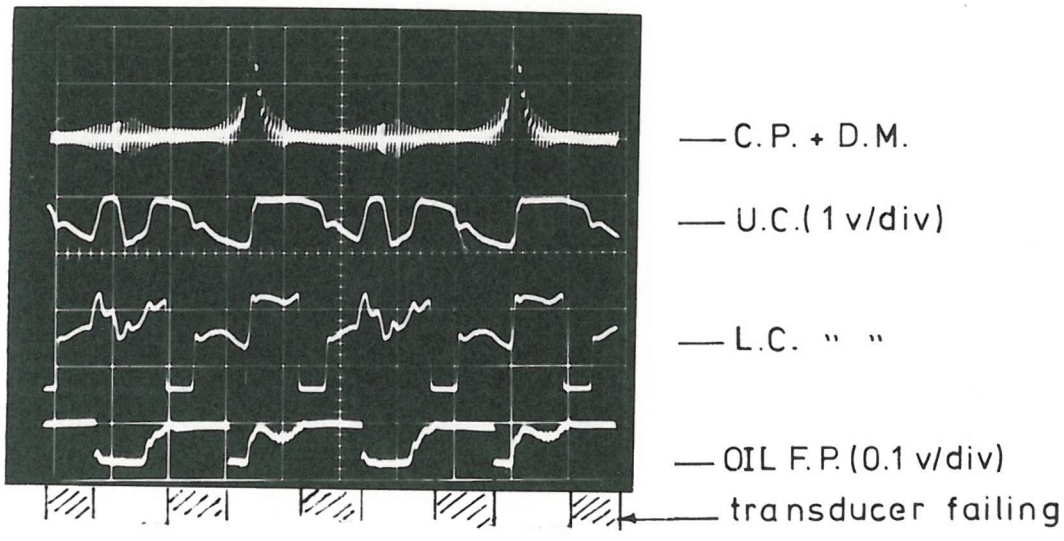

FULL LOAD

FIG. 7.29 PISTON MOVEMENT, CYLINDER PRESSURE AND OIL FILM PRESSURE IN NO 1 CYLINDER OF THE SA ENGINE RUNNING AT 2500 RPM

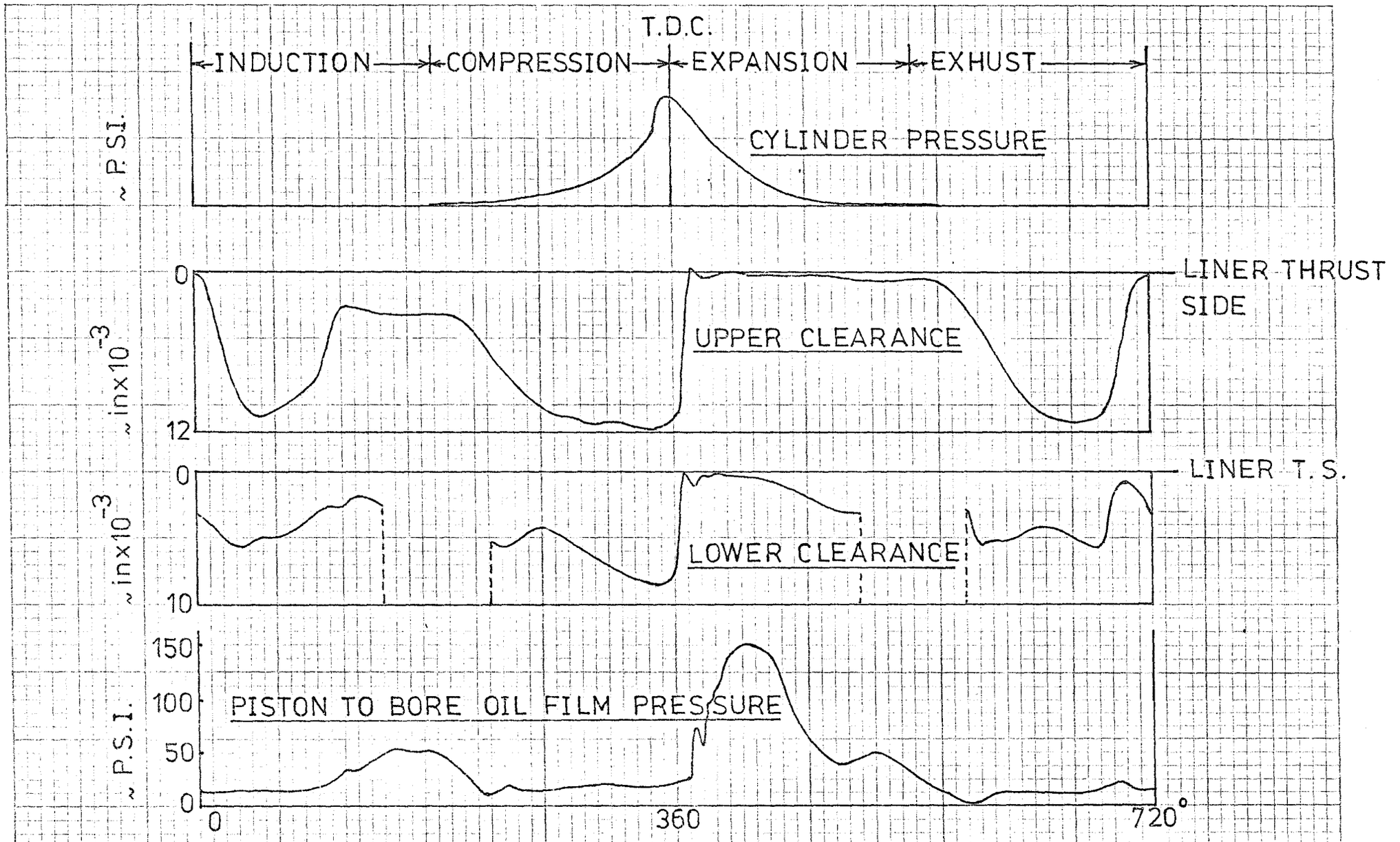

FIG. 7.30 RELATION BETWEEN CYLINDER PRESSURE, PISTON MOVEMENT AND PISTON TO BORE OIL FILM PRESSURE IN NO1 CYLINDER AT 1000 RPM NO LOAD. (ENGINE SA)

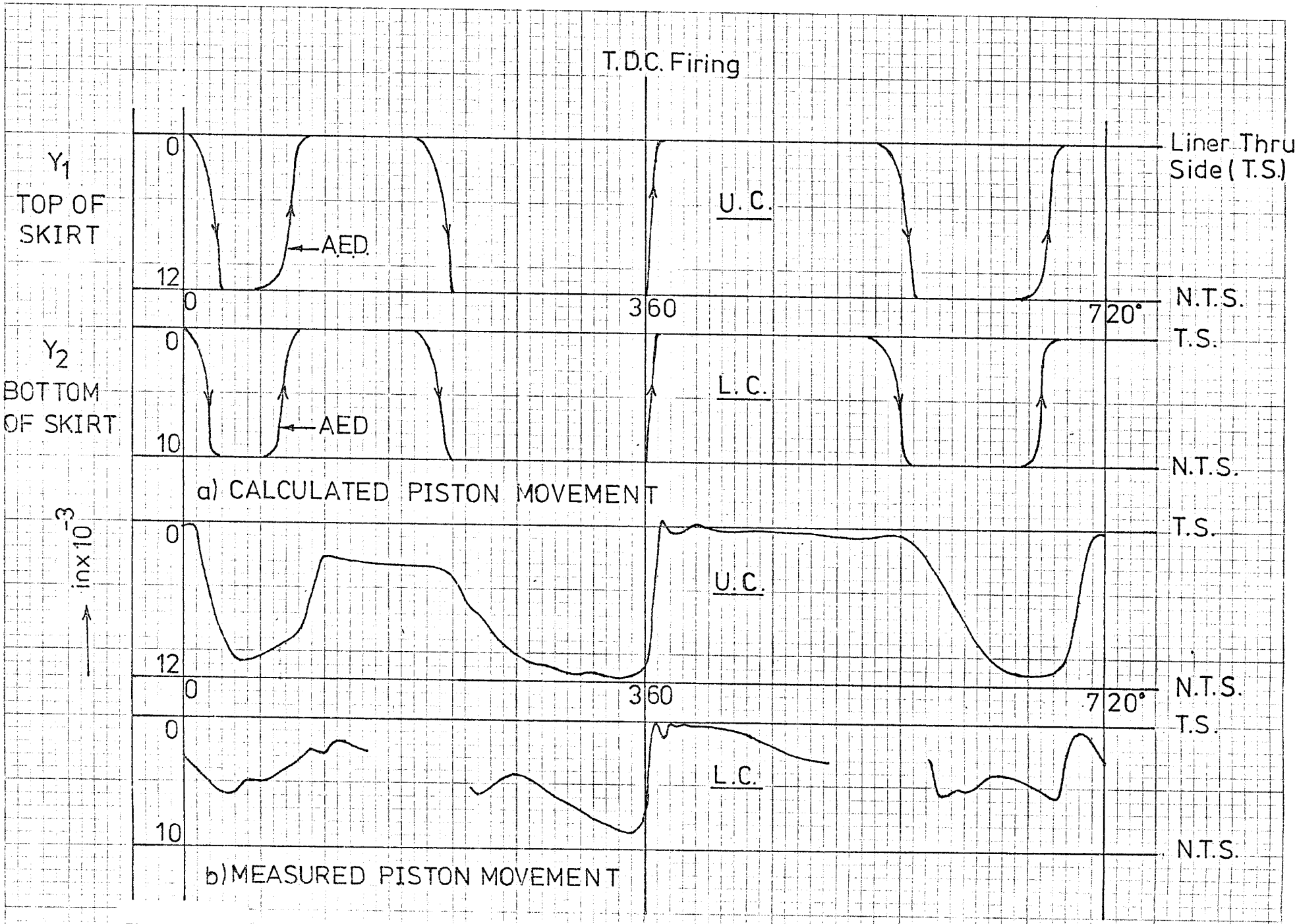

FIG. 7.31 COMPARISON OF CALCULATED AND MEASURED PISTON MOVEMENT PLOTS FOR ENGINE SA (7.7 L.) at 1000 RPM NO LOAD

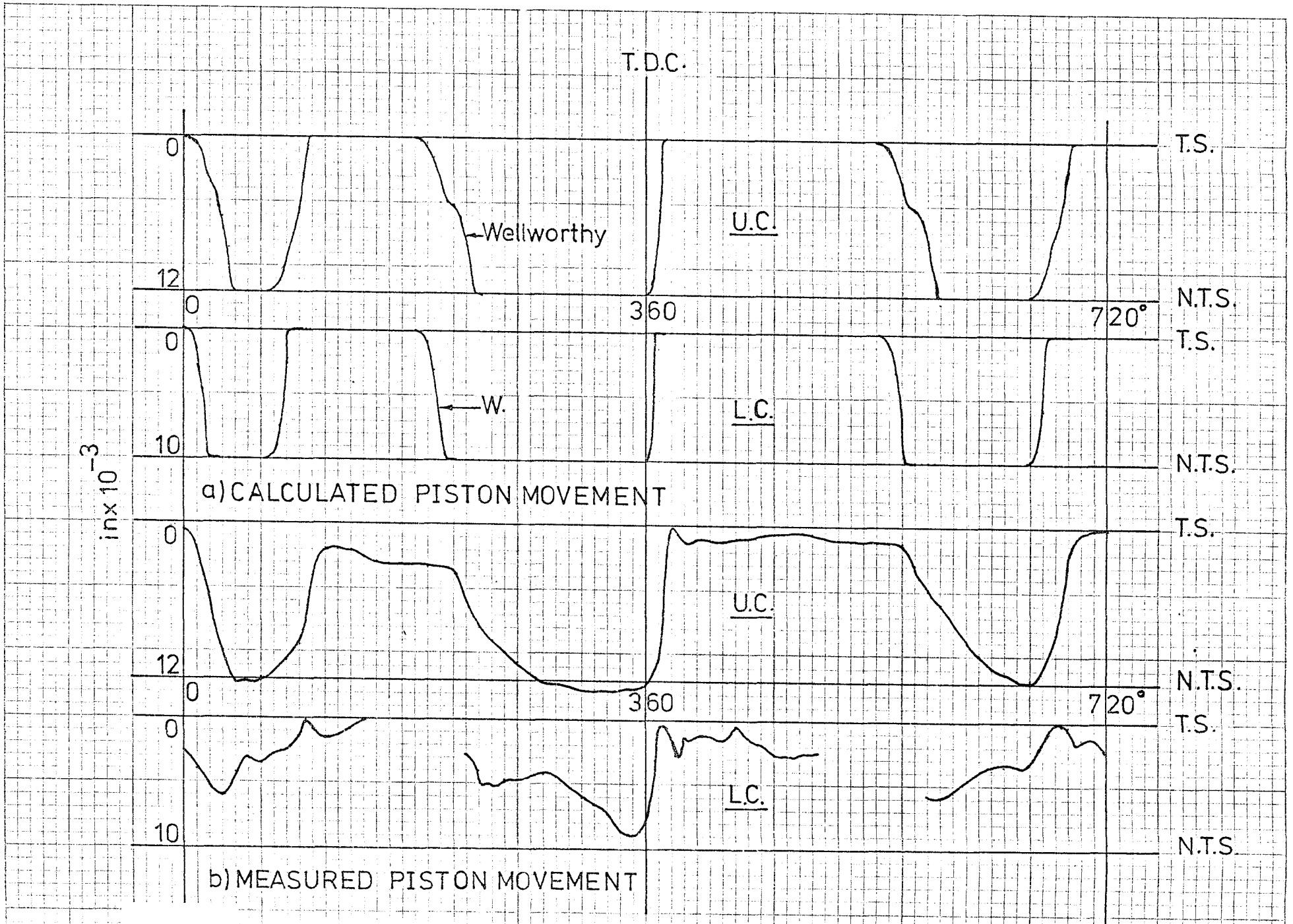

FIG. 7.32 COMPARISON OF CALCULATED AND MEASURED PISTON MOVEMENT PLOTS FOR ENGINE SA at 1500 RPM NO LOAD

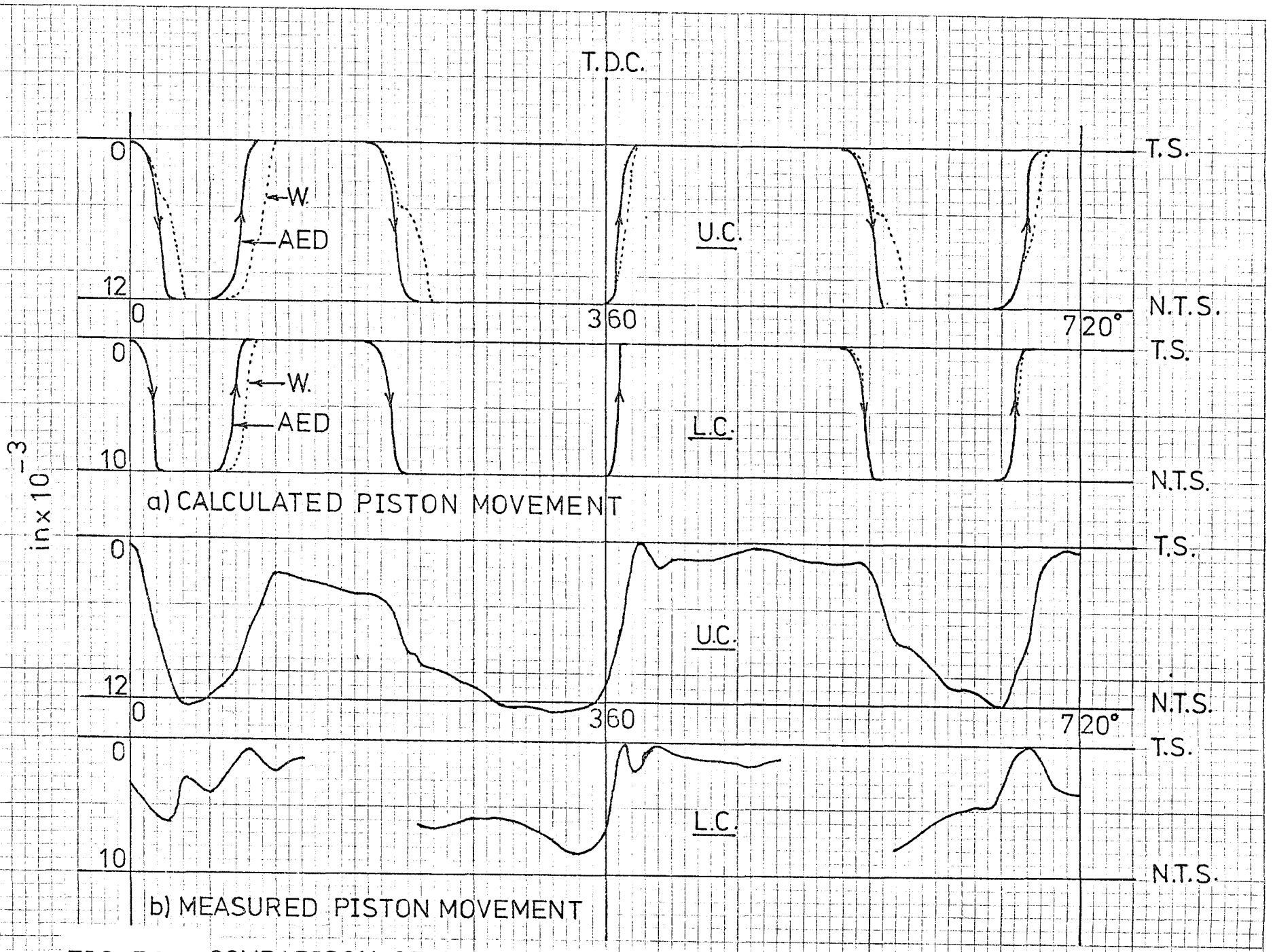

FIG. 7.33 COMPARISON OF CALCULATED AND MEASURED PISTON MOVEMENT PLOTS FOR ENGINE SA at 2000 RPM NO LOAD

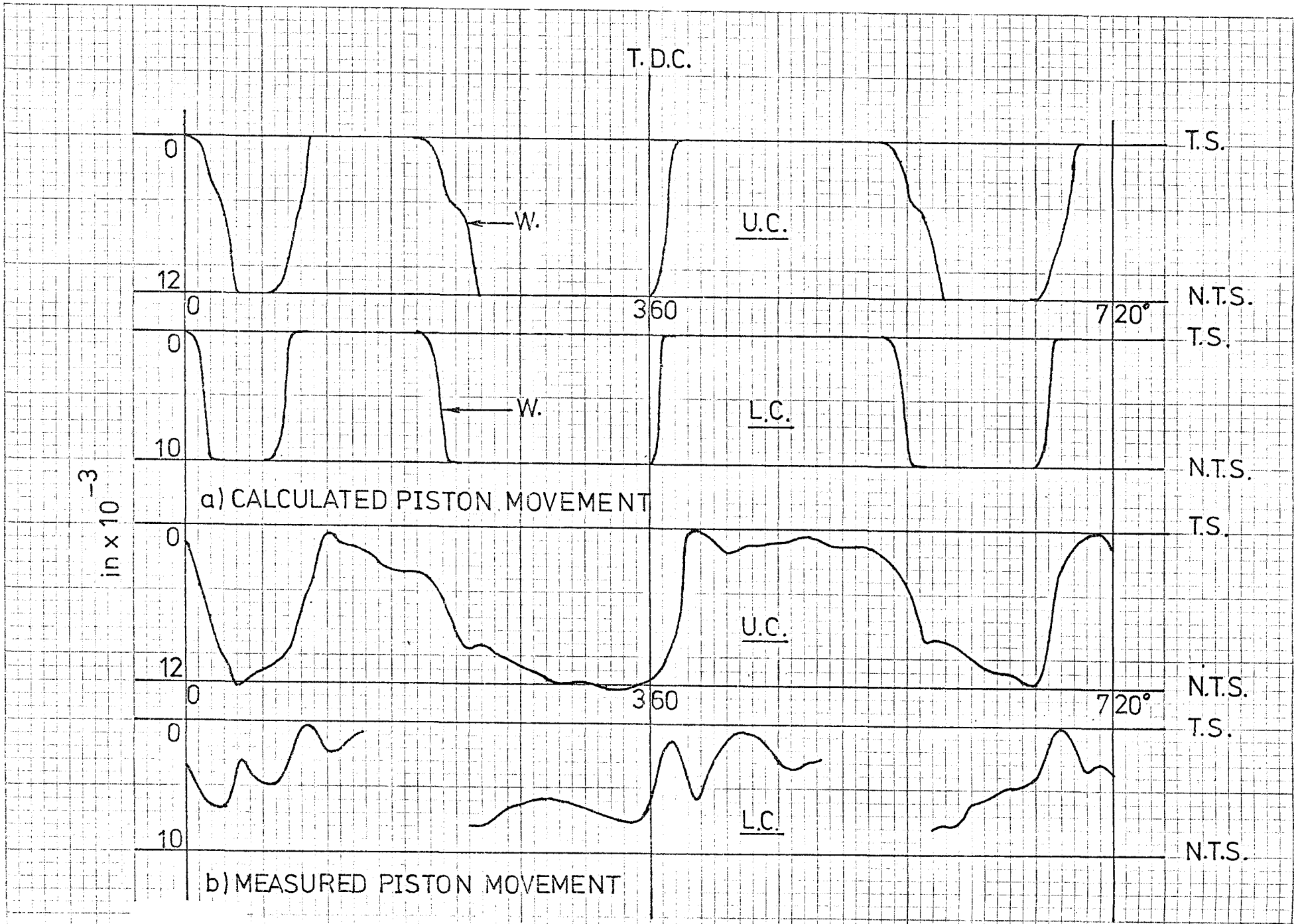

FIG. 7.34 COMPARISON OF CALCULATED AND MEASURED PISTON MOVEMENT PLOTS FOR ENGINE SA at 2500 RPM NO LOAD

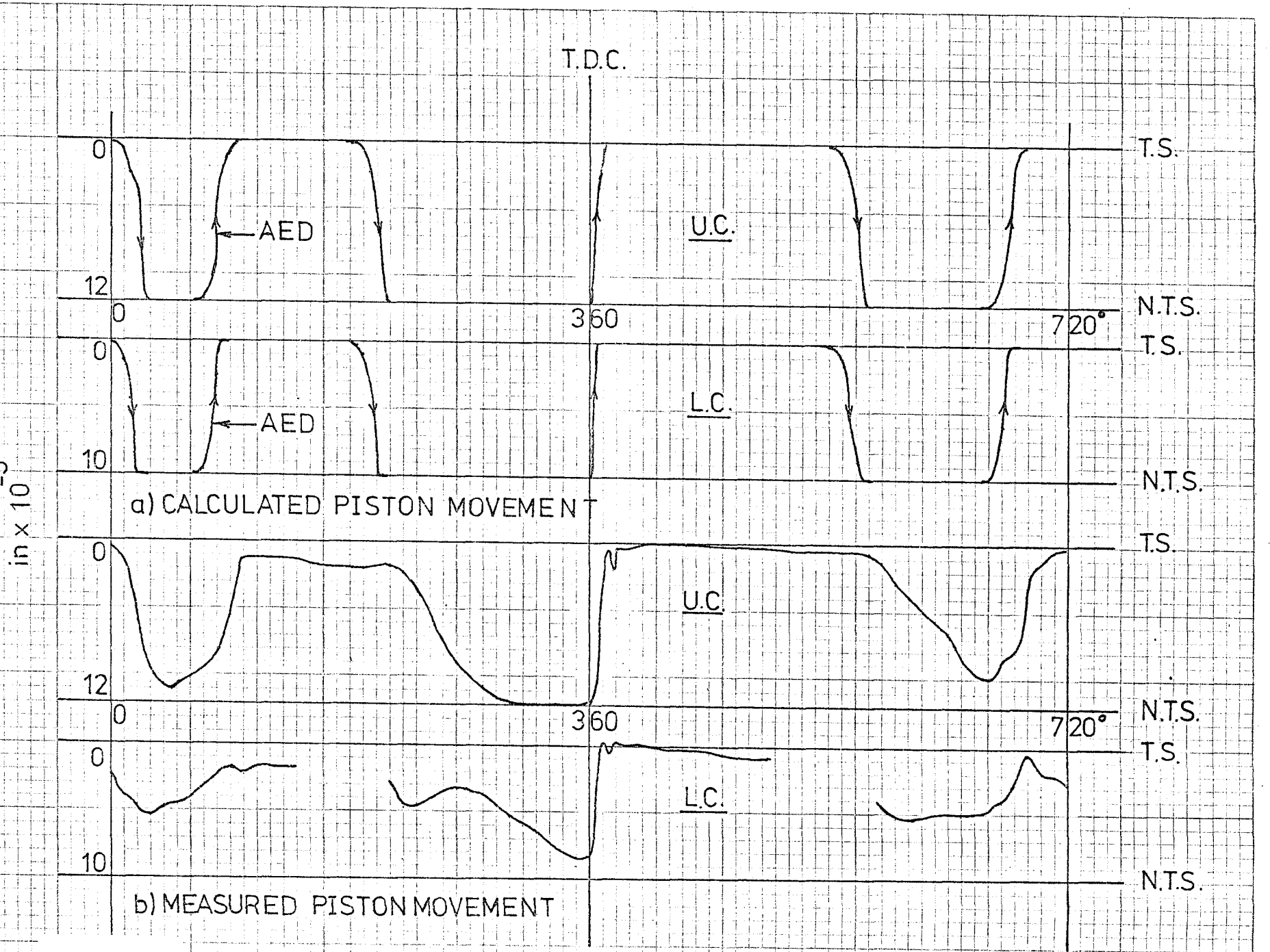

FIG. 7.35 COMPARISON OF CALCULATED AND MEASURED PISTON MOVEMENT PLOTS FOR ENGINE SA at 1000 RPM FULL LOAD

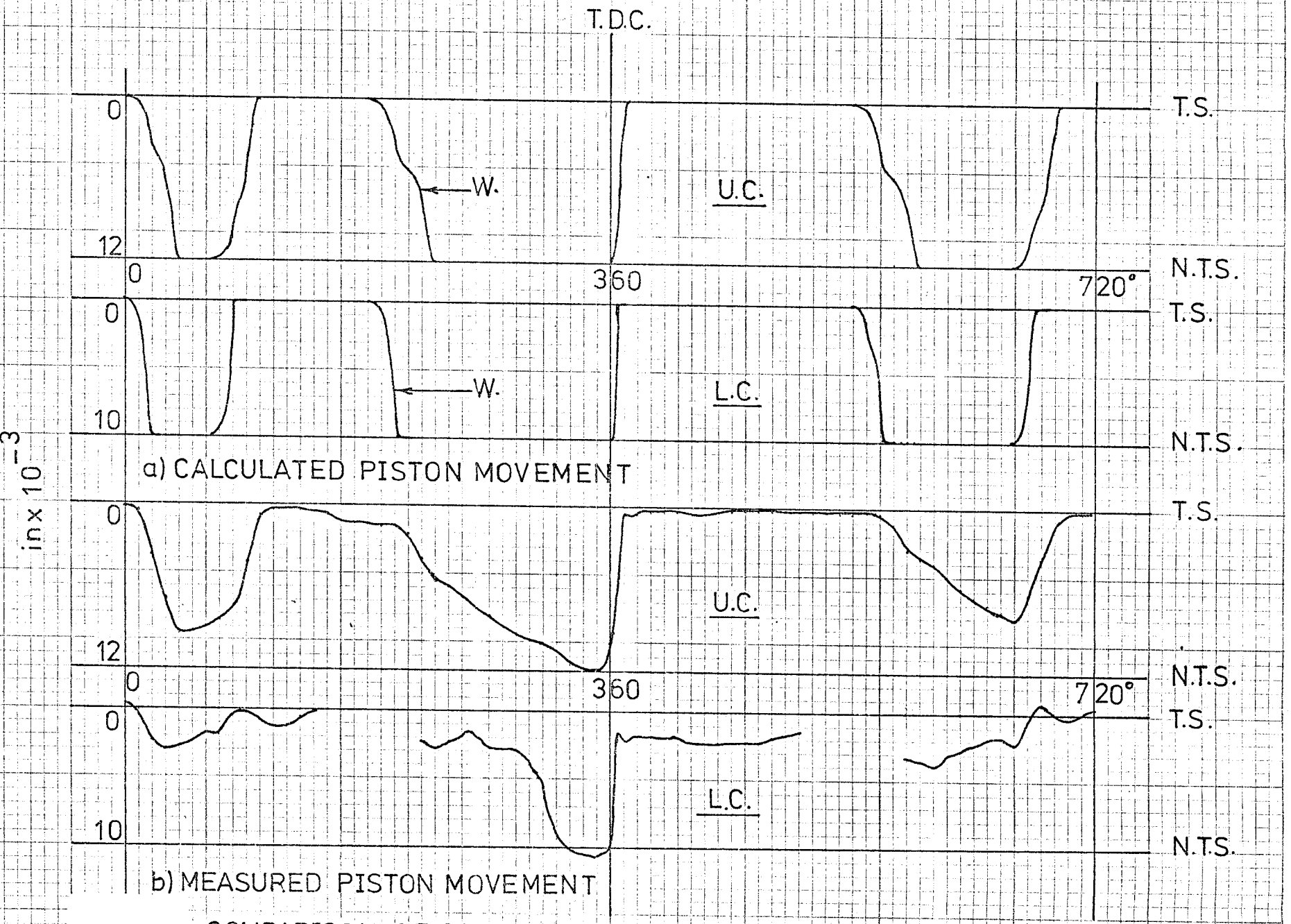

FIG. 7.36 COMPARISON OF CALCULATED AND MEASURED PISTON MOVEMENT PLOTS FOR ENGINE SA at 1500 RPM FULL LOAD

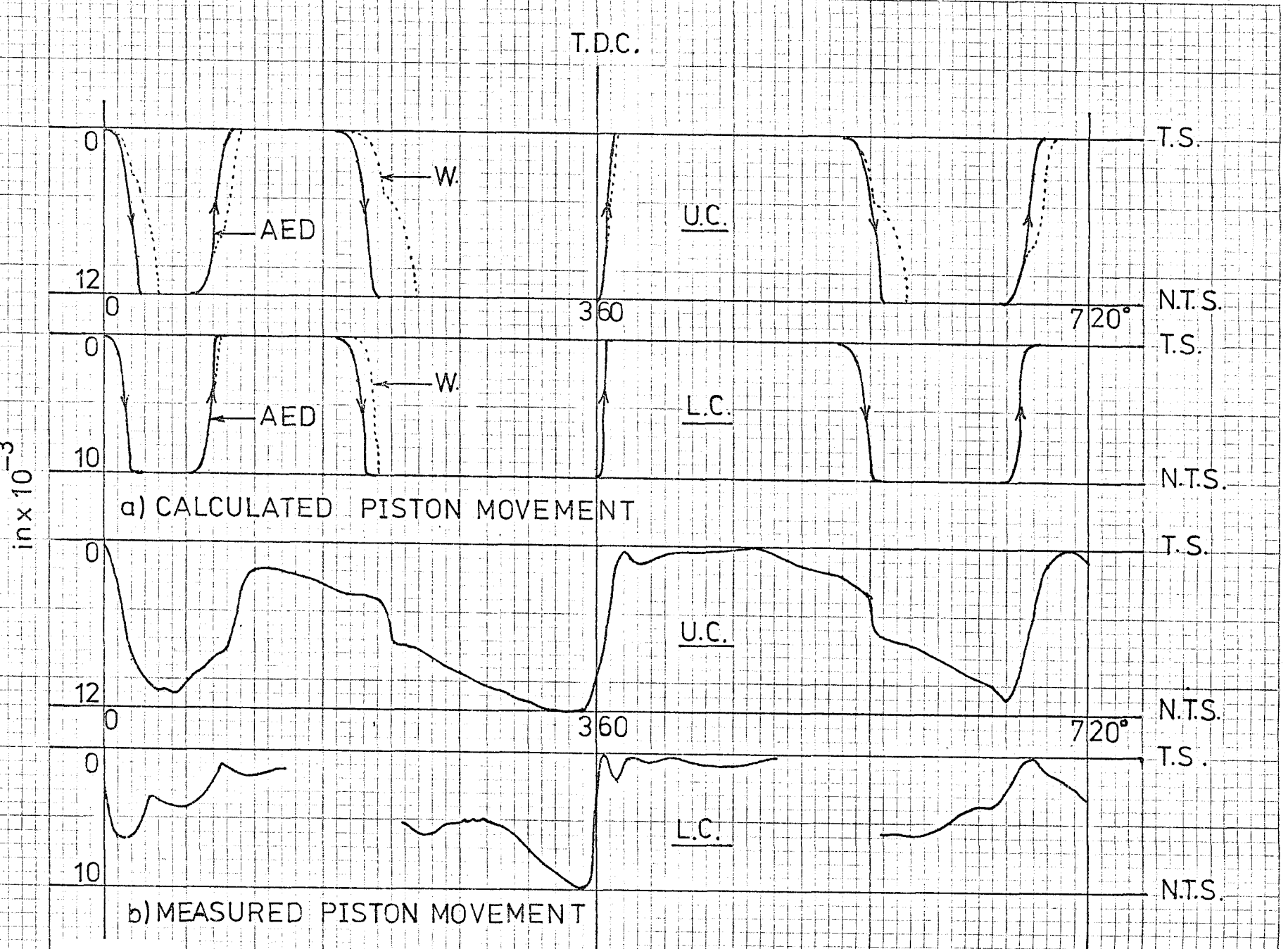

FIG. 7.37 COMPARISON OF CALCULATED AND MEASURED PISTON MOVEMENT PLOTS FOR ENGINE SA at 2000 RPM FULL LOAD

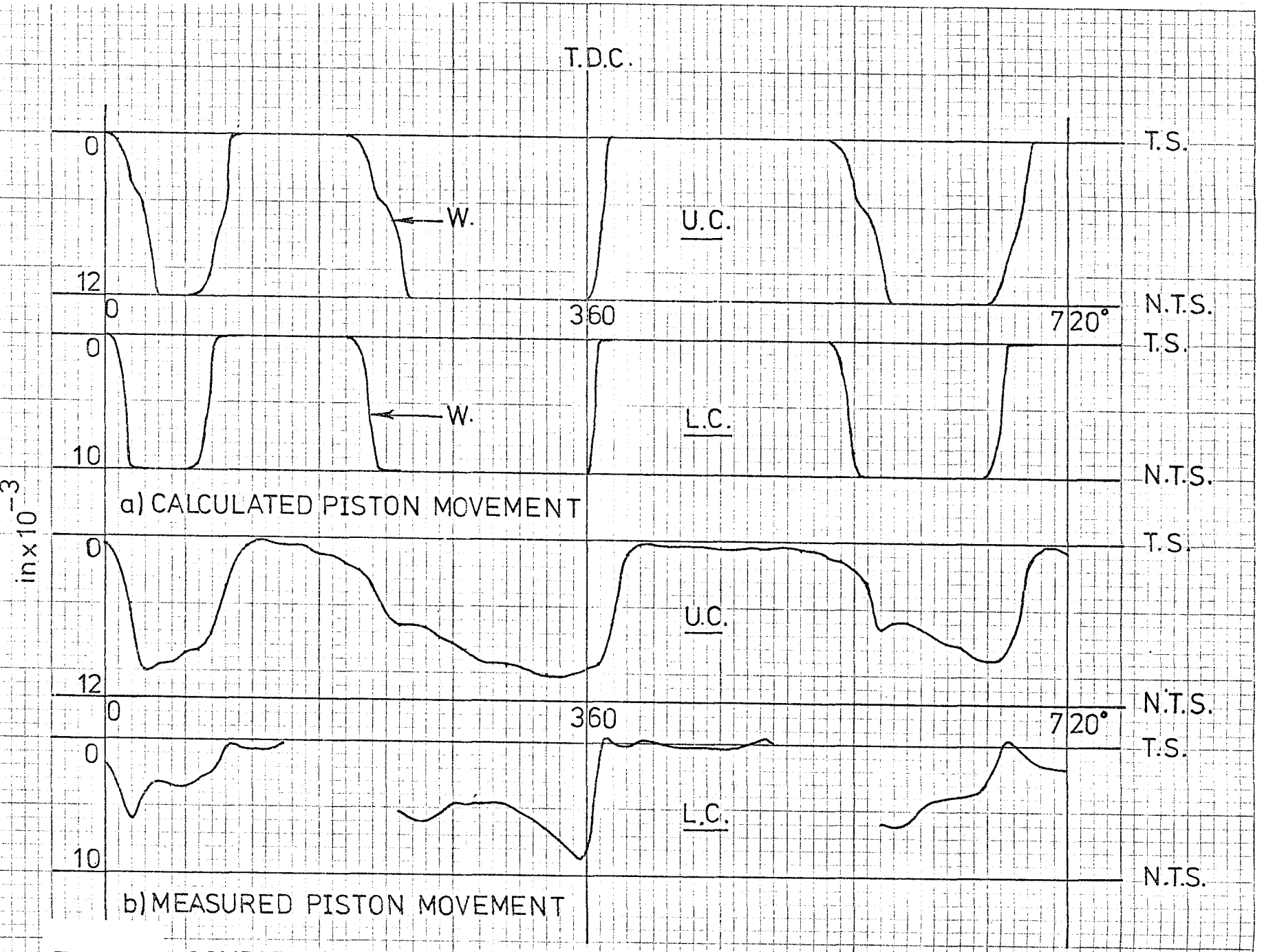

FIG. 7.38 COMPARISON OF CALCULATED AND MEASURED PISTON MOVEMENT PLOTS FOR ENGINE SA at 2500 RPM FULL LOAD

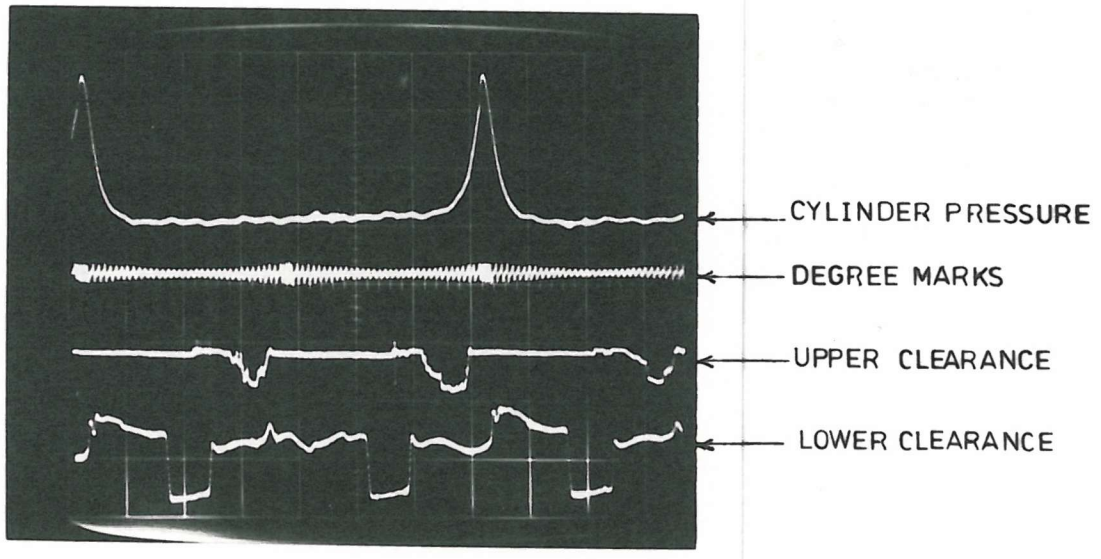

(a) TYPICAL PROXIMITY TRACES FOR THE RUNNING SA ENGINE (PISTON NO.1) AT 1000 RPM – PART LOAD

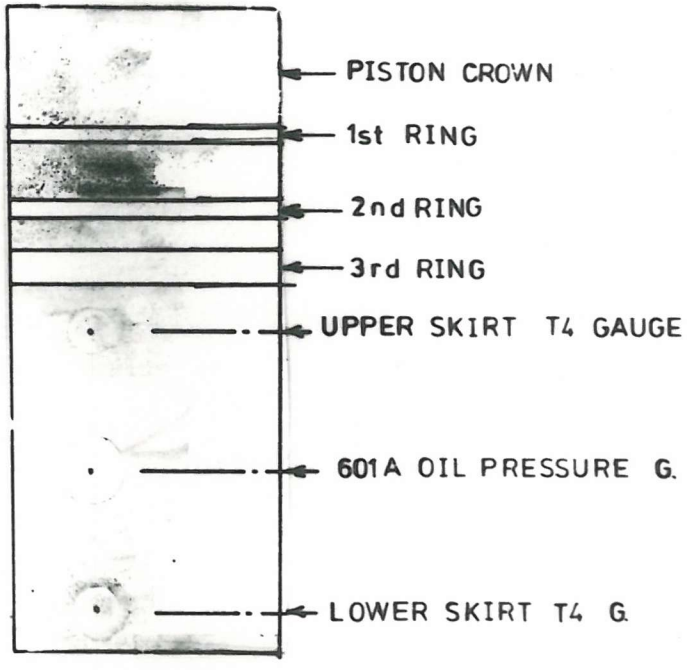

(b) LOCATION OF TRANSDUCERS IN PISTON SKIRT (THRUST SIDE) — full scale —

FIG. 7.39

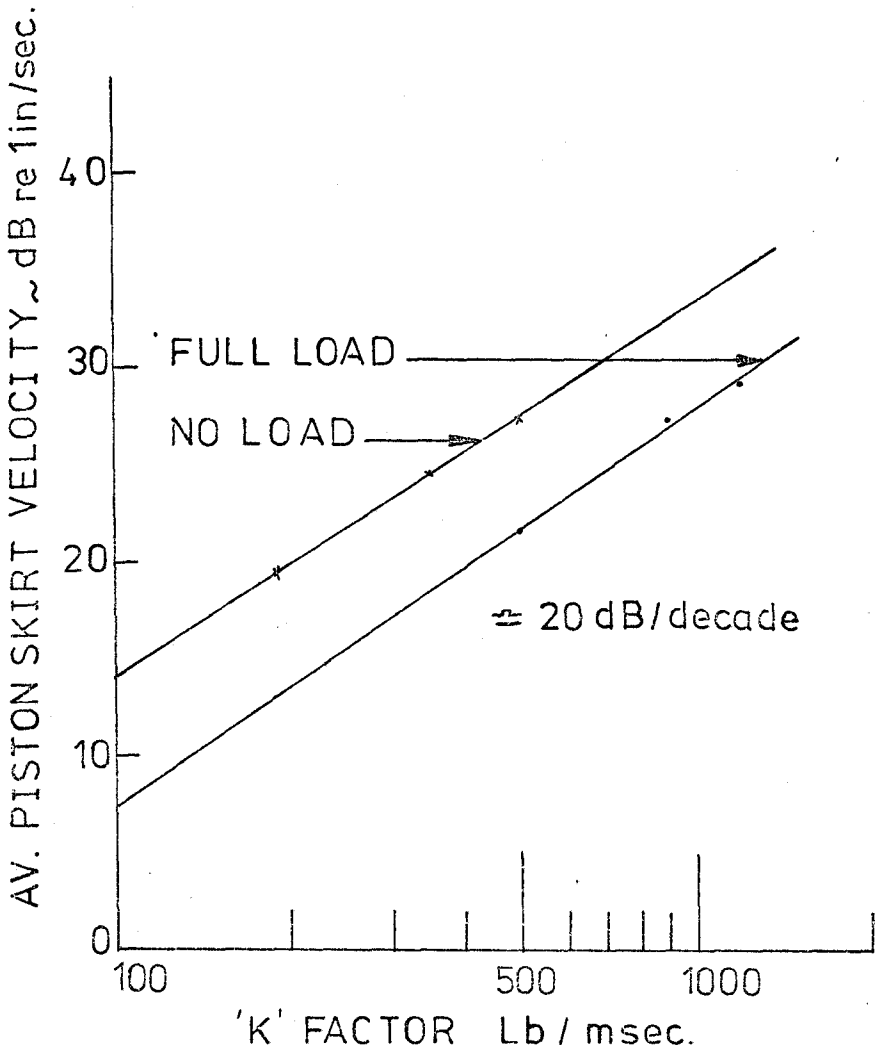

(a) RELATION BETWEEN AVERAGE PISTON IMPACT VELOCITY AND 'K' FACTOR — ENGINE SA

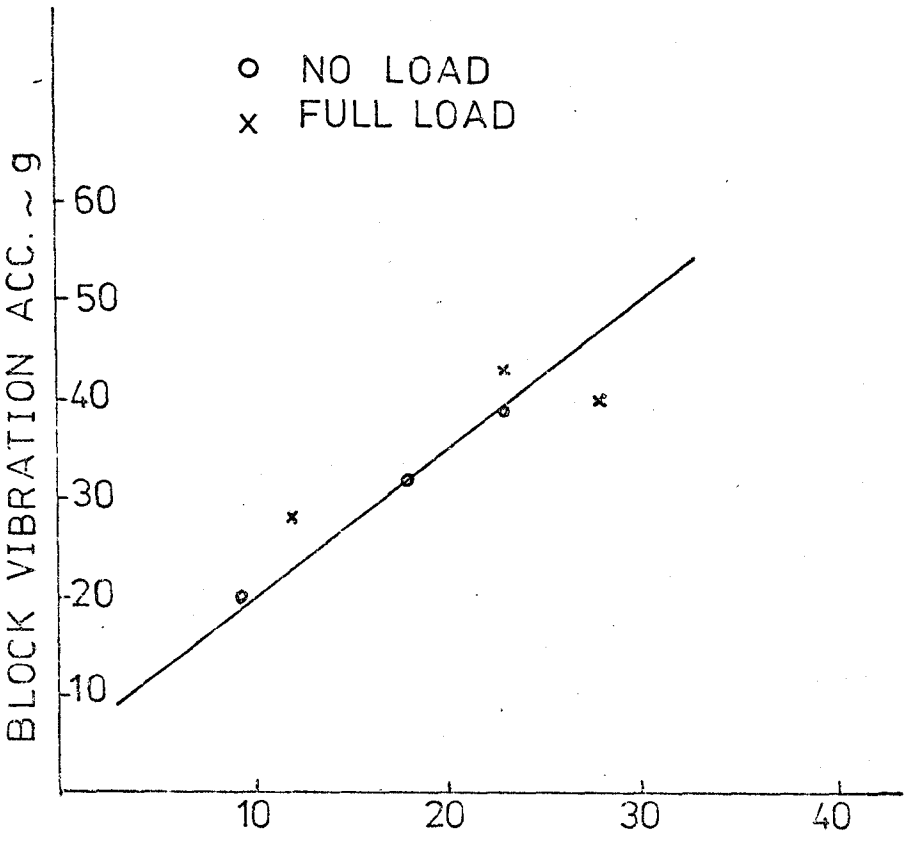

(b) TYPICAL RELATION BETWEEN PISTON IMPACT VELOCITIES AND RESULTANT ENGINE BLOCK VIBRATION - SA (G.P. Offset = 0)

FIG. 7.40

```
      LIST(LP)
      LIBRARY(SUBGROUPSRGP)
      LIBRARY(SUBGROUPS=RS)
      PROGRAM(V05D)
      INPUT 5=CRD
      OUTPUT 6=LPD
      COMPACT DATA
      TRACE
      END

      MASTER RCALC
      DIMENSION THETA(90),P(90),R(90),R1(90)
      DIMENSION TP(2),YT(1),XT(2)
      DATA TP(1)/12HPISTON  SLAP/
      DATA PN/4H940C/
      DATA YT(1)/8HFORCE/,XT(1)/11HCRANK ANGLE/
      REAL L,M,MM,MP,K2
      CALL LGP1(TP,1)
      CALL GRAPHNAME(PN)
      PI=3.14159626
      B=PI*PI/900.0/386.0
      READ (5,13) A,AA,BB,MM,M,MP,RR,L,K2
   13 FORMAT(9F0.0)
      DO 12 II=1,3
      READ(5,11) W
      READ (5,10) N
   10 FORMAT(I0)
      READ (5,11) (THETA(I),P(I),I=1,N)
   11 FORMAT(2F0.0)
      WRITE(6,21) RR,L,A
      GA=RR/L
      DO 3 I=1,N
      T=THETA(I)*PI/180.0
      S=SIN(T)
      R1(I)=P(I)*GA*S*A*(1.0+GA*GA*S*S/2.0+3.0*GA*GA*GA*GA*S*S*S*S/8.0)
      WRITE(6,20) THETA(I),P(I),R1(I)
    3 CONTINUE
   21 FORMAT('0PISTON SLAP FORCE=APPROX'//3F10.3//)
   20 FORMAT(1H ,3F10.3)
      WRITE(6,23)
   23 FORMAT('0PISTON SLAP FORCE=ACCURATE')
      DO 4 I=1,N
      T=THETA(I)*PI/180.0
      X=P(I)*A*SIN(T)*RR/L
      X=X+B*W*W*SIN(T)*((M+MP)*RR*RR/2.0+MM*(K2*AA+BB))/L/L
      X=X-B*W*W*RR*RR*SIN(2.0*T)*(M+MP)/2.0/L
      R(I)=X-B*SIN(3.0*T)*M*W*RR*RR*RR*(M+MP)/2.0/L/L
      WRITE(6,20) THETA(I),P(I),R(I)
    4 CONTINUE
      CALL LGP5A(0.0,720.0,-900.0,1500.0,12.0,8.0,XT,2,YT,1,1)
      CALL LGP6A(THETA,R,N,2,PI)
      CALL LGP6A(THETA,R1,N,2,PI)
   12 CONTINUE
      CALL LGP2
      STOP
      END
```

FIG. 7.41 ISVR COMPUTER PROGRAMME FOR CALCULATING AND PLOTTING ACCURATE AND APPROXIMATE PISTON SIDEWAYS FORCES FOR ENGINE SA

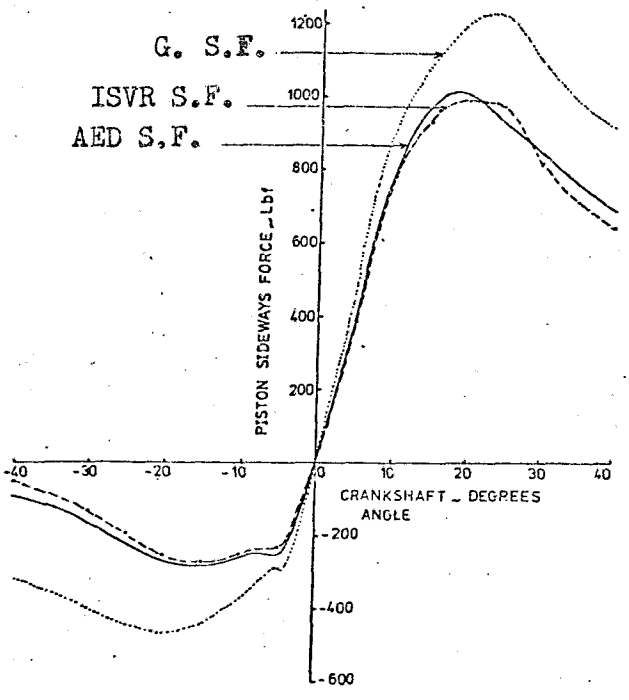

COMPARISON OF COMPUTED PISTON SIDE FORCES AROUND T.D.C. USING ISVR and AED PROGRAMMES AT 3000RPM FULL LOAD (ENGINE SA G.P. OFFSET = 0)

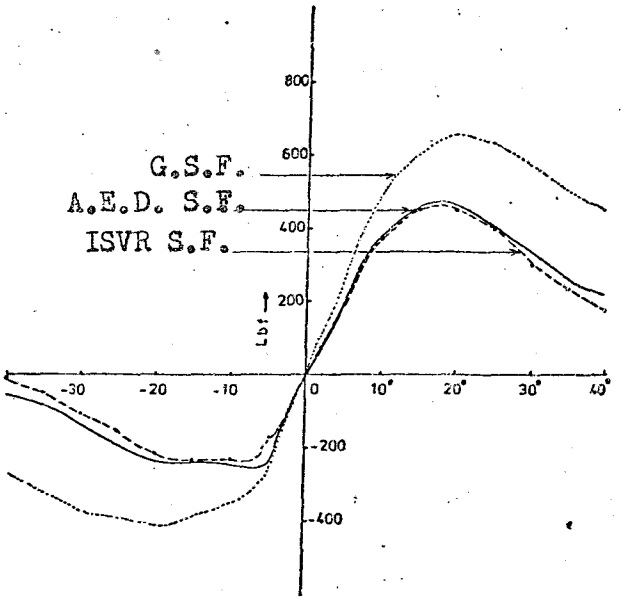

COMPARISON OF COMPUTE PISTON SIDE FORCES AROUND T.D.C. USING ISVR and AED PROGRAMMES AT 3000 RPM NO LOAD (ENGINE SA G.P. OFFSET = 0)

G. S.F. = PISTON SIDEWAYS FORCE DUE TO GAS FORCE ONLY

ISVR S.F. = SIDE FORCES DUE TO GAS FORCE AND INERTIA

AED S.F. = SIDE FORCES USING A.E.D. COMPUTER PROGRAMME

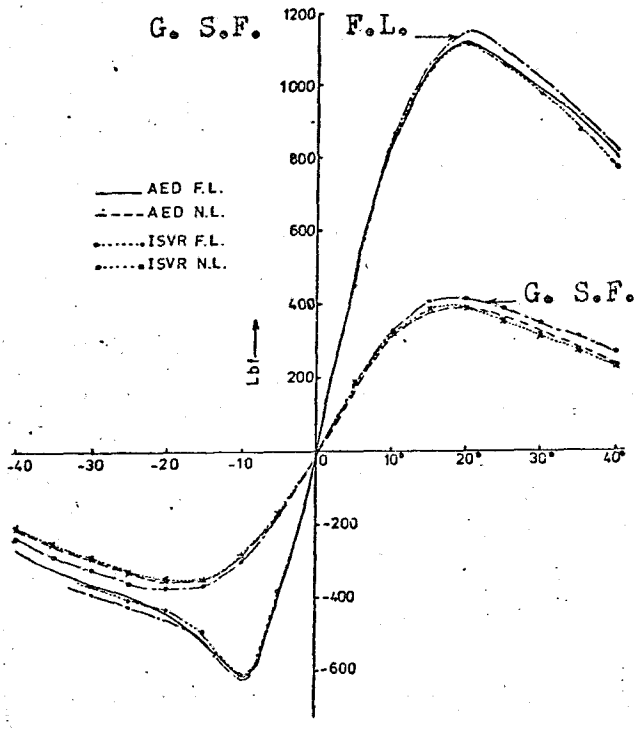

COMPARISON OF COMPUTED PISTON SIDE FORCES AROUND T.D.C. USING ISVR and AED PROGRAMMES AT 1000 RPM FULL AND NO LOAD (SA G.P.O. = 0)

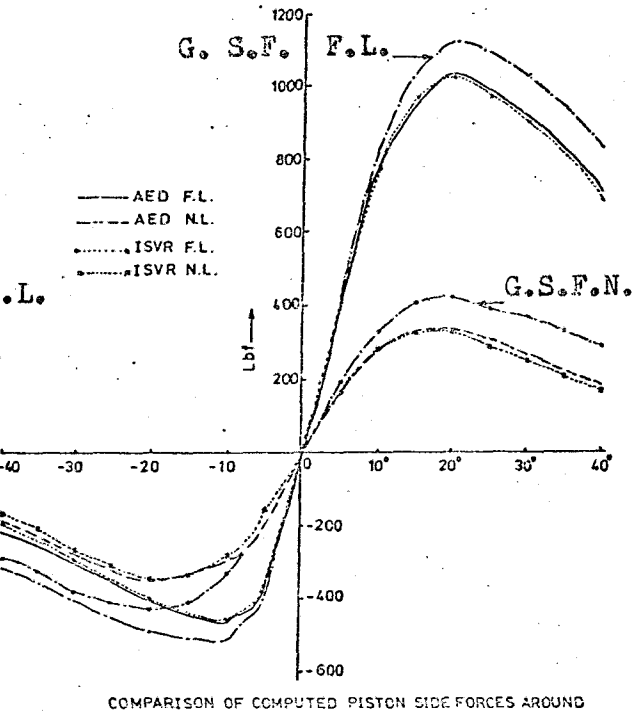

COMPARISON OF COMPUTED PISTON SIDE FORCES AROUND T.D.C. USING ISVR and AED PROGRAMMES AT 2000 RPM FULL AND NO LOAD (ENGINE SA G.P.O. = 0)

FIG. 7.42 CALCULATED PISTON SIDE FORCES (ENGINE SA)

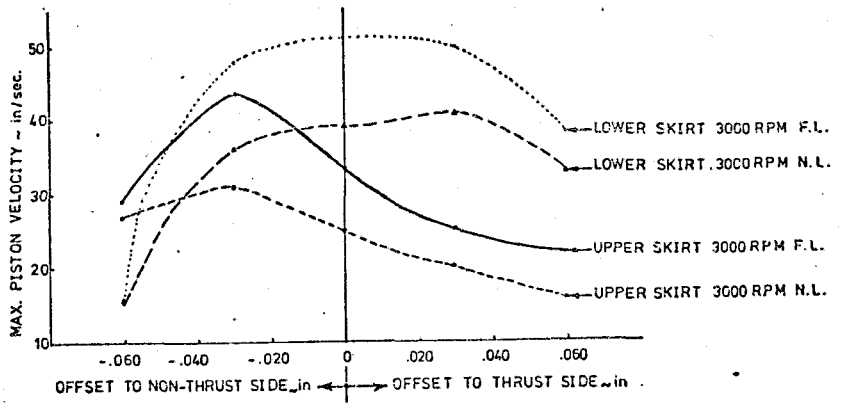

VARIATION OF MAXIMUM PISTON VELOCITY AROUND T.D.C. FIRING WITH GUDGEON PIN OFFSET — ENGINE SA

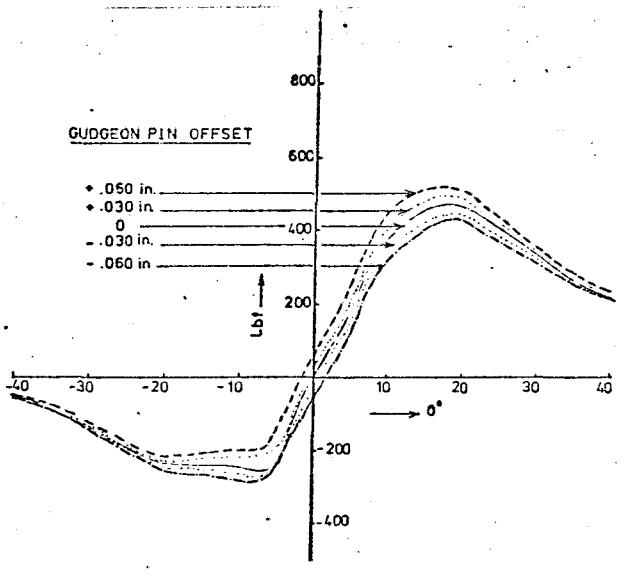

EFFECT OF GUDGEON PIN OFFSET ON PISTON SIDEWAYS FORCE AROUND T.D.C. AT 3000 RPM NO LOAD (ENGINE SA)

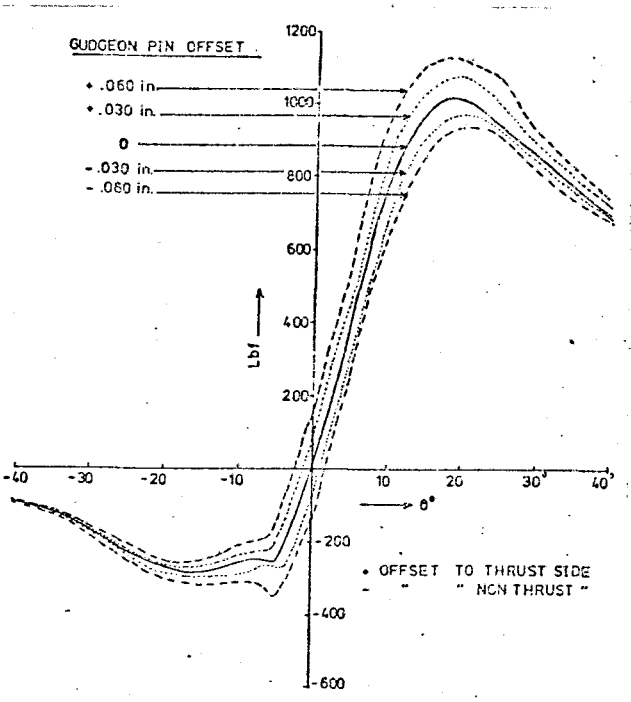

EFFECT OF GUDGEON PIN OFFSET ON PISTON SIDEWAYS FORCE AROUND T.D.C. AT 3000 FULL LOAD (ENGINE SA)

FIG. 7.43 EFFECT OF G.P. OFFSET

Chapter 8

GENERAL CONCLUSIONS

Many detailed conclusions have been drawn from the results of investigations presented in the foregoing chapters and these appear at the end of the relevant sections. The more important conclusions are summarised below:-

1. Piston slap excitation is, to a great extent, directly responsible for generating the bank to bank vibratory mode of Vee type engines. It is also indirectly responsible for the bulging or conical mode which is accentuated by piston-to-bore oil film pressure development.

2. Oscillographic techniques have proved to be an effective method in the identification of the relative magnitudes of the various sources of vibration on running engines.

3. The experimental piston slap rig simulation in a non-running engine has proved to be a useful method for the study of piston slap characteristics in isolation from other sources of vibration. It enables the effect of the controlling parameters to be ascertained. The rate of rise of piston sideways force (K) was found to be the most important parameter controlling piston slap induced cylinder block vibration.

4. Piston-to-bore oil film pressures measured in the running engine exhibit distinct regions of squeeze and hydrodynamic effects. The former being due to the application of piston sideways force and the latter due to the sliding movement of the piston in the bore. The sawtooth-like squeeze pressure due to the major slap after TDC is shown to be a significant source of excitation which can predominate over combustion excitation in the frequency range 1000 Hz upwards.

It is concluded that the effect of piston slap can be controlled by smoothing the impulsive piston to bore oil film pressure development. It is also suggested that the oil film forces can account for the differences in the calculated and measured piston movements.

APPENDIX A

Inertia Effect of the Back to Back Connecting Rods on the Vee Piston Slap Rig

1. Experimental method to show that the inertia effect of the back to back system is small for high forces:

Figure 1A shows the back to back system. Two studs were cemented at points C (on the con rod) and P (on the inner surface of the piston along centre line of gudgeon pin). Varying forces were applied and the corresponding vibration accelerations were measured at C and P.

If $\ddot{x}_c$ = vibration acceleration at C in g

$\ddot{x}_p$ = " " " P in g

and if the system has no inertia effect, then the angular acceleration about G should be equal, i.e.,

$$\frac{\ddot{x}_p}{\ell} = \frac{\ddot{x}_c}{\ell'} \qquad (1a)$$

where $\ell = 6"$ and $\ell' \simeq 2.7$ in.

Equation (1a) was applied to various conditions and was found to agree reasonably well especially for the application of higher forces.

2. Calculated inertia effect of the system

Neglecting resonances of the back to back system

$$F\ell = F'\ell + I\ddot{\theta} \qquad (2a)$$

where I = inertia of the back to back system about the bearing pivot,

F = force applied using shaker

F' = actual force applied by piston on the liner.

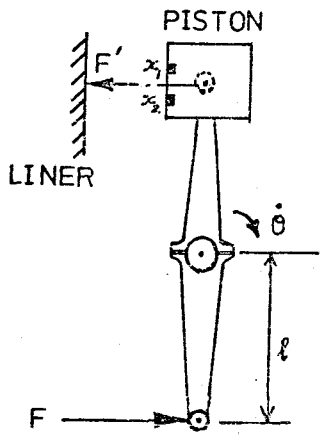

$$\therefore \quad \ell\ddot{\theta} = \frac{\ddot{x}_1 + \ddot{x}_2}{2} \qquad (3a)$$

where $\ddot{x}_1 = \frac{d^2x_1}{dt^2}$ and $\ddot{x}_2 = \frac{d^2x_2}{dt^2}$

x_1 = clearance at top of the skirt) measured using movement
) gauges installed in the
x_2 = clearance at bottom of the skirt) skirt.

Therefore, substituting (3a) in (2a)

$$F\ell = F'\ell + I\frac{\ddot{x}_1 + \ddot{x}_2}{2}$$

Therefore,

$$F' = F - \frac{I}{\ell^2}\left(\frac{\ddot{x}_1 + \ddot{x}_2}{2}\right) \qquad (4a)$$

i.e., the correction due to inertia is $\frac{I}{\ell^2}\left(\frac{\ddot{x}_1 + \ddot{x}_2}{2}\right)$.

This was calculated for few cases to determine the order of magnitude of this correction. Typical calculation is presented below for a case of applying a certain force ($\simeq \frac{1}{2}$ max) at a repetition rate of 50 Hz, where the effect of inertia should be highest.

Oscillographic pictures of the upper and lower piston movement traces were enlarged. As the proximity gauges are non-linear, calibration curves were previously obtained and used to draw the real piston movements. Figure 2A (x_1 and x_2) shows these compensated proximity plots for this particular case. By calculating the slopes, the velocity plots ($\dot{x}_1$ and $\dot{x}_2$) are obtained. Repeating the same process, the acceleration plots ($\ddot{x}_1$ and $\ddot{x}_2$) are obtained as in Figure 3A. Figure 4A shows the graphical addition to obtain $\ell\ddot{\theta}$ required in equation (3a) above.

Knowing $\ell\ddot{\theta}$ at any instant, the true F' can be calculated. As an example, calculate $\frac{I}{\ell^2}\ddot{x}$ for the maximum $\ell\ddot{\theta}$ from Figure 4A (where $\ddot{x} = \frac{\ddot{x}_1 + \ddot{x}_2}{2}$).

Mass of piston and two con rods = 11.94 lb

k^2 for the back to back system about crankshaft ≃ 17.94 in^2

Therefore, $I = 11.94 \times 17.94 = 214.2$ lb in^2

$\ell = 6$ in. Therefore, $\ell^2 = 36$ in^2

max. $\ell\ddot{\theta} \simeq 80$ in/sec^2 (from Figure 4A)

Therefore, $$\frac{I}{\ell^2}\ddot{x} = \frac{214.2}{36} \times 80 \times \frac{1}{386} \simeq \underline{1.25 \text{ lbf}}.$$

Remembering that the forces applied are in the order of 500-1000 lbf, it can be seen that this calculated correction is practically negligible.

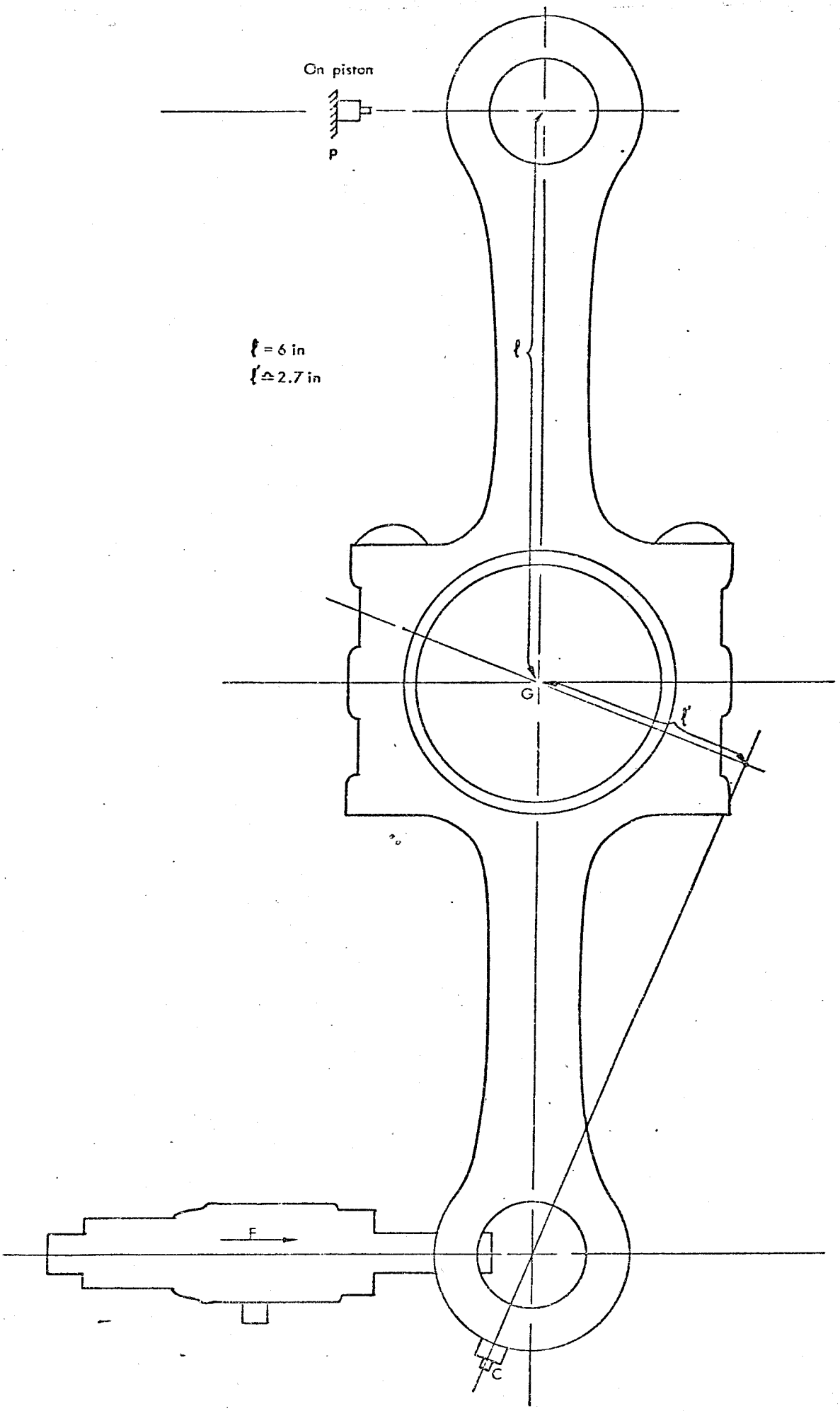

FIG 1A BACK TO BACK CONNECTING ROD SYSTEM

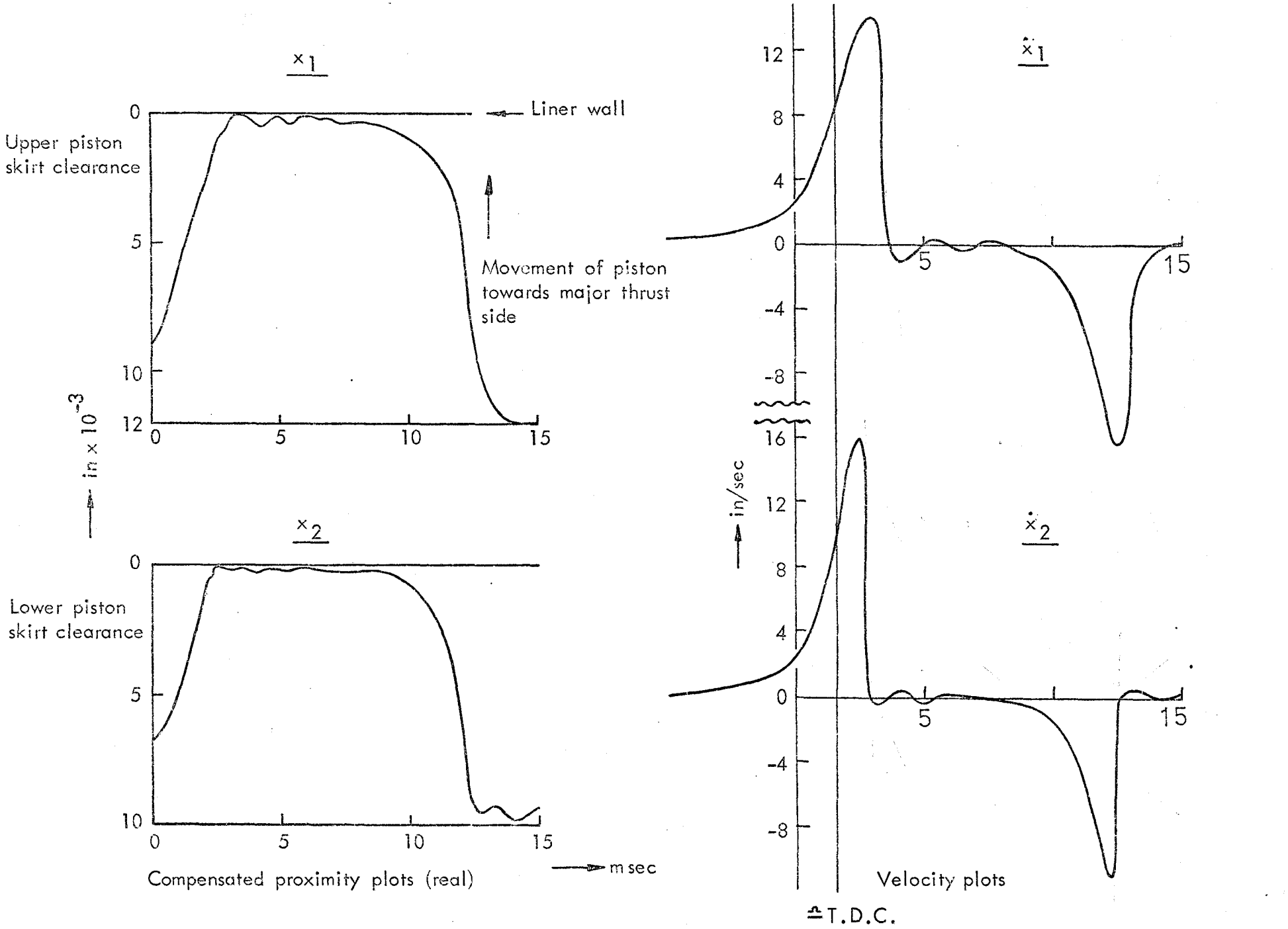

FIG 2A PROXIMITY AND VELOCITY PLOTS OF THE PISTON DUE TO A CERTAIN FORCE AT 50 Hz ≡ 3000 RPM (DRY CASE)

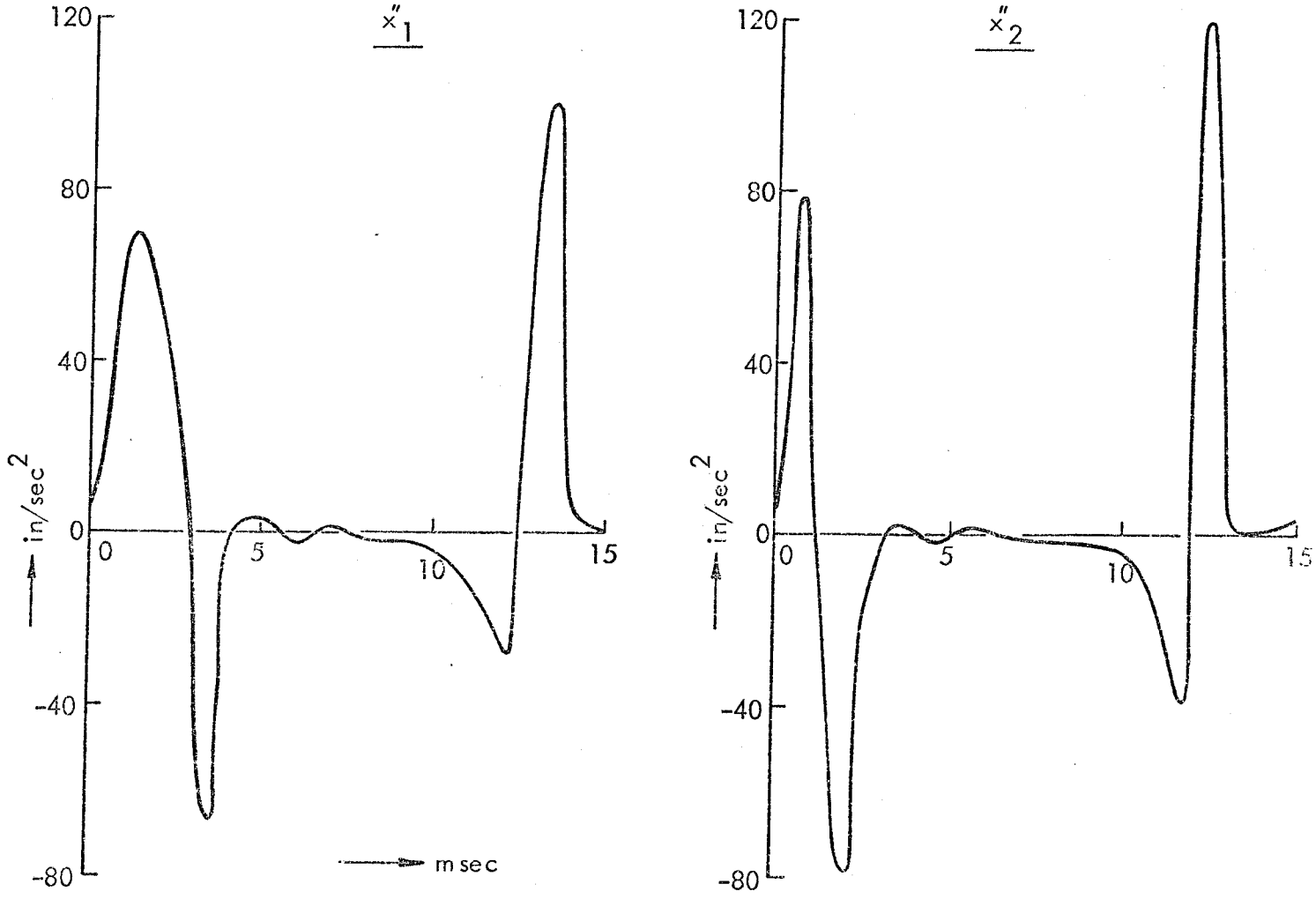

FIG 3A PISTON ACCELERATION PLOTS DERIVED FROM THE PLOTS IN 2A DUE TO A CERTAIN FORCE AT 50 Hz ≡ 3000 RPM (DRY CASE)

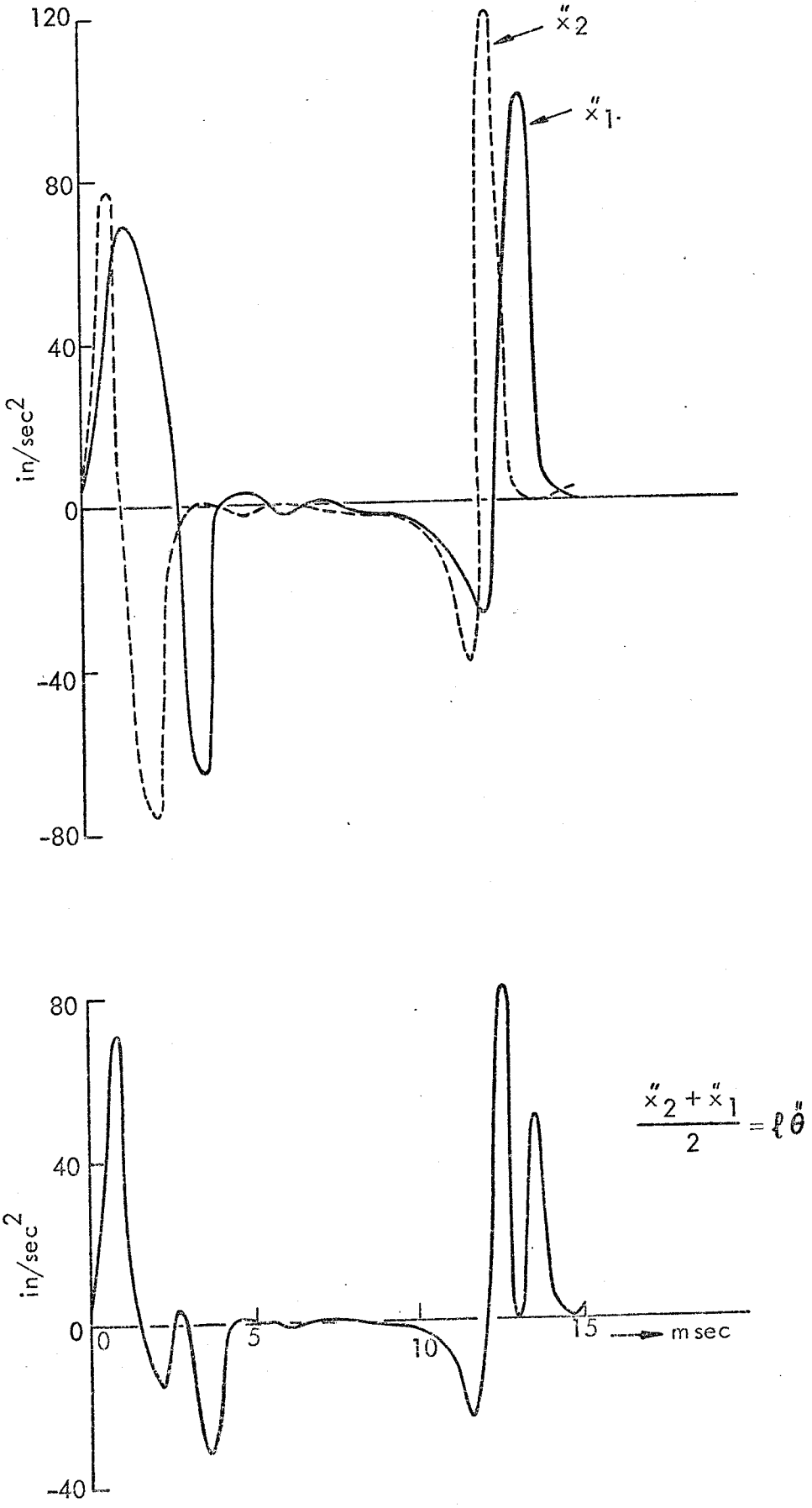

FIG 4A GRAPHICAL DERIVATION OF $\ell\ddot{\theta}$ FROM PLOTS OF 3A DUE TO A CERTAIN FORCE AT 50 Hz ≡ 3000 RPM .

APPENDIX B

A computer programme was written using equation (5.1) to calculate the piston sideways force for any running engine condition. The following table (1B) presents the maximum forces and rates of rise of forces around T.D.C. for the stated conditions.

TABLE 1B

Engine Speed rpm	Full Load		No Load	
	Max. Force x_{peak} lbf.	Rate of force rise: K lbf/msec	Max. Force x_{peak} lbf.	Rate of force rise: K lbf/msec
1000	1055	510	370	190
1500	1010	700	340	290
2000	970	900	320	350
2500	-	-	-	-
3000	920	1200	390	500
3300	-	-	-	-

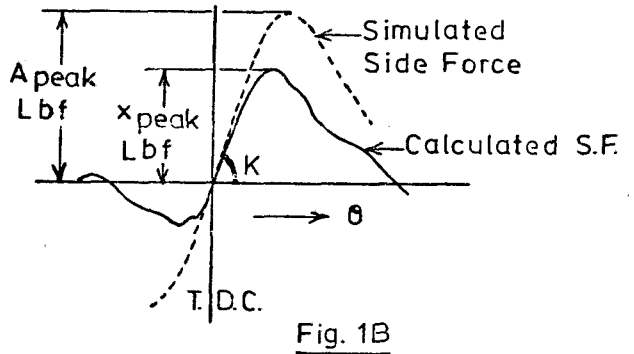

Fig. 1B

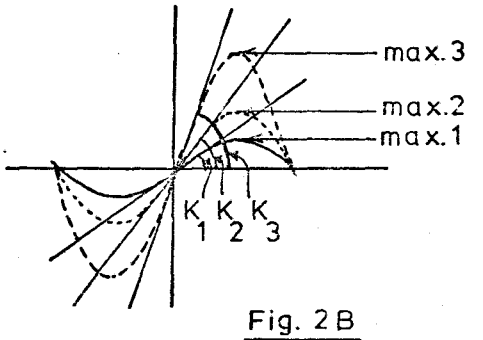

Fig. 2B

Figure 1B shows the general shape of the piston sideways force. To approximate this force to a sinusoidal shape as shown, then the peak force of this new waveform will be higher in order to keep the original rates of rise (K) which was found experimentally to be the most important parameter in deciding the response. That is, if S.F. = A sin ωt (1b)

$$\frac{d\ SF}{dt} = A\omega \cos \omega t = A_{peak}.\omega \quad @ \quad \theta \simeq 0 \qquad (2b)$$

Therefore,

$$A_{peak} = \left| \frac{d\ SF}{dt} \right|_{\theta=0} /\omega = K/\omega \qquad (3b)$$

where ω = engine speed in rad/sec.

K = rate of rise of piston sideways force in lbf/sec.

Using equation (3b) the following table (2B) is prepared showing this effect.

TABLE 2B

Engine Speed rpm	Repetition Rate c/s	Full Load x_{peak} lbf	Full Load A_{peak} lbf	No Load x_{peak} lbf	No Load A_{peak} lbf
1000	16.7	1055	4900	370	1830
1500	25	1010	4600	340	1720
2000	33.3	970	4300	320	1670
2500	41.7	-	-	-	-
3000	50	920	3820	390	1600
3300	55	-	-	-	-

APPENDIX C

Spectral Analysis of the Piston Slap Pulses for the Running Engine to Compare with Simulated Response

This exercise was conducted using the excellent facilities available at the Data Analysis Centre "Myriad Computer" of I.S.V.R. Vibration acceleration response at the top of the running engine block was recorded using a Nagra III one track tape recorder. The recordings were played back and plotted as shown in Figure 1C (top trace A). The time scale could be adjusted to enable clear identification of the piston slap pulses. The computer is then instructed to select each of these piston slap response pulses individually to be displayed on an expanded time scale as shown in Figure 1C (traces B and C). These pulses are then analysed and their total response presented.

The following programme was used to conduct this analysis:

```
/ACQUIRE ("A", 2000, 20000, 1)
/PLOT ("A", 20, 4, *0, # 0120)
 DO  2 K ← 1, 6
/INUM (I, J)
/KILL ("B", "C", "D")
/CONV ("A", "B", 2, I, J)
/PLOT ("B", 10, 5, *0, # 0120)
/FFTA ("B", "C")
/MOD PHASE ("C", "D", 2)
/F (K-1) 0, 0, 3
/CONV ("D", "E", 4)
GO TO 2
3 /ARITH ("E", "E", 4, "D")
2 CONTINUE
/PLOT ("F", 20, 20, *1, # 3120)
END
```

Figure 2C shows the narrow band vibration acceleration at $C\ell_3$ due to the six slapping pulses shown in Figure 1C (trace A) for the engine running at 2000 rpm full load.

Figure 3C shows the simulated 1/3 octave vibration acceleration response at $C\ell_3$ obtained on the V8 piston slap rig and corresponding to the running engine condition of 2000 rpm full load. This figure has been carried forward from Figure 5.25 to the same scale of Figure 2C for comparison purposes. Superimposing Figure 2C on Figure 3C shows the very close agreement in the two spectra. This also provides extra confidence in the validity of the simulation although it must be remembered that the piston slap pulses analysed for the running engine case may contain low levels of other mechanical sources.

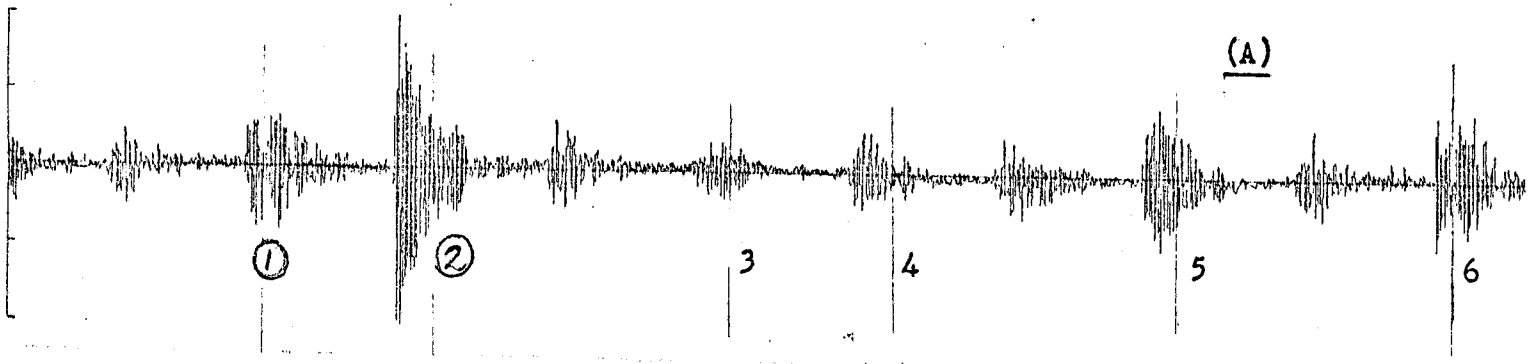

9 .10 .1972 NO 1
VVBOA X Y
ORIGIN 0.0000E00 0.0000E00
X SCALE 4.3987E00 MSECS /CM
Y SCALE 8.3253E-01 VOLT /CM
R VS Z

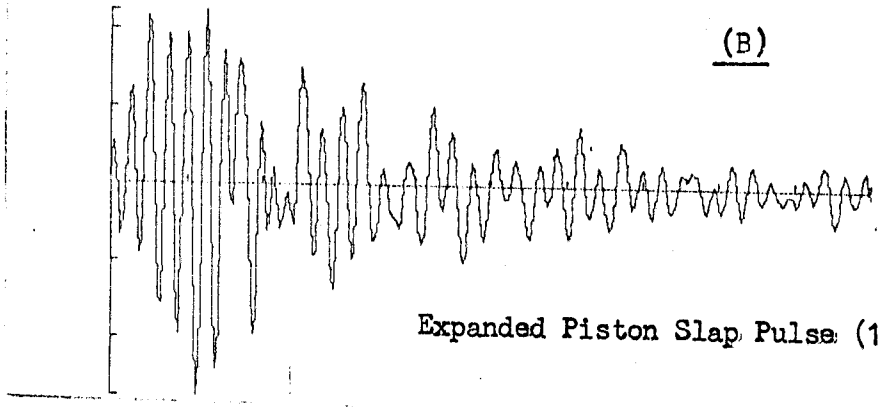

Expanded Piston Slap Pulse (1)

9 .10 .1972 NO 1
VVBOB
ORIGIN 1.7000E01 0.0000E00
X SCALE 7.9750E-01 MSECS /CM
Y SCALE 2.4316E-01 VOLT /CM
R VS Z

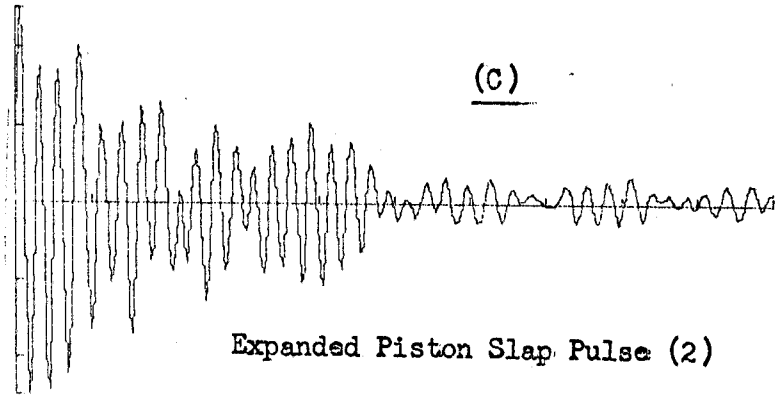

Expanded Piston Slap Pulse (2)

9 .10 .1972 NO 1
VVBOB
ORIGIN 2.6500E01 0.0000E00
X SCALE 7.9750E-01 MSECS /CM
Y SCALE 4.4141E-01 VOLT /CM
R VS Z

FIG. 1C Typical Vibration Osillographs at Cl_3 for the Running V8-470 Diesel Engine as Plotted through the D.A.C. of ISVR

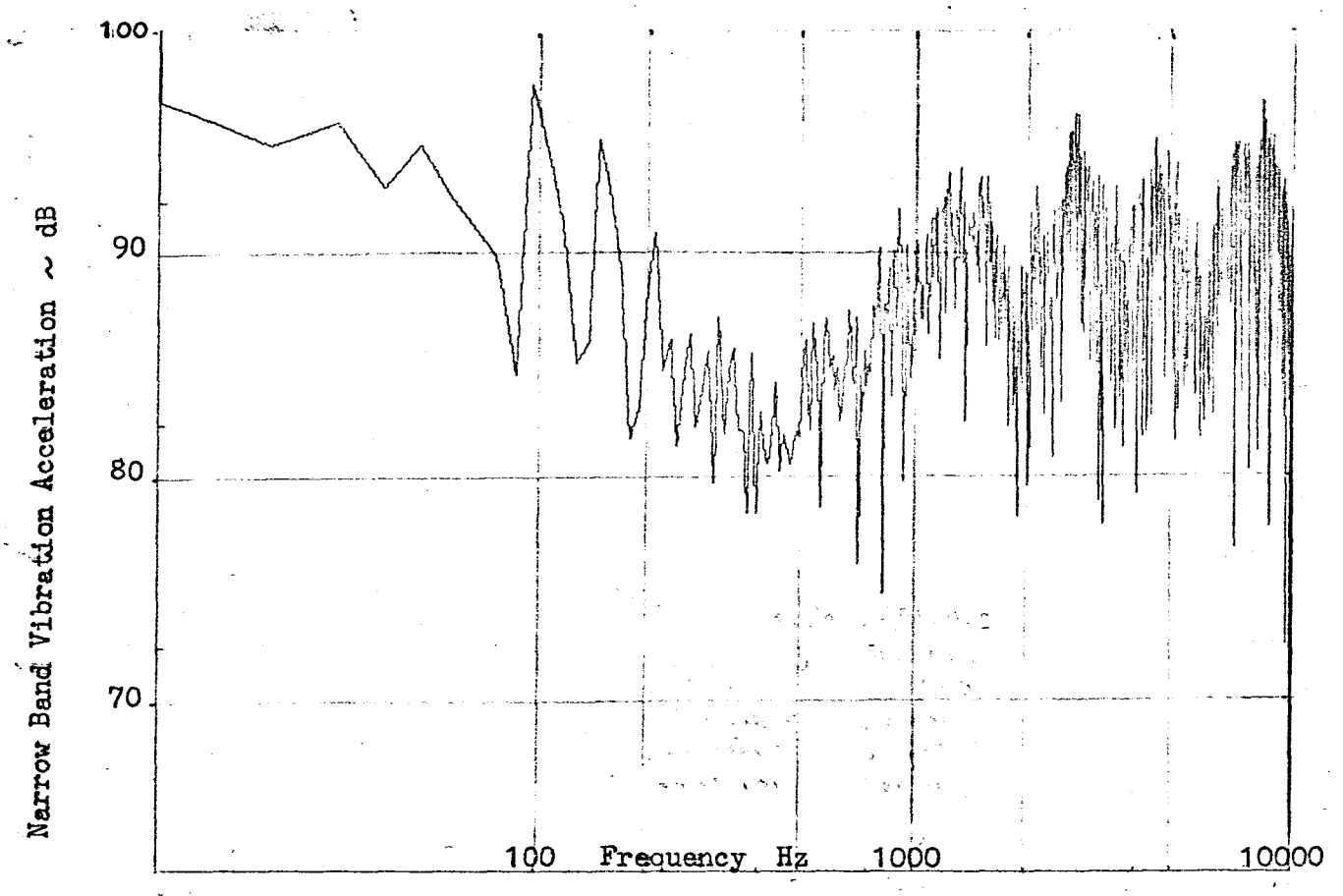

FIG. 2C Vibration Acceleration Response at Cl_3 due to Slapping Pulses in a running V8-470 Diesel Engine at 2000 r.p.m. Full Load.

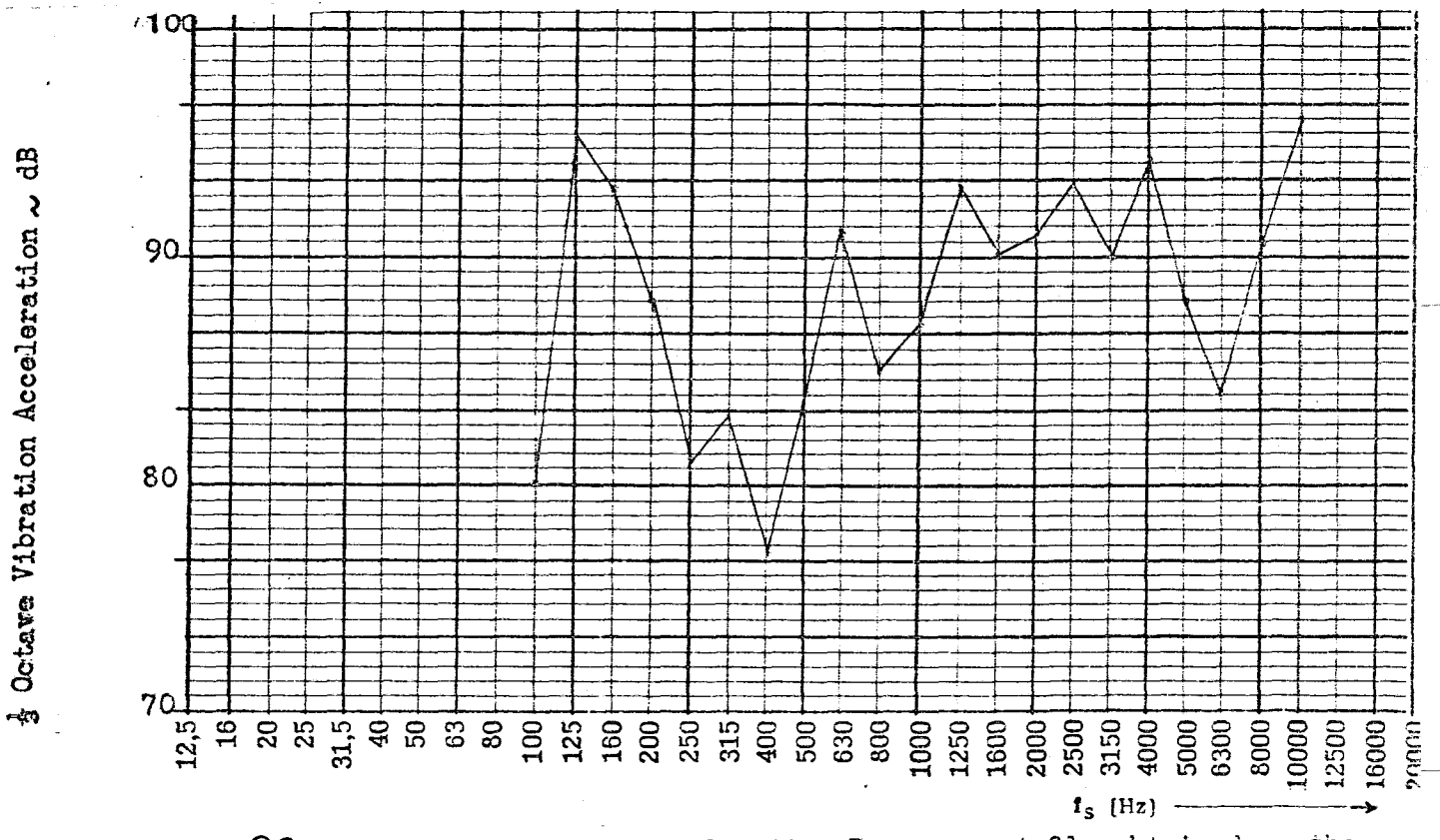

FIG. 3C Simulated Vibration Acceleration Response at Cl_3 obtained on the V8-470 Piston Slap Rig at 2000 r.p.m. ≡ 33.3 Hz for Full Load

(c.f.)

APPENDIX D

Natural Frequencies of Diesel Engine Cylinder Liners

The liner characteristics bear a great deal of importance in relation to piston slap and engine vibration response. Therefore the following theoretical analysis has been conducted to calculate the natural frequencies of engine cylinder liners.

The liner is treated as a thin walled cylinder enabling the application of the general Flügge's equations (ref. D.1).

In the present analysis the general Flügge's equations are further simplified to apply to the case of freely supported thin cylinders. Using the concept of the equivalent wavelength factor, equations for other conditions of support are derived (ref. D.2).

For the case of hinged-hinged ends the following expressions for displacement were assumed for the component directions, X, Y and Z (Figure 1Da).

$$u = A \cos \frac{m\pi x}{\ell} \cos n\phi \cos \omega t$$

$$v = B \sin \frac{m\pi x}{\ell} \sin n\phi \cos \omega t \qquad (1d)$$

$$w = C \sin \frac{m\pi x}{\ell} \cos n\phi \cos \omega t$$

where A, B and C = amplitude constants

m = number of axial half waves (in direction X)

m+1 = number of axial nodes

n = number of circumferential waves (in direction ϕ)

2n = number of circumferential nodes

ℓ = length of cylinder

$\omega/2\pi$ = the frequency of vibration

It is found that equations (1d) satisfy the end conditions and are compatible with the strain relations. By application of the Lagrange equation to the derived expressions for strain energy and kinetic energy, constants A, B and C may be eliminated to form the following cubic equation:

$$\Delta^3 - K_2\Delta^2 + K_1\Delta - K_o = 0 \tag{2d}$$

where
$$\left.\begin{aligned} K_o &= \tfrac{1}{2}(1-\sigma)^2(1+\sigma)\lambda^4 + \tfrac{1}{2}(1-\sigma)\beta\left|(\lambda^2+n^2)^4 - 2(4-\sigma^2)\lambda^4n^2\right. \\ &\qquad \left. - 8\lambda^2n^4 - 2n^6 + 4(1-\sigma^2)\lambda^4 + 4\lambda^2n^2 + n^4\right| \\ K_1 &= \tfrac{1}{2}(1-\sigma)(\lambda^2+n^2)^2 + \tfrac{1}{2}(3-\sigma-2\sigma^2)^2 + \tfrac{1}{2}(1-\sigma)n^2 \\ &\quad + \beta\left|\tfrac{1}{2}(3-\sigma)(\lambda^2+n^2)^3 + 2(1-\sigma)\lambda^4 - (2-\sigma^2)\lambda^2n^2\right. \\ &\quad \left. - \tfrac{1}{2}(3+\sigma)n^4 + 2(1-\sigma)\lambda^2 + n^2\right| \\ K_2 &= 1 + \tfrac{1}{2}(3-\sigma)(\lambda^2+n^2) + \beta\left|(\lambda^2+n^2)^2 + 2(1-\sigma)\lambda^2 + n^2\right| \end{aligned}\right\} \tag{3d}$$

$$f = \frac{1}{2\pi a}\sqrt{\frac{E\Delta g}{\rho(1-\sigma^2)}}, \qquad \beta = \frac{h^2}{12a^2} \tag{4d}$$

where K_o, K_1 and K_2 are constants for a given cylinder under a given nodal configuration.

f = the vibration frequency

σ = Poisson's ratio

a = mean radius of cylinder (inches)

E = Young's modulus

ρ = density of cylinder material

π = 3.141596

g = 386 in/sec^2

h = thickness of cylinder (inches)

λ = wavelength factor

As some terms in the equations (3d) are small compared with others and,

moreover, Δ^3 and $K_2\Delta^2$ are small compared with the other terms of the cubic equation (2d), the following linear equation is found to give good approximations.

$$\Delta = \frac{K_o}{K_1} + \frac{K_2}{K_1}\left(\frac{K_o}{K_1}\right)^2, \tag{5d}$$

where

$$K_o = \tfrac{1}{2}(1-\sigma)^2(1+\sigma)\lambda^4 + \tfrac{1}{2}(1-\sigma)\beta\left|(\lambda^2+n^2)^4 - 8\lambda^2n^4 - 2n^6 + n^4\right|$$

$$K_1 = \tfrac{1}{2}(1-\sigma)(\lambda^2+n^2)^2 + \tfrac{1}{2}(3-\sigma-2\sigma^2)\lambda^2 + \tfrac{1}{2}(1-\sigma)n^2 + \tfrac{1}{2}(3-\sigma)\beta(\lambda^2+n^2)^3 \tag{6d}$$

and $$K_2 = 1 + \tfrac{1}{2}(3-\sigma)(\lambda^2+n^2)$$

Therefore the final equations used for computing the natural frequencies of the freely supported cylinder are (4d), (5d) and (6d). However, in actual engines, the cylinder liners are either cantilevered (wet liners) or fixed-fixed (dry liners). Therefore these equations are progressed to deal with these two specific cases. For this the concept of equivalent wavelength factor is used as follows:

Equivalent Wavelength Factor = λ_e

This concept was established through theoretical-experimental approach by Warburton (ref. D.2). As explained diagrammatically in Figure 2D, λ_e refers to a fictitious non-dimensional quantity for a freely supported cylinder, which happens to have, under the same nodal arrangement, a frequency equal to that of the fixed-fixed (or cantilevered) cylinder under consideration.

In brief, Warburton's results are

$$\text{Theoretically} \quad \lambda_e = (m + c)\frac{\pi a}{\ell} \tag{7d}$$

and

$$\text{Experimentally} \quad \lambda_e = (m + 0.3)\frac{\pi a}{\ell} \quad \text{for the fixed-fixed} \tag{8d}$$

where he obtained $C \simeq 0.3$ for the fixed-fixed case. But c was not obtained

for the cantilevered case. In the present analysis, and instead of obtaining an experimental c value for the cantilevered case, another approach was followed. It was found that another way of determining an equivalent wavelength factor would be to use the numbers associated with the successive roots of the frequency equation for uniform beams with appropriate end conditions - ref. D.3.

Fixed-fixed

Considering firstly the case of both ends fixed (Figure 3D-1) the roots are 4.733, 7.855, 11.000, etc. These numbers would have to replace the terms $(m + c)\pi$ in equation (7d) above and would lead to an approximate equivalent wavelength factor, given by:

$$\lambda_{e_{(\text{fixed-fixed})}} = \pi a(m + 0.5)/\ell \qquad (9d)$$

This would give slightly higher natural frequencies than the original wavelength factor obtained in equation (8d) but was found to give better results (ref. D.3) and relatively small errors.

Fixed-free

Considering now a cantilevered case the corresponding numbers are: 1.876, 4.733, 7.855, etc., for the modes m = 1, 2, 3, etc. (Figure 3D-2).

This could be approximated as follows:

$$\lambda_{e_{\text{cantilevered}}} = \pi a(m + 0.5)/\ell \qquad \text{for } m > 1$$

and

$$\lambda_{e_{\text{cantilevered}}} = 1.876a/\ell \qquad \text{for } m = 1 \qquad (10d)$$

Validity of this method

1. If this method of the roots of the frequency equations is applied to cylindrical shells with hinged-hinged ends then the correct answers are obtained.

2. Some calculations of natural frequencies of thin cantilever cylindrical shells were determined, directly from a solution of Flügge's equations for the range of values of interest in our problem (ref. D.4) and shown to be close to those obtained using the approximations of λ_e in equations (10d).

Computer Programmes for Calculating Natural Frequencies of Liners

Having established that the above approximate equations are good for the particular dimensions associated with the problem, they were then used to write computer programmes to execute the calculation.

Figure 4D shows a sample computer programme using equations (4d), (5d), (6d) and (8d) to calculate the natural frequencies of Dry liners (fixed-fixed). Another programme using equation (9d) instead of (8d) for these calculations shows small difference which provides confidence in the roots technique compared with the Warburton's experimental method.

Figure 5D shows a sample computer programme using equations (4d), (5d), (6d) and (10d) to calculate the natural frequencies of Wet liners (cantilevered).

Figure 6D shows specimen results using the two computer programmes for the calculation of the natural frequencies of the liner investigated, when treated as wet and dry (in terms of fixing). The values of the wet liner case show that the fundamental 1st and 2nd harmonic frequencies could interfere with the piston impact range of frequencies and also the sensitive part of the noise spectrum of the engine. On the other hand, the dry liner has the advantage of pushing these frequencies to the rather unimportant part of the spectrum.

References

D.1 Flügge, W. "Statik und Dynamik der Schalen" (Julius Springer, Berlin). 1934.

D.2 Arnold, R.N., Warburton, G.B. "The Flexural Vibrations of Thin Cylinders". I. Mech. E. Paper. 1953.

D.3 Warburton, G.B. "Private communication", 15 October 1971.

D.4 Warburton, G.B., Higgs, J. "Natural Frequencies of Thin Cantilevered Cylindrical Shells". J. Sound Vib. (1970) 11(3), 335-338.

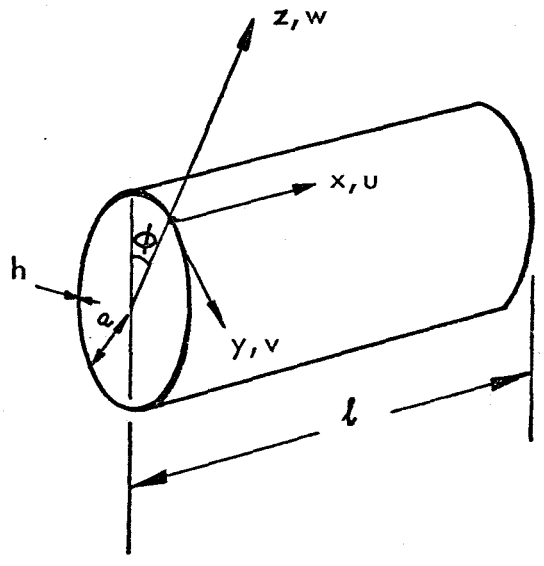

FIG. 1D.a

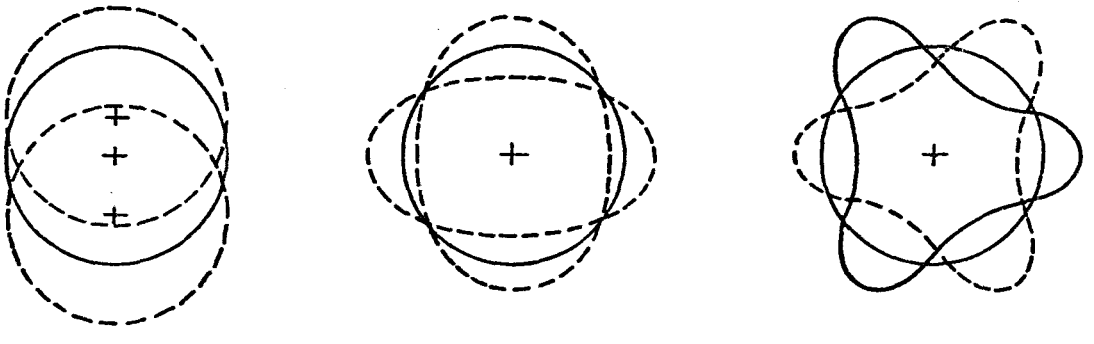

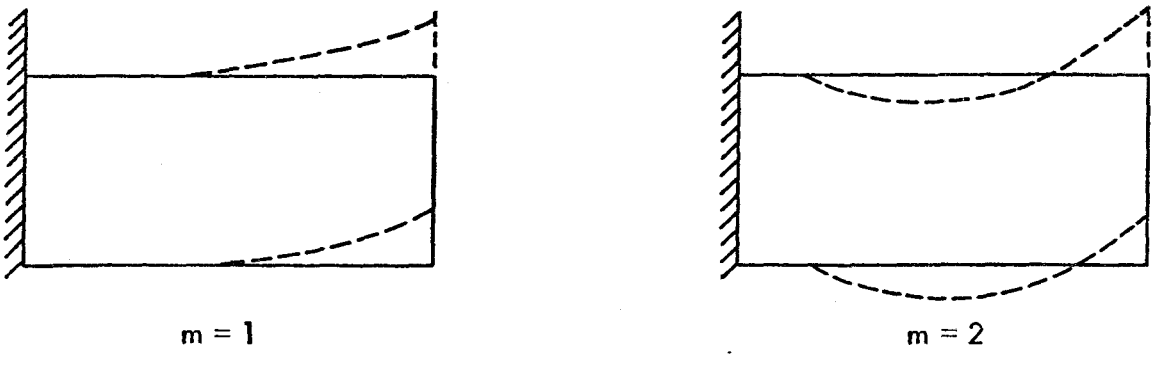

FIG. 1D.b SOME FORMS OF VIBRATION OF THIN CYLINDERS

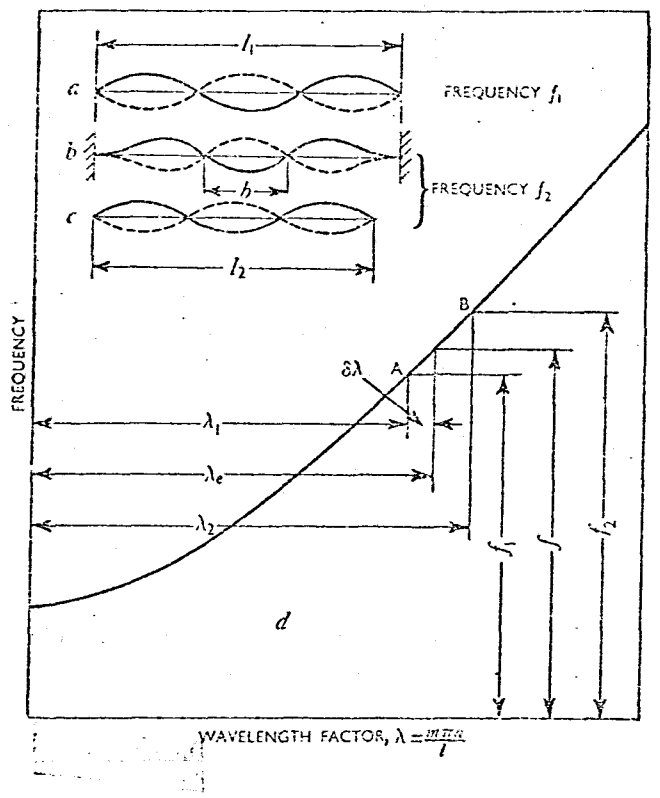

f_1 = frequency of freely supported

f_2 = frequency of fixed - fixed

f = frequency of fixed - fixed equivalent to freely supported

FIG. 2 D Diagram showing the Concept of the Equivalent Wavelength Factor λ_e (Warburton)

BEAMS OF UNIFORM SECTION AND UNIFORMLY DISTRIBUTED LOAD

ANGULAR NATURAL FREQUENCY $\omega_n = A\sqrt{\frac{EI}{\mu l^4}}$ RAD/SEC

WHERE E = YOUNG'S MODULUS, LB/IN.^{2}
I = AREA MOMENT OF INERTIA OF BEAM CROSS SECTION, IN.^{4}
l = LENGTH OF BEAM, IN.
μ = MASS PER UNIT LENGTH OF BEAM, LB-SEC^2/IN.^{2}
A = COEFFICIENT FROM TABLE BELOW

NODES ARE INDICATED IN TABLE BELOW AS A PROPORTION OF LENGTH l MEASURED FROM LEFT END

FIXED-FREE (CANTILEVER)	A = 3.52 (1.876)	0.774 A = 22.4 (4.733)	0.500 0.868 A = 61.7 (7.855)	0.356 0.644 0.906 A = 121.0	0.500 0.926 0.279 0.723 A = 200.0
HINGED-HINGED (SIMPLE)	A = 9.87	0.500 A = 39.5	0.333 0.667 A = 88.9	0.25 0.50 0.75 A = 158	0.20 0.40 0.60 0.80 A = 247
FIXED-FIXED (BUILT-IN)	A = 22.4 (4.733)	0.500 A = 61.7 (7.855)	0.359 0.641 A = 121 (11.000)	0.278 0.500 0.722 A = 200	0.409 0.773 0.227 0.591 A = 298
FREE-FREE	0.224 0.776 A = 22.4	0.132 0.500 0.868 A = 61.7	0.094 0.644 0.356 0.906 A = 121	0.277 0.723 0.073 0.500 0.927 A = 200	0.060 0.409 0.773 0.227 0.591 0.940 A = 298
FIXED-HINGED	A = 15.4	0.560 A = 50.0	0.384 0.692 A = 104	0.529 0.294 0.765 A = 178	0.429 0.810 0.238 0.619 A = 272
HINGED-FREE	0.736 A = 15.4	0.446 0.853 A = 50.0	0.308 0.616 0.898 A = 104	0.471 0.922 0.235 0.707 A = 178	0.363 0.763 0.130 0.581 0.937 A = 272

FIG. 3 D Vibration Modes of Uniform Beams.

```
      LIST(LP)
      PROGRAM(V05C)
      OUTPUT 6=LP0
      COMPACT DATA
      TRACE
      END

      MASTER FREQ3
      REAL L,K0,K1,K2
      R=0.3
      PI=3.141596
      L=6.49
      A=2.44
      E=28500000.0
      G=386.0
      S=0.284
      H=0.25
      R2=R*R
      BE=H*H/12.0/A/A
      TA=1.0-R
      TB=1.0+R
      DO 20 M=1,5
      XL=(M+0.3)*PI*A/L
      XL2=XL*XL
      XL4=XL2*XL2
      DO 30 N=1,5
      N2=N*N
      N4=N2*N2
      TC=XL2*N2
      TC2=TC*TC
      TC3=TC2*TC
      K0=0.5*TA*TA*TB*XL4+0.5*TA*BE*(TC3*TC-8.0*XL2*N4-2.0*N2*N4+N4)
      K1=0.5*TA*TC2+0.5*(3.0-R-2.0*R2)*XL2+0.5*TA*N2+0.5*(3.0-R)*BE*TC3
      K2=1.0+0.5*(3.0-R)*TC
      P=K0/K1+K2*K0*K0/K1/K1/K1
      F=SQRT(E*G*P/S/(1.0-R2))/2.0/PI/A
      WRITE(6,101) M,N,F
   30 CONTINUE
   20 CONTINUE
  101 FORMAT(1H ,2I10,3F15.4)
      STOP
      END
```

FIG.4D Computer Programme for Calculating the Natural Frequencies of Dry Type Engine Liners.

```
      LIST(LP)
      PROGRAM (V05B)
      OUTPUT =LPU
      COMPACT DATA
      TRACE
      END

      MASTER FREQ2
      REAL L,K0,K1,K2
      R=0.3
      PI=3.14159
      L=6.49
      A=2.44
      E=28500000.0
      G=306.0
      S=0.284
      H=0.25
      R2=R*R
      BE=H*H/12.0/A/A
      TA=1.0-R
      TB=1.0+R
      DO 20 M=1,5
      XL=PI*A*(M-0.5)/L
      IF (M.EQ. 1) XL=1.875*A/L
      XL2=XL*XL
      XL4=XL2*XL2
      DO 30 N=1,5
      N2=N*N
      N4=N2*N2
      TC=XL2+N2
      TC2=TC*TC
      TC3=TC*TC2
      K0=0.5*TA*TA*TB*XL4+0.5*TA*BE*(TC3*TC-8.0*XL2*N4-2.0*N4*N2+N4)
      K1=1.5*TA*TC2+0.5*(3.0-R-R2*2.0)*XL2+0.5*TA*N2+0.5*(3.0-R)*BE*TC3
      K2=1.0+0.5*(3.0-R)*TC
      P=K0/K1+K2*K0*K0/K1/K1/K1
      F=SQRT(E*G*P/S/(1.0-R2))/2.0/PI/A
         WRITE(6,101) M,N,F
   30 CONTINUE
   20 CONTINUE
  101 FORMAT(1H ,2I10,F15.4)
      STOP
      END
```

FIG.5D Computer Programme for Calculating the Natural Frequencies of Wet Type Engine Liners.

M	N	F_d	F_w
1	1	8774.9167	2948.03
1	2	4585.2409	1728.56
1	3	8313.9083	3229.04
1	4	14686.3505	5949.16
1	5	22726.0867	9470.13
2	1	11820.4226	8197.66
2	2	11903.5199	5570.79
2	3	25569.5311	5207.14
2	4	43569.0088	7201.31
2	5	64089.8894	10533.41
3	1	13539.3582	11265.54
3	2	23592.9510	9481.73
3	3	49610.2326	8830.72
3	4	80090.6257	
3	5	111730.4768	
4	1	15920.5271	
4	2	38596.4319	
4	3	77226.6277	
4	4	118418.6590	
4	5	158815.0943	
5	1	19580.1403	
5	2	55840.4972	
5	3	105964.4076	
5	4	156040.3647	
5	5	203999.1341	

F_d = Frequency of the Dry Type Liner (Hz.)

F_w = Frequency of the Wet Type Liner (Hz)

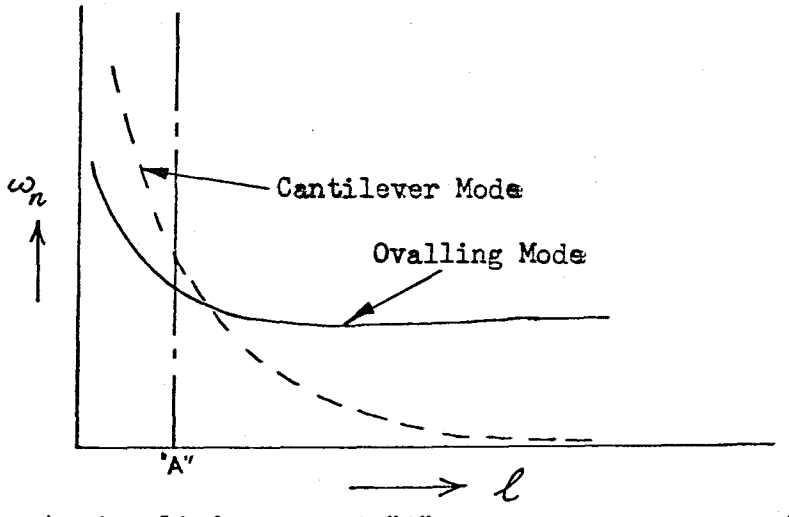

For short cylinders as at "A" , w_n cantilever mode $>$ w_n ovalling mode

FIG. 6D Calculated Natural Frequencies of the V8-470 Liner when treated as Wet (actual case) and Dry (future design).

APPENDIX E

Calculation of Modal Damping Ratios Using Impact Analysis

There are various methods for calculating the modal damping ratios of structures. One such method has been developed (ref. E.1) using the relationship

$$z = \frac{\log_e \frac{x_1}{x_n}}{2\pi n} \qquad \text{(e.1)}$$

where x_1 and x_n are the amplitudes of free vibration spaced (n) cycles apart. It can be shown that if two truncated Fourier transforms of equal data record lengths but with their starting points separated by time (t) are performed on the impulse response, then the damping ratio of the i^{th} mode z_i is given by

$$z_i = \frac{\log_e \frac{|FT(f_i)|_1}{|FT(f_i)|_2}}{2\pi f_i t} \qquad \text{(e.2)}$$

where f_i = the frequency of the i^{th} mode.

$|FT(f_i)|_1$ and $|FT(f_i)|_2$ are the maximum levels of the modulus spectra for the two successive transforms.

This relationship is free from inherent errors caused by dynamic range considerations and has been shown to work for a simulated system with ten natural frequencies (ref. E.1). This method was used to find:

z_γ = damping ratios between the two halves of the liner

and z_c = damping ratios between the liner and engine block.

For z_γ an impulsive force was applied to one side of the liner and the vibration acceleration response measured of the other side and tape recorded. This response was then fed into a Myriad data analysis computer to obtain the Fourier transforms as shown in figure 1E. Using equation (e.2),

damping ratios were calculated for every clear mode and plotted as shown in figure 3E. Therefore the average damping ratio could be estimated at any mode of interest.

The same procedure was followed to calculate z_c, where an impulsive force was applied on the inner part of the liner (as near as possible to where the piston is expected to impact the liner around T.D.C.) and the vibration acceleration response on the top of the block measured and recorded. Fourier transforms were then obtained as shown in figure 2E and the damping ratios calculated using equation (e.2) and plotted as shown in figure 4E. Figure 4E also shows the effect of pistons on the damping characteristics of engine structure.

Reference

E.1 G.C. Wright. "Dynamic behaviour of fibre reinforced materials". Structural Dynamics Conference, Southampton University, April, 1972.

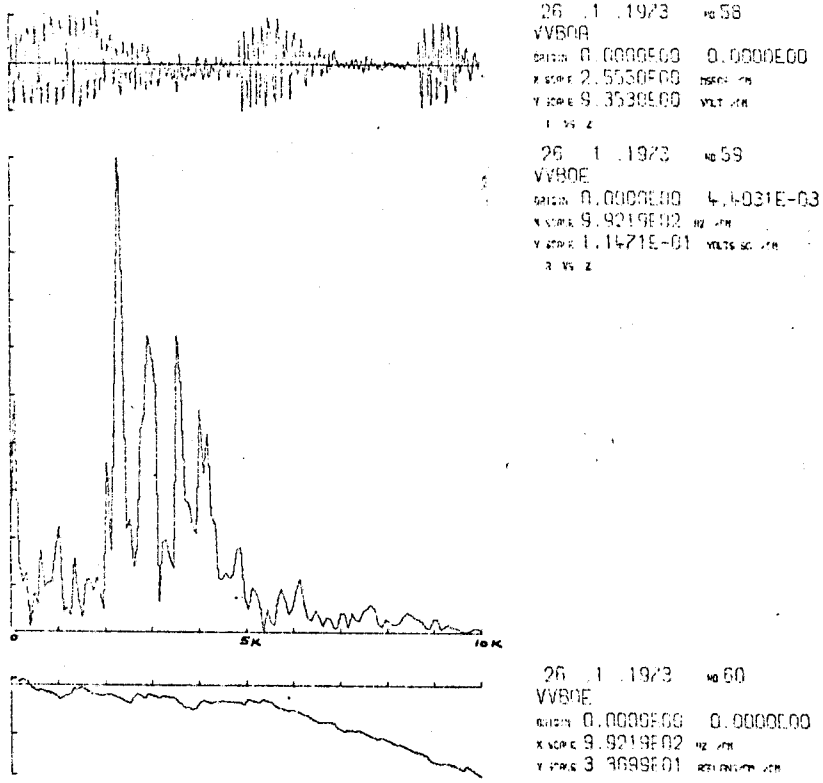

$$\zeta_g$$

$$t = 50/20000$$

$$\zeta_g @ f_i = \frac{\ln \frac{M_1}{M_2}}{\pi f_i \cdot \frac{1}{200}}$$

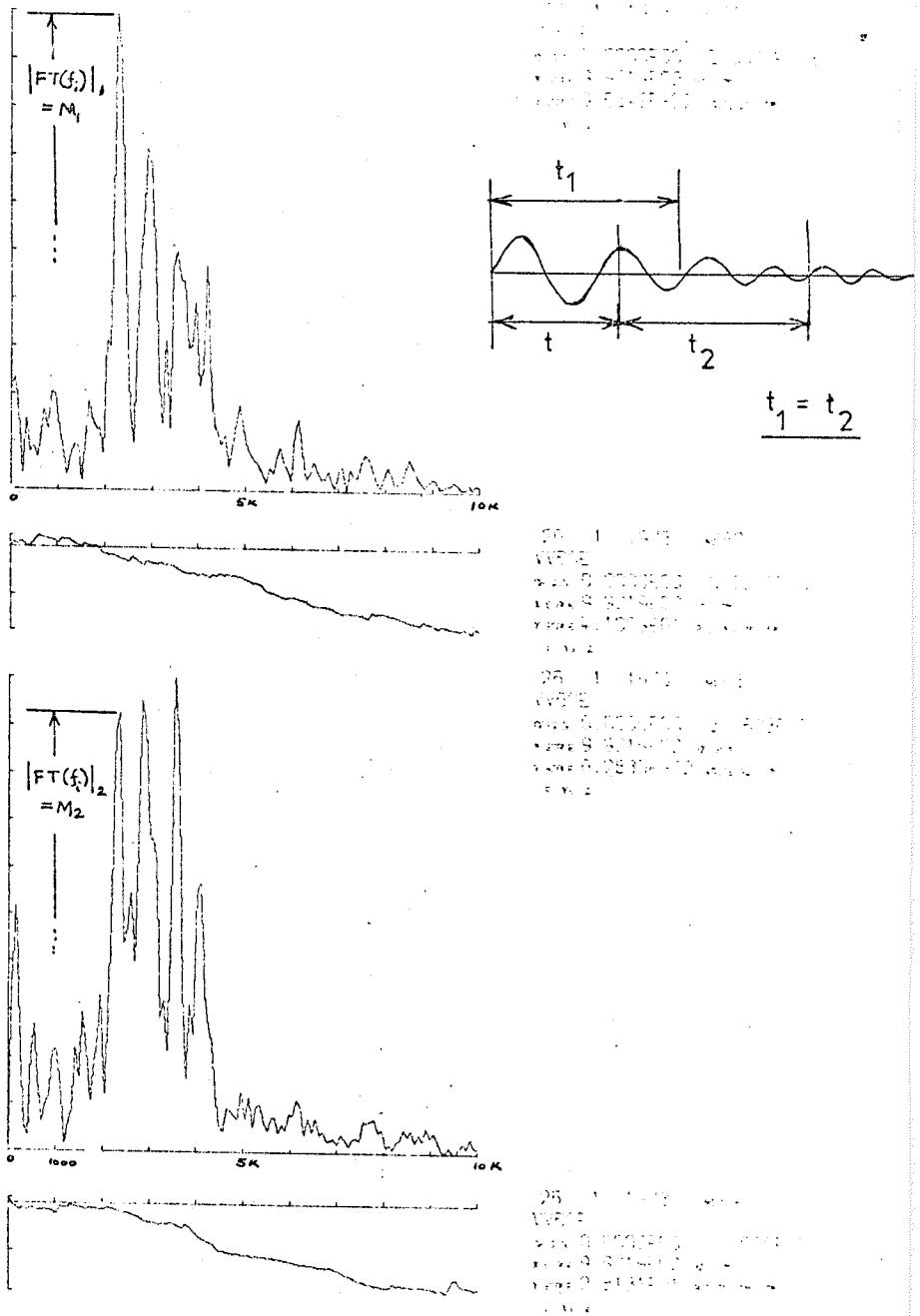

FIG. 1E NATURAL FREQUENCIES AND FOURIER TRANSFORMS FOR THE FOR THE CALCULATION OF MODAL DAMPING RATIOS BETWEEN THE TWO PARTS OF THE LINER FOR THE SA ENGINE (IN SITU).

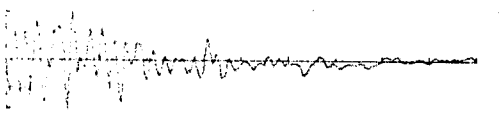

26 .1 .1973 NO 51
VV80B
ORIGIN 0.0000E00 0.0000E00
X SCALE 1.2750E00 HERTZ / CM
Y SCALE 7.8760E00 VOLTS / CM
R VS Z

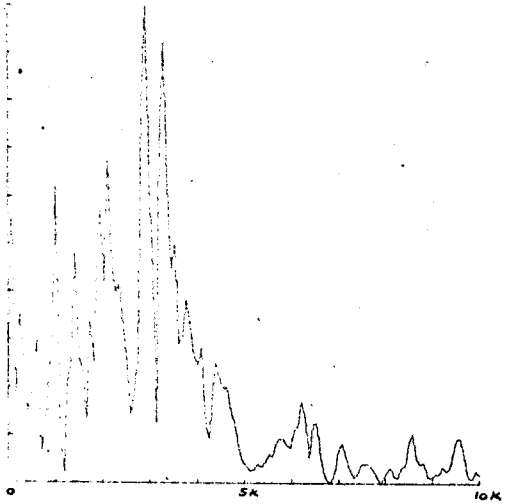

26 .1 .1973 NO 52
VV80E
ORIGIN 0.0000E00 4.0661E-03
X SCALE 9.9219E02 HZ / CM
Y SCALE 4.9268E-02 VOLTS SQ / CM
R VS Z

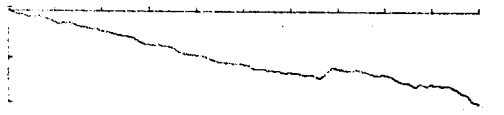

26 .1 .1973 NO 53
VV80E
ORIGIN 0.0000E00 0.0000E00
X SCALE 9.9219E02 HZ / CM
Y SCALE 4.1007E01 RADIANS / CM
I VS Z

ζ_c

$t = 50/20000$

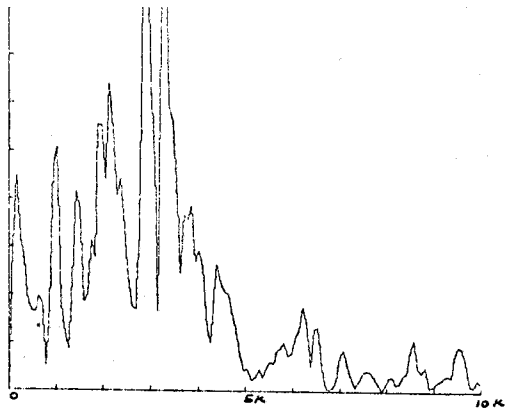

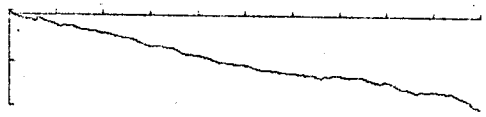

26 .1 .1973 NO 55
VV80E
ORIGIN 0.0000E00 0.0000E00
X SCALE 9.9219E02 HZ / CM
Y SCALE 4.4122E01 RADIANS / CM
I VS Z

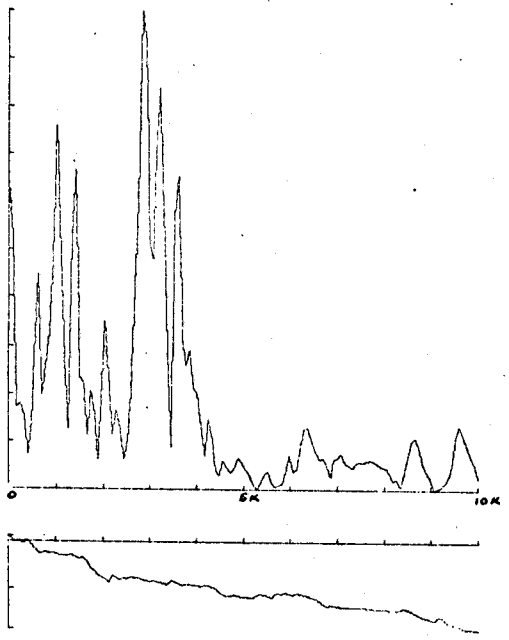

26 .1 .1973 NO 56
VV80E
ORIGIN 0.0000E00 5.4286E-04
X SCALE 9.9219E02 HZ / CM
Y SCALE 2.6853E-02 VOLTS SQ / CM
R VS Z

26 .1 .1973 NO 57
VV80E
ORIGIN 0.0000E00 0.0000E00
X SCALE 9.9219E02 HZ / CM
Y SCALE 2.5426E01 RADIANS / CM
I VS Z

FIG. 2E NATURAL FREQUENCIES AND FOURIER TRANSFORMS FOR THE CALCULATION OF MODAL DAMPING RATIOS BETWEEN THE LINER AND ENGINE BLOCK FOR THE SA ENGINE.

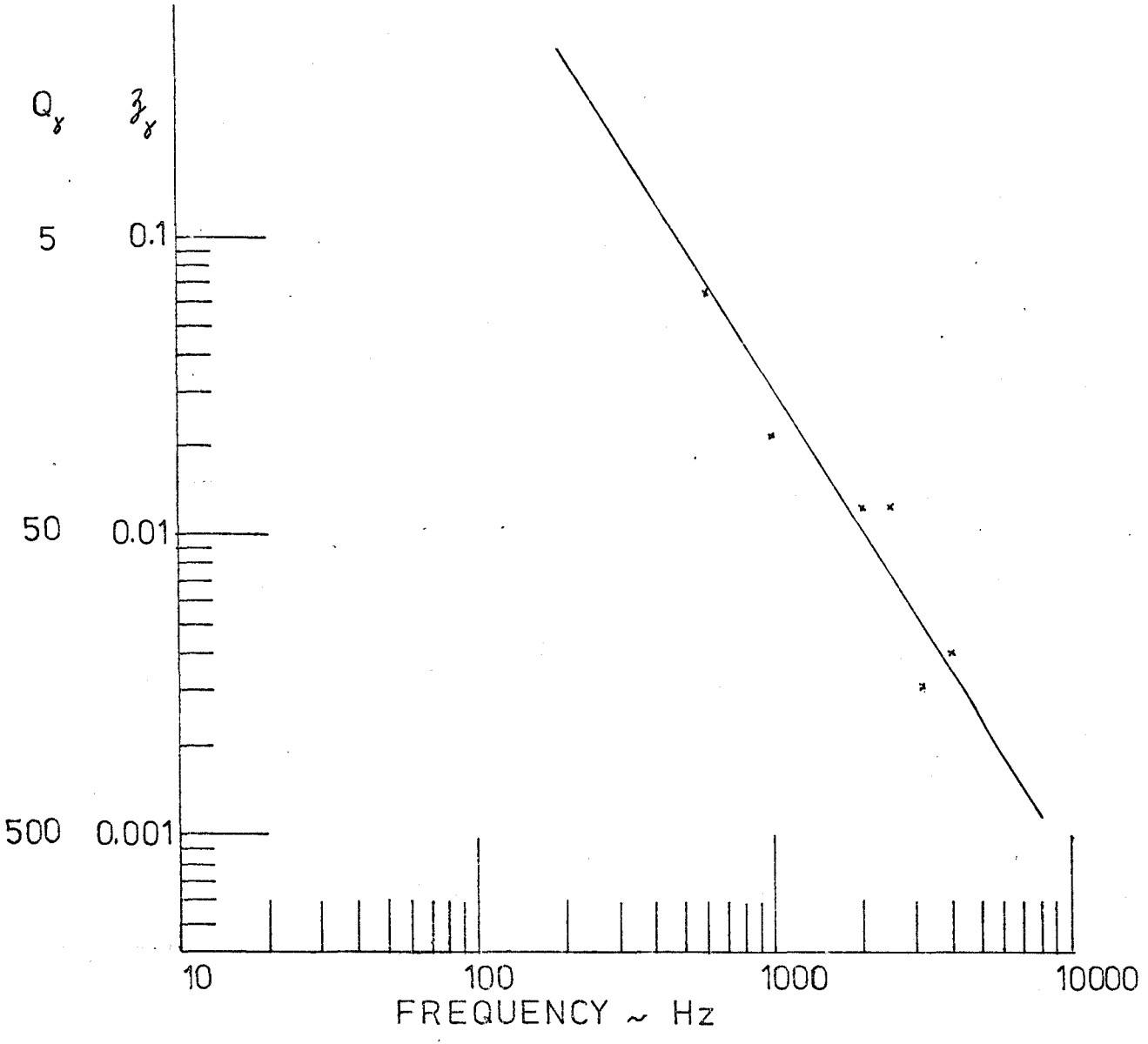

FIG. 3E MODAL DAMPING RATIOS BETWEEN THE TWO PARTS OF THE LINER OF V8 SA DIESEL ENGINE

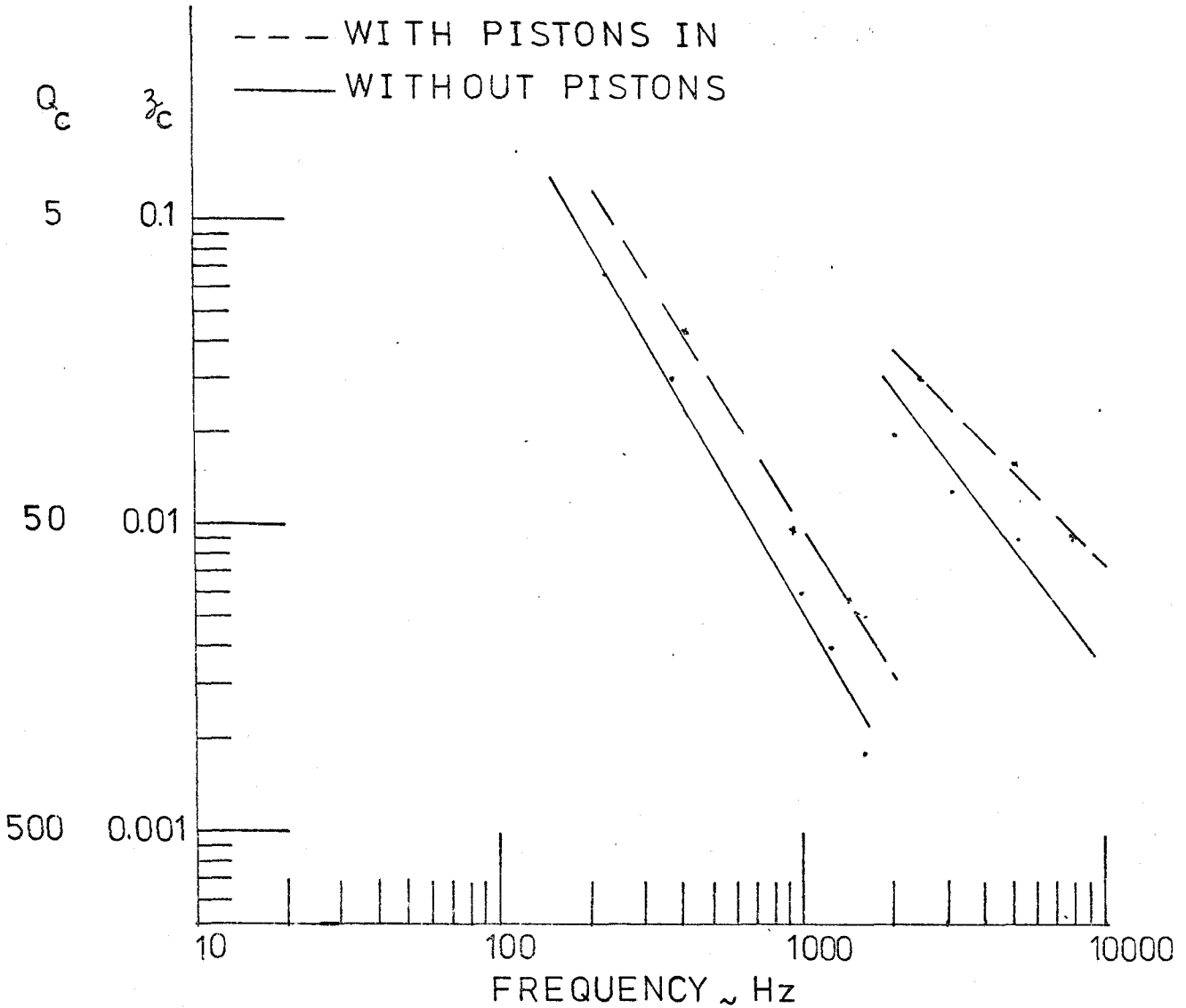

FIG. 4E MODAL DAMPING RATIOS BETWEEW THE LINER AND ENGINE BLOCK OF V8 SA DIESEL ENGINE

Appendix F

MEASUREMENT OF PISTON TO BORE CLEARANCE

Capacitive transducers are usually used for the measurement of displacement where linear calibration characteristics are desired. Such transducers were used in the first development of piston slap rig simulation. However, in the presence of lubricating oil, these transducers become unreliable. Also the measuring heads of these transducers are relatively large for installation in the skirt of a medium size piston. The recently developed inductive transducers are small in size and reliable in a wide range of environments. However they are non linear and calibration charts have to be prepared for each transducer. A pair of inductive Sangamo T4 proximity transducers were used throughout to measure the upper and lower displacements of the piston skirt. These were fitted in the skirt using special adaptors. The signals were then fed into an AE instrument comprising power supply module, oscillator and detector/filter modules (complete details of instrumentation and setting up procedure are given in ref. F.1).

Calibration of T4 gauges used on the Vee piston slap rig simulation

Before assembly in the piston, the gauges were calibrated using a precision anvil and thimble micrometer with a steel armature. Figures 1F and 2F show the calibration curves obtained for these gauges. The figures also illustrate the sensitivity at three carrier frequencies set up under the same condition. It can be seen that the 100 kHz carrier frequency gives the best sensitivity and so curves 'A' were used throughout. Figure 3F shows movement compensation using the relevant calibration curves for a typical case.

Calibration of T4 gauges used on the running engine

The gauges were firmly installed and cemented to the piston skirt using "Araldite". Because of the severe environment, the calibration of the gauges was checked frequently.

A rig is shown in figure 4F which enabled this calibration to be carried out in situ. Figure 5F shows the average calibration curves obtained for the two proximity gauges installed in piston No. 1 (thrust side) in the running engine.

The AET4 gauges used by AED in similar experiments were reported to show some change in calibration with operating temperatures (ref. 2.13). However, the manufacturers of the Sangamo T4 transducers (used in the present investigations) quote low sensitivity change with temperature (typically 0.1% change of inductance per ^{o}C) - ref. F.2.

References

F.1 Associated Engineering AET4 Instrumentation Manual.

F.2 Sangamo Weston Controls Ltd. Inductive type transducer manual.

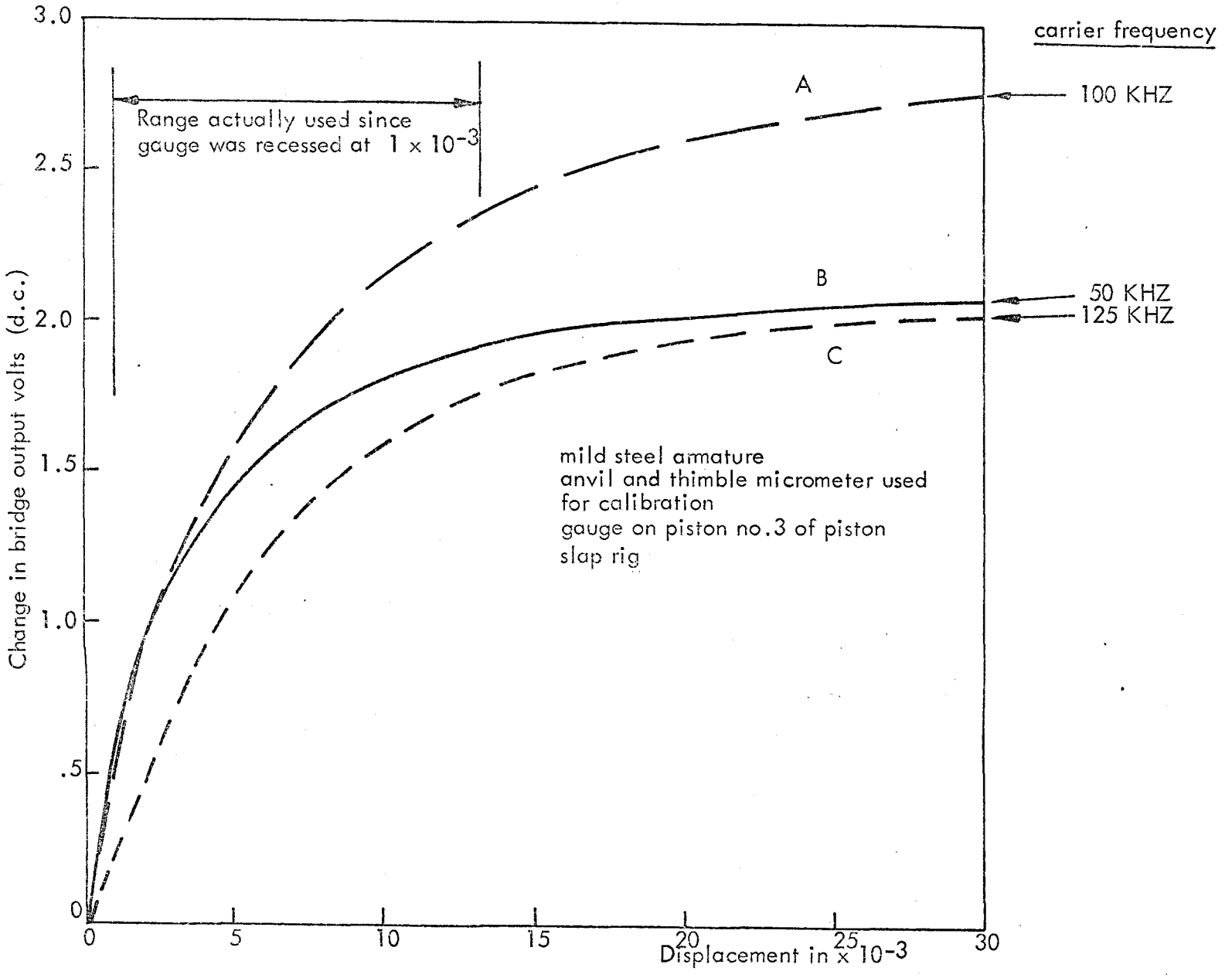

FIG. 1F CALIBRATION OF UPPER CLEARANCE AET 4 INDUCTIVE GAUGE

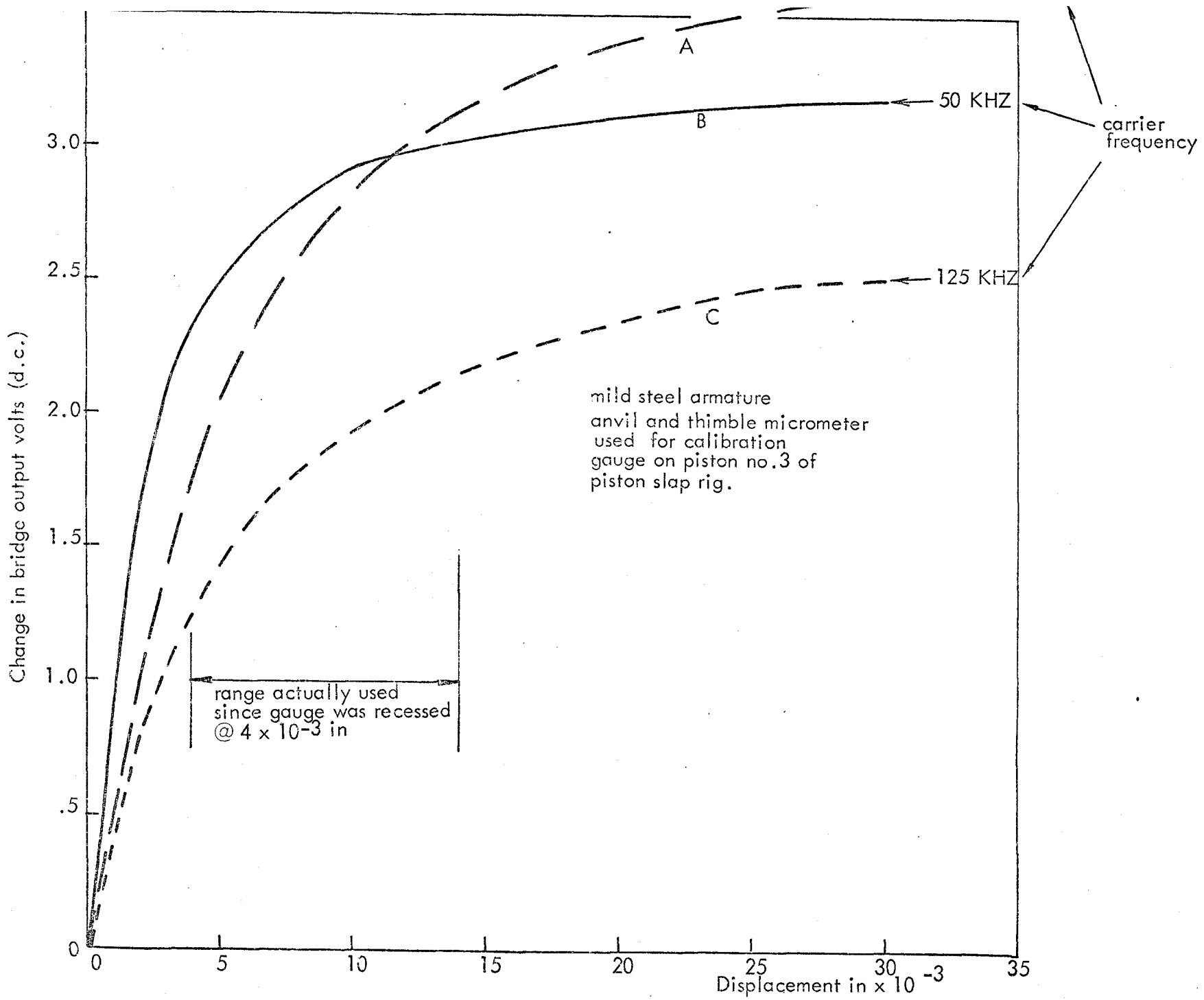

FIG. 2F CALIBRATION OF LOWER CLEARANCE AET 4 INDUCTIVE GAUGE

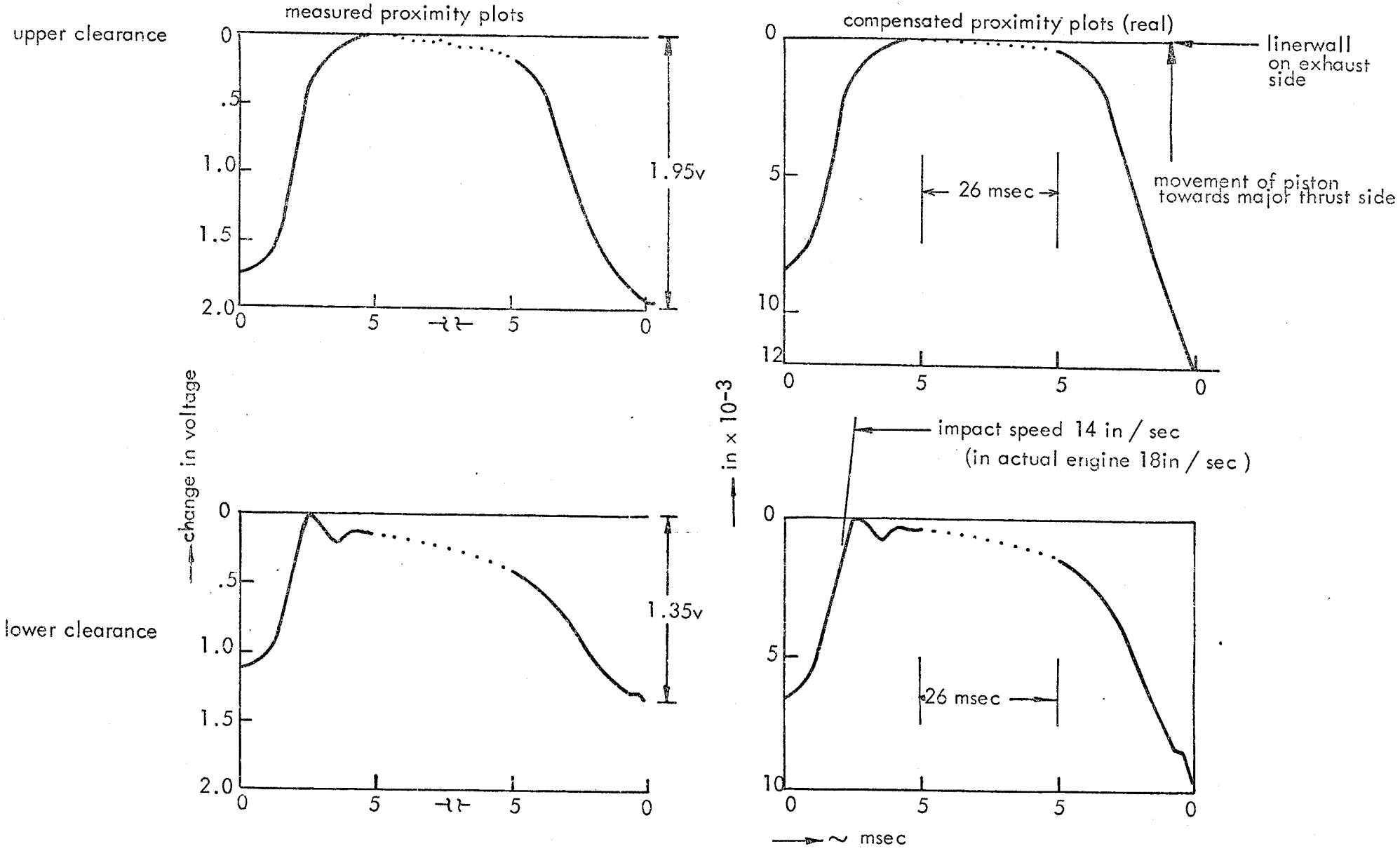

FIG. 3F PISTON MOVEMENT @ 16.7 HZ≡1000 rpm DRY CASE — PISTON SLAP RIG —

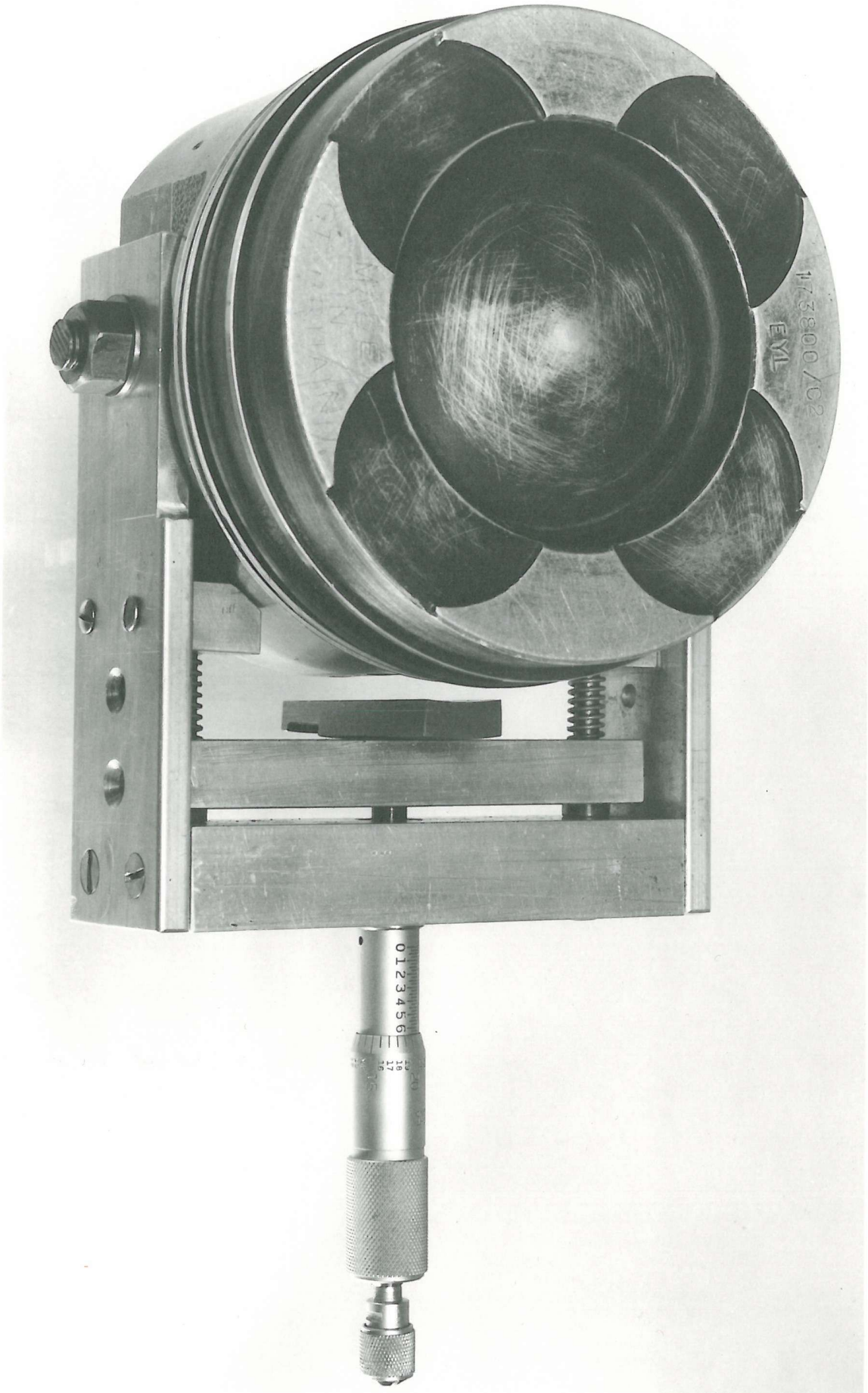

FIG. 4F RIG FOR CALIBRATING T4 GAUGES IN SITU

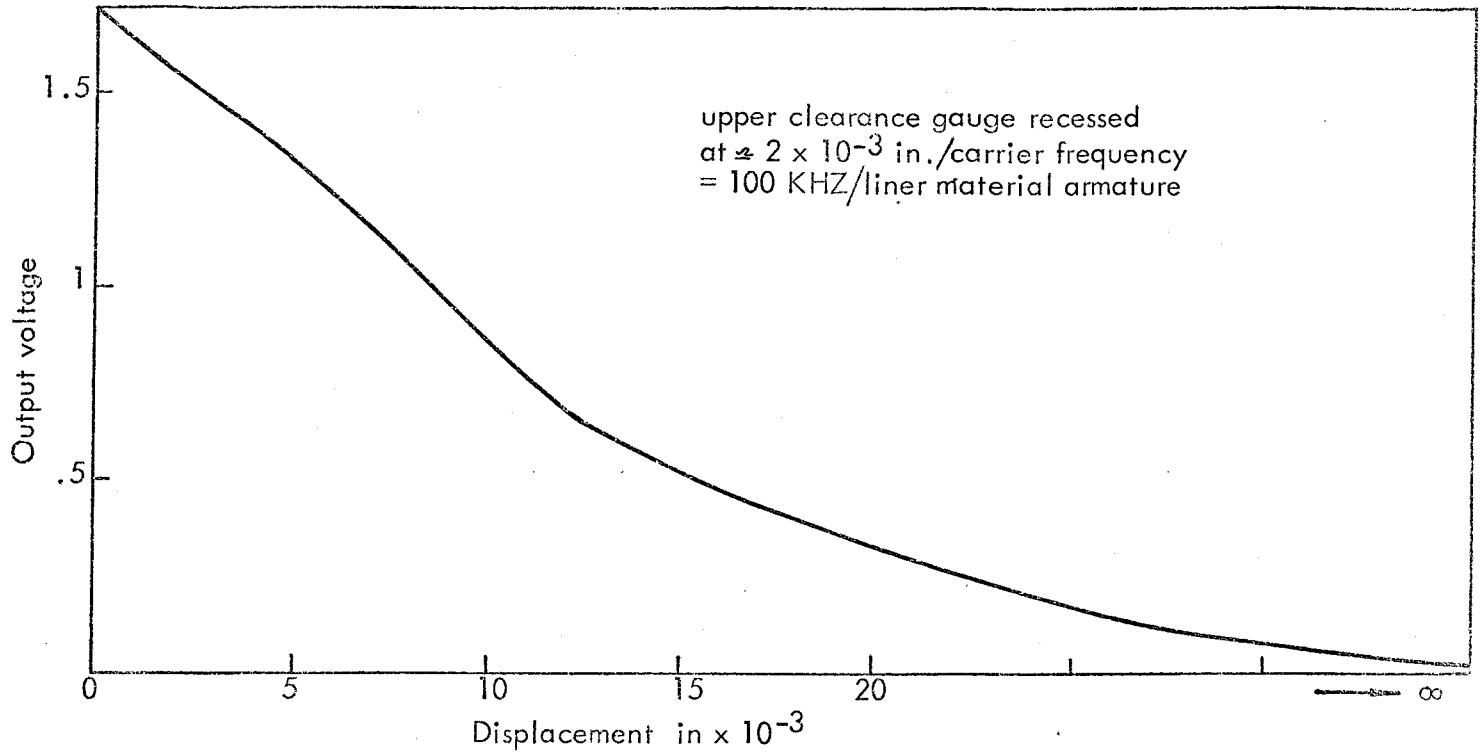

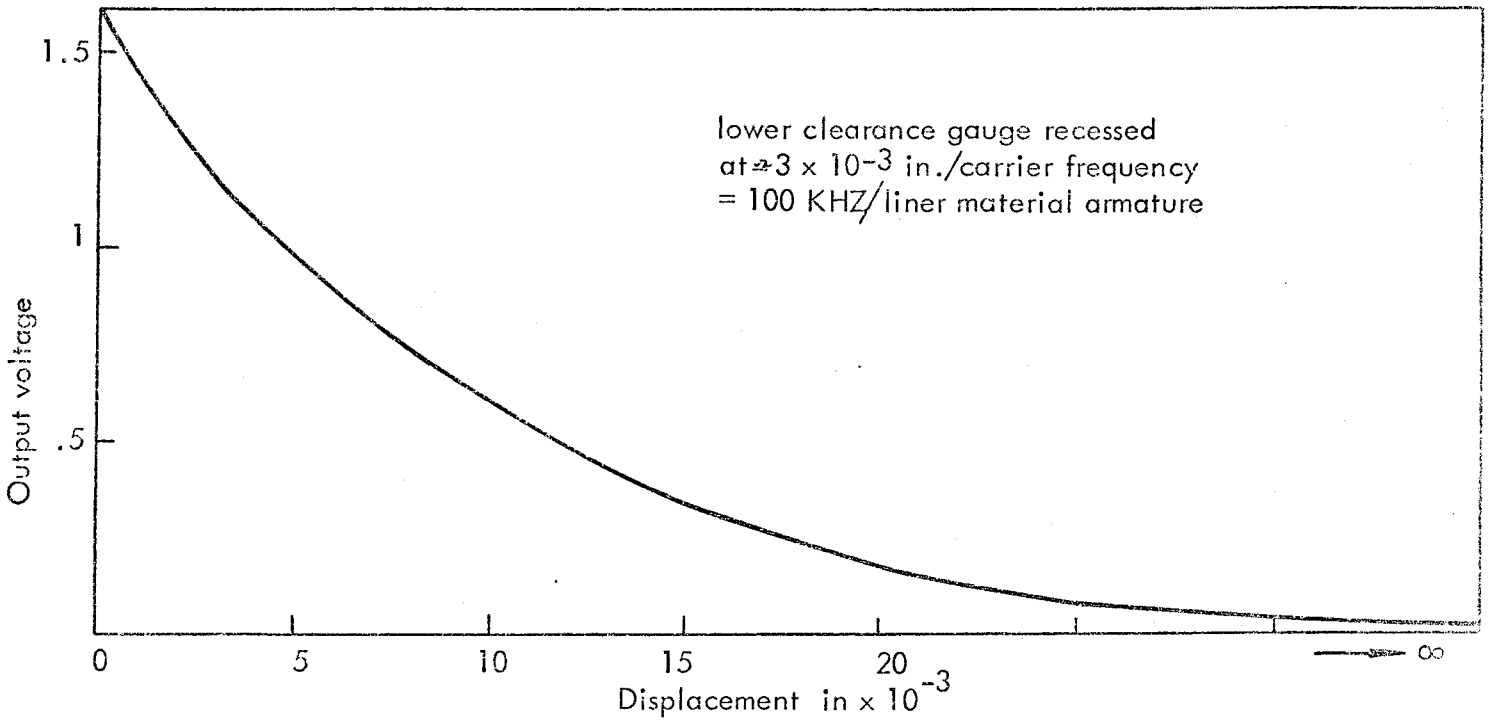

FIG. 5F CALIBRATION CURVES OF THE TWO AET 4 PROXIMITY GAUGES INSTALLED IN PISTON 1 OF V8 - 7.7 LITRE RUNNING ENGINE "WITH LINKAGE"

Appendix G

HARMONIC ANALYSIS

For a multi degree of freedom system vibrating freely, it is common for vibrations of several different frequencies to exist simultaneously. Such vibrations result in a complex waveform which is repeated periodically.

J. Fourier (1768-1830) showed that any periodic motion can be represented by a series of sines and cosines which are harmonically related by the following series:

$$x(t) = \frac{a_o}{2} + a_1 \cos \omega_1 t + a_2 \cos 2\omega_1 t + \ldots + b_1 \sin \omega_1 t + b_2 \sin 2\omega_1 t + \ldots \qquad (1g)$$

where $\omega_1 = \frac{2\pi}{\tau}$ = fundamental frequency

OR $f(x) = \frac{1}{2}a_o + \sum_{k=1}^{\infty} (a_k \cos kx + b_k \sin kx)$ (2g)

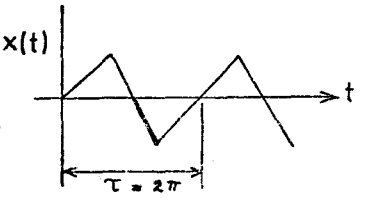

To determine the coefficients a_k and b_k, equation (2g) is multiplied by cos kx and integrated over the period τ (0 - 2π)

Therefore

$$\int_0^{2\pi} f(x) \cos kx \, dx = a_k \int_0^{2\pi} \cos mx \cos kx \, dx + b_k \int_0^{2\pi} \sin mx \cos kx \, dx \qquad (3g)$$

where $\int_0^{2\pi} \cos mx \cos kx \, dx = 0$ if $m \neq k$

$= \pi$ if $m = k$ (4g)

and $\int_0^{2\pi} \sin mx \cos kx \, dx = 0$ for all m and k (5g)

Therefore, for m = k (where m and k are integers)

$$a_k = \int_0^{2\pi} \cos^2 kx \, dx = \pi a_k \qquad (6g)$$

Therefore,

$$a_k = \frac{1}{\pi} \int_0^{2\pi} f(x) \cos kx \, dx \tag{7g}$$

Similarly, multiply equation (2g) by sin kx and integrate from x = 0 to x = 2π,

$$\int_0^{2\pi} \sin mx \sin kx \, dx = 0 \quad \text{if } m \neq k$$
$$= \pi \quad \text{if } m = k \tag{8g}$$

Therefore,

$$b_k = \frac{1}{\pi} \int_0^{2\pi} f(x) \sin kx \, dx \tag{9g}$$

It may be seen that for k=0

$$b_o = 0$$

and

$$a_o = \frac{1}{\pi} \int_0^{2\pi} f(x) dx \tag{10g}$$

Therefore, in general terms, and for a period length τ, equations (7g) and (9g) may be written as follows.

$$a_k = \frac{1}{\tau/2} \int_0^{\tau} f(x) \cos \frac{2\pi kx}{\tau} \, dx \tag{11g}$$

$$b_k = \frac{1}{\tau/2} \int_0^{\tau} f(x) \sin \frac{2\pi kx}{\tau} \, dx \tag{12g}$$

Returning to equation (1g) and examining the two terms of equations (11g) and (12g) at one of the frequencies, $k\omega_1$, their sum can be written as

$$a_k \cos k\omega_1 t + b_k \sin k\omega_1 t$$

$$= \sqrt{a_k^2 + b_k^2} \left\{ \frac{a_k}{\sqrt{a_k^2 + b_k^2}} \cos k\omega_1 t + \frac{b_k}{\sqrt{a_k^2 + b_k^2}} \sin k\omega_1 t \right\}$$

$$= c_k \cos (k\omega_1 t - \phi_k)$$

where $c_k = \sqrt{a_k^2 + b_k^2}$ (13g)

and $\tan \phi = \frac{b_k}{a_k}$ (14g)

where c_k = modulus of the harmonic

ϕ = phase of the harmonic

Thus c_k and ϕ_k completely define the harmonic contribution of the periodic waveform.

When c_k is plotted against frequency for all values of k, the result is a series of discrete lines at ω_1, $2\omega_1$, etc. For presentation, an envelope passing through the peaks is usually drawn. Such a plot is called the Fourier spectrum of the waveform.

Various digital computer programmes have been written to execute the Fourier analysis in the minimum of time (refs. G.1 and G.2). At ISVR a relatively simple and time saving programme has been developed (ref. G.3). This programme employs the Simpson's Rule with a weighting function to evaluate the sine and cosine integrals of the repetitive function $f(x)$. The programme was originally designed to Fourier analyse the cylinder pressure waveform. With slight modification to the hardware, it was used throughout for analysis of combustion force, piston sideways force, liner response and oil film pressure waveforms for the running engine.

The Sawtooth Waveform

The sawtooth waveform is an example of a simple waveform that can be calculated mathematically rather than use a computer programme. Calculating the amplitude at the fundamental frequency and knowing that this type of waveform has a spectrum decaying at 20 dB/decade, the overall spectrum may be plotted.

Take a sawtooth waveform as shown:

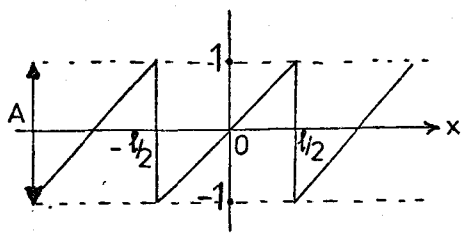

Since the waveform is skew-symmetrical about the values $x = 0$, $x = \ell/2$ and $x = -\ell/2$, the series expansion contains sine terms only (ref. G.4) and the following boundary conditions are satisfied, i.e.

$$F(x) = f(x) \sin kx$$

$$f(x) = f(\ell - x)$$

$$\sin kx = - \sin k(\ell - x)$$

Therefore,

$$F(x) = f(x) \sin kx = f(\ell - x) \sin k(\ell - x) = F(\ell - x)$$

Also,

$$\int_{x=0}^{\ell} F(x)dx = 2 \int_{x=0}^{\ell} F(x)dx \qquad (15g)$$

Hence, from equation (12g)

$$b_k = \frac{2}{\ell/2} \int_{-\ell/2}^{\ell/2} f(x) \sin \frac{2\pi kx}{\ell} dx$$

$$= \frac{4}{\ell} \{(- \frac{\ell}{2\pi k} \cdot \frac{\cos 2\pi kx}{\ell})_{-\ell/2}^{\ell/2} + \frac{\ell}{2\pi k} \int_{-\ell/2}^{\ell/2} \cos \frac{2\pi}{\ell} kx \, dx\}$$

$$= - \frac{2}{\ell\pi k} \{ \frac{\ell}{2} \cos k\pi + \frac{\ell}{2} \cos -k\pi\} = - \frac{2 \cos k\pi}{k\pi}$$

Therefore,

$$b_k = \frac{2}{k\pi} \quad \text{if } k \text{ is odd}$$

$$= - \frac{2}{k\pi} \quad \text{if } k \text{ is even} \qquad (16g)$$

In general

$$b_k = \frac{A}{k\pi} \quad \text{where } A = 2 \text{ for the analysed sawtooth waveform}$$

and

$$a_k = 0. \qquad \text{Therefore, } \underline{c_k = b_k}.$$

To calculate the sawtooth amplitude equivalent to noise level in dB (rms) the general relationship is used, i.e. $20 \log \frac{P}{P_{ref}}$

$$b_k \text{ (rms)} = \frac{A}{\sqrt{2}k\pi}$$

Therefore,

$$b_k \text{ (rms) dB} = 20 \log_{10} \frac{A}{k\pi\sqrt{2}\, P_{ref}} \qquad (17g)$$

where A = amplitude of waveform

k = the harmonic number

$P_{ref} = 2 \times 10^{-4}$ μbar = reference S.P.L.

Since A is usually measured in psi, then to convert to bars it must be divided by 14.7.

Therefore, equation (17g) becomes

$$b_k \text{ (in dB rms)} = 20 \log \frac{A \times 10^6}{k\pi\sqrt{2} \times 2 \times 10^{-4} \times 14.7} \qquad (18g)$$

which may be simplified to

$$\text{dB} = 160 + 20 \log_{10} \frac{A}{1.3k} \qquad (19g)$$

Therefore, equation (19g) may be used to calculate the Fourier spectrum for k = 1, 2, 3, ..., for any amplitude. Fig. 1G presents the calculated Fourier spectra of sawtooth waveforms showing the effect of varying the amplitude and the fundamental frequency.

For example, when k = 1 and A = 1000 psi, equation (19g) gives the amplitude of the spectrum as $b_1 \simeq 217.6$ dB at the fundamental frequency. That is, this value of amplitude may be shown at 8.33 Hz for engine speed of 1000 revs/min and at 16.7 Hz for engine speed of 2000 revs/min, and at 25 Hz for engine speed of 3000 revs/min. Similar relationships exist with varying amplitudes.

REFERENCES

G.1 J.W. Cooley and J.W. Tuckey. 'An algorithm for the machine calculation of complex series". Mathematics of computation 19: 90 (April 1965), pp. 297-301.

G.2 IEEE Trans. on Audio and Electroacoustics, Vol. AU-15, No. 2 (1967). 'Special Issue on Fast Fourier Transform'.

G.3 D. Anderton. 'Spectrum Analysis of recorded pressure diagrams by digital method'. ISVR Report 1967.

G.4 R.G. Manley 'Waveform Analysis'. Chapman & Hall, London 1950.

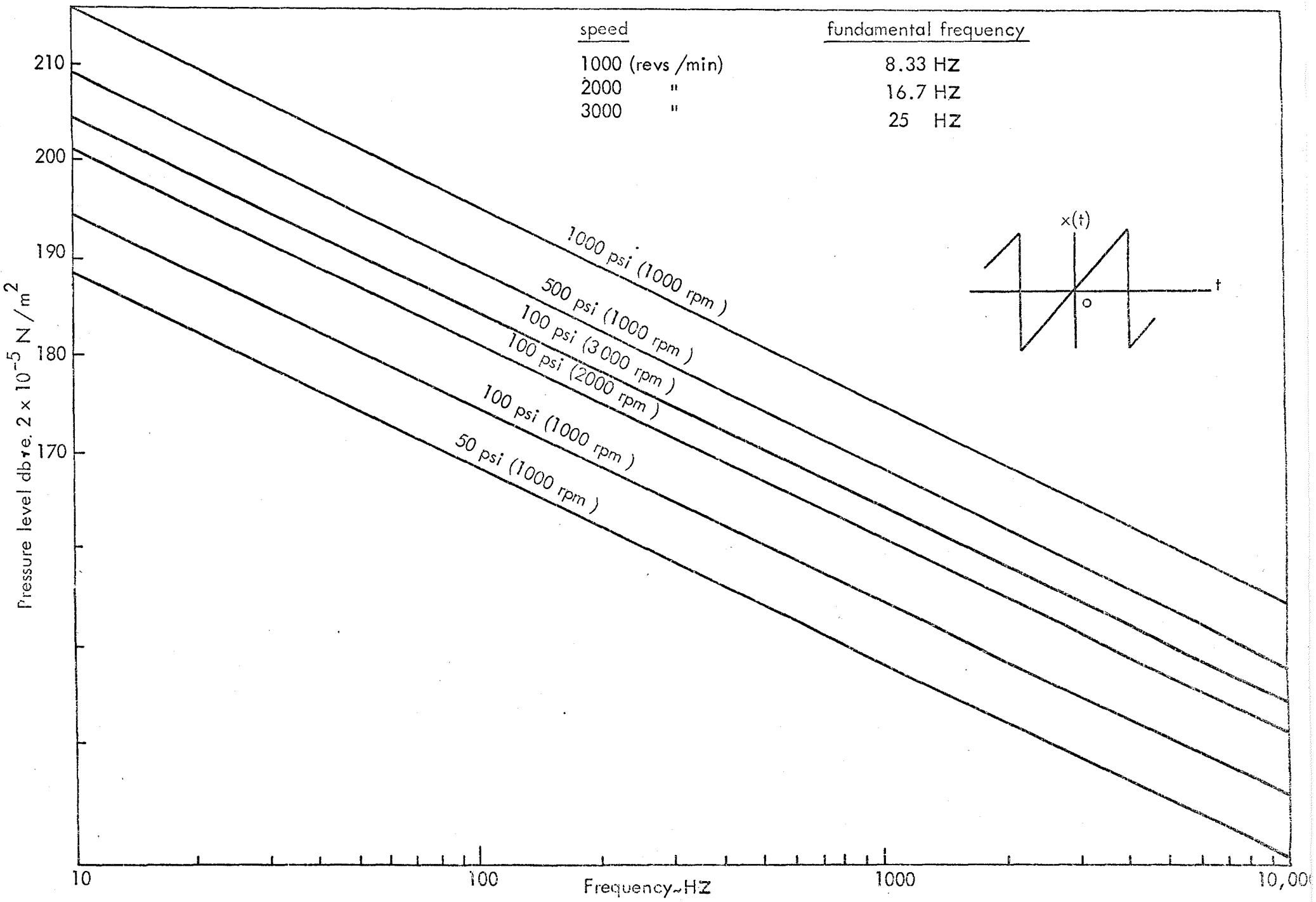

FIG. 1G FOURIER SPECTRA OF SAWTOOTH WAVEFORMS SHOWING THE EFFECT OF VARYING THE AMPLITUDE AND THE FUNDAMENTAL FREQUENCY

Appendix H

ESTIMATION OF ENGINE LINER RESPONSE DUE TO THE MAJOR PISTON IMPACT

The impact of the piston against the engine liner can be represented schematically as shown in the sketch. At the instant of impact at A, this point acquires a velocity (v_i). The beam or liner is then set in wave motion with relevant amplitudes at B, C, D and E.

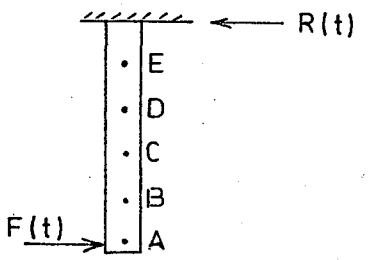

In such a system, the controlling factor determining the shape of R(t) is the ratio of:

$$\frac{\text{duration of impulse}}{\frac{1}{2}\text{ period of the fundamental mode}} .$$

If this ratio is small, the distortion becomes large, indicating the advantage of isolating the liner from the engine block to reduce transmitted vibration. The shape and magnitude of this distortion, or liner vibration response due to the major impact, is estimated as follows for the V8 engine at 1000 rev/min no load:

Assuming the following model to represent the piston-liner relationship at impact:-

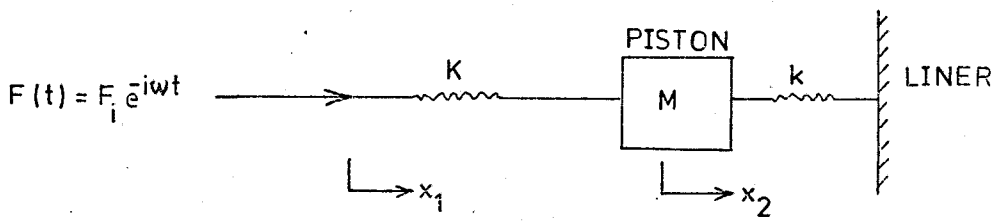

$$M\frac{d^2x_2}{dt^2} = -kx_2 + K(x_1 - x_2) \qquad (1h)$$

$$F_i e^{-i\omega t} = K(x_1 - x_2) \qquad (2h)$$

Put $x_1 = a_1 e^{-i\omega t}$ Therefore $\ddot{x}_1 = -\omega^2 a_1 e^{i\omega t}$

$x_2 = a_2 e^{-i\omega t}$ Therefore $\ddot{x}_2 = -\omega^2 a_2 e^{-i\omega t}$

Substituting in (1h) and (2h)

$$-\omega^2 M a_2 = -k a_2 + K(a_1 - a_2) \tag{3h}$$

$$F_i = K(a_1 - a_2) \tag{4h}$$

Rearranging (3h) and (4h)

$$F_i = K a_1 - K a_2$$

$$0 = a_1(-K) + a_2(-M\omega^2 + k + K)$$

Therefore,

$$F_i = a_2(-K - M\omega^2 + k + K)$$

$$k = F_i/a_2 + M\omega^2 \tag{5h}$$

where

a_2 = peak amplitude of piston oscillation

F_i = peak amplitude of applied force

M = mass of piston

ω = exciting frequency

k = stiffness between piston and liner at impact.

Since the inertia force part ($M\omega^2$) is relatively small, equation (5h) becomes:

$$k \simeq \frac{F_i}{a_2} . \tag{6h}$$

The average value of k may be found from the applied force-proximity relationship obtained on the piston slap rig simulation. For this it is assumed that the applied force deforms the liner in the manner described by equation (6h). It was found that at a repetition frequency of 16.7 Hz and applied force of 215 lbf peak, the peak amplitude of piston movement = 3×10^{-4} in.

Therefore,

$$k = \frac{215}{3 \times 10^{-4}} = 7.2 \times 10^5 \text{ lbf/in} = \underline{8.6 \times 10^6 \text{ lbf/ft.}}$$

Figure 1.H(a) shows a typical piston movement for the running V8 engine at 1000 revs/min no load. Using the relevant calibration curve, figure 1.H (b) is obtained showing the actual piston movement (a_2). The oscillatory part of this movement may be approximately regarded as the resultant liner deformation. Therefore, the resultant oscillatory liner response can be calculated as $F_i = ka_2$ and plotted in Fig. 1.H(c). Before TDC, the liner may be considered in relative smooth contact with the piston responding to the side force as shown in Fig. 2.H along ABC. At C (TDC) the piston leaves the minor thrust side and moves towards the major thrust side. During the period CD the other side of the liner does not see any force. However, at D, the piston has completed its movement across the piston to bore clearance with the application of a sudden force to the liner. The liner at this stage will respond to the piston sideways force with the oscillatory force superimposed on it. The resultant overall liner response due to piston movement around TDC, is shown in Figure 2.H.

Actual records of liner response (strain measurements) were obtained from a diesel engine and these show close agreement with the above estimated trend of liner response.

Analysis of liner response as an exciting source

The resultant liner response may be regarded as an exciting source initiating cylinder block vibration. To quantify its exciting propensities, a frequency analysis should be obtained (Appendix G).

Figure 3H compares the spectra of combustion and liner response for the V8 engine at 1000 revs/min no load. For realistic comparison both should be related to the same unit of pressure or force. Figure 3H shows three possible liner response spectra to compare with the combustion spectrum:

1. Spectrum (a), where the area of contact between the piston and liner is small ($\simeq$ 1 in^2). This case is very probable since the piston at impact tends to hit the liner at top or bottom of the skirt with the rest of the piston in space. That is, the effective area may be very small indeed.

2. Spectrum (b), where the area of contact at impact is considered as that subtended by an angle of 60^o. This assumption is commonly adopted for the analysis of lubricating films between two cylindrical objects. In this case the area is approximately 4 in^2, as shown in the following sketches:

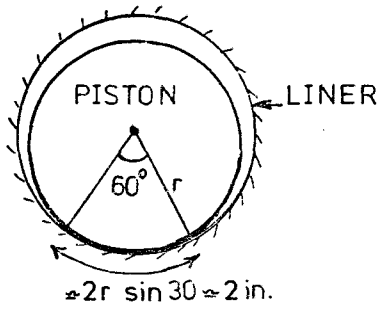

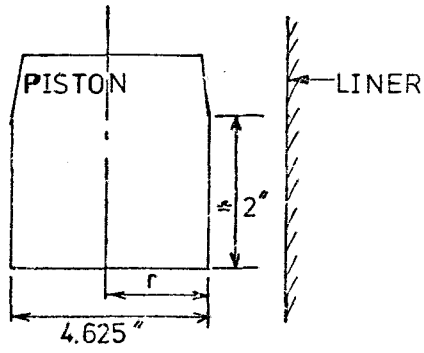

3. Spectrum (c) represents the extreme case of referring the liner response to an area equivalent to that of the piston cross section ($\simeq$ 16.8 in^2 in this case).

It can be seen from Fig. 3H that the liner response in all three cases discussed above predominates over the combustion force, especially in the frequency range from 500 Hz upwards. This indicates that the liner of a diesel engine can play a most important role in exciting the engine structure.

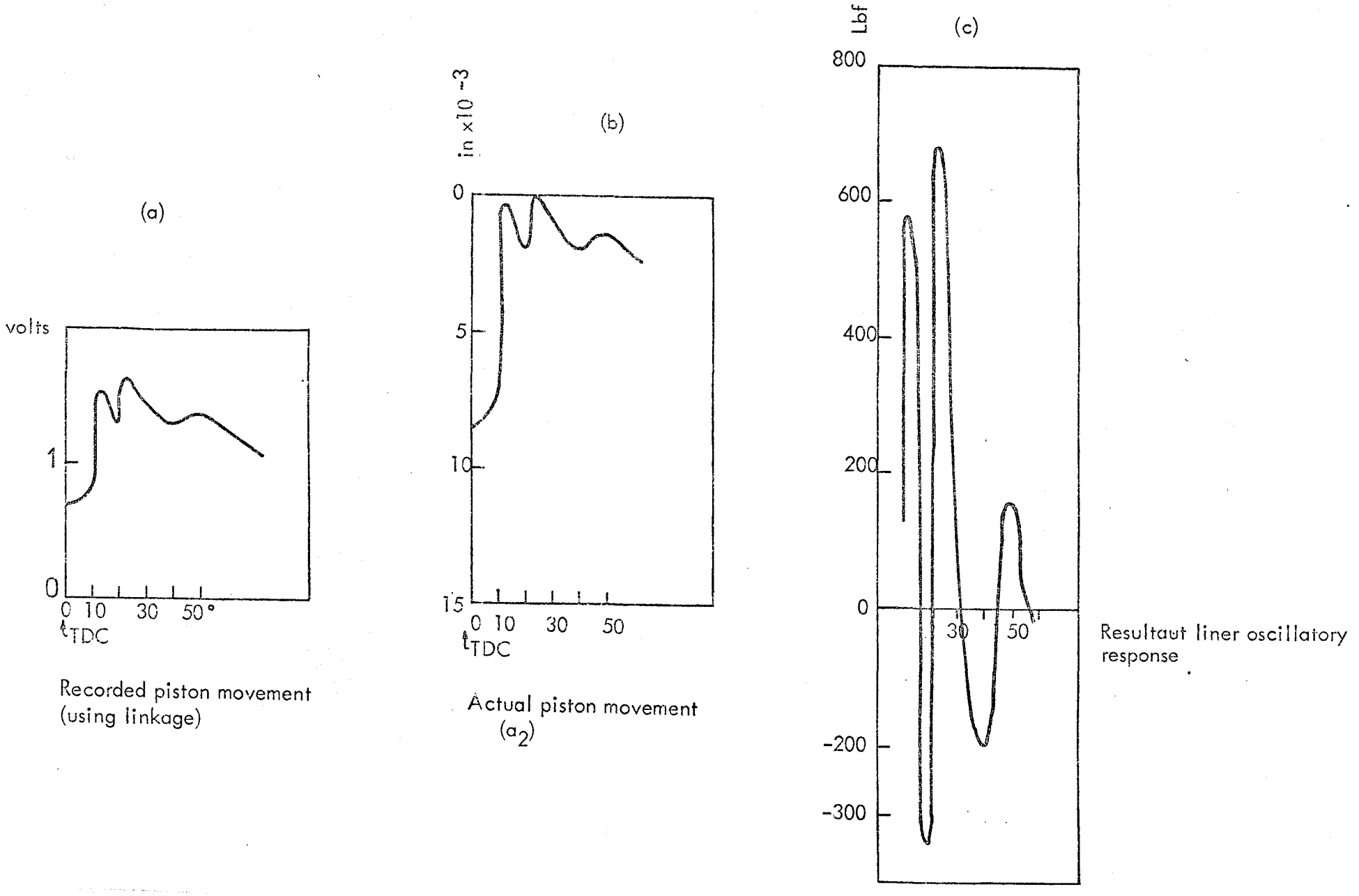

Recorded piston movement (using linkage)

Actual piston movement (a_2)

Resultaut liner oscillatory response

FIG. 1H MEASURED PISTON MOVEMENT AND THE RESULTANT LINER OSCILLATARY RESPONSE FORCE FOR A RUNNING V8 DIESEL ENGINE AT 1000 rev / min NO LOAD.

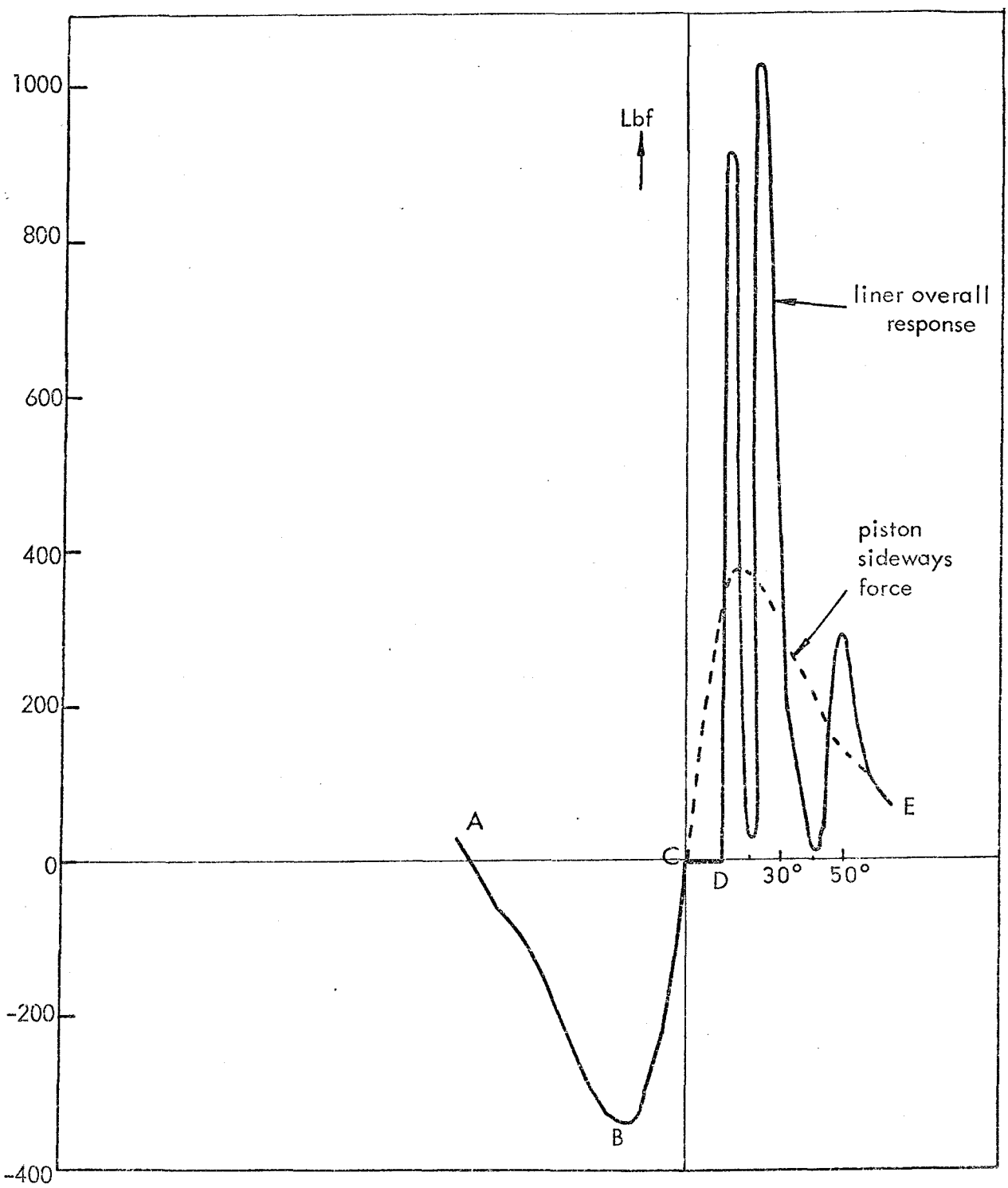

FIG. 2H RESULTANT LINER OVERALL RESPONSE DUE TO PISTON IMPACT AROUND TDC FOR A V8-7.7 LITRE DIESEL ENGINE @ 1000 revs/min NO LOAD

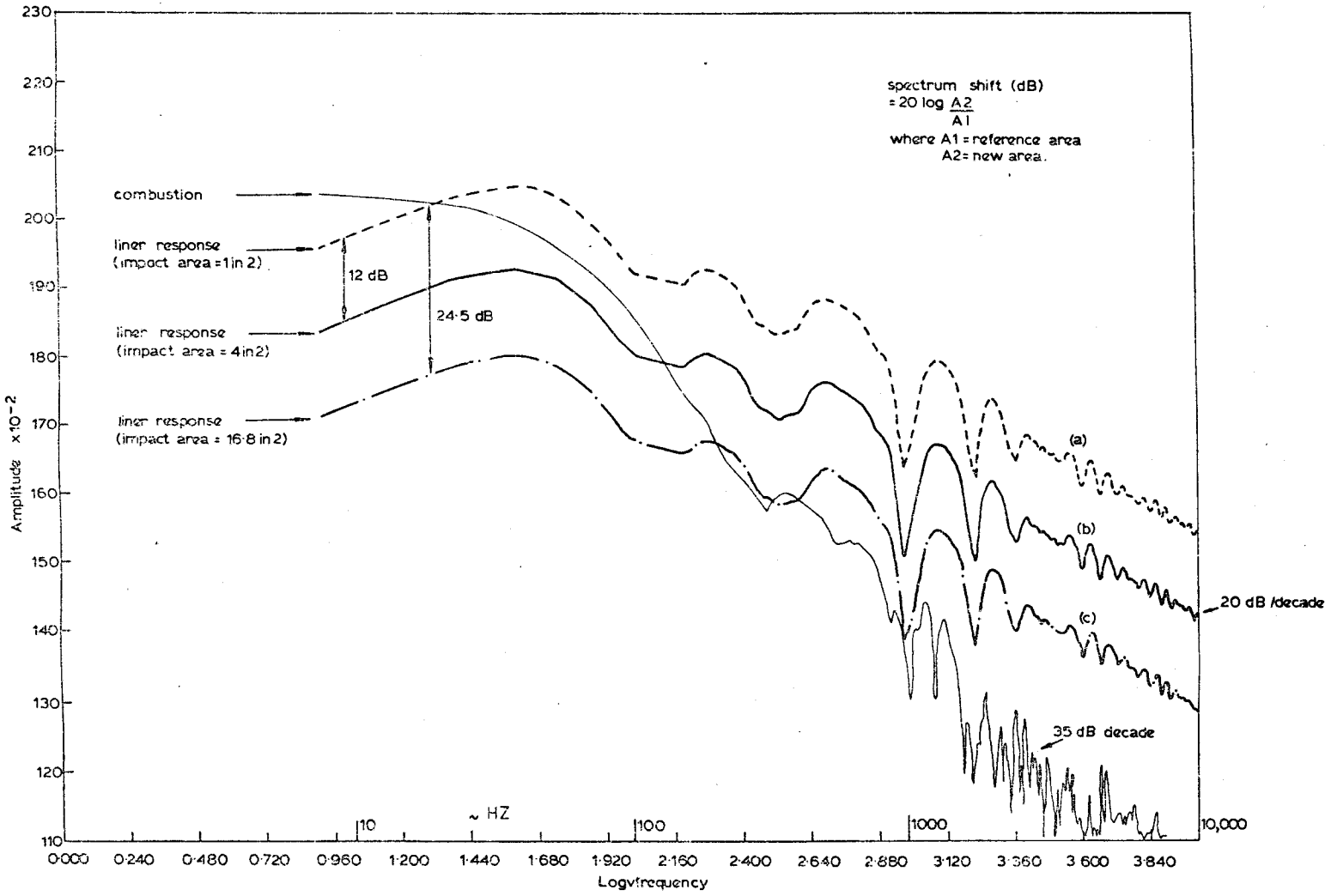

FIG. 3H . RELATIONSHIP BETWEEN COMBUSTION AND ENGINE UNER RESPONSE AT 1000 revs/min NO LOAD FOR A V8 7·7 LITRE DIESEL ENGINE.

DO NOT SCALE

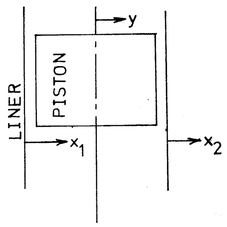

FORCE ON PISTON (INPUT)

$2 \times 10^{-6} F(t)$

PISTON

EQUATION

L.H. LINER

EQUATION

R.H. LINER

EQUATION

Logic 1, becoming Logic 0 when either impact occurs

Logic 0, becoming Logic 1 when either impact occurs

Logic 0, becoming 1 when impact with L.H. Liner occurs

COMP. A

L.H. LINER IMPACT

COMP. C

INITIAL CONDITION

COMP. B

R.H. LINER IMPACT

R.V. - 25 volts

DETECTOR

Logic 1, $y > 0$

Logic 0, $y < 0$

SELECTOR

DETECTOR

-10v.

RESTART SYSTEM

Logic 0, becoming 1 when impact with R.H. Liner occurs

+5 volts

INITIAL CONDITION COMPUTATION

COMP. "C"

Integrator Modes			
OP → / RS ↓		1	0
1		—	Reset
0		Compute	Hold

Sample Output

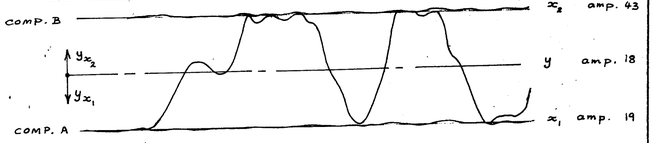

⊛ Amplifier inserted for $e m_p > m_c$

* " " " $e m_c > m_p$

† Pots 00,03 are set to zero for freely moving piston

SCALE

INSTITUTE OF SOUND AND VIBRATION RESEARCH
UNIVERSITY OF SOUTHAMPTON

TITLE	MATERIAL	DRAWN A. D. Nicholls
CIRCUIT FOR PISTON SLAP SIMULATION (for PACE TR-48)	FINISH	CHECKED P. W. Fortescue
	HEAT TREATMENT	DATE 4.11.1973
	DRAWING No. 6.TR48	

GAF S/P 2160/69